PhD

PROGRAM IN TRANSLATIONAL

AND MOLECULAR MEDICINE

DIMET

University of Milano-Bicocca

School of Medicine and Faculty of Science

Schwann cell dystroglycan regulates the architecture of nodes of Ranvier and internodes in the peripheral nervous system

Coordinator: Prof. Andrea Biondi

Tutor: Dr. Silvia Brunelli

Co-Tutor: Dr Laura Feltri

Dr. Cristina Colombelli

Matr. No. 600279

XXIV Cycle

Academic Year 2010-2011

Nothing is too wonderful to be true if it be consistent with the laws of nature.
(M. Faraday, 1870)

To the memory of Alberto

Table of contents

Chapter 1

Introduction

1.1 Overview

Perception of and reaction to the external environment is accomplished by the nervous system through bidirectional transmission of electrical impulses between the central nervous system (CNS) and the peripheral nervous system (PNS). The CNS is composed of the brain, the principal integrative area of the nervous system, and the spinal cord that functions as a conduit for nervous pathways to and from the brain and also acts as an integrative area for coordinating many subconscious nervous activities. The peripheral nervous system is made up of fibers that affiliate the brain and the spinal cord to the rest of the body, mediating information transfer either from the periphery to the CNS (sensory nervous system) or from the CNS to effector organs (motor nervous system). To achieve this connection two types of neurons are necessary: efferent or motor neurons, which transmit information away from the CNS, and afferent or sensory neurons, which are responsible for conveying signals to the CNS.

Moreover the PNS can be divided into the somatic and the autonomic or visceral parts. The first system includes somatic motor axons innervating skeletal muscles, and somatic afferent axons from the skin, joints and muscles. On the other hand, the autonomous system comprises visceral motor, autonomic axons to smooth muscle, cardiac muscle and glands, and visceral afferent axons from organs, and is mainly involved in involuntary functions such as heart rate, vasomotor

tone, bowel motility and saliva flow. It can be divided into the sympathetic and the parasympathetic system (Topp and Boyd, 2011).

The proper electrophysiological function of the PNS requires both cells that are directly involved in the process of signal transmission, i.e. neurons, muscle fibers and sensory endings, and a variety of cells that modulate these functions. This is demonstrated by the highly specialized relationships and profound intercellular cooperativity between different cellular components in the PNS. One of the most remarkable examples of this intimate cell-cell interaction is represented by the peripheral extension of the neuron, the axon, and its associated glial component, the Schwann cell, in myelinated fibers (Peters et al., 1991). The relevance of this mutual dependence is evidenced in several inherited diseases caused by mutations in Schwann cell genes that affect axonal structure and function, causing, in turn, motor and/or sensory disabilities.

As a result of this reciprocal communication, nerve fibers acquire structural features that allow them to maximize their conduction velocities. One such feature is the deposition of a specialized structure known as myelin sheath, that insulate the axon reducing the leak of current through the membrane in regions termed internodes. Another important feature is the differentiation of the axonal membrane into distinct molecular, structural and functional domains. This specialized structural organization is generated and maintained thanks to the formation of macromolecular complexes between axons and Schwann cells.

Functionally, the compartmentalization of the axon-Schwann cell unit allows the fast conduction of the electrical impulse by restricting the

regeneration of action potentials to nodes of Ranvier, specific regions of the axonal membrane devoid of the insulating myelin sheath and endowed with the molecular components involved in transmembrane ion movement. The node of Ranvier and its associated machinery mediate rapid, saltatory conduction (Hodgkin and Huxley, 1952), which means that each node acts as a booster station to ensure regeneration of the electric impulse and propagation of it to the next node. This kind of conduction gives the neuron the advantage of not having to constantly regenerate the impulse along every micron of axonal surface, with a striking reduction in the metabolic debt.

Besides the need of a compact myelin sheath along internodes and a proper nodal structure and function, another parameter that can influence the rate of nerve conduction is the length of internodes (Hursh, 1939; Brill et al., 1977; Jacobs, 1988; Court et al., 2004). It has been demonstrated that the proper Schwann cell cytoplasm compartmentalization in longitudinal and transverse bands, first described by Ramón y Cajal (Ramón y Cajal, 1933), is necessary for the correct internodal Schwann cell elongation. If such an organization is lost or altered, internodal lengths are affected and conduction velocity is slowed (Court et al., 2004 and 2009).

This thesis addresses the role of a Schwann cell laminin-receptor, dystroglycan, in the regulation of both nodal and internodal architecture, to provide the nerve with the proper structure that is ultimately needed to accomplish its electrical function.

1.2 Development of the peripheral nervous system

1.2.1 Cell types of the PNS and their origin

The two major cell types of the peripheral nervous system are neurons, or nerve cells, and the peripheral glial cells, termed Schwann cells (SCs) after the name of the german physiologist who first described them. Other cell types can be found in the supporting connective tissue, such as endoneurial and perineurial fibroblasts, and in blood vessels, like pericytes and endothelial cells.

Neurons

The basic makeup of a neuron consists in a cell body, or soma, with one long axon, the neurite, extending outwards to transmit impulses away from the cell body, and several dendrites, which are shorter in length and more branched, and whose role is to take signals in from other nerve cells.

The cell bodies of somatic motor neurons are located in the ventral horn of the spinal cord, whereas the cell bodies of autonomic motor neurons are located in the intermediolateral cell column of the T1-L2/L3 of the spinal cord for the sympathetic system, in the brainstem nuclei for cranial nerves III, VII, IX and X, or in the intermediolateral cell column of the S2-S4 spinal cord segments for the parasympathetic neurons. The cell bodies of both somatic and visceral sensory neurons locate in the dorsal root ganglia (DRG), also known as spinal ganglia, found within the intervertebral foramina. The neurons in the DRGs are pseudo-unipolar neurons that send their centrally directed axons through dorsal rootlets into the dorsal horn of the spinal cord. Efferent fibers send their axons through the ventral horn and into ventral

rootlets and are joined by sensory fibers from dorsal DRG to form a mixed, motor and sensory, spinal nerve. The spinal nerve divides almost immediately into dorsal and ventral branches, containing both motor and sensory axons. During development, the dorsal branches innervate the epiblast tissues, which will form the joints and deep muscles of the back and the overlying skin. The ventral branches innervate the hypoblast tissues, which will give rise to the joints, muscles and skin of the rest of the trunk and the limbs (Nakao and Ishizawa, 1994).

Neurons originate from the neural tube at specific locations along the dorso-ventral and rostro-caudal axes. In the ventral region, uncommitted, mitotically active progenitors give rise to motor neuron progenitors. This differentiation process is induced by the ventral to dorsal gradient of the transcription factor Sonic hedgehog (Shh), secreted from the underlying notochord and floor plate; this creates multiple motor neuron progenitor domains that give rise to distinct neuronal classes (Jacob et al., 2001). After specification of motor neuron subtypes, the correct innervation of their target structures is controlled by axon guidance cues, which are present in discrete locations along the pathway to the target zone.

Neurons of the sensory lineage derive from neural crest cells (NCCs) that delaminate from the neural tube and migrate in a ventral direction between the dermamyotome and the neural tube to produce cells of the dorsal root ganglia. During migration and shortly after coalescing into a DRG, NCCs commit to a sensory and neuronal fate and diversify into principal sensory subtypes such as nociceptive, mechanoreceptive and proprioceptive neurons. Only after neuronal

subtypes are specified, modality-specific central fields of terminations are established, with nociceptive neurons terminating in the dorsal horn, mechanoreceptors in deeper laminae of the dorsal spinal cord, proprioceptive neurons in the intermediate zone (for review, Marmigère and Ernfors, 2007).

Schwann cells

Schwann cells are the main glial cells in the PNS. They can be myelinating or non-myelinating depending on the diameter of the axon they come into contact with.

Such as sensory neurons, Schwann cells originate from neural crest stem cells. To achieve their adult phenotype, they have to undergo three main transitions: migrating NCCs give rise to Schwann cell precursor (SCPs), which then become immature SCs that eventually differentiate into either myelinating or non-myelinating Schwann cells (for review, Jessen and Mirsky, 2005) (Fig. 1).

The mechanisms that allow the population of crest cells to generate Schwann cells rather than neurons or melanocytes have been intensively studied. It is likely that some neural crest cells are already committed to the glial fate, whereas others are multipotent and a combination of positive and negative signals probably direct their differentiation as they are migrating through immature connective tissue before the time of nerve formation. Some evidence hints at β-neuregulin as an instructive signal that controls gliogenesis from the neural crest (Shah et al., 1994).

NCCs give rise to Schwann cell precursors, which colonize growing neurites directly through the ventro-lateral migratory stream and can

be found in mouse peripheral nerves at E12-13 (rat E14-15). SCPs are highly motile, flattened and with extensive cell-cell contacts. They can be found tightly associated to the surface of large bundles of axons or they can branch among the axons inside early nerves that are still compact and do not contain blood vessels or connective tissue yet. One peculiarity of SCPs is that they are wholly dependent on survival signals from axons, which are probably mediated to a large extent by axonal β-neuregulin acting via ErbB2/ErbB3 receptors on the precursors (Syroid et al., 1996; Jessen and Mirsky, 1999).

In a relatively abrupt transition SCPs convert to immature Schwann cells between E14 and E15 in mouse (rat E16-E17). Differently from precursors, immature Schwann cells are able to support their own survival by establishing an autocrine survival loop. *In vitro*, this has been shown to be mediated by insulin-like growth factor 2 (IGF2), neurotrophin 3 (NT3), platelet-derived growth factor-β (PDGFB), leukaemia inhibitory factor (LIF) and lysophosphatidic acid (LPA) (Dowsing et al., 1999; Meier et al., 1999; Weiner and Chun, 1999). Morphologically, immature Schwann cells contact with single large axon or with a bundle of small fibers. At this time connective tissue spaces also open up within the nerves, which become vascularized, and a distinct layer of developing perineurium appears at the nerve surface. A rudimentary basal lamina also appears on immature Schwann cells at this stage. The SCP-immature Schwann cell transition therefore correlates with an important step in the organogenesis of peripheral nerves. Each Schwann cell then selects an individual axon from a nerve bundle through a process called radial sorting (reviewed below).

At around the time of birth, immature Schwann cells give rise to myelinating and non-myelinating Schwann cells, also known as Remak bundles. Myelin-forming Schwann cells appear first and express a large amount of myelin proteins (P0, PMP22, MBP), whereas non-myelin forming Schwann cells, appear later and express markers such as glial fibrillary acidic protein (GFAP), N-CAM, L1 and p75.

Myelinating Schwann cells form a 1:1 relationship with axons prior to myelination (Webster et al., 1973). SCs with this morphology are often referred to as pro-myelinating Schwann cells. The different commitment of mature Schwann cells depends on the diameter of the axon they contact. Indeed, each mature Schwann cell has the potential to form myelin, but only the one that contact axons with a diameter greater than 1 μm can myelinate (Duncan, 1934; Voyvodic, 1989). More recently, this has been shown to correlate to the amount of neuregulin-1 type III that axons express on their surface (reviewed below).

Other cell types

Besides neurons and Schwann cells, peripheral nerves comprise other minor cell types. Among these, the ones contained in the three layers of connective tissues that surround and support peripheral nerves: endoneurium, perineurium and epineurium.

Endoneurium is the innermost connective tissue between individual nerve fibers and it consists of endoneurial fluid and a fine network of collagen fibers that are continuous with the basal laminae surrounding myelinated and unmyelinated fibers. In this compartment fibroblasts,

macrophages and mast cells are found. A Cre-recombinase fate mapping study has shown that SCPs are the source of the population of endoneurial fibroblasts residing in the nerve (Joseph et al., 2004).

Perineurial fibroblasts and a layer of dense connective tissue bundle single nerve fibers into fascicles, providing mechanical strength to the nerve. Perineurial fibroblasts are arranged in one to 15 layers, each provided with a basal lamina of type IV collagen, laminin, fibronectin and heparan-sulfate proteoglycan (HSPG). These cells may be mesodermally-derived (Bunge et al., 1989a).

Each group of nerve fascicles is in turn surrounded by the epineurium, containing dense and loose connective tissue and adipose tissue. It supports vessels and nerve fibers passing from extra-neural regions to the nerve fibers.

During embryonic development (mouse E14, rat E16), unknown signals recruit mesenchymal cells to surround the nerve and form a loose permeable sheath around it. It has been found that Desert Hedgehog (Dhh) from Schwann cells, probably together with other factors, is needed for the mesenchymal-epithelial transformation that turns this sheath into the multilayered, ordered perineurial sheath which forms a tight barrier between the nerve fibers and the surrounding tissue (Parmantier et al., 1999). Dhh is also involved in the formation of the epineurium, as it is extremely thin and with many fewer collagen fibrils in *dhh* null mice.

Pericytes and endothelial cells, that surround small blood vessels, are also present in peripheral nerves. The vascular supply is derived from segmental vessels that enter the epineurium and pass as arterioles and venules along the length of the nerve. Small arterioles pass obliquely

through the perineurial sheath, whereas continuous capillaries are present within the endoneurium (Bell and Weddell, 1984). The embryonic origin of these cells might be mesodermic.

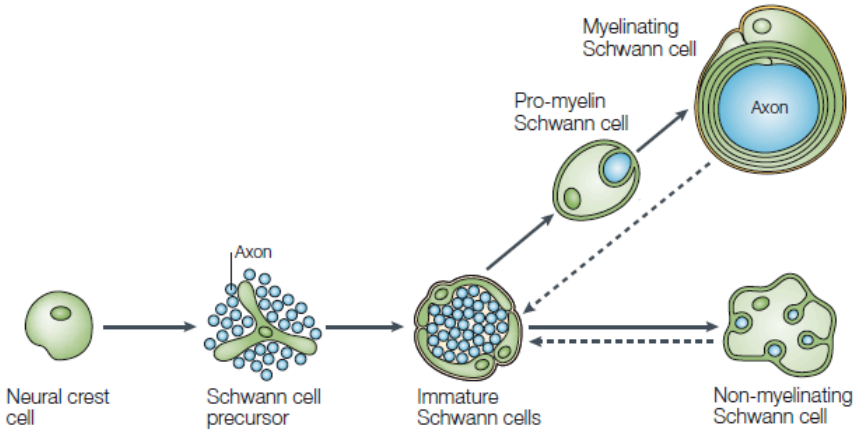

Fig. 1 Stages involved in Schwann cell development. As despicted in the diagram, the development of mature Schwann cells from neural crest cells involves two intermediate states, Schwann cell precursors and immature Schwann cells and three main transition events (from Jessen and Mirsky, 2005).

1.2.2 Formation of the myelinated fiber

As stated above, large caliber axons are myelinated by Schwann cells. The process that ends up in the formation of a myelinated fiber involves two sequential events: axonal, or radial, sorting and Schwann cell myelination. Both of them are thinly regulated by the interplay between axons, Schwann cells and the extracellular matrix (Fig. 2).

Axonal sorting

During late embryonic development, Schwann cells surround large bundles of axons forming the so-called Schwann cell 'families', contained in a common basal lamina (Webster et al., 1984). Each Schwann cell then selects an individual axon from the nerve bundle by extending sheet-like processes until they reach a 1:1 relationship. Axons larger than 1 μm in diameter are destined to be myelinated and are segregated away from axons that will remain unmyelinated (Webster et al., 1973). After larger axons have been sorted at the periphery of the bundle, their ensheathing Schwann cell detaches from the family and reorganizes its own basal lamina, in a process termed defasciculation.

Radial sorting is regulated by multiple signals from axons and from the extracellular matrix. The amount of neuregulin-1 type III (NRG1 type III) on the axon has been shown to be the instructive signal that determines whether a Schwann cell will myelinate a large axon or just encircle groups of multiple, small axons (Taveggia et al., 2005). Moreover, *in vivo* studies have shown that both laminins and their receptors (β1-integrins and dystroglycan) are required for different steps of radial sorting (Bradley and Jenkison, 1973; Feltri et al., 2002;

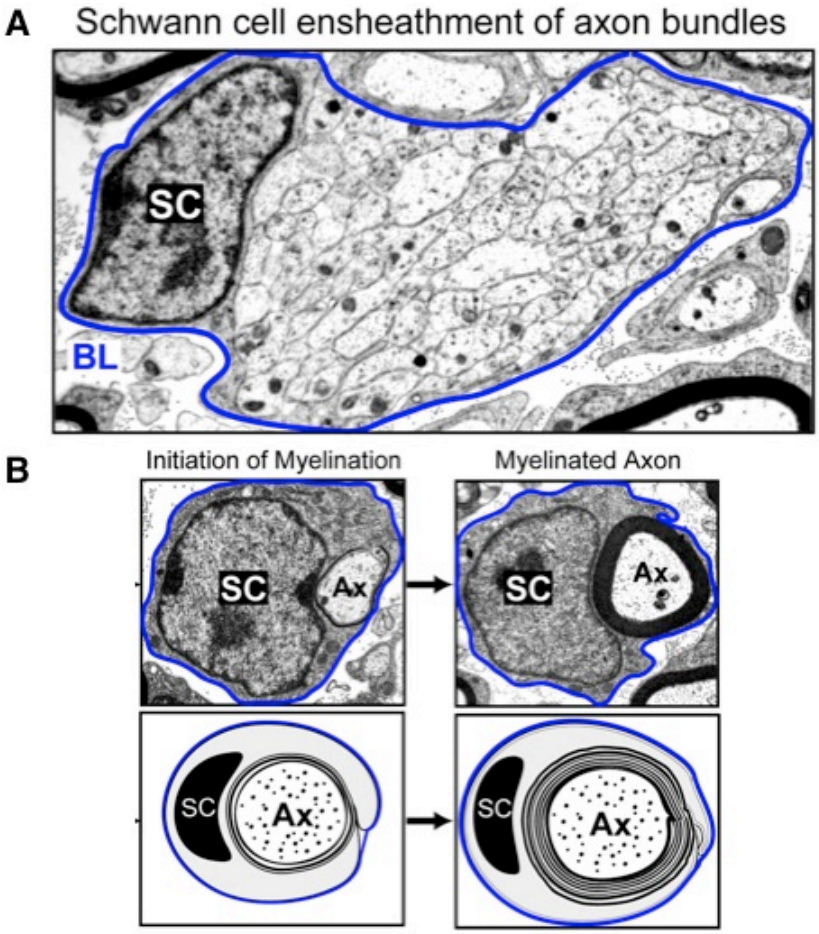

Fig. 2 Electron microscopy of Schwann cell (SC) development in the mouse sciatic nerve. During peripheral nerve development, Schwann cells proliferate, migrate, and ensheath axon (Ax) bundles (**A**). Schwann cells organize a basal lamina (BL, outlined in blue), which completely surrounds each individual cell and the associated axon(s). Upon receiving the appropriate signals from the local environment, SCs will sort through the axon bundle (not shown), isolate an individual axon at the periphery of the bundle, and then initiate myelination (**B**). Bottom panels are schematic representations of the electron micrographs in the top panels, and represent initial wrapping and myelination of a single axon (from Chan, 2007).

Chen and Strickland, 2003; Yang et al., 2005; Berti et al., 2011). It was found that laminin signaling promotes both the formation of SC processes via activation of the Rho-family GTPase Rac1 (Nodari et al., 2007) and SC proliferation and survival, necessary for the exact matching of SC-axon numbers, via activation of PI3K, Fak and Cdc42 (Yang et al., 2005; Benninger et al., 2007; Grove et al., 2007).

Myelination

Myelination starts at birth and is completed within the first 3-4 postnatal week in rodents, while is markedly more protracted in humans, extending over the first few years of life.

Once individual Schwann cells have associated with single axons along their lengths, they have reached a promyelinating phenotype, that means that their genetic expression program is modified to allow the synthesis of myelin constituents.

To form myelin the Schwann cell flattens into a spade-like shape and wraps its plasma membrane tightly around the axon, while removing the majority of cytoplasm from the spade. For the wrapping process two theories have been raised: the formation of myelin is achieved by either the progression of the inner (adaxonal) lip of the Schwann cell around the axon, or the movement of the outer (abaxonal) rim. In 1989, Bunge and colleagues monitored the movement of myelinating Schwann cell nucleus relative to the inner and outer lips of Schwann cell cytoplasm and suggested that the outer lip serves as an anchor, whereas spiral movements around the axon occur around the inner lip (Bunge et al., 1989b) (Fig. 3).

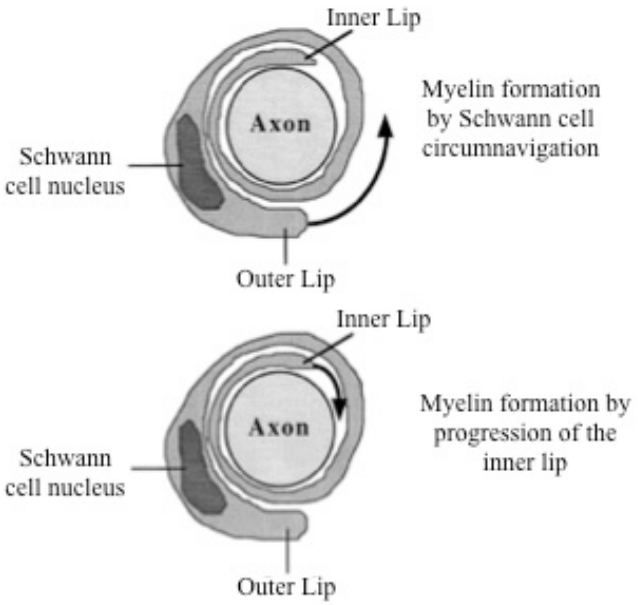

Fig. 3 Myelin formation by the Schwann cells: two hypotheses. The diagrams represent transverse sections of myelinating Schwann cells. The arrows indicate the direction of movement of the growing Schwann cell membranes (from Garbay et al., 2000).

Recent studies have shown that the regulation of actin filament polymerization by molecules as N-WASP and Rho GTPases and their downstream effector Rho kinase (ROCK) is crucial for coordinated spiraling of the internodal Schwann cell membrane around the axon, its longitudinal extension and myelination (Melendez-Vasquez et al., 2004; Novak et al., 2011; Jin et al., 2011).

After three to four turns of the Schwann cell process, the exclusion of cytoplasm and the association of adjacent extracellular membrane surfaces lead to the formation of a compact myelin sheath (Geren, 1954). Apposition of the cytoplasmic faces of the membranes is dependent on myelin basic protein (MBP) (Rosenbluth, 1980) and the

cytoplasmic tail of the integral membrane protein P0, the major protein of peripheral myelin; whereas the association of the extracellular faces of the membrane is achieved by the homophilic association of the extracellular domains of P0 (Filbin et al. 1990; D'Urso et al., 1990).

The number of myelin lamellae forming the sheath increases during the myelination period, reaching a mean number of myelin lamellae of 50 and 80 in the sciatic nerves of adult mice and rats, respectively, with a maximum of about 100 lamellae for the thickest fibers (Friede and Samorajski, 1968).

At the end of myelination, myelin presents two distinct domains, compact and non-compact myelin, each of which contains a non-overlapping set of proteins. Compact myelin represents the bulk of the myelin sheath and is a spiral of closely packed membranes with a periodicity of approximately 14 nm in conventional transmission EM and slightly greater (18 nm) in fresh nerves by X-ray diffraction. The apposed membranes form the intraperiod line and the thin space that separates the membranes is contiguous with the extracellular space. The major dense line is contiguous with the cytoplasm.

Non-compact regions of the Schwann cell plasma membrane containing cytoplasm, known as Schmidt-Lanterman incisures, radially transverse the compact myelin, providing a channel between the Schwann cell cytoplasm outside the myelin sheath (abaxonal compartment) and the cytoplasm adjacent to the axonal plasma membrane (adaxonal compartment) (Fig. 4).

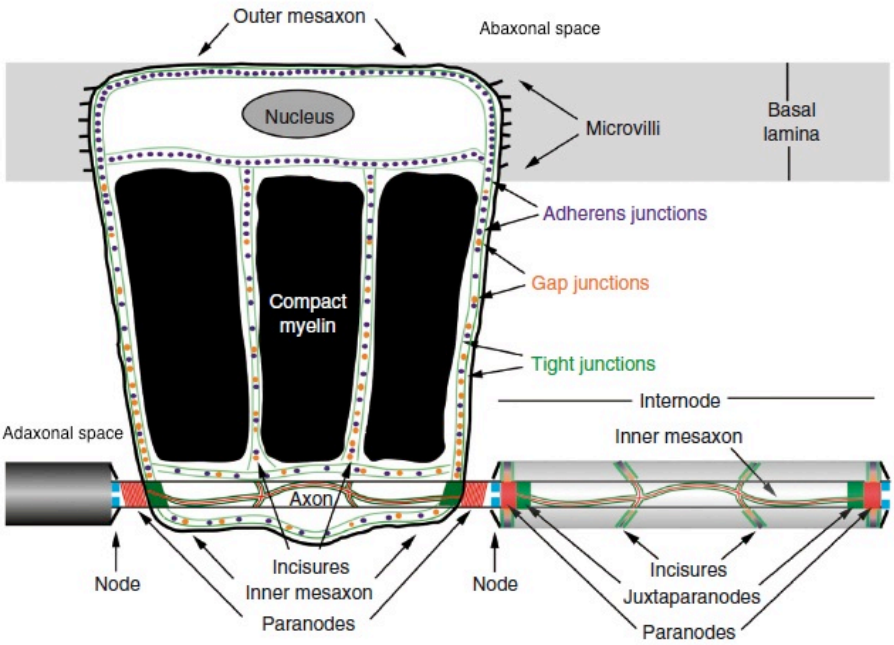

Fig. 4 Scheme of a myelinated axon. One myelinating Schwann cell has been unrolled, revealing the regions that form non-compact (Schmidt-Lanterman incisures and paranodes) and compact myelin. The abaxonal and adaxonal compartments are shown at the top and the bottom respectively (adapted from Scherer and Arroyo, 2002).

Regulation of myelin thickness

The thickness of the myelin sheath varies according to the diameter of the axon: bigger axons have thicker myelin, and vice versa (Friede and Samorajski, 1967). The optimal myelin thickness is reached when the 'g-ratio' (i.e. the numeric ratio between the diameter of the axon and that of the myelinated axon) is close to 0.68. As noted in very early studies, for most vertebrates this ratio is remarkably well maintained independent of the specific axon diameter (Donaldson and

Hoke, 1905). This requires axon size to be perceived by myelinating SCs, to make the correct number of myelin wraps. Via ErbB2/ErbB3 co-receptors, Schwann cells sense an axonal size-related signal, which has been demonstrated to be the amount of NRG1 type III (Michailov et al., 2004). Altering the levels of axonal NRG1 type III alters the amount of deposited myelin: mice haploinsufficient for the neuregulin 1 (*Nrg1*) gene have thinner peripheral myelin sheaths than controls, whereas transgenic *Nrg1* overexpressing mice show hypermyelination (Michailov et al., 2004; Taveggia et al., 2005).

Although NRG1 type III plays a pivotal role in determining myelin thickness, it is possible that other signaling systems, like p75 and BDNF, might participate in determining the extent of myelin synthesis (Tolwani et al., 2004).

Control of the internodal length

The influence of growth, or the lack of it, upon internodal length has been demonstrated by studies in developing animals and in nerves from parts of the body which show different rates of growth (Ranvier, 1872; Vizoso, 1948 and 1950). This has suggested that elongation of the nerve controls the longitudinal size of Schwann cells. Furthermore, internodal length (IL) is positively related to axonal diameter, so that nodes of Ranvier are farther apart in large fibers than in small ones (Ranvier, 1875; Hiscoe, 1947). This can be explained as a consequence of the fact that large fibers are sorted and myelinated first and are therefore subjected to the longest period of growth (extension in length), whereas small fibers myelinate later and are therefore shorter. Nonetheless, several pieces of evidence suggest that

length and thickness of the myelin sheath are independently regulated (Hara et al., 2003; Michailov et al., 2004).

This 'classical' model suggests that the final internodal length depends on two parameters: the time at which a Schwann cell associates to an individual axon and the subsequent growth of the nerve fiber that determines the growth rate of the associated Schwann cell.

In the last few years Court et al. showed that indeed internodal extension is precisely matched to nerve growth in normal fibers, but the ability of Schwann cells to elongate is cell-autonomous and depends on their capacity to properly organize their outermost region of cytoplasm in two compartments: transverse cytoplasmic areas termed Cajal bands, and areas in which the Schwann cell membrane is closely apposed to the myelin sheath, known as appositions or patches (Court et al., 2004 and 2009) (Fig 5). These studies have shown that SC compartmentalization and the establishment of correct internodal length depend on periaxin (Court et al., 2004), and require the presence of glycosylated dystroglycan, utrophin and extracellular laminin α2, which are proteins that link the extracellular matrix to the SC cytoskeleton, regulating the formation of SC compartments by maintaining actin and tubulin fences that dictate the localization of Cajal bands (Court et al., 2009). The finding that the formation of Cajal bands/appositions is determined by a primordial cytoskeletal pattern that outlines the areas that will subsequently be compartmentalized goes along with the fact that actin filaments contribute to the elongation of Schwann cells on axons.

Another great advance of these studies was the experimental

confirmation of the relation between internodal length and conduction velocity, in accordance with previous theoretical predictions from mathematical models (Brill et al., 1977; McIntyre et al., 2002).

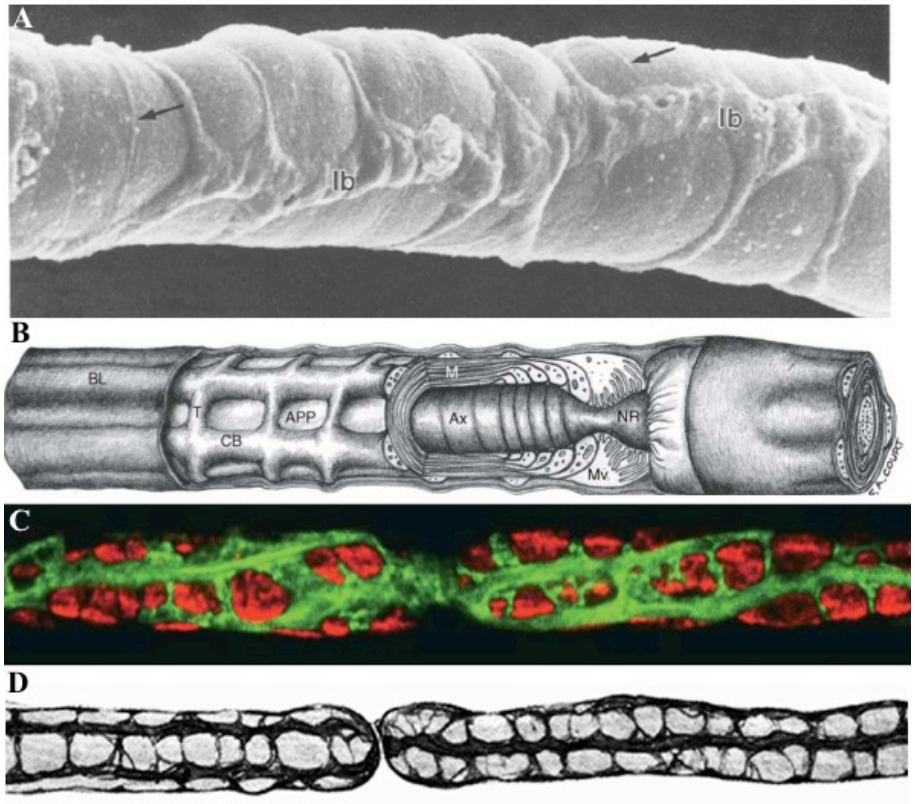

Fig. 5 Distribution of bands of Cajal and appositions in the outer cytoplasm of a myelinating Schwann cell. A, Scanning electron microscopy of the surface of a myelin forming Schwann cell showing the longitudinal arrangement of the cytoplasmic channels (lb) with fine *trabeculae* (arrows) connecting them (from Ushiki and Ide, 1987). **B**, Schematic drawing with cut away sections displays the architecture of the myelinated fiber, with Cajal bands (CB), *trabeculae* (T), and appositions (APP). Microvilli (Mv) at nodes (NR), the outer basal lamina (BL), compact myelin (M) and the axon (Ax) are shown (from Court et al., 2006). **C**, Teased fibers stained with fluorescent-conjugated phalloidin (green) and an antibody against DRP2 (red). Schwann cell cytoplasmic domains are excluded from spheroidal clusters immunopositive for DRP2 (from Court et al., 2004). **D**, Longitudinal and transverse protoplasmic bands silver-stained by Ramón y Cajal (from Ramón y Cajal, 1933).

1.3 Structure of the peripheral myelinated fiber

The myelin sheath was a unique and transformative vertebrate acquisition, which enabled great increases in impulse propagation along axons at low metabolic and spatial costs. This facilitated both predatory and escape behaviours, permitting the evolution of very large vertebrate body sizes. It is likely that myelin evolved first in the oldest jawed fishes, the placoderms, during the Devonian period (Zalc and Colman, 2000). It has also been hypothesized that the myelin sheath in vertebrates arose in conjunction with the neural crest, which gives rise to the jaw apparatus and most of the peripheral nervous system (Zalc et al., 2008).

The myelinating Schwann cell-axon unit represents a striking example of cell-cell interaction, in which the two cellular components are completely interdependent. The result of this intimate coordination is the organization of both the glial and the axonal counterparts in structurally, molecularly and functionally distinct subcellular domains. Along the longitudinal length of a myelinated fiber two main domains can be distinguished: the node of Ranvier and the internode. The first eponymous structures (Ranvier, 1871) are short periodical interruptions of the myelin sheath, where action potentials are continuously regenerated; internodes are the myelin segments extending from node to node, through which electrical signals are rapidly propagated. Nodes of Ranvier and internodes are separated by two further specialized domains, the paranodes and juxtaparanodes. Indeed, the entire axon and Schwann cell, including their cytoskeleton, organelle content and transport machinery are differentially organized at these sites (Fig. 6).

In the next section, I will review these defined domains that have profound implications for the electric properties of the SC-axon unit.

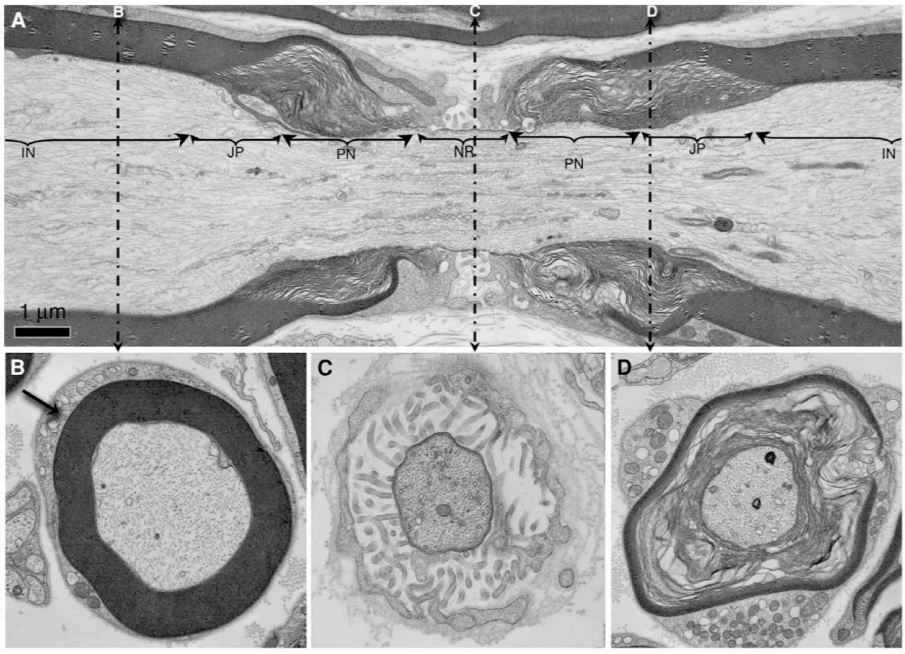

Fig. 6 Domain organization of the peripheral myelinated fiber. A, Electron micrograph of a longitudinal section of an adult rat ventral spinal root with the nodal (NR), paranodal (PN) and internodal areas (IN) marked. Cross sections through each corresponding region are represented in **B-D**. **B**, Section through the internodal region is characterized by the presence of a compact myelin sheath. The arrow marks the outer layer of Schwann cell cytoplasm that is reduced to narrow channels running continuously from the cell body to the nodal region. **C**, Section through the midpoint of the nodal membrane. Numerous Schwann cell microvilli can be seen surrounding and closely apposing the axonal nodal membrane. The basal lamina covers the entire nodal region. **D**, Section through the paranodal region of an axon, showing the uncompacted myelin of the paranodal loops (from Sosinsky et al., 2005).

1.3.1 Internodes

Internodes represent the most extended site of interaction between axons and SCs, comprising nearly 99% of total segment length. They are approximately 100 times the axon diameter, ranging up to 1 mm or more in larger fibers of adult mammalian PNS (Hess and Young, 1952; Abe et al., 2004).

Each internode comprises the myelin sheath deposited by a single Schwann cell (Webster, 1971). In the internodal region the myelin sheath can be divided in two contiguous domains: compact myelin, forming the bulk of the myelin sheath, and non-compact myelin, comprising the Schmidt-Lanterman incisures (SLIs) and the inner and outer mesaxons.

Compact myelin

One of the most peculiar biochemical feature that distinguishes myelin from other cellular membranes is its high lipid to protein ratio: overall, lipids account for 70-80% and proteins make up for 20-30% of myelin dry weight (Garbay et al., 2000). The high lipid content ensures the insulating function during electrical impulse conveyance, while proteins are considered important to guarantee the stability of the sheath.

There is not a myelin-specific pattern of lipids, but all the main classes of lipids (cholesterol, phospholipids, sphingolipids) are represented in PNS myelin. Cholesterol, which accounts for 20-30% of the total lipid content, is required for normal myelination as mice with reduced cholesterol synthesis show severe hypomyelination (Saher et al., 2005). The importance of lipids is also evidenced by the congenital

hypomyelination developed by mice lacking a protein that actively regulates the expression of genes involved in myelin lipid synthesis (Verheijen et al., 2009).

While there are no myelin-specific lipids, a number of proteins exists that are unique to myelin. The most abundant proteins are the glycoproteins Myelin Protein Zero (P0; 50-70% of total myelin proteins) and Peripheral Myelin Protein 22 kDa (PMP22; 2-5%) and the basic proteins Myelin Basic Protein (MBP; 5-15%) and PMP2/P2 (1-10%).

The fundamental role of myelin proteins and the need of a fine regulation of their dosage/stoichometry are underlined by the fact that many mutations or copy number variation in their genes are responsible for a variety of peripheral neuropathies. More than 40 mutations in *PMP22* sequence have been associated with hereditary neuropathies, among which the most common is gene duplication and causes Charcot-Marie-Tooth 1A (CMT1A; Pentao et al., 1992), while its deletion is responsible for hereditary neuropathy with liability to pressure palsies (HNPP; Chance et al., 1993) in humans. Various mutations in the human *MPZ* gene can cause demyelination (CMT1B) by a dose-related decrease in the amount of P0 protein or by a gain of toxic function of the mutant protein (Scherer and Wrabetz, 2008).

Non-compact myelin, cytoplasmic components of the Schwann cell

Along the internodal region, the cytoplasmic domain at the outer (abaxonal) Schwann cell surface is contiguous with the cytoplasmic channels that either traverse the compact myelin (Schmidt-Lanterman incisures) or surround the axon (inner or adaxonal surface). This

complex cytoplasmic channel network runs both longitudinally along the internode and transversely through the myelin sheath, providing a continuous connection between all the cytoplasmic compartments of the SC. This continuity is required for the metabolic support of the entire cell and for signal communication between the axon and the Schwann cell.

At the adaxonal side of the myelin sheath, the inner membrane of the Schwann cell is uniformly separated from the underlying axon by a periaxonal space of 12-14 nm and is closely apposed to the myelin sheath except for a single cytoplasmic channel that traverses the entire internode. This cytoplasmic compartment is believed to be involved in transduction of signals that regulate myelin formation; indeed, two studies have shown that nectin-like (Necl) proteins on the adaxonal Schwann cell surface and on the axon mediate heterophilic binding that may allows proper communication of the signals that trigger myelination (Maurel et al., 2007; Spiegel et al., 2007).

The abaxonal surface displays multiple cytoplasmic channels that where first described by Santiago Ramón y Cajal, using silver staining methods (Ramón y Cajal, 1933) (Fig. 5). He proposed that this network of cytoplasm was required for the efficient transport of nutrients along the internode to the more distal regions of the Schwann cell. Considering that the SC nucleus together with all the machinery for protein synthesis and transport are positioned in this domain, it is not difficut to believe that these cytoplasmic channels are needed to expand and maintain the myelin internode (Trapp and Kidd, 2003).

The major channels, termed Cajal bands, run longitudinally over the

entire length of the internode, whereas the smaller ones connecting different Cajal bands are called *trabeculae*. These channels are rich in microtubules, filamentous actin and other cytoskeletal components, like spectrin and ankyrin, for transport and stability, and mitochondria for energy. Moreover, their membranes contain caveolin-1 (Mikol et al., 1999), a protein involved in the formation of *caveolae*, which are invaginations of the plasma membrane known to regulate signal transduction and cholesterol transport. Regions devoid of cytoplasm (appositions) are located between cytoplasmic rich domains, in close apposition with the outermost loop of compact myelin (Ushiki and Ide, 1987) (Fig. 5). These regions are characterized by the presence of dytroglycan-related protein 2 (DRP2) in association with the protein L-periaxin, which can be mutated in autosomal recessive forms of the demyelinating neuropathy CMT4F (Sherman et al., 2001). DRP2-periaxin associates with the dystroglycan receptor which links the extracellular matrix to the Schwann cell cytoskeleton (reviewed below).

How the compartmentalization of Schwann cell outer cytoplasm in Cajal bands and appositions is achieved has been unveiled only recently. A study demonstrated that during early postnatal development actin filaments first deposit in areas that will become Cajal bands, forming a net-like structure around empty gaps that will be subsequently filled with DRP2 (Court et al., 2009).

The cytoplasmic outer and inner regions of the internode are connected by Schmidt-Lanterman incisures, a series of cytoplasmic openings of the compact myelin that are in register with each others (Robertson et al., 1958; Ghabriel and Allt, 1981). SLIs contain

cytoplasm, certain types of microtubules, filamentous actin, and several types of junctions (adherens, tight and gap) (Fig. 4). The role of incisures as conduits for metabolic material to the myelin sheath has been proposed. In accordance with this role, the number of incisures along the internode increases with fiber diameter (Hiscoe, 1947), suggesting that there exists an upper limit to the amount of myelin that can be maintained in a single region between two incisures. In addition, radial diffusion of small ions has been reported to occur through gap junctions formed by the protein connexin-32 and linking apposed membranes of SLIs (Balice-Gordon et al., 1998).

Each one of the aforementioned Schwann cell cytoplasmic areas has its specific protein composition. However, the two major protein markers shared by the majority of non-compact myelin domains are myelin-associated glycoprotein (MAG) (Trapp et al., 1990) and 2',3'-cyclic nucleotide 3'-phospodiesterase (CNP).

1.3.2 Node of Ranvier

Nodes of Ranvier are periodic annular constrictions of the myelinated fibers first described by Louis-Antoine Ranvier in 1871. They are small gaps, less than 1 μm in length, devoid of myelin, where the axonal membrane is directly exposed to and communicate with the extracellular milieu. At nodes the axon is typically constricted in its diameter, being reduced to as little as 20% of the internode in large fibers.

This decrease in axonal caliber results in a higher packing density of microtubules, membranous vesicles and neurofilaments. The decreased neurofilament spacing depends on a reduced sidearm

extension due to less phosphorylation of tyrosine residues (Mata et al., 1992).

Nodal axolemma

The main function of nodes of Ranvier is to regenerate action potentials that initially arise at the axon initial segment (AIS), thus allowing saltatory conduction of the nerve impulse. The molecular organization of the node is specialized for its electrical function. In light of this structure/function relationship, the nodal axolemma is highly enriched in voltage-gated sodium channels (Nav) that reach a density of 1200-1500/μm^2, much higher than the internodal density, estimated to be less than 25/μm^2. Such a high concentration of Nav has been first envisaged by freeze fracture studies that detected a remarkable enrichment of intramembranous particles (IMPs) at nodes compared to internodes (Rosenbluth, 1976). These IMPs, associated to the outer leaflet (E face), were thought to correspond largely to Nav and this has been confirmed by subsequent electrophysiologic studies. In addition to Nav, a dense undercoating of 25-35 nm subjacent to the axolemma represents several transmembrane and cytoskeletal proteins forming multiprotein complexes that link ion channels with the cortical cytoskeleton of the axon. Among others, the cytoskeletal protein ankyrin-G, whose major isoforms at the node of Ranvier are 270 and 480 kDa (Kordeli et al., 1995), has an essential role in organizing and stabilizing the nodal, axonal complex (Dzhashiashvili et al., 2007). Ankyrin-G binds directly to Nav (Bouzidi et al., 2002; Lemaillet et al., 2003), and βIV-spectrin, an actin-binding protein highly enriched at nodes and AISs (Berghs et al., 2000). βIV spectrin

physically stabilizes the nodal axolemma and regulates the clustering of Nav at the nodes by providing a link between the Nav complex and the actin cytoskeleton (Komada and Soriano, 2002). Mice deficient in βIV spectrin exhibit enlarged axon diameters and aberrant protrusions of the axon membrane at the node (Yang et al., 2004).

Ankyrin-G also interacts with two members of the L1 subgroup of IgG cell adhesion molecules superfamily (L1 CAM), NrCAM and neurofascin-186 (Nf186), which are found at nodes of Ranvier (Davis et al., 1996). Binding of ankyrin-G to Nf186 and NrCAM is mediated by phosphorylation of the tyrosine residue of the FIGQY conserved sequence in their cytoplasmic domains (Zhang et al., 1998); only when this motif is dephosphorylated, the binding occurs (Garver et al., 1997; Tuvia et al., 1997). Both NrCAM and Nf186 cluster early at some sites presumed to be nascent nodes, before Nav and ankyrin-G (Lambert et al., 1997), and they have been hypothesized to act as pioneer molecules in node formation (Lustig et al., 2001). Indeed, mice specifically lacking axonal neurofascin (Nf186) are not able to cluster Nav (Sherman et al., 2005; Thaxton et al., 2011), whereas *NrCAM* null mutants show a delay in Nav and ankyrin-G sequestration at developing nodes (Custer et al., 2003).

In addition to Nav, some voltage-gated potassium channels are also expressed at nodes, in particular KCNQ2 and KCNQ3 (Devaux et al., 2004), which have a conserved sequence that mediates their binding to ankyrin-G (Pan et al., 2006) and may be important in the control of repetitive discharges (Cooper and Jan, 2003). The importance of these channels is shown by a dominant mutation in the human *KCNQ2* gene; the mutant KCNQ2 reduces the activity of both KCNQ2 and

KCNQ3, and it produces repetitive firing of motor axons (known as neuromyotonia or neuromyokymia). An isoform of Na^+/K^+-ATPase is highly concentrated in the nodal axolemma as well, where it is needed for the maintenance of sodium and potassium gradients required for action potential propagation. (Ariyasu et al. 1985; Mata et al. 1991).

Other proteins have recently been identified as enriched at nodes of Ranvier, including IKK (IkBα kinase) (Politi et al., 2008), an isoform of schwannomin-interacting protein-1 (IQCJ-SCHIP-1) (Martin et al., 2008), and the FGF homologous factors FHF2 (Wittmack et al., 2004). The FHF family has been implicated in modulating the activity of sodium channels (Goldfarb et al., 2007; Buzhdygan, 2011).

Voltage-gated sodium channels

At nodes, the action potential is generated by the opening and subsequent inactivation of voltage-gated sodium channels and, with a slight delay, the opening of voltage-gated potassium channels (reviewed below).

Mammalian Nav are multimeric complexes that consist of a highly glycosylated 260 kDa pore-forming α-subunit associated with one or more auxiliary β-subunits, that can be linked with α via disulfide bonds (β2 and β4) or non-covalently (β1 and β3) (Catterall et al., 2005). These subunits are encoded by nine α- (*Scn1a-Scn9a*) and four β-subunit genes (*Scn1b-Scn4b*) in mammals. The Nav α-subunits (Nav1.1-9) contain the ion-selective pore and are composed of four homologous membrane domains (I-IV) each containing six transmembrane α helices (S1-S6) (Fig.7). S5 and S6 segments from the four domains form the Na^+ selective pore and the S4 helix contains

positively-charged amino acid residues that serve as gating charges whose movements induce pore opening in response to depolarization of the membrane. The short intracellular loop connecting domains III and IV acts as the inactivation gate, folding into the channel structure and blocking the pore from the inside during sustained depolarization of the membrane. The α subunit is sufficient for functional expression of Nav, but the kinetics and amplitude of sodium currents are modulated by the β subunits (Qu et al., 2001; Arman et al., 2009). Although the exact stoichiometry and composition of the sodium channel α/β subunit complex at the node is not yet known, both β1 and β2 are localized at this site, whereas whether β3 and β4 are present at nodes remains to be determined (Chen et al., 2004). The four β subunits share a similar topology, containing an extracellular immunoglobulin (Ig)-like domain, which mediates homophilic interactions, as well as binding to other nodal components. For instance, the β1 and β2-subunits interact in *cis* with Nf186 and NrCAM (Ratcliffe et al., 2001; McEwen and Isom, 2004), suggesting a mechanism for Nav recruitment to nodes through the β subunits. In support of this, mice deficient in β1 have defects in nodal architecture and both β1 and β2 knock out mice show altered nerve conduction, characteristic of a reduced Nav density (Chen et al., 2002 and 2004). However, it is likely that β subunits are involved primarly in Nav cluster maintenance rather than formation, as an Nf186 mutant deficient in ankyrin-binding but capable of binding β subunits fails to cluster Nav at nodes *in vitro* (Dzhashiashvili et al., 2007). Some investigators (Malhotra et al., 2002), but not others (Bouzidi et al., 2002; Lemaillet et al., 2003) also reported a direct interaction of β

subunits to ankyrin-G. Furthermore, the β1- and β2-subunits can interact with the extracellular matrix molecules tenascin-C and tenascin-R (Srinivasan et al., 1998; Xiao et al., 1999), as well as with phosphacan (Ratcliffe et al., 2000), the secreted form of receptor protein tyrosine phosphatase β (Rptpβ).

Many subtypes of sodium channels can be targeted to nodes of Ranvier and during development several subtypes are found at neonatal nodes. In the adult mammal almost all nodes of Ranvier in the PNS contain predominantly one subtype, Nav1.6 (Caldwell et al., 2000). Nav1.6 exhibits user-dependent potentiation, which may be particularly useful during the high frequency firing characteristic of nodes of Ranvier (Zhou and Goldin, 2004). Mutations or conditional disruption of the Nav1.6 coding gene, *Scn8a*, result in a remarkable decrease or absence of nodal Nav and elongated and disorganized nodes in mice (Rieger et al., 1984; Burgess et al., 1995; Kohrman et al., 1996, Sharkey et al., 2009).

During development, the Nav1.2 isoform is uniformly distributed along unmyelinated fibers and appears first at immature nodes; as myelination progresses Nav1.2 are eventually replaced by Nav1.6 both in CNS and in peripheral nerves (Boiko et al., 2001). However, in PNS a substantial fraction of newly forming nodes contain Nav1.6 already at P1 (Schafer et al., 2006). The Nav isoform switch takes place in the first postnatal days and is completed by P7 in sciatic nerves (Rasband and Trimmer, 2001). The functional significance of this switch is currently unclear, but it might allow neurons to adapt to high-frequency firing. Strikingly, paranodal junctions seem to have a prominent role in the differential expression of Nav1.2 and Nav1.6

types at nodes, as mice with altered paranodes exhibit incomplete replacement of Nav1.2 by Nav1.6 (Rios et al., 2003).

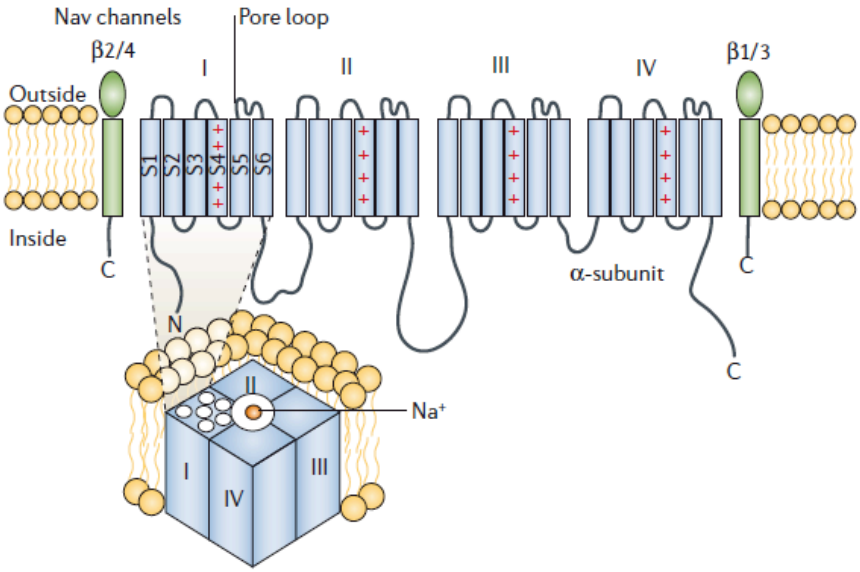

Fig. 7 General structural topology of Nav. Nav channels are formed from a single polypeptide that consists of four domains (I-IV), each of which has six transmembrane segments (S1-S6). The fourth transmembrane segment of each domain contains positively charged arginines that are primarily responsible for voltage sensing, as well as the S5-pore loop-S6 region, which forms the pore domain through which sodium ions flow. The β-subunits, β1/3 and β2/4, are single transmembrane proteins that have an immunoglobulin-like extracellular domain that co-assembles with the Nav α-subunits (from Lai and Jan, 2006).

Schwann cell microvilli and the nodal gap

At peripheral nodes of Ranvier, the nodal axolemma is closely apposed by interdigitating cytoplasmic processes that extend from the outer collars of two neighbouring Schwann cells (Ichimura and Ellisman, 1991). These projections are termed microvilli. Owing to their differential staining properties, Ramón y Cajal and Louis Ranvier first observed Schwann cell microvilli and the so called 'cementing disc of Ranvier', which consists in the specialized substance in which microvilli are immersed, in that area known as nodal gap (Landon and Langley, 1971) (Fig. 6B). Microvilli appear to be connected to one another via tight junctions (Berthold and Rydmark, 1983), and claudin-2 is specifically localized at these sites (Poliak et al., 2002). Morphologically they are similar to microvilli of other cell types, with a diameter of 70-80 nm and a central core of 4-6 microfilaments; in larger fibers, they are organized into a regular hexagonal array. Nodal microvilli contain F-actin, myosin and spectrin (Trapp et al., 1989; Zimmermann, 1996), the homologous cytoskeletal-associated proteins, ezrin, radixin and moesin (ERM proteins), ezrin-binding protein (EBP50) and RhoA-GTPase (Hayashi et al., 1999; Melendez-Vasquez et al., 2001; Scherer et al., 2001). ERM proteins might act as crosslinkers between the cytoskeleton and the plasma membrane, being able of binding transmembrane proteins with their N-terminal domain and actin cytoskeleton with their C-terminal half. Their cross-linking activity is activated by phosphorylation of a conserved threonine residue (Matsui et al., 1998). During development, the ERM proteins become concentrated at the lateral tips of Schwann cells before MBP expression, and these

ERM-positive SC processes overlie and associate closely with nascent nodes of Ranvier, suggesting a role in node formation (Gatto et al., 2003).

The importance of microvilli in the formation and maintenance of a proper nodal architecture is evidenced by several nodal-environment mutant mice that show disorganization and impaired attachment of microvilli to the nodal axolemma, associated with alterations in Nav clustering (Saito et al., 2003; Feinberg et al., 2010). These mutants lack gliomedin, NrCAM or dystroglycan, three transmembrane proteins that are enriched at SC microvilli (Eshed et al., 2005; Occhi et al., 2005; Feinberg et al., 2010). Gliomedin and glial NrCAM are cleaved from their transmembrane precursors in a furin-dependent manner and their extracellular domains are shed in the nodal gap (Eshed et al., 2007; Feinberg et al., 2010). Here they form a multiprotein complex with extracellular matrix proteins (heparan sulfate proteoglycans) and interact with axonal CAMs (Nf186 and NrCAM), directing the clustering of Nav (Feinberg et al., 2010), and the maintenance of nodes of Ranvier (Amor et al., 2011). Dystroglycan is expressed at SC microvilli with its SC specific dystrophin isoform Dp116 (Occhi et al., 2005), but how it influences Nav clustering and microvilli formation is still not known and is one of the aims of this thesis (see Chapter 2).

In addition, SC microvilli express the inwardly rectifying potassium channels Kir2.1 and Kir2.3 that have been suggested to play a role in K^+ buffering, indicating that even inexcitable cells as SCs participate actively to maintain a microenvironment for the regeneration of the action potential at the node (Mi et al., 1996). This is probably similar

to the buffering role of astrocytes in the CNS. Another type of potassium channel, Kv1.5, is enriched on the outer surface of the Schwann cells in the vicinity of the node. Rather than being involved in K^+ buffering, Kv1.5 has been proposed to serve for the subsequent efflux of K^+ from the Schwann cell (Mi et al., 1995). Extruded K^+ may travel a short distance in the extracellular space and then be recaptured by the axon via the Na^+/K^+-ATPase pump, which has also been localized at the nodal axonal membrane.

As stated above, SC microvilli are embedded within a poorly defined filamentous matrix, the nodal gap substance, which consists of proteoglycans and non-sulfated mucopolysaccharides, which contribute to the ability of methylen blue and a wide variety of metal salts to label nodes of Ranvier (Hess and Young, 1952; Quick and Waxman, 1977). The nodal gap is also stained by *Griffonia simplicifolia*-B4 isolectin and peanut agglutinin (PNA), lectins that recognize terminal α- and β-D-galactose, an epitope of the GM1 ganglioside. Proteoglycans that are present at nodes include the V1 isoform of versican (Apostolski et al., 1994; Melendez-Vasquez et al., 2005), the chondroitin sulfate proteoglycan NG2 (Martin et al., 2001) and syndecan-3 and 4 (Goutebroze et al., 2005; Melendez-Vasquez et al., 2005). Syndecan-3 is a transmembrane HSPG, which localizes to nodes at early stages of development and is subject to metalloproteinase cleavage in cultured Schwann cells and P4-P10 nerves, raising the possibility that its ectodomain is shed into the nodal gap (Asundi et al., 2003). This could suggest a role for syndecan-3 in node organization, however, the analysis of adult *syndecan-3* null mice has not identified significant defects in Nav

clustering or nodal morphology (Melendez-Vasquez et al., 2005). NG2 knock out mice were also analyzed for their nodal architecture, but no obvious abnormalities were found (Colombelli and Feltri, unpublished observation).

Finally, the nodal matrix is also enriched in laminins, in particular laminin 211 and 511 (Occhi et al., 2005), and collagen α4(V) that is known to interact with syndecan-3 (Chernousov et al., 1996).

1.3.3 Paranodes

Flanking the node of Ranvier, the compact myelin sheath opens and forms a cytoplasmic corridor that spirals around the axon and tightly associates to the axolemma by junctional complexes, known as axoglial or paranodal junctions (PNJs). Observed in longitudinal sections they appear as cytoplasmic loops derived from each turn of the myelin wrap (Fig. 6C). Axoglial junctions appear relatively late during myelination, first generated closer to the nodes by the most outer paranodal loop and then forming gradually as additional loops are attached to the axon. Paranodal loops are held in register with one another by autotypic adherens and tight junctions (Fannon et al., 1995; Scheiermann et al., 2007) and communicate between each other through gap junctions (Meier et al., 2004).

In the paranode, the glial and neuronal cell maintain their closest apposition, 2.5-3 nm, and the pockets of the Schwann cell lamellae indent the surface of the axon, connecting with it through a series of ridges (transverse bands) that are reminiscent of invertebrate septate junctions. Freeze-fracture EM revealed that these junctions are composed of rows of large particles on the glial membrane that are in

register with a double row of smaller particles on the axolemma (Wiley and Ellisman, 1980). The molecular composition of these paranodal septate junctions remained elusive until the identification of proteins that localized to *Drosophila* septate junctions, like neurexin IV (Baumgartner et al., 1996). Subsequently, three independent studies identified the vertebrate homologue of neurexin IV, referred to as contactin-associated protein (caspr), paranodin, or NCP1, which localizes to paranodal septate junctions (Einheber et al., 1997; Menegoz et al., 1997; Peles et al., 1997). Caspr is expressed at the paranodal axolemma where it forms a complex in *cis* with the GPI-anchored protein contactin that in turn binds in *trans* the 155 kDa isoform of neurofascin (Nf155) on the glial, paranodal loops (Rios et al., 2000; Charles et al., 2002). The association between caspr and contactin occurs in the endoplasmic reticulum, is required for the efficient export of caspr from the ER to the plasma membrane (Faivre-Sarrailh et al., 2000), and regulates the glycosylation and the transport of contactin (Gollan et al., 2003). Accordingly, in contactin mutant mice caspr remains in the soma and is not transported into the axon or the paranodes (Boyle et al., 2001) and in *caspr* null mice paranodal contactin is either absent or undetectable (Bhat et al., 2001).

Genetic inactivation of caspr, contactin and Nf155 have further confirmed that these proteins are essential for the formation of the axoglial junction and the conduction of action potentials, as knock out mice exhibit major defects of the paranodes and decreased conduction velocities (Bhat et al., 2001; Boyle et al., 2001; Sherman et al., 2005; Pillai et al., 2009). Particularly, in these mutants transverse bands are absent and the paranodal loops are less tightly apposed to the axon

with some everted terminal loops, intrusion of microvillar processes between the loops and the axon, and an increased periaxonal space. Disruption of the paranodal septa minimally affects the distribution of nodal Nav, with a small increase in nodal length and a mild reduction in intramembranous particles at the nodal axolemma (Bhat et al., 2001). Both the paranodal and the nodal phenotype of *caspr* and *contactin* null mice is more pronounced in CNS than PNS, suggesting that interactions mediated by the nodal microvilli and with the basal lamina may contribute to paranodal stability in peripheral nerves. However, both in CNS and PNS the absence of septate junctions alters the distribution of potassium channels Kv1.1/1.2 that are re-distributed to the paranodes instead of being located to juxtaparanodes (see below). Therefore, paranodal junctions are considered sort of fences that separate lateral axonal domains, acting as barriers for ion diffusion away from the node and by spatially separating voltage-activated sodium channels (Nav) and voltage-activated potassium channels (Kv) between the node and the juxtaparanode, respectively.

The functional importance of septate junctions is further demonstrated by mice deficient in the myelin glycolipids galactocerebroside and sulfatide (*Cgt* and *Cst* null) which lack the caspr-contactin complex from paranodes and exhibit paranodal defects comparable to those of the aforementioned paranodal mutants (Dupree et al., 1998; Honke et al., 2002). The precise role of these glycolipids in junction assembly is still not understood, but it has been hypothesized that they may be required for appropriate trafficking and partitioning of glial receptors to paranodal lipid rafts (Schafer et al., 2004). This is in accordance with the paranodal abnormalities observed in animals that lack MAL

(myelin and lymphocyte protein), a raft component implicated in the apical secretion of membrane proteins in epithelial cells (Schaeren-Wiemers et al., 2004).

The molecular link between the paranodal septate junctions and the axonal cytoskeleton is provided by caspr through the protein 4.1B, which is enriched in paranodes and juxtaparanodes (Ohara et al., 2000). The short intracellular tail of caspr contains a sequence motif, identified as GNP (glycophorin C, neurexin IV, paranodin), that provides a site of anchorage for the FERM domain of 4.1B (Denisenko-Nehrbass et al., 2003). This interaction is required for the stable membrane retention of caspr at the paranodes (Gollan et al., 2002) and for the generation of an efficient membrane barrier at the PNJ, as caspr mutants lacking their 4.1B binding sequence are not able to rescue the paranodal invasion of Kv1 in caspr null mice (Horresh et al., 2010). In support of this, Kv1 are abnormally distributed at paranodes in the *shambling* mutant mouse, which expresses a truncated caspr protein lacking its entire cytoplasmic domain (Sun et al., 2009). Furthermore, two recently generated *4.1B* null mice show mislocalization of caspr and destabilization of PNJs, establishing a relevant role for 4.1B as an adaptor protein that links axoglial complexes to the axonal actin-spectrin cytoskeleton, ensuring long-term stability of axonal domains (Buttermore et al., 2011; Cifuentes-Diaz et al., 2011).

The axonal cytoskeleton at the paranodes is highly specialized and also contains ankyrin-B and αII and βII spectrins, that form a macromolecular complex with 4.1B (Ogawa et al., 2006). Examination of *caspr* null mice showed that ankyrin-B fails to

accumulate at paranodes in the absence of PNJs, suggesting that neuron-glia interactions are important for the organization of the axonal cytoskeleton. In zebrafish, αII spectrin is also transiently expressed at nodes and promotes proper Nav clustering at these sites (Voas et al., 2007).

Less is known about the SC cytoskeleton. No ankyrins have been reported to be expressed in myelinating glial cells. However, it was shown that the 4.1G protein is enriched at paranodes (Ohno et al., 2006), although a study on *4.1G* null mice has not revealed any abnormalities in PNJ formation (Terada et al., 2011). Nonetheless, a very recent work shows that 4.1G is also localized at the periaxonal membrane, where it is required for the polarized distribution of either glial or axonal proteins along internodes (Ivanovic et al., 2012).

1.3.4 Juxtaparanodes

The juxtaparanode lies just under the internodal compact myelin sheath, immediately adjacent to the innermost paranodal loop. This domain extends into the internodes for 5-15 μm, and is characterized by high densities of two delayed rectifier potassium channels of the *Shaker*-type, Kv1.1 and Kv1.2, with their β subunits and a complex of adhesion molecules that anchors the channels to this site (Wang et al., 1993). Although the role of juxtaparanodal Kv1 channels is still unknown, they are thought to have an important physiological function, acting as an active damper of re-entrant excitation to maintain the internodal resting potential (Vabnick et al., 1999). The finding that Kv1.1 null mice have abnormal impulse generators near the neuromuscular junctions supports this idea (Zhou et al., 1998).

Similarly, mutations in the human *KCNAC1* gene are associated with ectopic impulse generators in the distal aspects of motor axons. Kv may also provide a pathway for the movement of K^+ ions that accumulate with electrical activity, from the axoplasm into the periaxonal space, being then removed through connexin-29 hemichannels located at the adaxonal membrane of the myelinating Schwann cell (Altevogt et al., 2002).

Kv1.1 and Kv1.2 form a macromolecular complex with the adhesion molecule Caspr2 and the GPI-anchored transient axonal glycoprotein-1 (TAG-1) on the axon and TAG-1 on the glial membrane (Poliak et al., 1999; Traka et al., 2003). Adhesion is mediated by homophilic trans interactions of TAG-1. This complex is essential for the accumulation of Kv1 in the juxtaparanodes as disruption of *caspr2* or *TAG-1* results in a remarkable decrease of Kv1 enrichment at these sites (Poliak et al., 2003; Traka et al., 2003).

Caspr2 interacts with 4.1B on the axon via its FERM domain, such as caspr at paranodes (Denisenko-Nehrbass et al., 2003). Furthermore, in its C-terminal domain it also contains a PDZ-binding sequence that can bind the membrane-associated guanylate kinases (MAGUK) PSD-93 and PSD-95, which are both localized to juxtaparanodes (Rasband et al., 2002; Horresh et al., 2008) and able to simultaneously bind the α subunit of Kv1. Different studies have demonstrated that PSD-93 and PSD-95 are dispensable, whereas 4.1B is necessary for the proper juxtaparanodal localization of Kv1 (Rasband et al., 2002; Horresh et al., 2008 and 2010). A recent study has identified a disintegrin and metalloproteinase 22 (ADAM22) as a novel component of the Kv1 protein complex; ADAM22 is required to recruit PSD-93 and PSD-95,

but not Kv1 and Caspr2 to juxtaparanodes and has been suggested to play a role in the modulation of Kv1 function (Ogawa et al., 2010).

1.3.5 Mechanisms of domain assembly

How the Schwann cell-axon unit succeeds in assembling such differently specialized domains along the myelinated fiber has been subject of several studies. In the last decade, the mechanisms of nodal domain formation have been gradually revealed by *in vivo* developmental studies and the analysis of both SC-DRG co-culture systems and mice deficient in key domain components.

Up to now it has been shown that domains assemble in progression, starting with nodes, paranodes and juxtaparanodes that form sequentially as myelination proceeds, during the first postnatal days (Salzer et al., 2003). Furthermore, it is well established that, far from being considered merely as a passive contributor, peripheral myelinating glia has an active role in directing the formation of axonal domains, directly regulating neuron excitability and structure. As early *in vitro* studies suggested, peripheral nodes are not intrinsically specified by the neuron, but are assembled from the outside in, meaning that an interaction between Schwann cells and the axon is necessary for Nav to cluster (Ching et al., 1999). This finding further supported the observation that Nav aggregate in the vicinity of SC cell processes also *in vivo* (Vabnick et al., 1996). Specifically, as the Schwann cell wraps the axon, Nav present at lower levels along the internode, or possibly newly synthetized Nav, starts to aggregate in close association with SC microvilli, forming pairs of clusters between two neighbouring Schwann cells (known as heminodes or

node intermediates) that eventually fuse to form a node of Ranvier (Vabnick et al., 1996; Pedraza et al., 2001).

The formation of proper nodes of Ranvier requires different mechanisms: the glial recruitment of nodal proteins, the retention and stabilization of nodal clusters on axons through interaction with cytoskeleton and scaffolding proteins, and the restriction of membrane protein mobility through the formation of paranodal junctions.

Initially, gliomedin and glial NrCAM, expressed early at SC microvilli, are secreted and incorporated in the surrounding ECM (Eshed et al., 2007; Feinberg et al., 2010). At this site, they bind the ectodomain of Nf186, which is cleared from internodes (Dzhashiashvili et al., 2007) and forms an initial cluster with axonal NrCAM. When these CAMs are positioned, they function as a docking site for ankyrin-G, which in turn forms a scaffold for the retention of Nav, KCNQs and βIV spectrin, the latter ensuring the tethering of the complex to the nodal cytoskeleton. In the PNS, the structural stability of the nodal complex is also provided by the Schwann cell, that mechanically maintains the position of the nodal cluster through microvilli (Occhi et al., 2005).

To ensure that Nav are found at high density at nodes, Schwann cells have evolved a second mechanism that is cooperating with, yet independent from the one described above. This second mechanism occurs when paranodal junctions form and acts like a snow-plough, excluding nodal proteins from beneath the myelin sheath and restricting them to nodes of Ranvier. This idea that two backup systems exist for Nav clustering at nodes is experimentally supported: first, *gliomedin* and *NrCAM* null, as well as *caspr* null mice still

assemble nodes, although with slight defects (Bhat et al., 2001; Custer et al., 2003; Feinberg et al., 2010); second, double mutants lacking both gliomedin or NrCAM and caspr have dramatically impaired node formation (Feinberg et al., 2010), suggesting that PNJ and ECM-CAM interactions are overlapping mechanisms to facilitate Nav clustering (Fig. 9). However, in contrast with the idea that paranodes may suffice to induce Nav clustering in the absence of nodal CAMs, a recent study has shown that paranodal domains fail to rescue the Nav clustering defect in mice lacking Nf186 (Thaxton et al., 2011). Furthermore, these authors suggest that Nf186 complex acts itself as a molecular boundary to prevent the lateral mobility of the flanking paranodes into the nodal space. These discrepancies between the two studies may reflect the different experimental conditions respectively used.

As myelin lamellae are elaborated, their lateral edges form the paranodal loops; those closest to the node are generated first. PNJs similarly mature in a sequence beginning with loops closest to the node, progressing inward (Tao-Cheng and Rosenbluth, 1983). Even the assembly of the paranodal junctions requires axo-glial interactions. Caspr accumulates at paranodes shortly after gliomedin, ank-G and Nav at nodes, whereas the glial-specifc splice variant of the neurofascin gene (Nf155) is expressed and concentrated at paranodal loops subsequently to its neuronal isoform. The establishment of a distinct detergent-resistant, low-density lipid environment is also a good candidate for the initiation of the clustering of paranodal proteins to PNJs, thus excluding nodal and juxtaparanodal components solely on the basis of their inability to partition into

paranodal membranes (Schafer et al., 2004).

Like nodes of Ranvier, the proper assembly of juxtaparanodes also depends on at least two distinct neuron-glia interactions. On one hand the PNJs exclude Kv1 from the paranodal region, as evidenced by the paranodal invasion of Kv1 in paranodal mutants (Bhat et al., 2001; Boyle et al., 2001), on the other hand, the formation of the juxtaparanodal tripartite complex between glial TAG1 and Caspr2/TAG1 on the axon induces Kv1 clustering, as demonstrated by mice lacking either one of these proteins (Poliak et al, 2003; Traka et al., 2003). Temporally, Kv1 are transiently expressed at nodes (Vabnick et al., 1999), then, together with Caspr2, are detected in the paranodes, but are soon displaced to juxtaparanodes as caspr and contactin accumulate.

Fig. 8 Organization and composition of domains of peripheral myelinated fibers. A, Sciatic nerve teased fiber stained for nodal Nav (blue), paranodal caspr (red) and juxtaparanodal Kv1.1 (green). **B-C**, Scheme of a longitudinal cross section through a myelinated axon; the axon, with intracellular organelles concentrated in the nodal region, is in red and myelinating SCs are in light blue. The node of Ranvier (blue) is contacted by microvillar processes arising from the outer collar of the Schwann cells; the nodal gap substance and basal lamina are not shown. The paranodal junctions (green) flank either side of the node. The location of the juxtaparanodes (violet) and internodes (red) are shown. Major components of these different domains of the Schwann cell including nodal matrix components synthesized by the Schwann cell (top row) and axonal components including cell adhesion molecules (CAMs), cytoskeletal proteins, and ion channels are listed (from Salzer et al., 2008).

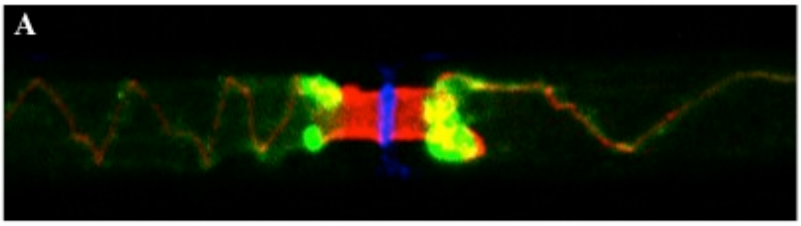

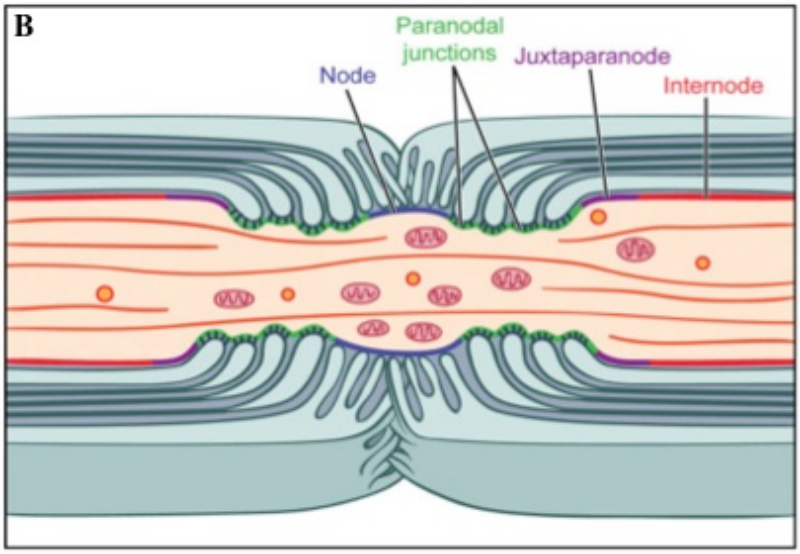

C	Node	Paranodes	Juxta-paranodes	Internode
Schwann Cell	NrCAM ERMs DG Gliomedin Laminin HSPGs Collagen V	NF155	TAG1	Necl4, 2 MAG
Axonal CAMs	NF186 NrCAM	Contactin Caspr	TAG1 Caspr2	Necl1, 2
Axonal Channels	Nav1.6 KCNQ2,3		Kv1.1 Kv1.2	
Axonal Cytoskeleton	AnkG ßIV spectrin	4.1B AnkB αII/βII spectrin	4.1B αII/βII spectrin	

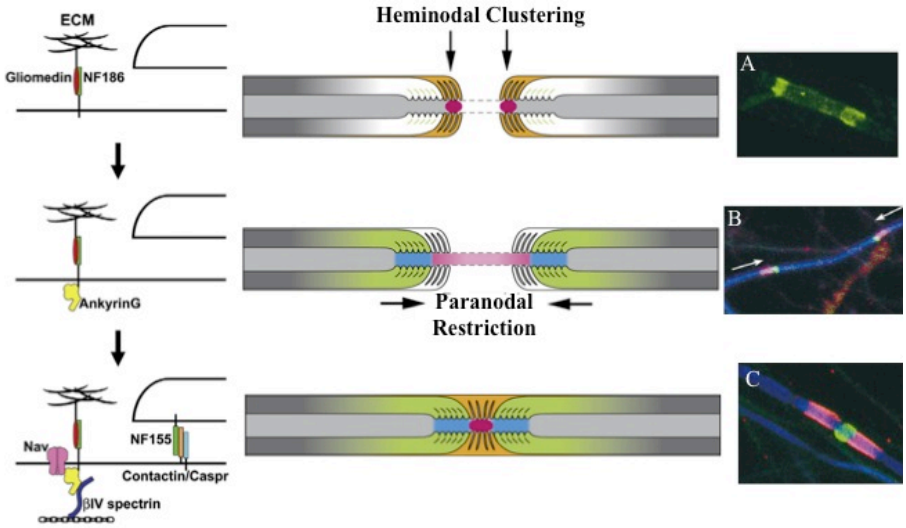

Fig. 9 Mechanism of Nav clustering. As depicted in the diagrams, PNS nodes are assembled through three cooperating mechanisms: interaction of gliomedin and glial NrCAM with axonal Nf186, which allows Nav to initially cluster at heminodes; restriction by the paranodal diffusion barrier (caspr/contactin-Nf155); and stabilization of the clusters by interactions with the underlying cytoskeleton (modified from Susuki and Rasband, 2008 and Feinberg et al., 2010). On the right, myelinating co-cultures of DRGs and SCs were immunolabeled for Nav (green in **A**, **B**, **C**), caspr (red) and neurofilament (blue). The elongation of SCs along the axon causes Nav clusters to move (**B**) until two heminodes fuse in a mature node (**C**) (from Pedraza, 2001).

1.4 Schwann cell basal lamina

The whole Schwann cell-axon unit is surrounded by a basal lamina (BL), which is synthetized and deposited by both myelinating and non-myelinating Schwann cells on their abaxonal surfaces. At the ultrastructural level, BLs are sheet-like structures that generally range from 50 to 100 nm in thickness and that can be visualized with

periodic acid Schiff and silver staining.

As in other tissues, Schwann cell basal lamina is a basement membrane whose extracellular matrix components organize giving rise to an internal lamina, known as *lamina lucida*, which faces and is linked to the cell membrane, and an external, fibrillar matrix, called *lamina densa*. The composition of basal lamina is cell-specific and changes in space and time, with differences not only among different tissues, but also in sub-regions of the same tissue, and during development. In adult Schwann cells, the outer BL electron-dense layer is enriched in collagen fibrils (type-I and III), whereas the inner electrolucent layer contains sulphated proteoglycans (agrin, perlecan, syndecans), nidogen-1/entactin, collagens (type-IV and V) and is particularly enriched in laminins. Moreover, the cell-anchored galactosyl-sulphatide binds laminins and this interaction is believed to promote BL assembly (Li et al., 2005). The highly organized supramolecular architecture of BLs is at least in part guaranteed by the self-binding of laminin and collagen IV molecules to form a mesh-like polymer, and by the binding interactions among individual laminins, nidogens, collagens and other components.

In the last few years, the role of basal lamina has emerged to be much more than merely structural, implying BL components and their cellular receptors in the control of many cellular functions, such as migration, proliferation and survival, actin-cytoskeleton dynamics, polarization and differentiation (for review, Reichardt and Prokop, 2011). Particularly, in the PNS an example is represented by the role of collagens, laminins and their receptors in controlling the proper ensheathment and myelination of axons (Feltri and Wrabetz, 2005;

Chernousov et al., 2008).

During peripheral nerve development, ECM components are secreted and a rudimentary basal lamina starts to be deposited by immature SCs at E15-16 in mice. Although this early BL can be discontinuous and less well organized, signals from laminins are processed probably by Schwann cells via α6β1 integrin receptor to sort large caliber axons destined to be myelinated away from smaller axons. Laminins promote radial extension of cytoplasmic processes around axons and support SC proliferation and survival to match their number to that of axons. When at the promyelinating stage, SCs have reached a 1:1 relationship with axons and the nerve fiber is encircled by a completely mature basal lamina. At this stage, SCs express laminin receptors as dystroglycan and integrin α6β4. From P1 onwards, signals from laminins through the dystroglycan receptor are required for proper morphogenesis of myelinated axons (reviewed below).

1.4.1 Schwann cell basal lamina constituents

One of the prominent components of SC basal lamina are laminins, whose structure and functions are reviewed in the next section. A brief description of the heparan sulfate proteoglycans perlecan and agrin is also added, being relevant for this thesis.

Laminins

Laminins are secreted heterotrimeric glycoproteins composed of one α, one β and one γ chain (αβγ). Each chain is encoded by different genes and a wide diversity in the laminin trimers is generated through the combinatorial assembly of five α, four β and three γ subunits. So

far at least 15 different heterotrimers have been observed in nature (Miner, 2008). Laminin heterotrimers are relatively large proteins (with molecular masses ranging from 400 to 900 kDa) and exist as cross-shaped molecules with two or three short arms and one long arm.

The α chains contain a large (100 kDa) C-terminal globular domain, the G-domain, that can be subdivided into five self-folding β-sandwich modules, termed laminin G (LG1-5) modules, with a hinge-like region between LG3 and LG4. LG modules are generally involved in the interaction with several cellular receptors. In particular, epitopes located along the LG1-3 domains have been shown to interact preferentially with integrin receptors, while glycoconjugate-type receptors, including heparan sulfates, galactosylsulfatide (a glycolipid), and α-dystroglycan, are focused at sites on the LG4 and LG5 domains. Moreover, all the α chains contain a long coiled-coil domain (I/II) that mediates heterotrimer assembly with similar domains contained in the β and γ chains. Almost all the α chains have also laminin N-terminal domains VI (LN VI), which make the heterotrimers capable of polymerization into a network via inter-trimer domain VI interactions. Although, when present, the N-terminal short arm domains share a high sequence homology, different laminin isoforms show the greatest variability in arm length and domain number in the short arm. Based on these short arm differences, laminins can be divided into three different subfamilies, known as cruciform, Y-shaped and rod-shaped, with chains α1, α2 or α5 having full complements of domains in each short arm, or chains α3A or α4 carrying extensive, if not complete, truncations in their

short arms (Fig. 10G).

All laminin chains have N-terminal secretion signals that target them to the ER, where trimers are assembled. Initially, disulfide-linked dimers of the β- and γ-subunits form; then, the βγ dimer is retained in the cytoplasm and requires α subunit incorporation, and therefore trimerization, to drive secretion (Yurchenco et al., 1997). As laminin chains make their way through the secretory pathway, they also become glycosylated.

Once in the extracellular space, both laminin self-polymerization (interaction between same trimers) and laminin co-polymerization (interaction between different isoforms) occur; these processes are dependent on the binding of LN domains on the short arm of each trimer and occur when the laminin molecule is bound to cell surface receptors (Cohen et al., 1997). Moreover, following their secretion and deposition, laminins interact with several matrix proteins, and this might affects laminin deposition, BL organization and stabilization.

Besides organizing basement membrane assembly on cell surfaces (Yurchenco and Patton, 2009), laminins play two additional and overlapping roles in mammals: they provide attachment sites for cells via cell surface proteins, by linking BL to the underlying cytoskeleton (Henry and Campbell, 1996); and they act as ligands for receptors on cells (e.g. integrins, DG), initiating signals that influence cell behaviour and survival (Schwartz, 2001).

During PNS development, the major laminin isoforms expressed are LM 211 (old designation, α2β1γ1) and LM 411 (α4β1γ1). In postnatal peripheral nerves, adult SCs express LM 211, LM 411 and LM 511 (α5β1γ1), whereas LM 421 (α4β2γ1) and LM 521 (α5β2γ1) are

present in the basal lamina of perineurial cells. Laminin 211 is the major laminin isoform expressed in PNS and it is present all along the basal lamina, with enrichments at nodes of Ranvier (Masaki et al., 2002; Occhi et al., 2005). Laminin 411 is expressed at higher levels in embryonic and early postnatal endoneurium, but it continues to be expressed, albeit at lower levels, in adult BL. Laminin 511 is enriched around nodes and paranodes (Vagnerova et al., 2003; Occhi et al., 2005) and it becomes expressed and polarized to nodes relatively late during postnatal development (Colombelli and Feltri, unpublished observation). It is worth noting that the SC basal lamina is longitudinally polarized, similar to the axon underneath (Fig. 10A-F).

Schwann cells require laminins throughout nerve development, for the sorting of axons before birth, and the formation of myelin internodes after birth.

The importance of laminins in peripheral nerve development and maintenance has been evidenced by Schwann cell-neuron co-cultures that showed that laminin deposition is required for myelination *in vitro* (Fernandez-Valle et al., 1993). This was confirmed by *in vivo* evidences: first, the observation that laminin α2-chain mutant mice, also known as dystrophic (*Lama2*$^{dy/dy}$ and *Lama*$^{dy2J/dy2J}$; see below) mice, have naked axon bundles lacking ensheathment and myelination, and show reduced internodal lengths and altered Nav clustering at nodes (Bradley and Jenkison, 1973; Stirling, 1975; Occhi et al., 2005; Court et al., 2009); second, mice lacking laminin γ1 specifically from SCs have amyelinated nerve fibers, with most axons naked and tightly compacted, impaired SC proliferation, a dramatic reduction in conduction velocity, absence of a continuous BL and

altered Nav clustering (Chen and Strickland, 2003; Yu et al., 2005; Occhi et al., 2005); third, even laminin α4 null mice show hypomyelination and polyaxonal myelination in the distal nerve (Yang et al., 2005; Rasi et al., 2010).

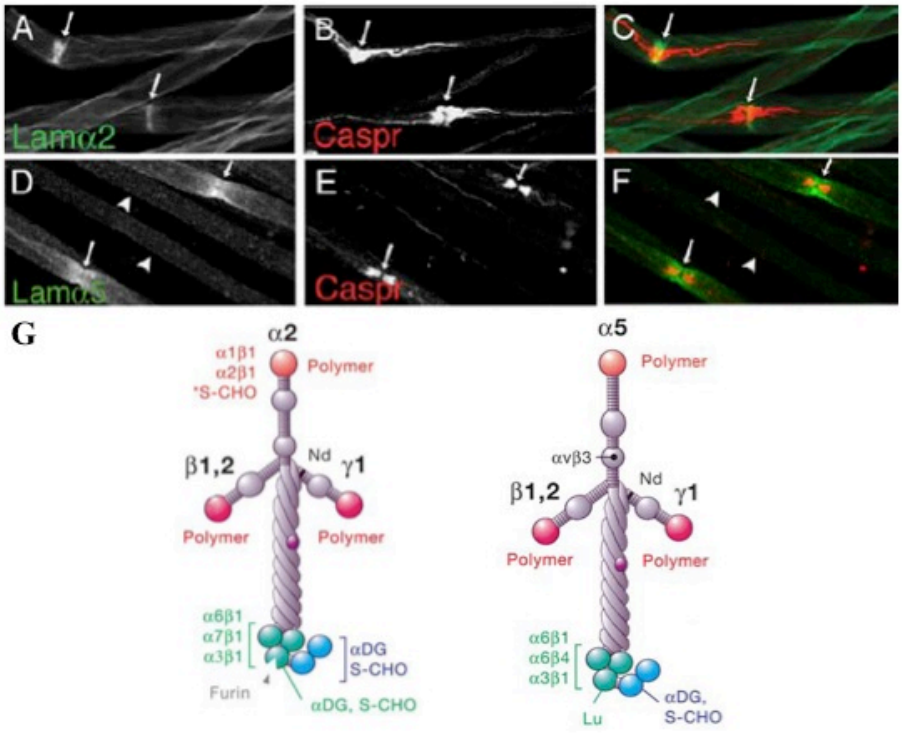

Fig. 10 Laminins are polarized along SC basal lamina. Laminin 211 is enriched at nodes of Ranvier (**A-C**), while laminin 511 is localized around nodes and paranodes (**D-F**) (from Occhi et al., 2005). **G**, Schematic drawing of laminin 211 and 511: they are αβγ trimers with the classic cruciform structure. The domains of binding to other basal membrane components - nidogen (Nd), agrin, other laminins (Polymer), - and to surface receptors - αβ integrins, dystroglycan (α-DG), Lu/BCAM (Lu) - or sulfated-carbohydrates (s-CHO) are indicated (from Miner and Yurchenco, 2004).

Perlecan

Perlecan is one of the most abundant heparan sulfate proteoglycans in vertebrate basement membranes and it is expressed in the Schwann cell basal lamina as well (Eldridge et al., 1986). Its eponym reflects a 'beads on a string' domain structure as visualized by rotary shadowing electron microscopy (Bix and Iozzo, 2008).

Its core protein is large (~400 kDa) and consists of five distinct domains, including the fourth and fifth regions that are comprised of Ig-like repeats and LG domains, sites of interaction with a host of matrix molecules and cell surface receptors. These associations include nidogen-1 and collagen IV (domain IV), integrin α2β1 and α-dystroglycan (domain V). Laminins, through their interactions with nidogen-1, can also form ternary complexes with perlecan.

Perlecan heparan sulfate (HS) side chains, located primarily in the N-terminal domain I, have the potential to bind laminins and type IV collagen, and to tether FGF2 and other growth factors, functioning as a growth factor reservoir, that regulate their transport and accessibility.

Despite these many interactions and its widespread deposition in BLs, perlecan does not appear to have a principal role in basement membrane assembly. Basement membranes develop normally both in mutant mouse embryos homozygous for a null allele of the perlecan gene (*Hspg2*), which survived to between E10.5 and E19 (Arikawa-Hirasawa et al., 1999; Costell et al., 1999), and in patients with various mutations of *HSPG2* gene. However, perlecan may have a critical role in the maintenance of the integrity and stability of the

basement membranes especially in tissues that are subject to mechanical stress (Costell et al., 1999).

In humans, two rare skeletal disorders, the severe neonatal lethal dyssegmental dysplasia, Silverman-Handmaker type (DDSH), and the relatively mild Schwartz-Jampel syndrome (SJS), are both due to mutations in *HSPG2* gene (Arikawa-Hirasawa et al., 2001; Nicole et al., 2000). The phenotypic differences between DDSH and SJS patients are due to 'quantitative' changes, that is, the phenotype severity depends on the amount of functional perlecan in the matrix. DDSH is a lethal autosomal recessive disorder, in which truncated perlecan molecules are not properly secreted into the extracellular space. In contrast, patients with SJS, a nonlethal, autosomal recessive disorder, secrete truncated forms of perlecan generally lacking domain V or parts of domain V, thus only partially functional. The SJS phenotype is complex and includes varying degrees of myotonia and chondrodysplasia. The former is thought to occur because perlecan is required for binding to acetylcholinesterase at the neuromuscular junction (Peng et al., 1999).

In this thesis two *Hspg2* mutant mice are analyzed. The first is a compound heterozygote of the null allele and an allele carrying a missense mutation, C1532Y, corresponding to a human familial SJS mutation (Stum et al., 2008). Almost no perlecan is secreted in the BLs of these mice, which suffer from chondrodysplasia and muscle stiffness with spontaneous activity at rest on electromyogram (EMG). This latter feature has been associated with peripheral nerve hyperexcitability (Echaniz-Laguna et al., 2009).

The second animal model is the $Hspg2^{\Delta 3/\Delta 3}$ mouse, lacking exon 3 of

Hspg2, which causes the loss of the three HS attachment sites in domain I, without altering perlecan expression or secretion (Rossi et al., 2003). These mice are viable and fertile, with no obvious macroscopical alterations under physiologic conditions, apart from structural abnormalities in the lens capsule. However, loss of HS chains results in impaired angiogenesis, delayed wound healing, and retarded tumor growth due to a decreased trapping and presentation of FGF2 (Zhou et al., 2004). This result could suggest that perlecan HS chains might have a similar role in different ligand sequestration and presentation to their high-affinity receptors in other tissues.

Agrin

A second heparan sulfate proteoglycan of basement membranes is agrin, a large (more than 400 kDa) multi-domain HSPG that exists in several variant forms generated through alternative splicing and transcription initiation sites. The most known isoform is the 'active' one, with a short N-terminal domain, that is expressed by motor neurons at the neuromuscular junction, where it directs the clustering of acetylcholine receptors (AChRs) (Ruegg and Bixby, 1998). The predominant agrin isoform in BL contains an N-terminal NtA domain, which binds the laminin γ1 subunit of laminins 111, 211 and 221 (Mascarenhas et al., 1993). The C-terminal laminin globular (LG) domain region of agrin contains sites of interaction with α-dystroglycan and is required for heparan binding (Gesemann et al., 1998). Agrin LG binding to dystroglycan has the highest affinity of all of the LG domains tested. The affinity of NtA-agrin for both laminin and dystroglycan may serve to increase laminin anchorage to cell

surfaces in some tissues. This is consistent with the improvement in sarcolemma basement membrane structure and function seen by over-expression of a shortened version of agrin in *lama2* deficient mice (Moll et al., 2001).

It was shown that Schwann cells express several agrin isoforms, including the active one, which is able to induce the clustering of AchR (Yang et al., 2001). This study suggested that perisynaptic SCs may play a role in AchR clustering both *in vitro* and *in vivo*, although not during synaptogenesis as the active form is expressed only in regenerating axons, after nerve injury. Axonal SCs express both the active and the inactive isoforms; whether active agrin could play a role along myelinated fibers at sites different from NMJ is still not known.

1.4.2 Laminin receptors

The laminin receptors expressed in peripheral nerves are integrins and dystroglycan. During embryonic development Schwann cells express α6β1 integrin, while α6β4 integrin and dystroglycan start to be synthetized by SCs at the pro-myelinating stage; α7β1 integrin instead is expressed later by mature SCs (Previtali et al., 2003).

In the next session I will focus on dystroglycan.

Dystroglycan

In 1987 a laminin-binding membrane protein was found in brain tissue and was termed cranin (Smalheiser and Schwartz, 1987). Eight years passed until this protein proofed to be identical with dystroglycan, which was previously only thought to be associated with muscle

membranes (Smalheiser and Kim, 1995). In the same years dystroglycan was also identified in other non-muscle tissues, in particular in PNS, where it is expressed at the SC abaxonal membrane that faces the endoneurial basal lamina (Matsumura et al., 1993).

Dystroglycan is encoded by a single gene (*DAG1*) and cleaved into two proteins, α-DG and β-DG, by post-translational processing (Holt et al., 2000). The role of this cleavage and the protease or proteases involved are still unknown. The two resultant proteins immediately associate again by a non-covalent bond to form a tightly bound heterodimer. This complex is anchored in the cell membrane by the membrane-spanning β-DG and binds to extracellular partners via α-DG (Ibraghimov-Beskrovnaya et al., 1992). The interaction with extracellular matrix ligands, as laminins, agrin, perlecan, neurexin or pikachurin, depends on post-translational modification (mainly glycolsylation) of α-DG. Schwann cell dystroglycan is known to bind LM 211 and agrin (Yamada et al., 1994 and 1996).

α-dystroglycan

α-DG is composed of three distinct domains: N-terminal, mucin-like and C-terminal, with the globular N- and C-terminal domains connected by the central mucin-like domain, which is highly glycosylated by O-linked sugar chains (Brancaccio et al., 1995) (Fig. 11J). A recent study has identified a phosphorylated O-mannosyl glycan on the mucin-like domain that is required for laminin binding (Yoshida-Moriguchi et al., 2010). Extended glycosylation is the reason why, although the α-DG core protein is 70 kDa, it migrates at 120 kDa in brain and peripheral nerve and at 156 kDa in skeletal

muscle. A series of glycosyltransferases have been implicated in α-DG glycosylation: POMT1 and POMT2, POMGnT1, fukutin, fukutin-related protein (FKRP), and LARGE. In addition, it has been recently shown that LARGE functions as a bifunctional glycosyltransferase, with both xylosyltransferase and glucuronyltransferase activities, which produce repeating units of [-3-xylose-α1,3-glucuronic acid-β1-] that allow α-DG to bind LG domain-containing ECM ligands (Inamori et al., 2012).

Mutations in some of these enzymes have been identified in patients with a subclass of congenital muscular dystrophies (CMDs), also known as α-dystroglycanopathies, affecting skeletal muscle, eye, brain and peripheral nerve to different extents. This suggests that α-DG glycosylation is very important for its function in these districts (Muntoni et al., 2008).

Another post-translational modification that involves α-DG is the processing of its N-terminal domain by a proprotein convertase (PC), called furin (Kanagawa et al., 2004; Singh et al., 2004). The N-terminal domain has a sequence that is highly conserved between different species, with a dumbbell-like shape structure that constitutes an indipendent folding unit (Bozic et al., 2004). It is made up of two autonomous domains: an Ig-like domain and a domain resembling the rRna binding protein S6, connected by a long flexible linker. It spans from residue 30 to 316, at the beginning of the mucin-like domain. At residue 312, a putative cleavage site for furin has been found. Cleavage at this site removes a 312 amino acid long peptide (α-DG-N), both N- and O- sialylated, with a molecular weight of 37-45 kDa. α-DG-N is secreted in a furin-dependent manner from multiple cell

types into culture medium. Moreover, it has been found at detectable levels in human serum, cerebrospinal fluid and urine (Saito et al., 2011; Hesse et al., 2011). Nonetheless, the physiological significance of α-DG-N is still unclear. Some authors demonstrated that it functionally serves as an essential recognition site for the glycosyltransferase LARGE during the maturation process of DG (Kanagawa et al., 2004), others showed that recombinant α-DG-N promotes neurite extension of PC12 cells and it can bind laminins 211, 221 and 111, fibronectin and fibrinogen (Hall et al., 2003). It is also not known whether the proteolytic cleavage takes place inside the cell or when DG is already inserted in the membrane.

β-dystroglycan

On the other extremity α-DG is anchored to β-DG in the Schwann cell membrane. β-DG is a type-I transmembrane protein with a single transmembrane domain and a 120 amino acid long C-terminal cytoplasmic tail. β-DG has a molecular weight of 43 kDa and it is only slightly glycosylated in its extracellular part. It has been shown that in Schwann cells β-DG can be cleaved extracellularly by matrix metalloproteinase 2 and 9 (MMP-2, MMP-9), yielding a transmembrane protein unable to bind α-DG, thus disrupting the interaction with BL (Yamada et al., 2001; Zhong et al., 2006).

In the PNS, β-DG C-terminal domain is anchored to the cytoskeleton through three dytrophin isoforms or homologues, which are Dp116, dystrophin-related protein 2 (DRP2) and utrophin. Although it is generally believed that dystrophins mediate β-DG interaction with cytoskeletal proteins, a direct interaction between β-DG and F-actin

was also reported (Chen et al., 2003). The interaction between β-DG and dystrophins involves its WW C-terminal domain and it is negatively regulated by phosphorylation (Sotgia et al., 2001).

Dp116 is a SC-specific isoform of dystrophin, that derives from an alternative promoter usage of the dystrophin gene, that generates a 5.2 kb transcript initiating 850 nucleotides upstream of the *DMD* exon 56, only in Schwann cells (Byers et al., 1993). The protein product represents the C-terminal domain of dystrophin, lacking actin-binding and spectrin-like rod domains. β-DG binds Dp116 either with high affinity, through 15 C-terminal aa of DG C-tail, or with low affinity, via 26 N-terminal aa of the C-terminal domain (Saito et al., 1999).

Instead, DRP2 is a dystrophin homologue encoded by a separate gene (Roberts et al., 1996) and highly enriched in SCs. Here it binds β-DG and periaxin, a SC-specific protein that in turn binds the cytoskeleton (Sherman et al., 2001).

Utrophin is very similar in overall structure to dystrophin, it is not SC-specific, but, differently from Dp116 and DRP2, directly binds F-actin (Love et al., 1989).

Intracellularly, the dystroglycan complex directly or indirectly interacts with various scaffolding proteins as well. α1-dystrobrevin and four syntrophin isoforms (α1, β1, β2 and γ2), which can bind utrophin and dystrophin, are expressed in Schwann cells (Saito et al., 2003; Albrecht et al., 2008). Moreover, β-, δ-, ε- and ζ-sarcoglycans and sarcospan have been detected in sciatic nerves (Saito et al., 2003). The four sarcoglycan isoforms seem to form a stable tetrameric sarcoglycan complex that associates with DG and Dp116 to constitute a larger dystrophin-glycoprotein complex (DGC) in Schwann cells as

in skeletal muscle (Imamura et al., 2000; Cai et al., 2007).

The Schwann cell abaxonal surface is organized into two distinctive compartments: a cytoplasm rich domain, known as Cajal bands, and appositions, in which the plasma membrane is tightly apposed to the last turn of the myelin sheath (Fig. 5). Several studies have shown that the molecular composition of the DGC is different between these two domains (Albrecht et al., 2008; Court et al., 2009 and 2011). In the former compartment, β-DG forms a complex with Dp116, utrophin, α1-dystrobrevin, syntrophins and the ABCA1 cholesterol transporter. Appositions, instead, are enriched in β-DG linked to DRP2 and periaxin (Fig. 12). Furthermore, our lab demonstrated that the composition and localization of these different DG complexes along the SC outer membrane depend on cleavage of β-DG by MMP-2 and 9; specifically, the cleaved form of β-DG, not capable to bind laminin, preferentially associates to Dp116 and utrophin in Cajal bands, whereas full-lenght β-DG, capable of laminin binding, interacts with DRP2/periaxin, along appositions (Court et al., 2011; see Chapter 3). We proposed that this is a physiological process through which SCs remodel their cytoplasmic compartments.

The polarization of different DG complexes in different SC domains also regards the node of Ranvier. Here, the major intracellular partner of β-DG are Dp116 and utrophin, whereas DRP2 has not been detected (Occhi et al., 2005).

Besides the 'classical' molecules involved in the DGC, a myriad of other proteins and signaling molecules have been shown to interact with dystroglycan in non peripheral nervous tissues. One example is ezrin, an ERM expressed at nodal microvilli, that have been reported

to bind β-DG and to play a role in filopodia formation in epithelial cells (Spence et al., 2004).

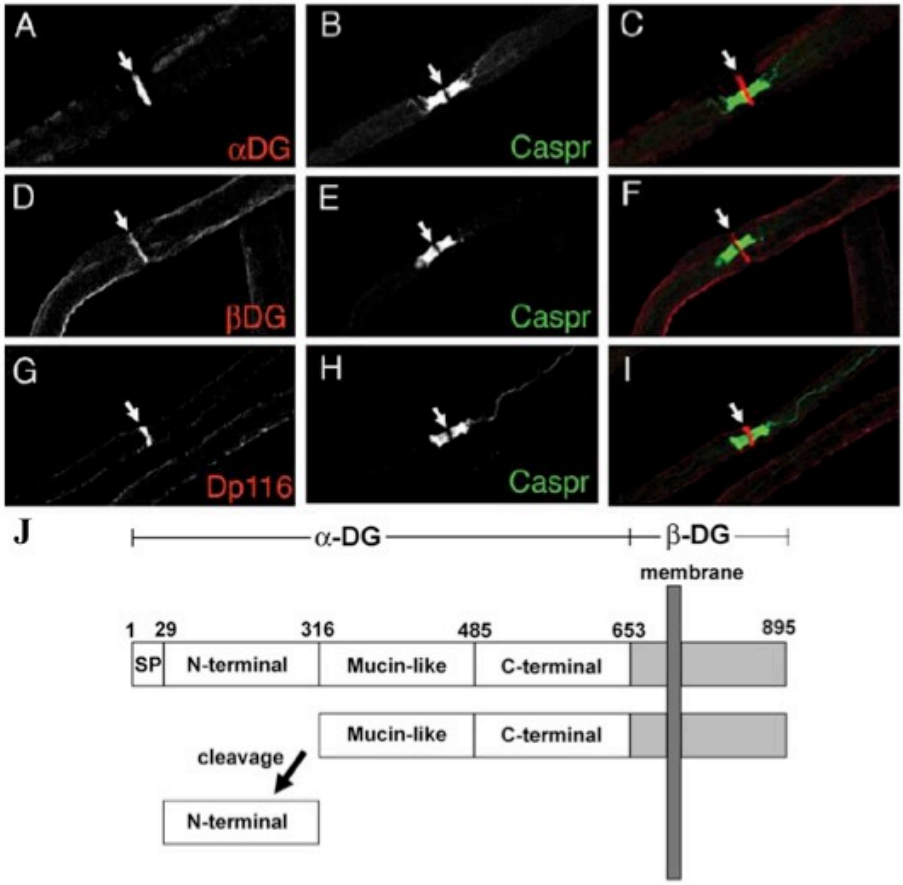

Fig. 11 α- and β-dystroglycan are enriched at nodes of Ranvier, with the 116 kDa dystrophin isoform. Teased fibers of adult rat sciatic nerves stained with antibodies against α-DG (**A**), β-DG (**D**), or Dp116 (**G**) and the paranodal marker caspr (green) (from Occhi et al., 2005). **J**, Schematic representation of dystroglycan. DG is synthesized as a single polypeptide of 895 residues that is post-translationally cleaved in α- and β-DG. α-DG consists of three domains: mucin-like, C-terminal and N-terminal. The latter can be further processed by a furin protease. Instead, β-DG can be cleaved by MMP-2 and -9 in its extracellular domain (not shown; adapted from Saito et al., 2008).

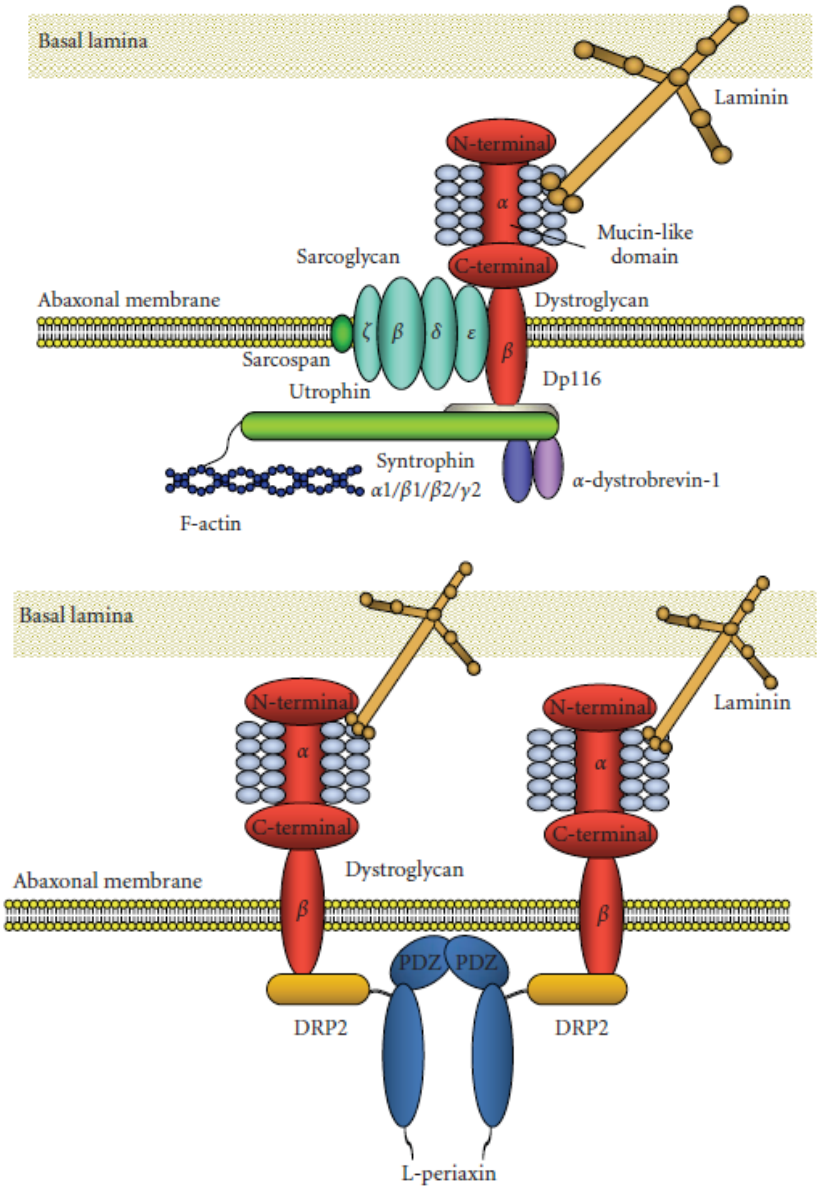

Fig. 12 Distinct DGC are differently compartmentalized in Schwann cell cytoplasm. In Cajal bands DG associates with Dp116 and utrophin that in turn interacts with F-actin (top). In membrane portions directly apposed to myelin sheath, DG binds DRP2, which in turn interacts with periaxin. This type of DGC lacks syntrophins and dystrobrevin (bottom) (from Masaki and Matsumura, 2010).

1.5 Animal models

Insights into the role of dystroglycan in the peripheral nervous system have come mainly from studies on animal models. The constitutive DG knock out is embryonic lethal (~E5.5), due to disruption of Reichert's membrane, one of the first basement membranes that form during early murine development (Williamson et al., 1997). To bypass this obstacle, mice in which dystroglycan was disrupted selectively in Schwann cells were generated using the P0 protein promoter and Cre-loxP technology (Saito et al., 2003). Moreover, mice with α-glycosylation defects were analyzed in the PNS to elucidate the role of α-DG glycosylation (Hewitt, 2010). The function of some DGC-associated proteins was assessed through the analysis of the sarcoglycan null hamster (Cai et al., 2007), the periaxin null mouse (Gillespie et al., 2000), and the utrophin null mouse (Court et al., 2009). The deficiency or mutation of the major DG extracellular ligand in PNS, laminin 211, are modeled by the dystrophic mouse and its many variants.

Recently, a new mouse model was generated harbouring a missense mutation (T190M) in the α-DG N-terminal domain, which was identified in a patient with limb-girdle muscular dystrophy (LGMD) and cognitive impairment. Unfortunately the peripheral nerve was not evaluated in this report (Hara et al., 2011).

1.5.1 Dystroglycan null mouse

The Schwann cell dystroglycan null mouse (dgko) exhibits a variety of morphological and functional abnormalities. Altered myelination has been detected by the presence of polyaxonal myelination,

redundant myelin loops, most commonly forming comma-shaped extensions along the entire internode, and abnormally folded myelin sheaths that are more frequent and irregularly thickened in older mice. Only few hypomyelinated fibers were observed, as well as axonal degeneration and signs of demyelination/remyelination that were occasionally seen only in the motor component of old mice (Saito et al., 2003; Figlia et al., 2011). Recently, a study has also shown that in a specific genetic background the loss of DG can cause an arrest in radial sorting, mostly in spinal roots, which resembles the defect found in laminin α2 mutants (Berti et al., 2011). Another remarkable abnormality of DG deficient mice is represented by the altered clustering of Nav at nodes of Ranvier. Nav clusters are less intense, abnormally shaped, lack definite corners, and are diffusive (Occhi et al., 2005). The nodal abnormality is also evidenced by variable degrees of microvilli disorganization and blunting, and axonal abnormalities as presence of elongated axonal protrusions, known as domes or spines, in the nodal gap (Saito et al., 2003). The analysis of the Nav clustering defects in these mice is one the objectives of the present work (see Chapter 2).

Another feature of DG null mice is the shortening of internodes, which has been associated to the disruption of Cajal bands/appositions in the outer SC cytoplasm (Court et al., 2009). This, together with the Nav clustering defect, is probably the prominent cause of the electrophysiological abnormalities found in both motor and sensory nerves, where conduction velocity is slowed and action potential amplitudes are reduced (Saito et al., 2003).

1.5.2 Mice with α-glycosylation defects

Peripheral nerve involvement in human α-dystroglycanopathies, namely congenital muscular dystrophy 1D (CMD1D), muscle-eye-brain disease (MEB), Walker-Warburg disease (WWS) and Fukuyama congenital muscular dystrophy (FCMD), has not been extensively studied. However, three different mouse models have been analyzed in PNS: the two LARGE mutants, *myd* and *enr* (Rayburn and Peterson, 1978; Levedakou et al., 2005), and the fukutin-deficient chimeric mouse (Saito et al., 2007). All the three models show a radial sorting defect similar to that found in DG deficient mice. Moreover, internodal lengths are shorter in LARGE^{myd} mice and conduction velocity and amplitude are reduced as well. Hence, the link between reduced α-DG glycosylation and laminin binding, and loss of functional dystroglycan is supported by the production of similar phenotypes in DG null and glycosyltransferase mutants. However, one difference with DG deficient mice is that the aberrant Nav clustering has not been observed in LARGE mutants (Levedakou et al., 2005).

1.5.3 Sarcoglycan null hamster

The importance of the DGC in peripheral nerves is also demonstrated by the phenotype of sarcoglycan null hamsters (BIO14.6). In these mutants, the loss of the sarcoglycan complex leads to a reduction of both α-DG and Dp116, with a consequent decrease of DGC stability, that induces age-dependent myelin disruption, abnormal foldings, disorganized SLIs. However, Nav clusters are not altered (Cai et al., 2007).

1.5.4 Periaxin null mouse

Studies of periaxin null mice revealed a unique aspect of DGC biological function in Schwann cells. Periaxin null mice do not show any defect in peripheral nerve development, instead they show progressive demyelination and abnormal myelin foldings in sciatic nerve, suggesting unstable myelin sheath. Moreover, these mutants exhibit abnormal Schwann cell compartmentalization and reduced internodes associated with a remarkable decrease in conduction velocity (Gillespie et al., 2000; Court et al, 2004). Loss of periaxin due to mutations in *PRX* gene is responsible for a human hereditary demyelinating neuropathy, CMT4F, with sensory-motor involvement. The homozygous *PRX* mutation C715X, causing expression of a truncated form of L-periaxin, results in a relatively milder phenotype of CMT neuropathy with sensory dominant involvement. Nerve biopsy shows loss of myelinated fibers, onion bulbs, focal thickening of myelin sheath, and myelin folding, which were similar to the nerve pathology of periaxin null mice (Takashima et al., 2002). Similar features, indicative of acute demyelination, have been detected also in old DG deficient mice and are aggravated by the ablation of β4 integrin (Nodari et al., 2008).

1.5.5 Utrophin null mouse

The PNS of utrophin null mice has been described by Court et al., who determined shortened internodes and disrupted Cajal bands/appositions, suggesting that this dystrophin isoform mediates the linkage between laminin 211/DG and the actin cytoskeleton, guiding the formation of proper SC compartments (Court et al., 2009).

1.5.6 Dystrophic mouse

There is a series of dystrophic mice carrying different mutations or disruption of the laminin α2 chain coding gene, that are used as models for the human disorder known as congenital muscular dystrophy 1A (MDC1A; see below). The most studied are the naturally occuring *dystrophia muscularis* dy/dy (Michelson et al., 1955) and dy2J/dy2J mice (Meier and Southard, 1970), and the targeted inactivated dy3k/dy3k (Miyagoe et al., 1997). In dy/dy mice, laminin α2 expression is absent in nerves and muscles and, although mapped to the *Lama2* locus, the causative mutation has not been found. Dy2J/dy2J mutants carry a point mutation causing an in-frame deletion of the α2 LN VI domain that results in a protein unable to polymerize, therefore not functional (Xu et al., 1994; Sunada et al; 1995a). The dy3k/dy3k is a full targeted knock out, not expressing laminin α2 and exhibiting a severe phenotype. Dy2J/dy2J has a peripheral nerve phenotype similar to that of dy/dy and dy3k/dy3k, but is more benign due to a more slowly progressive skeletal muscle degeneration. Thus, it has a longer lifespan and it is more suitable for experimental use.

All these dystrophic mice provide a strong experimental model of the human disease, accurately reflecting the variable extent of both muscle and peripheral nerve pathology in the affected human patient population. The demonstration that the peripheral neuropathy significantly contributes to the disease phenotype came from the transgenic rescue of laminin defect in muscle of dy/dy mice, in which improvement in muscle morphology and function did not eliminate a progressive lameness of hind legs, suggestive of a nerve defect

(Kuang et al., 1998).

In general, dystrophic mice are not able to polymerize a normal endoneurial basal lamina (Madrid et al., 1975) and exhibit a dysmyelinating neuropathy with different developmental defects. The main abnormality is the radial sorting defect characterized by the presence of bundles of naked axons, more evident in spinal roots that are severely amyelinated (Bradley and Jenkison, 1973; Stirling, 1975; Nakagawa et al., 2001). In the peripheral nerves, both laminins α4 and α1 are upregulated in the endoneurium, possibly accounting for the milder phenotype (Patton et al., 1997; Previtali et al., 2003).

Some fibers of the proximal PNS and most fibers in the distal PNS bypass the sorting block and myelinate. However, myelinated fibers present several abnormalities: thin or abnormally thickened myelin sheaths are present (Jaros and Bradley, 1979); internodes are up to 50% shorter and the SC cytoplasm compartmentalization in Cajal bands and appositions is altered (Jaros and Jenkison, 1983; Court et al., 2009); nodes of Ranvier can be abnormally wide, some microvilli are hypotrophic and nodal Nav clusters show reduced density, similar to DG deficient mice (Bradley et al., 1977; Occhi et al., 2005). As expected, conduction velocity is decreased in dystrophic fibers to as little as 5% of normal over bundles of bare axons in roots, and to 70-75% of normal in sciatic and caudal nerves (Rasminsky et al., 1978; Nakagawa et al., 2001; Occhi et al., 2005).

Interestingly, these abnormalities are not found homogeneously, either within or among different nerves. For example, internodal lengths are shorter and nodal gaps are larger in sciatic nerves but normal in caudal nerves (Rasminsky et al., 1978). It is not clear whether these

differences are due to region-specific compensation by other laminins, as for the sorting defect (Feltri and Wrabetz, 2005).

Importantly, a recent study has shown that overexpression of a transgenic laminin α1 lacking the binding sites for dystroglycan (LG4-5 domains) is not able to rescue the defects in peripheral nerves of dy3k/dy3k mice (Gawlik et al., 2010). This result strongly suggests the need of laminin 211/DG binding to guarantee the correct axon-SC interaction required for proper sorting, myelination and maintenance of peripheral myelin.

1.6 MDC1A

In humans, the absence of laminin α2, earlier designated merosin, causes merosin deficient congenital muscular dystrophy (MD-CMD), also known as congenital muscular dystrophy 1A (MDC1A). It was first described in 1994 by means of immunohistochemical analysis of tissue samples lacking laminin α2 (Tomé et al., 1994), and subsequently linked to human chromosome 6q2 by homozygosity mapping (Hillaire et al., 1994). The *LAMA2* mutations found in MDC1A patients are recessive, loss of function mutations that cause either absence or synthesis of non-functional laminin α2. Generally nucleotide substitutions, small deletions, or insertions that induce complete merosin deficiency, are associated with an early onset and a severe phenotype. Instead, the spectrum of the phenotypes of MDC1A patients with partial merosin deficiency is wider, ranging from milder forms to later onset muscular dystrophies, or even predominant PNS or CNS abnormalities.

MDC1A is the most frequent type of congenital muscular dystrophy

in Europe, accounting for about 50% of classical CMDs. Hence the original name of 'occidental type of cerebromuscular dystrophy'. In contrast, this disorder was reported to be relatively rare in Asia, with about 6% of CMD Japanese patients carrying *LAMA2* mutations (Miyagoe-Suzuki et al., 2000).

MDC1A characteristically involves skeletal muscle and both peripheral and central nervous systems. The muscle pathology resembles the myopathy described for other types of CMDs, as Duchenne or Becker muscular dystrophies, characterized by muscle weakness and atrophy, diffuse joint contractures, variable inability to stand and walk, and markedly raised creatine kinase level in blood serum. Muscle histopathology shows dystrophic features as marked variation in fiber size, signs of degenerating and regenerating processes, interstitial fibrosis and adipose tissue infiltration (Fig. 13B-D) (Conti Reed, 2009).

In the central nervous system, white matter abnormality was strikingly visible on brain magnetic resonance imaging (MRI) and may be a valuable criterion for diagnosis of MDC1A (Fig. 13A). In addition, some affected patients show structural abnormalities, mainly involving the occipital cortex, like occipital agyria, hypoplasia of cerebellum and pons and ventricular dilation (Sunada et al., 1995b; Vainzof et al., 1995; Philpot et al., 1999). However, mental retardation is very rare.

Like dystrophic mice, patients with MDC1A also develop a peripheral neuropathy, due to defective signaling within Schwann cells, leading to various abnormalities in Schwann cell-axon interactions. Although the involvement of PNS in MDC1A has been well characterized in

dystrophic mice, careful electrophysiological and histopathological studies were performed only on a minority of patients. However, nerve conduction velocities are moderately decreased in most of them, with a major impairment of the motor component, as it was previously reported for the dystrophic mouse (Rasminsky et al., 1978; Shorer et al., 1995; Quijano-Roy et al., 2004). It is worth noting that the fact that routine electrophysiological studies measure conduction velocity of the distal portions of PNS could overshadow a phenotype that is expected to be more severe in proximal PNS, as expected from mouse models. Unfortunately, the lack of post-mortem autopsies cannot confirm the presence of radial sorting defects in the spinal roots of MDC1A patients. However, when measured, F-wave latencies were significantly prolonged, suggesting root involvement (Di Muzio et al., 2003).

The dysmyelinating neuropathy has been evidenced in several case reports, where both sural nerve biopsies and teased nerve fibers revealed several abnormalities in myelinated fibers, such as: reduction of large myelinated fibers, hypomyelination and hypermyelination, presence of thickened myelin especially at paranodes, tomacula with uncompacted myelin (Deodato et al., 2002; Di Muzio et al., 2003) (Fig. 14). Moreover, the slowing in nerve conduction has been associated to the observations of short internodes and enlarged nodes of Ranvier (Di Muzio et al., 2003). Specifically, the same alterations in Nav clustering found in the animal model were also observed in a patient homozygous for a missense mutation (G600R) in the *LAMA2* gene, displaying a sensory-motor dysmyelinating neuropathy (Occhi et al., 2005). In the same patient, the absence of laminin α2 also

caused a defect in Schwann cell cytoplasm compartmentalization that may be at the basis of the decreased internodal length (Fig. 14) (Court et al., 2009).

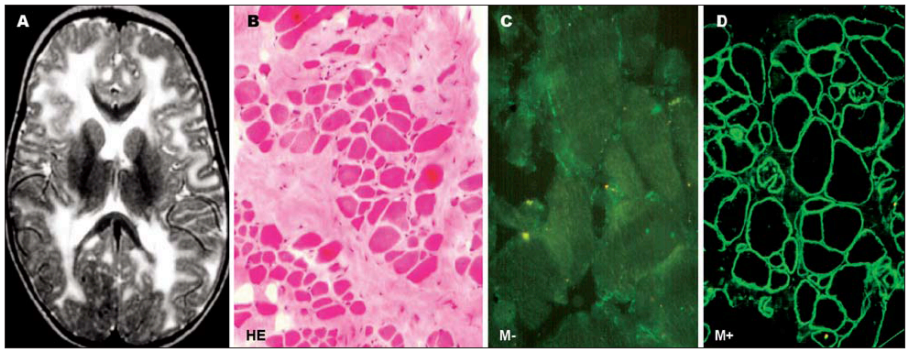

Fig. 13 Brain and muscle abnormalities in a child with MDC1A. **A**, Extensive white matter changes on magnetic resonance imaging, which is diffuse, bilateral and quite symmetrical. **B**, Dystrophic pattern on hematoxylin and eosin (HE) staining of a muscular biopsy. **C-D**, Immunohistochemical analysis of laminin α2 (merosin, M) on muscular biopsy showing absence of expression (M-), compared to control with a merosin-positive congenital muscular dystrophy (from Conti Reed, 2009).

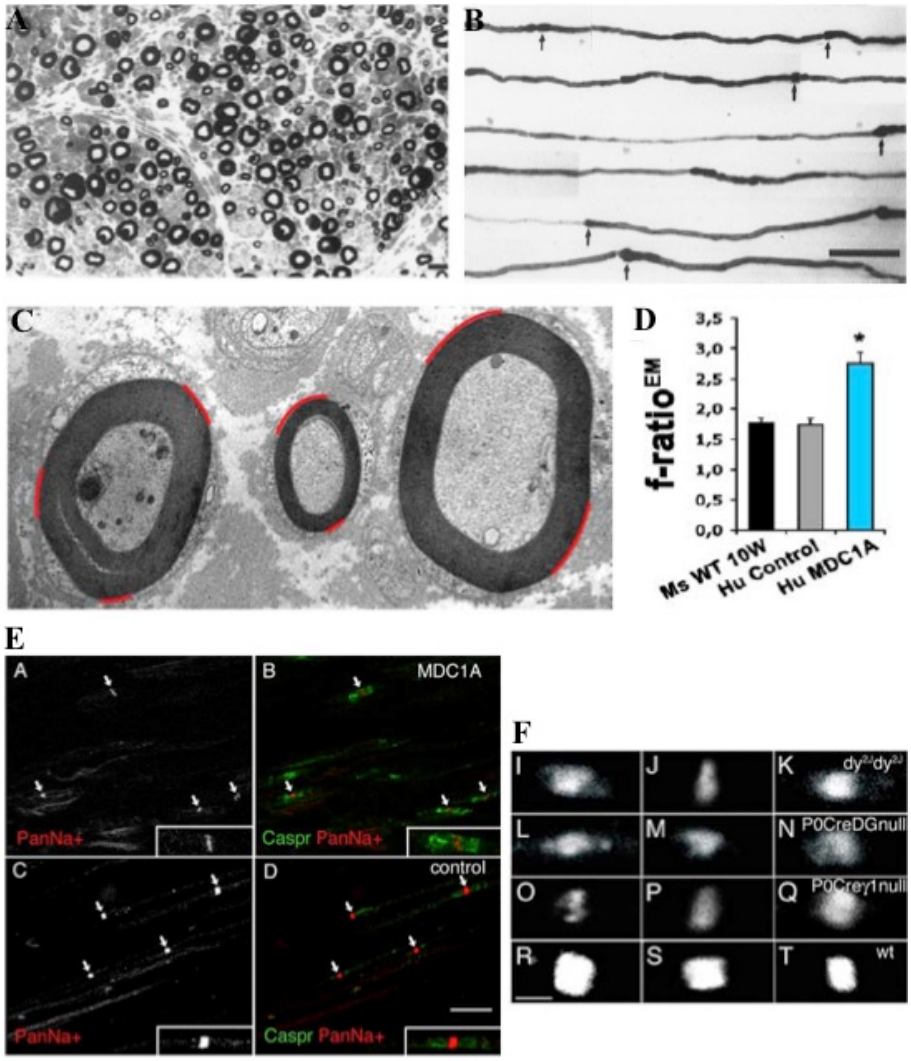

Fig. 14 Peripheral nerve abnormalities in a patient with MDC1A. **A,** Semithin section from a sural nerve biopsy showing reduction of myelinated fibers and presence of thickened and irregularly folded myelin sheath in some fibers. **B**, Osmicated teased nerve fibers display short internodes with irregularly thinned or thickened myelin in paranodal regions (from Di Muzio et al., 2003). **C-D**, EM section from sural nerve derived from the same MDC1A patient. *f*-ratio^{EM}, a measure of Schwann cell compartmentalization is increased,

demonstrating presence of smaller appositions (outlined in red) when compared to a control patient (not shown) (from Court et al., 2009). **E**, Longitudinal sections of sural nerve biopsies from an MDC1A patient (top) and a control (bottom) double stained with antibodies against all isoforms of sodium channels (panNav, red) and the paranodal marker caspr (green). A reduction in the intensity of staining for Nav clusters (arrows, enlarged in insets) is observed on MDC1A nerves compared with control nerves (from Occhi et al., 2005). **F**, Examples of Nav cluster abnormalities in a mouse model of MDC1A (dy2J/dy2J), and in mice lacking dystroglycan (P0CreDGnull) and laminin γ1-chain (P0Creγ1null) specifically from SCs. Defects in murine models are comparable to the ones found in the MDC1A patient (from Occhi et al., 2005).

1.7 References

- Abe I, Ochiai N, Ichimura H, Tsujino A, Sun J, and Hara Y. (2004) Internodes can nearly double in length with gradual elongation of the adult rat sciatic nerve. *J Orthop Res* 22: 571-577.
- Albrecht DE, Sherman DL, Brophy PJ, and Froehner SC. (2008) The ABCA1 cholesterol transporter associates with one of two distinct dystrophin-based scaffolds in Schwann cells. *Glia* 56(6): 611-618.
- Altevogt BM, Kleopa KA, Postma FR, Scherer SS, and Paul DL. (2002) Connexin29 is uniquely distributed within myelinating glial cells of the central and peripheral nervous systems. *J Neurosci 22*: 6458-6470.
- Amor V, Feinberg K, Eshed-Eisenbach Y, Grumet M, and Peles E. (2011) NrCAM and gliomedin are necessary for the maintenance of nodes of Ranvier in the peripheral nervous system. Abstract at *Myelin Satellite Meeting*.
- Apostolski S, Sadiq SA, Hays A, Corbo M, Suturkova-Milosevic L, Chaliff P, Stefansson K, LeBaron RG, Ruoslahti E, Hays AP, and Latov N. (1994) Identification of Gal(beta 1-3)GalNAc bearing glycoproteins at the nodes of Ranvier in peripheral nerve. *J Neurosci Res* 38(2): 134-41.
- Arikawa-Hirasawa E, Watanabe H, Takami H, Hassell JR, and Yamada Y. (1999) Perlecan is essential for cartilage and cephalic development. *Nat Genet* 23: 354-8.
- Arikawa-Hirasawa E, Wilcox WR, Le AH, Silverman N, Govindraj P, Hassell JR, and Yamada Y. (2001) Dyssegmental dysplasia Silverman-Handmaker type, is caused by functional null mutations of the perlecan gene. *Nat Genet* 27: 431-434.
- Ariyasu RG, Nichol JA, and Ellisman MH (1985) Localization of sodium/ potassium adenosine triphosphatase in multiple cell types of the

murine nervous system with antibodies raised against the enzyme from kidney. *J Neurosci* 5: 2581-2596.

- Arman TK, Grieco-Calub TM, Chen C, Rusconi R, Slat EA, Isom LL, and Raman IM. (2009) Regulation of persistent Na current by interactions between β subunits of voltage-gated Na channels. *J Neurosci* 29(7): 2027-2042.
- Asundi VK, Erdman R, Stahl RC, and Carey DJ. (2003). Matrix metalloproteinase-dependent shedding of syndecan-3, a transmembrane heparan sulfate proteoglycan, in Schwann cells. *J Neurosci Res* 73: 593-602.
- Balice-Gordon RJ, Bone LJ, and Scherer SS. (1998) Functional gap junctions in the Schwann cell myelin sheath. *J Cell Biol* 142: 1095-1104.
- Baumgartner S, Littleton JT, Broadie K, Bhat MA, Harbecke R, Lengyel JA, Chiquet-Ehrismann R, Prokop A, and Bellen HJ. (1996) A *Drosophila* neurexin is required for septate junction and blood-nerve barrier formation and function. *Cell* 87: 1059-1068.
- Bell MA, and Weddell AG. (1984) A descriptive study of the blood vessels of the sciatic nerve in the rat, man and other mammals. *Brain* 107(3): 871-98.
- Benninger Y, Thurnherr T, Pereira JA, Krause S, Wu X, Chrostek-Grashoff A, Herzog D, Nave KA, Franklin RJ, Meijer D, Brakebusch C, Suter U, and Relvas JB. (2007) Essential and distinct roles for cdc42 and rac1 in the regulation of Schwann cell biology during peripheral nervous system development. *J. Cell Biol* 177: 1051-1061.
- Berghs S, Aggujaro D, Dirkx R, Maksimova E, Stabach P, Hermel JM, Zhang JP, Philbrick W, Slepnev V, Ort T, and Solimena M. (2000) βIV spectrin, a new spectrin localized at axon initial segments and nodes of Ranvier in the central and peripheral nervous system. *J Cell Biol* 151: 985-1002.

- Berthold CH, and Rydmark M. (1983) Electron microscopic serial section analysis of nodes of Ranvier in lumbosacral spinal roots of the cat: ultrastructural organization of nodal compartments in fibres of different sizes. *J Neurocytol* 12, 475-505.
- Berti C, Bartesaghi L, Ghidinelli M, Zambroni D, Figlia G, Chen Z-L, Quattrini A, Wrabetz L, and Feltri ML. (2011) Non-redundant function of dystroglycan and β1 integrins in radial sorting of axons. *Dev* 138: 4025-4037.
- Bhat MA, Rios JC, Lu Y, Garcia-Fresco GP, Ching W, St Martin M, Li J, Einheber S, Chesler M, Rosenbluth J, Salzer JL, and Bellen HJ. (2001) Axon-glia interactions and the domain organization of myelinated axons requires neurexin IV/Caspr/Paranodin. *Neuron* 30: 369-383.
- Bix G, and Iozzo RV. (2008) Novel interactions of perlecan: unraveling perlecan's role in angiogenesis. *Micro Res Tech* 71(5): 339-48.
- Boiko T, Rasband M, Levinson S, Caldwell J, Mandel G, Trimmer J, and Mathews G. (2001) Compact myelin dictates the differential targeting of two sodium channel isoforms in the same axon. *Neuron* 30: 91-104.
- Bouzidi M, Tricaud N, Giraud P, Kordeli E, Caillol G, Deleuze C, Couraud F, and Alcaraz G. (2002) Interaction of the Nav1.2α subunit of the voltage dependent sodium channel with nodal ankyrin-G. *In vitro* mapping of the interacting domains and association in synaptosomes. *J Biol Chem* 277: 28996-29004.
- Boyle ME, Berglund EO, Murai KK, Weber L, Peles E, and Ranscht B. (2001) Contactin orchestrates assembly of the septate-like junctions at the paranode in myelinated peripheral nerve. *Neuron* 30: 385-397.
- Bozic D, Sciandra F, Lamba D, and Brancaccio A. (2004) The structure of the N-terminal region of murine skeletal muscle α-dystroglycan

discloses a modular architecture. *J Biol Chem* 279: 44812-44816.

- Bradley WG, and Jenkison M. (1973) Abnormalities of peripheral nerves in murine muscular dystrophy. *J Neurol Sci* 18: 227-247.
- Bradley WG, Jaros E, and Jenkison M. (1977) The nodes of Ranvier in the nerves of mice with muscular dystrophy. *J Neuropathol Exp Neurol* 36: 797-806.
- Brancaccio A, Schulthess T, Gesemann M, and Engel J. (1995) Electron microscopic evidence for a mucin-like region in chick muscle α-dystroglycan. *FEBS Lett* 368: 139-142.
- Brill MH, Waxman SG, Moore JW, and Joyner RW. (1977) Conduction velocity and spike configuration in myelinated fibres: computed dependence on internode distance. *J Neurol Neurosurg Psychiatry* 40: 769-774.
- Bunge MB, Wood PM, Tynan LB, Bates ML, and Sanes JR. (1989a) Perineurium originates from fibroblasts: demonstration *in vitro* with a retroviral marker. *Science* 243: 229-231.
- Bunge RP, Bunge MB, and Bates ML. (1989b) Movements of the Schwann cell nucleus implicate progression of the inner (axon-related) Schwann cell process during myelination. *J Cell Biol* 109: 273-284.
- Burgess DL, Kohrman DC, Galt J, Plummer NW, Jones JM, Spear B, and Meisler MH. (1995) Mutation of a new sodium channel gene, *Scn8a*, in the mouse mutant 'motor endplate disease'. *Nat Genet* 10: 461-465.
- Buttermore ED, Dupree JL, Cheng G Jr, An X, Tessarollo L, and Bhat MA. (2011) The cytoskeletal adaptor protein Band 4.1B is required for the maintenance of paranodal axoglial septate junctions in myelinated axons. *J Neurosci* 31(22): 8013-8024.
- Buzhdygan T, Shavkunov A, Panova-Elektronova N, and Laezza F. (2011) CK2-dependent regulation of the FGF14:Nav channel complex.

Abstract 760.23 at *Soc for Neurosci Meeting*.

- Byers TJ, Lidov HGW, and Kunkel LM. (1993) An alternative dystrophin transcript specific to peripheral nerve. *Nat Gen* 4(1): 77-81.
- Caldwell JH, Schaller KL, Lasher RS, Peles E, and Levinson SR. (2000) Sodium channel Na(v)1.6 is localized at nodes of Ranvier, dendrites, and synapses. *Proc Natl Acad Sci USA* 97: 5616-5620.
- Catterall WA, Goldin AL, and Waxman SG. (2005) International Union of Pharmacology. 465 XLVII. Nomenclature and structure-function relationships of voltage-gated sodium channels, *Pharmacol Rev* 57: 397-409.
- Chan JR. (2007) Myelination: all about Rac 'n' roll. *J Cell Biol* 177(6): 953-955.
- Chance PF, Alderson MK, Leppig KA, Lensch MW, Matsunami N, Smith B, Swanson PD, Odelberg SJ, Disteche CM, and Bird TD. (1993) DNA deletion associated with hereditary neuropathy with liability to pressure palsies. *Cell* 72: 143-151.
- Charles P, Tait S, Faivre-Sarrailh C, Barbin G, Gunn-Moore F, Denisenko-Nehrbass N, Guennoc AM, Girault JA, Brophy PJ, and Lubetzki C. (2002) Neurofascin is a glial receptor for the paranodin/Caspr-contactin axonal complex at the axoglial junction. *Curr Biol* 12: 217-220.
- Chen C, Bharucha V, Chen Y, Westenbroek RE, Brown A, Malhotra JD, Jones D, Avery C, Gillespie PJ, Kristin A. Kazen-Gillespie KA, Kazarinova-Noyes K, Shrager P, Saunders TL, Macdonald RL,. Ransom BR, Scheuer T, Catterall WA, and Isom LL. (2002) Reduced sodium channel density, altered voltage dependence of inactivation, and increased susceptibility to seizures in mice lacking sodium channel β2-subunits. *Proc Natl Acad Sci USA* 99(26): 17072-17077.
- Chen C, Westenbroek RE, Xu X, Edwards CA, Sorenson DR, Chen Y,

McEwen DP, O'Malley HA, Bharucha V, Meadows LS, Knudsen GA, Vilaythong A, Noebels JL, Saunders TL, Scheuer T, Shrager P, Catterall WA, and Isom LL. (2004) Mice lacking sodium channel β1 subunits display defects in neuronal excitability, sodium channel expression, and nodal architecture. *J Neurosci* 24: 4030-4042

- Chen YJ, Spence HJ, Cameron JM, Jess T, Ilsley JL, and Winder SJ. (2003) Direct interaction of β-dystroglycan with F-actin. *Biochem* 375(2): 329-337.
- Chen ZL, and Strickland S. (2003) Laminin γ1 is critical for Schwann cell differentiation, axon myelination, and regeneration in the peripheral nerve. *J Cell Biol* 163: 889-899.
- Chernousov MA, Stahl RC, and Carey DJ. (1996) Schwann cells secrete a novel collagen-like adhesive protein that binds N-syndecan. *J Biol Chem* 271: 13844-13853.
- Chernousov MA, Yu W-M, Chen Z-L, and Carey DJ, and Strickland S. (2008) Regulation of Schwann cell function by the extracellular matrix. *Glia* 56: 1498-1507.
- Ching W, Zanazzi G, SR Levinson, and Salzer JL. (1999) Clustering of neuronal sodium channels requires contact with myelinating Schwann cells. *J* Neurocytol 28: 295-301.
- Cifuentes-Diaz C, Chareyre F, Garcia M, Devaux J, Carnaud M, Levasseu G, Niwa-Kawakita M, Harroch S, Girault JA, Giovannini M, and Goutebroze L. (2011) Protein 4.1B contributes to the organization of peripheral myelinated axons. *PlosOne* 6(9): 1-15.
- Cohen MW, Jacobson C, Yurchenco PD, Morris GE, and Carbonetto S. (1997) Laminin-induced clustering of dystroglycan on embryonic muscle cells: comparison with agrin-induced clustering. *J Cell Biol* 136: 1047-1058.
- Conti Reed U. (2009) Congenital muscular dystrophy. *Arq*

Neuropsiquatr 67(2-A): 343-362.

- Cooper EC, and Jan LY. (2003) M-channels: Neurological diseases, neuromodulation, and drug development. *Arch Neurol* 60: 496-500.
- Costell M, Gustafsson E, Aszódi A, Mörgelin M, Bloch W, Hunziker E, Addicks K, Timpl R, and Fässler R. (1999) Perlecan maintains the integrity of cartilage and some basement membranes. *J Cell Biol* 147, 1109-1122.
- Court FA, Sherman DL, Pratt T, Garry EM, Ribchester RR, Cottrell DF, Fleetwood-Walker SM, and Brophy PJ. (2004) Restricted growth of Schwann cells lacking Cajal bands slows conduction in myelinated nerves. *Nature* 431: 191-195.
- Court FA, Wrabetz L, and Feltri ML. (2006) Basal lamina: Schwann cells wrap to the rhythm of space-time. *Curr Opin Neurobiol* 16: 501-507.
- Court FA, Hewitt JE, Davies K, Patton BL, Uncini A, Wrabetz L, and Feltri ML. (2009) A laminin-2, dystroglycan, utrophin axis is required for compartmentalization and elongation of myelin segments. *J Neurosci* 29(12): 3908-19.
- Court FA, Zambroni D, Pavoni E, Colombelli C, Baragli C, Figlia G, Sorokin L, Ching W, Salzer JL, Wrabetz L, and Feltri ML. (2011) MMP2-9 cleavage of dystroglycan alters the size and molecular composition of Schwann cell domains. *J Neurosci* 31(34): 12208-17.
- Custer AW, Kazarinova-Noyes K, Sakurai T, Xu X, Simon W, Grumet M, and Shrager P. (2003) The role of the ankyrin-binding protein NrCAM in node of Ranvier formation. *J Neurosci* 23(31): 10032-10039.
- Davis JQ, Lambert S, and Bennett V. (1996) Molecular composition of the node of Ranvier: identification of ankyrin-binding cell adhesion molecules neurofascin (mucin1/third FNIII domain-) and NrCAM at nodal axon segments. *J Cell Biol* 135: 1355-1367.

- Denisenko-Nehrbass N, Oguievetskaia K, Goutebroze L, Galvez T, Yamakawa H, Ohara O, Carnaud M, and Girault JA. (2003) Protein 4.1B associates with both Caspr/paranodin and Caspr2 at paranodes and juxtaparanodes of myelinated fibres. *Eur J Neurosci* 17: 411-416.
- Deodato F, Sabatelli M, Ricci E, Mercuri E, Muntoni F, Sewry C, Naom I, Tonali P, and Guzzetta F. (2002) Hypermyelinating neuropathy, mental retardation and epilepsy in a case of merosin deficiency. *Neuromuscul Disord* 12: 392-398.
- Devaux JJ, Kleopa KA, Cooper EC, and Scherer SS. (2004) KCNQ2 is a nodal K^+ channel. *J Neurosci* 24: 1236-1244.
- Di Muzio A, De Angelis MV, Di Fulvio P, Ratti A, Pizzuti A, Stuppia L, Gambi D, and Uncini A. (2003) Dysmyelinating sensory-motor neuropathy in merosin-deficient congenital muscular dystrophy. *Muscle Nerve* 27: 500-506.
- Donaldson HH, and Hoke GW. (1905) On the areas of the axis cylinder and medullary sheath as seen in cross sections of the spinal nerves of vertebrates. *J Comp Neurol* 15: 1-16.
- Dowsing BJ, Morrison WA, Nicola NA, Starkey GP, Bucci T, and Kilpatrick TJ. (1999) Leukemia inhibitory factor is an autocrine survival factor for Schwann cells. *J Neurochem* 73(1): 96-104.
- Duncan D. (1934) The importance of diameter as a factor in myelination. *Science* 79(2051): 363.
- Dupree JL, Coetzee T, Blight A, Suzuki K, and Popko B. (1998) Myelin galactolipids are essential for proper node of Ranvier formation in the CNS. *J Neurosci* 18(5): 1642-1649.
- D'Urso D, Brophy PJ, Staugaitis SM, Gillespie CS, Frey AB, Stempak JG, and Colman DR. (1990) Protein zero of peripheral nerve myelin: biosynthesis, membrane insertion, and evidence for homotypic interaction. *Neuron* 4: 449-460.

- Dzhashiashvili Y, Zhang Y, Galinska J, Lam I, Grumet M, Salzer JL. (2007) Nodes of Ranvier and axon initial segments are ankyrin G dependent domains that assemble by distinct mechanisms. *J Cell Biol* 177: 857-870.
- Einheber S, Zanazzi G, Ching W, Scherer S, Milner TA, Peles E, and Salzer JL. (1997) The axonal membrane protein Caspr/neurexin IV is a component of the septate-like paranodal junctions that assemble during myelination. *J Cell Biol* 139: 1495-1506.
- Echaniz-Laguna A, Rene F, Marcel C, Bangratz M, Fontaine B, Loeffler J-P, and Nicole S. (2009) Electrophysiological studies in a mouse model of Schwartz-Jampel syndrome demonstrate muscle fiber hyperactivity of peripheral nerve origin. *Muscle Nerve* 40(1): 55-61.
- Eldridge CF, Sanes JR, Chiu AY, Bunge RP, and Cornbrooks CJ. (1986) Basal lamina-associated heparin sulphate proteoglycan in the rat PNS: characterization and localization using monoclonal antibodies. *J Neurocytol* 15: 37-51.
- Eshed Y, Feinberg K, Poliak S, Sabanay H, Sarig-Nadir O, Spiegel I, Bermingham JR Jr, and Peles E. (2005) Gliomedin mediates Schwann cell-axon interaction and the molecular assembly of nodes of Ranvier. *Neuron* 47(2): 215-29.
- Eshed Y, Feinberg K, Carey DJ, and Peles E. (2007) Secreted gliomedin is a perinodal matrix component of peripheral nerves. *J Cell Biol* 177: 551-562.
- Faivre-Sarrailh C, Gauthier F, Denisenko-Nehrbass N, Le Bivic A, Rougon G, and Girault JA. (2000) The GPI-anchored adhesion molecule F3/contactin is required for surface transport of paranodin/caspr. *J Cell Biol* 149: 491-502.
- Fannon AM, Sherman DL, Ilyina-Gragerova G, Brophy PJ, Friedrich VL, Jr., and Colman DR. (1995) Novel E-cadherin-mediated adhesion in

peripheral nerve: Schwann cell architecture is stabilized by autotypic adherens junctions. *J Cell Biol* 129: 189-202.

- Feinberg K, Eshed-Eisenbach Y, Frechter S, Amor V, Salomon D, Sabanay H, Dupree JL, Grumet M, Brophy PJ, Shrager P, and Peles E. (2010) A glial signal consisting of gliomedin and NrCAM clusters axonal Na^+ channels during the formation of nodes of Ranvier. *Neuron* 65: 490-502.
- Feltri ML, Graus Porta D, Previtali SC, Nodari A, Migliavacca B, Cassetti A, Littlewood-Evans A, Reichardt LF, Messing A, Quattrini A, Mueller U, and Wrabetz L. (2002) Conditional disruption of β1 integrin in Schwann cells impedes interactions with axons. *J. Cell Biol.* 156: 199-209.
- Feltri ML, and Wrabetz L. (2005) Laminins and their receptors in Schwann cells and hereditary neuropathies. *J Periph Nerv Syst* 10: 128-143.
- Fernandez-Valle C, Fregien N, Wood PM, and Bunge MB. (1993) Expression of the protein zero myelin gene in axon-related Schwann cells is linked to basal lamina formation. *Dev* 119: 867-880.
- Figlia G, Dina G, Colombelli C, Ungaro D, Del Carro U, Riva N, Wrabetz L, Comi G, Feltri ML, and Quattrini A. (2011) Deletion of Schwann cell dystroglycan determines a spontaneous and purely motor polyradiculoneuritis. Presented at *Periph Nerve Soc Meeting*.
- Filbin MT, Walsh FS, Trapp BD, Pizzey JA, and Tennekoon GI. (1990) Role of myelin P0 protein as a homophilic adhesion molecule. *Nature* 344(6269): 871-1
- Friede RL, and Samorajski T. (1967) Relation between the number of myelin lamellae and axon circumference in fibers of vagus and sciatic nerves of mice. *J Comp Neurol* 130: 223-231.
- Friede RL, and Samorajski T. (1968) Myelin formation in the sciatic

nerve of the rat. A quantitative electron microscopic, histochemical and radioautographic study. *J Neuropathol Exp Neurol* 27: 546-570.

- Garbay B, Heape MA, Sargueil F, and Casagne C. (2000) Myelin synthesis in the peripheral nervous system. *Prog. Neurobiol* 61: 267-304.
- Garver TD, Ren Q, Tuvia S, and Bennett V. (1997) Tyrosine phosphorylation at a site highly conserved in the L1 family of cell adhesion molecules abolishes ankyrin binding and increases lateral mobility of neurofascin. *J Cell Biol* 137: 703-714.
- Gatto CL, Walker BJ, and Lambert S. (2003) Local ERM activation and dynamic growth cones at Schwann cell tips implicated in efficient formation of nodes of Ranvier. *J Cell Biol* 162: 489-498
- Gawlik KI, Akerlund M, Carmignac V, Elamaa H, and Durbeej M. (2010) Distinct roles for laminin globular domains in laminin α1 chain mediated rescue of murine laminin α2 chain deficiency. *PLoS One* 5(7): e11549.
- Geren BB. (1954) The formation from the Schwann cell surface of myelin peripheral nerves of chick embryos. *Exp Cell Res* 7: 558-562.
- Gesemann M, Brancaccio A, Schumacher B, and Ruegg MA. (1998) Agrin is a high-affinity binding protein of dystroglycan in non-muscle tissue. *J Biol Chem* 273, 600-605.
- Ghabriel MN, and Allt G. (1981) Incisures of Schmidt-Lanterman. *Prog Neurobiol* 17: 25-58.
- Gillespie CS, Sherman DL, Fleetwood-Walker SM, Cottrell DF, Tait S, Garry EM, Wallace VCJ, Ure J, Griffiths IR, Smith A, and Brophy PJ. (2000) Peripheral demyelination and neuropathic pain behavior in periaxin deficient mice. *Neuron* 26(2): 523-531.
- Goldfarb M, Schoorlemmer J, Williams A, Diwakar S, Wang Q, Huang X, Giza J, Tchetchik D, Kelley K, Vega A, Matthews G, Rossi P, Ornitz

DM, and D'Angelo E. (2007) Fibroblast growth factor homologous factors control neuronal excitability through modulation of voltage-gated sodium channels. *Neuron* 55: 449-463.

- Gollan L, Sabanay H, Poliak S, Berglund EO, Ranscht B, and Peles E. (2002) Retention of a cell adhesion complex at the paranodal junction requires the cytoplasmic region of Caspr. *J Cell Biol* 157: 1247-1256.
- Gollan L, Salomon D, Salzer JL, and Peles E. (2003) Caspr regulates the processing of contactin and inhibits its binding to neurofascin. *J Cell Biol* 163: 1213-1218.
- Goutebroze L, Carnaud M, Denisenko N, Boutterin MC, and Girault JA. (2003) Syndecan-3 and syndecan-4 are enriched in Schwann cell perinodal processes. *BMC Neurosci* 4: 29-37.
- Grove M, Komiyama NK, Nave KA, Grant SG, Sherman DL, and Brophy PJ. (2007) FAK is required for axonal sorting by Schwann cells. *J Cell Biol* 176: 277-282.
- Hall H, Bozic D, Michel K, and Hubbell JA. (2003) N-terminal α-dystroglycan binds to different extracellular matrix molecules expressed in regenerating peripheral nerves in a protein mediated manner and promotes neurite extension of PC12 cells. *Mol Cell Neurosci* 24: 1062-1073.
- Hara Y, Shiga T, Abe I, Tsujino A, Ichimura H, Okado N, and Ochiai N. (2003) P0 mRNA expression increases during gradual nerve elongation in adult rats. *Exp Neurol* 184(1): 428-35.
- Hara Y, Balci-Hayta B, Yoshida-Moriguchi T, Kanagawa M, Beltran-Valero de Bernabé D, Gündeşli H, Willer T, Satz JS, Crawford RW, Burden SJ, Kunz S, Oldstone MBA, Accardi A, Talim B, Muntoni F, Topaloğlu H, Dincer P, and Campbell KP. (2011) A dystroglycan mutation associated with Limb-Girdle Muscular Dystrophy. *N Engl J Med* 364(10): 939-946.

- Hayashi K, Yonemura S, Matsui T, Tsukita S, and Tsukita S. (1999). Immunofluorescence detection of ezrin/radixin/moesin (ERM) proteins with their carboxyl-terminal threonine phosphorylated in cultured cells and tissues: application of a novel fixation protocol using trichloroacetic acid (TCA) as a fixative. *J Cell Sci* 112: 1149-1158.
- Henry MD, and Campbell KP. (1996) Dystroglycan: an extracellular matrix receptor linked to the cytoskeleton. *Curr Opin Cell Biol* 8: 625-631.
- Hess A, and Young JZ. (1952) The Nodes of Ranvier. *Proc R Soc Lond B* 140: 301-320.
- Hesse C, Johansson I, Mattsson N, Bremell D, Andreasson U, Halim A, Anckarsäter R, Blennow K, Anckarsäter H, Zetterberg H, Larson G, Hagberg L, and Grahn A. (2011) The N-terminal domain of α-dystroglycan is released as a 38 kDa protein and is increased in cerebrospinal fluid in patients with Lyme neuroborreliosis. *Biochem Biophys Res Comm* 412(3): 494-9.
- Hewitt J. (2010) Investigating the functions of Large: lessons from mutant mice. *Meth Enzymol* 479 (21): 367-386.
- Hillaire D, Leclerc A, Faure S, Topaloglu H, Chiannilkulchai N, Guicheney P, Grinas L, Legos P, Philpot J, Evangelista TRouton M-C, Mayer M, Pellissier J-F, Estournet B, Barois A, Hentati F, Feingold N, Beckmann JS, Dubowitz V, Tomé FMS, and Fardeau M. (1994) Localization of merosin-negative congenital muscular dystrophy to chromosome 6q2 by homozygosity mapping. *Hum Mol Genet* 3: 1657-1661.
- Hiscoe HB. (1947) Distribution of nodes and incisures in normal and regenerated nerve. *Anat Record* 99: 447-475.
- Hodgkin AL, and Huxley AF. (1952) A quantitative description of membrane current and its application to conduction and excitation in

nerve. *J Physiol* 117: 500-544.

- Holt KH, Crosbie RH, Venzke DP, and Campbell KP. (2000) Biosynthesis of dystroglycan: processing of a precursor propeptide. *FEBS Lett* 468: 79-83.
- Honke K, Hirahara Y, Dupree J, Suzuki K, Popko B, Fukushima K, Fukushima J, Nagasawa T, Yoshida N, Wada Y, and Taniguchi N. (2002) Paranodal junction formation and spermatogenesis require sulfoglycolipids. *Proc Natl Acad Sci USA* 99: 4227-4232.
- Horresh I, Poliak S, Grant S, Bredt D, Rasband MN, and Peles E. (2008) Multiple molecular interactions determine the clustering of Caspr2 and Kv1 channels in myelinated axons. *J Neurosci* 28: 14213-14222.
- Horresh I, Bar V, Kissil JL, and Peles E. (2010). Organization of myelinated axons by Caspr and Caspr2 requires the cytoskeletal adapter protein 4.1B. *J Neurosci* 30: 2480 -2489.
- Hursh JB. (1939) Conduction velocity and diameter of nerve fibers. *Am J Physiol* 127: 131-139.
- Ibraghimov-Beskrovnaya O, Ervasti JM, Leveille CJ, Slaughter CA, Sernett SW, and Campbell KP. (1992) Primary structure of dystrophin-associated glycoproteins linking dystrophin to the extra cellular matrix. *Nature 355*: 696-702.
- Ichimura T, and Ellisman MH. (1991) Three-dimensional fine structure of cytoskeletal-membrane interactions at nodes of Ranvier. *J Neurocytol 20*: 667-681.
- Imamura M, Araishi K, Noguchi S, and Ozawa E. (2000) A sarcoglycan-dystroglycan complex anchors Dp116 and utrophin in the peripheral nervous system. *Hum Mol Gen* 9(20): 3091-3100.
- Inamori K, Yoshida-Moriguchi T, Hara Y, Anderson ME, Liping Y, and Campbell KP. (2012) Dystroglycan function requires xylosyl- and glucuronyltransferase activities of LARGE. *Science* 335: 93-96.

- Ivanovic A., Horresh I, Golan N, Spiegel I, Sabanay H, Frechter S, Ohno S, Terada N, Möbius W, Rosenbluth J, Brose N, and Peles E. (2012) The cytoskeletal adapter protein 4.1G organizes the internodes in peripheral myelinated nerves. *J Cell Biol* 196(3): 1-8.
- Jacob J, Hacker A, and Guthrie S. (2001) Mechanisms and molecules in motor neuron specification and axon pathfinding. *Bioessays 23*: 582-595.
- Jacobs JM. (1988) On internodal length. *J. Anat.* 157: 153-162.
- Jaros E, and Bradley WG (1979) Atypical axon-Schwann cell relationships in the common peroneal nerve of the dystrophic mouse: an ultrastructural study. *Neuropathol Appl Neurobiol* 5: 133-147.
- Jaros E, and Jenkison M. (1983) Quantitative studies of the abnormal axon-Schwann cell relationship in the peripheral motor and sensory nerves of the dystrophic mouse. *Brain Res* 258: 181-196.
- Jessen KR, and Mirsky R. (1999) Schwann cells and their precursors emerge as major regulators of nerve development. *Trends Neurosci* 22: 402-410.
- Jessen KR, and Mirsky R. (2005) The origin and development of glial cells in peripheral nerves. *Nat Rev Neurosci* 6: 671-682.
- Jin F, Dong B, Georgiou J, Jiang Q, Zhang J, Bharioke A, Qiu F, Lommel S, Feltri ML, Wrabetz L, Roder JC, Eyer J, Chen X, Peterson AC, and Siminovitch KA. (2011) N-WASp is required for Schwann cell cytoskeletal dynamics, normal myelin gene expression and peripheral nerve myelination. *Dev* 138: 1329-1337.
- Joseph NM, Mukouyama Y, Mosher JT, Jaegle M, Crone SA, Dormand E-L, Lee K-F, Meijer D, Anderson DJ, and Morrison SJ. (2004) Neural crest stem cells undergo multilineage differentiation in developing peripheral nerves to generate endoneurial fibroblasts in addition to Schwann cells. *Development* 131: 5599-5612.

- Kanagawa M, Saito F, Kunz S, Yoshida-Moriguchi T, Barresi R, Kobayashi YM, Muschler J, Dumanski JP, Michele DE, Oldstone BA, and Campbell KP. (2004) Molecular recognition by LARGE is essential for expression of functional dystroglycan. *Cell* 117: 953-964.
- Kohrman DC, Smith MR, Goldin AL, Harris J, and Meisler MH (1996) A missense mutation in the sodium channel Scn8a is responsible for cerebellar ataxia in the mouse mutant *jolting*. *J Neurosci* 16: 5993-5999.
- Komada M, and Soriano P. (2002) βIV-spectrin regulates sodium channel clustering through ankyrin-G at axon initial segments and nodes of Ranvier. *J Cell Biol* 156: 337-348.
- Kordeli E, Lambert S, Bennett V. (1995) Ankyrin G. A new ankyrin gene with neural-specific isoforms localized at the axonal initial segment and node of Ranvier. *J Biol Chem* 270: 2352-2359.
- Kuang W, Xu H, Vachon PH, Liu L, Loechel F, Wewer UM, and Engvall E. (1998) Merosin-deficient congenital muscular dystrophy: partial genetic correction in two mouse models. *J Clin Invest* 102(4): 844-852.
- Lai HC, and Jan LY. (2006) The distribution and targeting of neuronal voltage-gated ion channels. *Nat Rev* 7: 548-562.
- Lambert S, Davis JQ, and Bennett V. (1997) Morphogenesis of the node of Ranvier: co-clusters of ankyrin and ankyrin-binding integral proteins define early developmental intermediates. *J Neurosci* 17: 7025-7036.
- Landon DN, and Langley OK. (1971) The local chemical environment of nodes of Ranvier: a study of cation binding. *J Anat* 108: 419-432.
- Lemaillet G, Walker B, and Lambert S. (2003) Identification of a conserved ankyrin-binding motif in the family of sodium channel α subunits. *J Biol Chem* 278: 27333-27339.
- Levedakou EN, Chen XJ, Soliven B, and Popko B. (2005) Disruption of the mouse Large gene in the enr and myd mutants results in nerve,

muscle, and neuromuscular junction defects. *Mol Cell Neurosci* 28: 757-769.

- Li S, Liquari P, McKee KK, Harrison D, Patel R, Lee S, and Yurchenco PD. (2005) Laminin-sulfatide binding initiates basement membrane assembly and enables receptor signaling in Schwann cells and fibroblasts. *J Cell Biol* 169: 179-189.
- Love DR, Hill DF, Dickson G, Spurr NK, Byth BC, Marsden RF, Walsh FS, Edwards YH, and Davies KE. (1989) An autosomal transcript in skeletal muscle with homology to dystrophin. *Nature*, 339: 55-58.
- Lustig M, Zanazzi G, Sakurai T, Blanco C, Levinson SR, Lambert S, Grumet M, and Salzer JL. (2001) Nr-CAM and neurofascin interactions regulate ankyrin G and sodium channel clustering at the node of Ranvier. *Curr Biol* 11: 1864-1869.
- Madrid RE, Jaros E, Cullen MJ, and Bradley WG. (1975) Genetically determined defect of Schwann cell basement membrane in dystrophic mouse. *Nature* 257: 319-21.
- Malhotra JD, Koopmann MC, Kazen-Gillespie KA, Fettman N, Hortsch M, and Isom LL. (2002) Structural requirements for interaction of sodium channel β1 subunits with ankyrin. *J Biol Chem 277*: 26681-26688.
- Marmigère F, and Ernfors P. (2007) Specification and connectivity of neuronal subtypes in the sensory lineage. *Nat Rev Neurosci* 8: 114-127.
- Martin PM, Carnaud M, Garcia del Cano G, Irondelle M, Irinopoulou T, Girault JA, Dargent B, and Goutebroze L. (2008). Schwannomin-interacting protein-1 isoform IQCJ-SCHIP-1 is a late component of nodes of Ranvier and axon initial segments. *J Neurosci* 28: 6111-6117.
- Martin S, Levine AK, Chen ZJ, Ughrin Y, and Levine JM. (2001) Deposition of the NG2 proteoglycan at nodes of Ranvier in the peripheral nervous system. *J. Neurosci.* 21: 8119-8128.

- Masaki T, Matsumura K, Hirata A, Yamada H, Hase A, Arai K, Shimizu T, Yorifuji H, Motoyoshi K, and Kamakura K. (2002) Expression of dystroglycan and the laminin-α2 chain in the rat peripheral nerve during development. *Exp Neurol* 174, 109-117.
- Mascarenhas JB, Ruegg MA, Winzen U, Halfter W, Engel J, and Stetefeld J. (1993) Mapping of the laminin-binding site of the N-terminal agrin domain (NtA). *EMBO J* 22: 529-536.
- Mata M, Fink DJ, Ernst SA, and Segal GJ. (1991) Immunocytochemical demonstration of Na^+, K^+-ATPase in internodal axolemma of myelinated fibers of rat sciatic and optic nerves. *J Neurochem* 57: 184-192.
- Mata M, Kupina N, and Fink DJ. (1992) Phosphorylation-dependent neurofilament epitopes are reduced at the node of Ranvier. *J Neurocytol* 21: 199-210.
- Matsui T, Maeda M, Doi Y, Yonemura S, Amaono M, Kaibuchi K, Tsukita S, and Tsukita S. (1998) Rho-kinase phosphorylates COOH terminal threonines of ezrin/radixin/moesin (ERM) proteins and regulates their head-to-tail association. *J Cell Biol* 140: 647-657.
- Matsumura K, Yamada H, Shimizu T, and Campbell KP. (1993) Differential expression of dystrophin, utrophin and dystrophin-associated proteins in peripheral nerve. *FEBS Lett* 334: 281-285.
- Maurel P, Einheber S, Galinska J, Thaker P, Lam I, Rubin MB, Scherer SS, Murakami Y, Gutmann DH, and Salzer JL. (2007) Nectin-like proteins mediate axon-Schwann cell interactions along the internode and are essential for myelination. *J Cell Biol* 178: 861-874.
- McEwen DP, and Isom LL. (2004) Heterophilic interactions of sodium channel β1 subunits with axonal and glial cell adhesion molecules. *J Biol Chem* 279: 52744-52752.
- McIntyre CC, Richardson AG, and Grill WM. (2002) Modeling the excitability of mammalian nerve fibers: influence of afterpotentials on

the recovery cycle. *J Neurophysiol* 87: 995-1006.

- Meier C, Parmantier E, Brennan A, Mirsky R, and Jessen KR. (1999) Developing Schwann cells acquire the ability to survive without axons by establishing an autocrine circuit involving IGF, NT-3 and PDGF-BB. *J Neurosci* 19: 3847-3859.
- Meier C, Dermietzel R, Davidson KG, Yasumura T, and Rash JE. (2004) Connexin32-containing gap junctions in Schwann cells at the internodal zone of partial myelin compaction and in Schmidt-Lanterman incisures. *J Neurosci* 24: 3186-3198.
- Meier H, and Southard JL. (1970) Muscular dystrophy in the mouse caused by an allele at the dy-locus. *Life Sci* 9: 137-144.
- Melendez-Vasquez CV, Rios JC, Zanazzi G, Lambert S, Bretscher A, and Salzer JL. (2001) Nodes of Ranvier form in association with ezrin-radixin-moesin (ERM)-positive Schwann cell processes. *Proc Natl Acad Sci USA* 98: 1235-1240.
- Melendez-Vasquez CV, Einheber S, and Salzer JL. (2004) Rho kinase regulates Schwann cell myelination and formation of associated axonal domains. *J Neurosci* 24: 3953-3963.
- Melendez-Vasquez CV, Carey DJ, Zanazzi G, Reizes O, Maurel P, and Salzer JL. (2005) Differential expression of proteoglycans at central and peripheral nodes of Ranvier. *Glia* 52: 301-308.
- Menegoz M, Gaspar P, Le Bert M, Galvez T, Burgaya F, Palfrey C, Ezan P, Arnos F, and Girault JA. (1997) Paranodin, a glycoprotein of neuronal paranodal membranes. *Neuron* 19: 319-331.
- Mi H, Deerinck TJ, Ellisman MH, and Schwarz TL. (1995) Differential distribution of closely related potassium channels in rat Schwann cells. *J Neurosci* 15(5): 3761-3774.
- Mi H, Deerinck TJ, Jones M, Ellisman MH, and Schwarz TL. (1996) Inwardly rectifying K^+ channels that may participate in K^+ buffering are

localized in microvilli of Schwann cells. *J Neurosci* 16: 2421-2429.

- Michailov GV, Sereda MW, Brinkmann BG, Fischer TM, Haug B, Birchmeier C, Role L, Lai C, Schwab MH, and Nave KA. (2004) Axonal neuregulin-1 regulates myelin sheath thickness. *Science* 304: 700-703.
- Michelson A, Russell E, and Harman P. (1955) Dystrophia Muscularis: a hereditary primary neuropathy in the mouse. *Proc Natl Acad Sci USA* 41: 1079-1084.
- Mikol DD, Hong HL, Cheng HL, and Feldman EL. (1999) Caveolin-1 expression in Schwann cells. *Glia* 27: 39-52.
- Miner JH, and Yurchenco PD. (2004) Laminin functions in tissue morphogenesis. *Annu Rev Cell Dev Biol* 20: 255-284.
- Miner JH. (2008) Laminins and their roles in mammals. *Micr Res Tech* 71(5): 349-56.
- Moll J, Barzaghi P, Lin S, Bezakova G, Lochmuller H, Engvall E, Muller U, and Ruegg MA. (2001) An agrin minigene rescues dystrophic symptoms in a mouse model for congenital muscular dystrophy. *Nature* 413: 302-7.
- Miyagoe Y, Hanaoka K, Nonaka I, Hayasaka M, Nabeshima Y, Arahata K, and Takeda S. (1997) Laminin α2 chain null mutant mice by targeted disruption of the *Lama2* gene: a new model of merosin (laminin 2)-deficient congenital muscular dystrophy. *FEBS Lett.* 415: 33-39.
- Miyagoe-Suzuki Y, Nakagawa M, and Takeda S (2000) Merosin and congenital muscular dystrophy. *Microsc Res Tech* 48: 181-191.
- Muntoni F, Torelli S, and Brockington M. (2008) Muscular dystrophies due to glycosylation defects. *Am Soc Exp NeuroTherap* 5: 627-632.
- Nakagawa M, Miyagoe-Suzuki Y, Ikezoe K, Miyata Y, Nonaka I, Harii K, and Takeda S. (2001) Schwann cell myelination occurred without

basal lamina formation in laminin α2 chain-null mutant (*dy*3K/*dy*3K) mice. *Glia* 35: 101-110.

- Nakao T, and Ishizawa A. (1994) Development of the spinal nerves in the mouse with special reference to innervation of the axial musculature. *Anat Embryol* (Berl) 189(2): 115-138.
- Nicole S, Davoine CS, Topaloglu H, Cattolico L, Barral D, Beighton P, Ben Hamida C, Hammouda H, Cruaud C, White PS, Samson D, Urtizberea JA, Lehmann-Horn F, Weissenbach J, Hentati F, and Fontaine B. (2000) Perlecan, the major proteoglycan of basement membranes, is altered in patients with Schwartz-Jampel syndrome (chondrodystrophic myotonia). *Nat Genet* 26: 480-3.
- Nodari A, Zambroni D, Quattrini A, Court FA, D'Urso A, Recchia A, Tybulewicz VL, Wrabetz L, and Feltri ML. (2007) β1 integrin activates Rac1 in Schwann cells to generate radial lamellae during axonal sorting and myelination. *J Cell Biol* 177: 1063-1075.
- Nodari A, Previtali SC, Dati G, Occhi S, Court FA, Colombelli C, Zambroni D, Dina G, Del Carro U, Campbell KP, Quattrini A, Wrabetz L, and Feltri ML. (2008) α6β4 integrin and dystroglycan cooperate to stabilize the myelin sheath. *J Neurosci* 28(26): 6714-6719.
- Novak N, Bar V, Sabanay H, Frechter S, Jaegle M, Snapper SB, Meijer D, and Peles E. (2011) N-WASP is required for membrane wrapping and myelination by Schwann cells. *J Cell Biol* 192: 243-250.
- Occhi S, Zambroni D, Del Carro U, Amadio S, Sirkowski EE, Scherer SS, Campbell KP, Moore SA, Chen ZL, Strickland S, Di Muzio A, Uncini A, Wrabetz L, and Feltri ML. (2005) Both laminin and Schwann cell dystroglycan are necessary for proper clustering of sodium channels at nodes of Ranvier. *J Neurosci* 25(41): 9418-9427.
- Ogawa Y, Schafer DP, Horresh I, Bar V, Hales K, Yang Y, Susuki K, Peles E, Stankewich MC, and Rasband MN (2006) Spectrins and

ankyrinB constitute a specialized paranodal cytoskeleton. *J Neurosci* 26: 5230-5239.

- Ogawa Y, Oses-Prieto J, Kim MY, Horresh I, Peles E, Burlingame AL, Trimmer JS, Meijer D, and Rasband MN (2010) ADAM22, a Kv1 channel-interacting protein, recruits membrane-associated guanylate kinases to juxtaparanodes of myelinated axons. *J Neurosci* 30: 1038-1048.
- Ohara R, Yamakawa H, Nakayama M, and Ohara O. (2000) Type II brain 4.1 (4.1B/KIAA0987), a member of the protein 4.1 family, is localized to neuronal paranodes. *Mol Brain Res 85*: 41-52.
- Ohno N, Terada N, Yamakawa H, Komada M, Ohara O, Trapp BD, Ohno S. (2006) Expression of protein 4.1G in Schwann cells of the peripheral nervous system. *J Neurosci Res* 84: 568-577.
- Pan Z, Kao T, Horvath Z, Lemos J, Sul JY, Cranstoun SD, Bennett V, Scherer SS, and Cooper EC. (2006) A common ankyrin-G-based mechanism retains KCNQ and NaV channels at electrically active domains of the axon. *J Neurosci* 26: 2599-2613.
- Parmantier E, Lynn B, Lawson D, Turmaine M, Sharghi Namini S, Chakrabarti L, McMahon AP, Jessen KR, and Mirsky R. (1999) Schwann cell-derived Desert Hedgehog controls the development of peripheral nerve sheaths. *Neuron* 23: 713-724.
- Patton BL, Miner JH, Chiu AY, and Sanes JR. (1997) Distribution and function of laminins in the neuromuscular system of developing, adult, and mutant mice. *J Cell Biol* 139(6): 1507-1521.
- Pedraza L, Huang JK, and Colman DR. (2001) Organizing principles of the axoglial apparatus. *Neuron* 30: 335-344.
- Peles E, Nativ M, Lustig M, Grumet M, Schilling J, Martinez R, Plowman GD, and Schlessinger J. (1997) Identification of a novel contactin associated transmembrane receptor with multiple domains

implicated in protein-protein interactions. *EMBO J* 16: 978-988.

- Peng HB, Xie H, Rossi SG, and Rotundo RL. (1999) Acetylcholinesterase clustering at the neuromuscular junction involves perlecan and dystroglycan. *J Cell Biol* 145: 911-21.
- Pentao L, Wise CA, Chinault AC, Patel PI, and Lupski JR. (1992) Charcot-Marie-Tooth type 1A duplication appears to arise from recombination at repeat sequences flanking the 1.5 Mb monomer unit. *Nat Gen* 2: 292-300.
- Peters A, Palay SL, and Webster H. (1991) The fine structure of the nervous system: Neurons and their supporting cells. Third Edition, Oxford University Press.
- Philpot J, Cowan F, Pennock J, Sewry C, Dubowitz V, Bydder G, and Muntoni F. (1999) Merosin-deficient congenital muscular dystrophy: the spectrum of brain involvement on magnetic resonance imaging. *Neuromusc Disord* 9: 81-85.
- Pillai AM, Thaxton C, Pribisko AL, Cheng JG, Dupree JL, and Bhat MA. (2009) Spatio-temporal ablation of myelinating glia-specific neurofascin ($Nfasc^{NF155}$) in mice reveals gradual loss of paranodal axoglial junctions and concomitant disorganization of axonal domains. *J Neurosci Res* 87: 1773-1793.
- Poliak S, Gollan L, Martinez R, Custer A, Einheber S, Salzer JL, Trimmer JS, Shrager P, and Peles E. (1999) Caspr2, a new member of the neurexin superfamily, is localized at the juxtaparanodes of myelinated axons and associates with K1 channels. *Neuron* 24: 1037-1047.
- Poliak S, Matlis S, Ullmer C, Scherer SS, and Peles E. (2002) Distinct claudins and associated PDZ proteins form different autotypic tight junctions in myelinating Schwann cells. *J Cell Biol* 159: 361-372.
- Poliak S, Salomon D, Elhanany H, Sabanay H, Kiernan B, Pevny L,

Stewart CL, Xu X, Chiu SY, Shrager P, Furley AJ, and Peles E. (2003) Juxtaparanodal clustering of Shaker-like K^+ channels in myelinated axons depends on Caspr2 and TAG-1. *J Cell Biol* 162: 1149-1160.

- Politi C, Del Turco D, Sie JM, Golinski PA, Tegeder I, Deller T, and Schultz C. (2008) Accumulation of phosphorylated IkBα and activated IKK in nodes of Ranvier. *Neuropathol Appl Neurobiol* 34: 357-365.
- Previtali SC, Nodari A, Taveggia C, Pardini C, Dina G, Villa A, Wrabetz L, Quattrini A, and Feltri ML (2003) Expression of laminin receptors in Schwann cell differentiation: evidence for distinct roles. *J Neurosci* 23: 5520-5530.
- Qu Y, Curtis R, Lawson D, Gilbride K, Ge P, DiStefano PS, Silos-Santiago I, Catterall WA, and Scheuer T. (2001) Differential modulation of sodium channel gating and persistent sodium currents by the β1, β2, and β3 subunits. *Mol Cell Neurosci* 18: 570-580.
- Quick DC, and Waxman SG. (1977) Ferric ion, ferrocyanide, and inorganic phosphate as cytochemical reactants at peripheral nodes of Ranvier. *J Neurocytol* 6(5): 555-70.
- Quijano-Roy S, Renault F, Romero N, Guicheney P, Fardeau M, and Estournet B. (2004) EMG and nerve conduction studies in children with congenital muscular dystrophy. *Muscle Nerve* 29: 292-299.
- Ramón y Cajal S. (1933) Histology. London: Bailliere, Tindall & Cox.
- Ranvier L. (1871) Sur les éléments conjonctifs de la moelle épinière. *Compt Rend* 73: 1168-1171.
- Ranvier L. (1872) Des étranglements annulaires et des segments interannulaires chez les Raies et les Torpilles. *CR Acad Sci, Paris* 75: 1129-1132.
- Rasband MN, and Trimmer JS. (2001) Developmental clustering of ion channels at and near the node of Ranvier. *Dev Biol* 236, 5-16.
- Rasband MN, Park EW, Zhen D, Arbuckle MI, Poliak S, Peles E, Grant

SG, and Trimmer JS (2002) Clustering of neuronal potassium channels is independent of their interaction with PSD-95. *J Cell Biol* 159: 663-672.

- Rasi K, Hurskainen M, Kallio M, Staven S, Sormunen R, Heape AM, Avila RL, Kirschner D, Muona A, Tolonen U, Tanila H, Huhtala P, Soininen R, and Pihlajaniemi T. (2010) Lack of collagen XV impairs peripheral nerve maturation and, when combined with laminin-411 deficiency, leads to basement membrane abnormalities and sensorimotor dysfunction. *J Neurosci* 30: 14490-14501.
- Rasminsky M, Kearney RE, Aguayo AJ, and Bray GM. (1978) Conduction of nervous impulses in spinal roots and peripheral nerves of dystrophic mice. *Brain Res* 143: 71-8.
- Ratcliffe CF, Qu Y, McCormick KA, Tibbs VC, Dixon JE, Scheuer T, and Catterall WA. (2000) A sodium channel signaling complex: modulation by associated receptor protein tyrosine phosphatase β. *Nat Neurosci* 3: 437-444.
- Ratcliffe CF, Westenbroek RE, Curtis R, and Catterall WA. (2001) Sodium channel β1 and β3 subunits associate with neurofascin through their extracellular immunoglobulin-like domain. *J. Cell Biol* 154: 427-434.
- Rayburn HB, and Peterson AC. (1978) Naked axons in myodystrophic mice. *Brain Res* 146: 380-384.
- Reichardt L, and Prokop A. (2011) The role of extracellular matrix in nervous system development and maintenance. *Dev Neurobiol* 71(11): 883-8.
- Rieger R, Pincon-Raymond M, Lombet A, Ponzio G, Lazdunski M, and Sidman RL. (1984) Paranodal dysmyelination and increase in tetrodotoxin binding sites in the sciatic nerve of the motor end-plate disease (med/med) mouse during postnatal development. *Dev Biol* 101:

401-409.

- Rios JC, Melendez-Vasquez CV, Einheber S, Lustig M, Grumet M, Hemperly J, Peles E, and Salzer JL. (2000) Contactin-associated protein (Caspr) and contactin form a complex that is targeted to the paranodal junctions during myelination. *J Neurosci* 20: 8354-8364.
- Rios JC, Rubin M, St Martin M, Downey RT, Einheber S, Rosenbluth J, Levinson SR, Bhat M, and Salzer JL. (2003) Paranodal interactions regulate expression of sodium channel subtypes and provide a diffusion barrier for the node of Ranvier. *J Neurosci* 23: 7001-11.
- Roberts GR, Freeman TC, Kendall E, Vetrie DLP, Dixon AK, Shaw-Smith C, Bone Q, and Bobrow M. (1996) Characterization of DRP2, a novel human dystrophin homologue. *Nat Gen* 13: 223-226.
- Robertson JD. (1958) The ultrastructure of Schmidt-Lanterman clefts and related shearing defects of the myelin sheath. *J Biophys Biochem Cytol* 4: 39-44.
- Rosenbluth J. (1976) Intramembranous particle distribution at the node of Ranvier and adjacent axolemma in myelinated axons of the frog brain. *J Neurocytol* 5: 731-745.
- Rosenbluth J. (1980) Peripheral myelin in the mouse mutant Shiverer. *J Comp Neurol* 193: 729-739.
- Rossi M, Morita H, Sormunen R, Airenne S, Kreivi M, Wang L, Fukai N, Olsen BR, Tryggvason K, and Soininen R. (2003) Heparan sulfate chains of perlecan are indispensable in the lens capsule but not in the kidney. *EMBO J* 22(2): 236-245.
- Ruegg MA, and Bixby JL. (1998) Agrin orchestrates synaptic differentiation at the vertebrate neuromuscular junction. *Trends Neurosci* 21: 22-27.
- Saher G, Brugger B, Lappe-Siefke C, Mobius W, Tozawa R, Wehr MC, Wieland F, Ishibashi S,and Nave KA. (2005). High cholesterol level is

essential for myelin membrane growth. *Nat Neurosci* 8(4): 468-475.

- Saito F, Masaki T, Kamakura K, Anderson LVB, Fujita S, Fukuta-Ohi H, Sunada Y, Shimizu T, and Matsumura K. (1999) Characterization of the transmembrane molecular architecture of the dystroglycan complex in Schwann cells. *J Biol Chem* 274(12): 8240-8246.
- Saito F, Moore SA, Barresi R, Henry MD, Messing A, Ross-Barta SE, Cohn RD, Williamson RA, Sluka KA, Sherman DL, Brophy PJ, Schmelzer JD, Low PA, Wrabetz L, Feltri ML, and Campbell KP. (2003) Unique role of dystroglycan in peripheral nerve myelination, nodal structure, and sodium channel stabilization. *Neuron* 38: 747-758.
- Saito F, Masaki T, Saito Y, Nakamura A, Takeda S, Shimizu T, Toda T, and Matsumura K. (2007) Defective peripheral nerve myelination and neuromuscular junction formation in fukutin-deficient chimeric mice. *J.Neurochem.* 101: 1712-1722.
- Saito F, Saito-Arai Y, Nakamura A, Shimizu T, and Matsumura K. (2008) Processing and secretion of the N-terminal domain of α-dystroglycan in cell culture media. *FEBS Lett* 582(3): 439-44.
- Saito F, Saito-Arai Y, Nakamura-Okuma A, Ikeda M, Hagiwara H, Masaki T, Shimizu T, and Matsumura K. (2011) Secretion of N-terminal domain of α-dystroglycan in cerebrospinal fluid. *Biochem Biophys Res Commun* 411(2): 365-9.
- Salzer JL. (2003) Polarized domains of myelinated axons. *Neuron* 40: 297-318.
- Salzer JL, Brophy PJ, and Peles E. (2008) Molecular domains of myelinated axons in the peripheral nervous system. *Glia* 56: 1532-540.
- Schaeren-Wiemers N, Bonnet A, Erb M, Erne B, Bartsch U, Kern F, Mantei N, Sherman D, and Suter U. (2004) The raft-associated protein MAL is required for maintenance of proper axon-glia interactions in the central nervous system. *J Cell Biol* 166: 731-742.

- Schafer DP, Bansal R, Hedstrom KL, Pfeiffer SE, and Rasband MN. (2004) Does paranode formation and maintenance require partitioning of neurofascin 155 into lipid rafts? *J Neurosci* 24: 3176-3185.
- Schafer DP, Custer AW, Shrager P, and Rasband MN. (2006) Early events in node of Ranvier formation during myelination and remyelination in the PNS. *Neur Glia Biol* 2(2): 69-79.
- Scheiermann C, Meda P, Aurrand-Lions M, Madani R, Yiangou Y, Coffey P, Salt TE, Ducrest-Gay D, Caille D, Howell O, Reynolds R, Lobrinus A, Adams RH, Yu AS, Anand P, Imhof BA, and Nourshargh S. (2007) Expression and function of junctional adhesion molecule-C in myelinated peripheral nerves. *Science* 318**:** 1472-1475.
- Scherer SS, and Arroyo EJ. (2002) Recent progress on the molecular organization of myelinated axons. *J Periph Nerv Syst* 7: 1-12.
-
- Scherer SS, Xu T, Crino P, Arroyo EJ, and Gutmann DH. (2001) Ezrin, radixin, and moesin are components of Schwann cell microvilli. *J Neurosci Res* 65: 150-164.
- Scherer SS, and Wrabetz L. (2008) Molecular mechanisms of inherited demyelinating neuropathies. *Glia* 56: 1578-1589.
- Schwartz MA. (2001) Integrin signaling revisited. *Trends Cell Biol* 11: 466-470.
- Shah NM, Marchionni MA, Isaacs I, Stroobant P, and Anderson DJ. (1994) Glial growth factor restricts mammalian neural crest stem cells to a glial fate. *Cell* 77: 349-360.
- Sharkey LM, Cheng X, Drews V, Buchner DA, Jones JM, Justice MJ, Waxman SG, Dib-Hajj SD, and Meisler M.H. (2009) The *ataxia3* mutation in the N-terminal cytoplasmic domain of sodium channel Nav1.6 disrupts intracellular trafficking. *J Neurosci* 29(9): 2733-2741.
- Sherman DL, Fabrizi C, Gillespie CS, and Brophy PJ. (2001) Specific

disruption of a Schwann cell dystrophin-related protein complex in a demyelinating neuropathy. *Neuron* 30: 677-687.

- Sherman DL, Tait S, Melrose S, Johnson R, Zonta B, Court FA, Macklin WB, Meek S, Smith AJ, Cottrell DF, and Brophy PJ. (2005) Neurofascins are required to establish axonal domains for salutatory conduction. *Neuron* 48: 737-742.
- Shorer Z, Philpot J, Muntoni F, Sewry C, and Dubowitz V. (1995) Demyelinating peripheral neuropathy in merosin-deficient congenital muscular dystrophy. *J Child Neurol* 10: 472-475.
- Singh J, Itahana Y, Knight-Krajewski S, Kanagawa M, Campbell KP, Bissell MJ, and Muschler J. (2004) Proteolytic enzymes and altered glycosylation modulate dystroglycan function in carcinoma cells. *Canc Res* 64, 6152-6159.
- Smalheiser NR, and Schwartz NB. (1987) Cranin: a laminin-binding protein of cell membranes. *Proc Natl Acad Sci USA* 84**:** 6457-6461.
- Smalheiser NR, and Kim E. (1995) Purification of cranin, a laminin binding membrane protein. Identity with dystroglycan and reassessment of its carbohydrate moieties. *J Biol Chem* 270: 15425-15433.
- Sosinsky GE, Deerinck TJ, Greco R, Buitenhuys CH, Bartol TM, and Ellisman MH. (2005) Development of a model for microphysiological simulations. *Neuroinformatics* 3(2): 133-62.
- Sotgia F, Lee H, Bedford MT, Petrucci T, Sudol M, and Lisanti MP. (2001) Tyrosine phosphorylation of β-dystroglycan at its WW domain binding motif, PPxY, recruits SH2 domain containing proteins. *Biochem* 40: 14585-14592.
- Spence HJ, Chen YJ, Batchelor CL, Higginson JR, Suila H, Carpen O, and Winder SJ. (2004) Ezrin-dependent regulation of the actin cytoskeleton by β-dystroglycan. *Hum Mol Gen* 13(15): 1657-1668.
- Spiegel I, Adamsky K, Eshed Y, Milo R, Sabanay H, Sarig-Nadir O,

Horresh I, Scherer SS, Rasband MN, and Peles E. (2007) A central role for Necl4 (SynCAM4) in Schwann cell-axon interaction and myelination. *Nat Neurosci* 10: 861-869.

- Srinivasan J, Schachner M, and Catterall WA. (1998) Interaction of voltage-gated sodium channels with the extracellular matrix molecules tenascin-C and tenascin-R. *Proc Natl Acad Sci USA* 95: 15753-15757.
- Stirling CA. (1975) Abnormalities in Schwann cell sheaths in spinal nerve roots of dystrophic mice. *J Anat* 119: 169-180.
- Stum M, Girard E, Bangratz M, Bernard V, Herbin M, Vignaud A, Ferry A, Davoine CS, Echaniz-Laguna A, René F, Marcel C, Molgó J, Fontaine B, Krejci E, and Nicole S. (2008) Evidence of a dosage effect and a physiological endplate acetylcholinesterase deficiency in the first mouse models mimicking Schwartz-Jampel syndrome neuromyotonia. *Hum Mol Genet* 17(20): 3166-79.
- Sun XY, Takagishi Y, Okabe E, Chishima Y, Kanou Y, Murase S, Mizumura K, Inaba M, Komatsu Y, Hayashi Y, Peles E, Oda SI, and Murata Y (2009) A novel Caspr mutation causes the *shambling* mouse phenotype by disrupting axoglial interactions of myelinated nerves. *J Neuropathol Exp Neurol* 68: 1207-1218.
- Sunada Y, Bernier SM, Utani A, Yamada Y, and Campbell KP (1995a) Identification of a novel mutant transcript of laminin α2 chain gene responsible for muscular dystrophy and dysmyelination in dy2J mice. *Hum Mol Genet* 4:1055-1061.
- Sunada Y, Edgar TS, Lotz BP, Rust RS, and Campbell KP. (1995b) Merosin-negative congenital muscular dystrophy associated with extensive brain abnormalities. *Neurol* 45: 2084-2089.
- Susuki K, and Rasband MN. (2008) Molecular mechanisms of node of Ranvier formation. *Curr Opin Cell Biol* 20(6): 616-23.

- Syroid DE, Maycox PR, Burrola PG, Liu N, Wen D, Lee KF, Lemke G, and Kilpatrick TJ. (1996) Cell death in the Schwann cell lineage and its regulation by neuregulin. *Proc Natl Acad Sci USA* 93: 9229-9234.
- Takashima H, Boerkoel CF, De Jonghe P, Ceuterick C, Martin JJ, Voit T, Schroder JM, Williams A, Brophy PJ, Timmerman V, and Lupski JR. (2002) Periaxin mutations cause a broad spectrum of demyelinating neuropathies. *Ann Neurol* 51: 709-715.
- Tao-Cheng JH, and Rosenbluth J. (1983) Axolemmal differentiation in myelinated fibers of rat peripheral nerves. *Brain Res* 285: 251-263.
- Taveggia C, Zanazzi G, Petrylak A, Yano H, Rosenbluth J, Einheber S, Xu X, Esper RM, Loeb JA, Shrager P, Chao MV, Falls DL, Role L, and Salzer JL. (2005) Neuregulin-1 type III determines the ensheathment fate of axons. *Neuron* 47(5): 681-94.
- Terada N, Saitoh Y, Ohno N, Komada M, Saitoh S, Peles E, and Ohno S. (2011) Essential function of protein 4.1G in targeting of membrane protein palmitoylated 6 into Schmidt-Lanterman Incisures in myelinated nerves. *Mol Cell Biol* 32(1): 199-205.
- Thaxton C, Pillai AM, Pribisko AL, Dupree JL, and Bhat MA. (2011) Nodes of Ranvier act as barriers to restrict invasion of flanking paranodal domains in myelinated axons. *Neuron* 69: 244-257.
- Tolwani RJ, Cosgaya JM, Varma S, Reza J, Kuo LE, and Shooter EM. (2004) BDNF overexpression produces a long-term increase in myelin formation in the peripheral nervous system. *J Neurosci Res* 77: 662-669.
- Tomé FMS, Evangelista T, Leclerc A, Sunada Y, Manole E, Estournet B, Barois A, Campbell KP, and Fardeau M. (1994) Congenital muscular dystrophy with merosin deficiency. *CR Acad Sci* 317: 351-357.
- Topp KS, and Boyd BS. (2011) Peripheral nerve: from the microscopic functional unit of the axon to the biomechanically loaded macroscopic structure. *J Hand Ther*, Special Issue: 1-10.

- Trapp BD, Andrews SB, Wong A, O'Connell M, and Griffin JW. (1989) Colocalization of the myelin-associated glycoprotein and the microfilament components, F-actin and spectrin, in Schwann cells of myelinated nerve fibres. *J Neurocytol* 18: 47-60.
- Trapp BD. (1990) The myelin-associated glycoprotein: location and potential functions. Editors: Colman D, Duncan I, Skoff R. Myelination and dysmyelination. The New York Academy of Sciences. 29-43.
- Trapp BD, and Kidd GJ. (2004) Structure of the myelinated axon. In: Myelin Biology and its disorders. R.A. Lazzarini. San Diego: Elsevier Academic.
- Traka M, Goutebroze L, Denisenko N, Nifli A, Havaki S, Iwakura Y, Fukamauchi F, Watanabe K, Soliven B, Girault JA, and Karagoges D. (2003) Association of TAG-1 with Caspr2 is essential for the molecular organization of juxtaparanodal regions of myelinated fibers. *J Cell Biol* 162: 1161-1172.
- Tuvia S, Garver TD, and Bennett V. (1997) The phosphorylation state of the FIGQY tyrosine of neurofascin determines ankyrin binding activity and patterns of cell segregation. *Proc Natl Acad Sci USA* 94: 12957-12962.
- Ushiki T, and Ide C. (1987) Scanning electron microscopic studies of the myelinated nerve fibres of the mouse sciatic nerve with special reference to the Schwann cell cytoplasmic network external to the myelin sheath. *J Neurocytol* 16: 737-747.
- Vabnick I, Novakovic SD, Levinson SR, Schachner M, and Shrager P. (1996) The clustering of axonal sodium channels during development of the peripheral nervous system. *J Neurosci* 16**:** 4914-4922.
- Vabnick I, Trimmer JS, Schwarz TL, Levinson SR, Risal D, and Shrager P. (1999) Dynamic potassium channel distributions during axonal development prevent aberrant firing patterns. *J Neurosci* 19: 747-758.

- Vagnerova K, Tarumi YS, Proctor TM, and Patton BL. (2003) A specialized basal lamina at the node of Ranvier. Abstract 351.18 at *Soc for Neurosci Meeting*.
- Vainzof M, Marie SK, Reed UC, Schwartzman JS, Pavanello RC, Passos-Bueno MR, and Zatz M. (1995) Deficiency of merosin (laminin M or a α2) in congenital muscular dystrophy associated with cerebral white matter alterations. *Neuroped* 26: 293-297.
- Verheijen MHG, Camargo N, Verdier V, Nadra K, de Preux Charles A-S, Médard J-J, Luoma A, Crowther M, Inouye H, Shimano H, Chene S, Brouwers JF, Helms B, Feltri ML, Wrabetz L, Kirschner D, Chrast R, and Smit AB. (2009) SCAP is required for timely and proper myelin membrane synthesis. *Proc Natl Acad Sci USA* 106(50): 21383-21388.
- Vizoso AD, and Young JZ. (1948) Internode length and fibre diameter in developing and regenerating nerves. *J Anat* 82: 110-134.
- Vizoso AD. (1950) The relationship between internodal length and growth in human nerves. *J Anat* 84: 342-353.
- Voas MG, Lyons DA, Naylor SG, Arana N, Rasband MN, and Talbot WS. (2007) αII-spectrin is essential for assembly of the nodes of Ranvier in myelinated axons. *Curr Biol* 17: 562-568.
- Voyvodic JT. (1989) Target size regulates calibre and myelination of sympathetic axons. *Nature* 342: 430-433.
- Wang H, Kunkel DD, Martin TM, Schwartzkroin PA, and Tempel BL. (1993) Heteromultimeric K^+ channels in terminal and juxtaparanodal regions of neurons. *Nature 365*: 75-79.
- Webster HD. (1971) The geometry of peripheral myelin sheaths during their formation and growth in rat sciatic nerves. *J Cell Biol* 48: 348-367.
- Webster HD, Martin R, and O'Connell MF. (1973) The relationships between interphase Schwann cells and axons before myelination: a quantitative electron microscopic study. *Dev Biol* 32: 401-416.

- Webster HD, Frail DE, and Favilla JT. (1984) In *Peripheral Neuropathy* 2nd ed. Eds Dyck PJ, Thomas PK, Lambert EH, and Bunge RP. 329 (W. B. Saunders, Philadelphia).
- Weiner JA, and Chun J. (1999) Schwann cell survival mediated by the signaling phospholipid lysophosphatidic acid. *Proc. Natl Acad. Sci. USA* 96: 5233-5238.
- Wiley CA, and Ellisman MH. (1980) Rows of dimeric particles within the axolemma and juxtaposed particles within glia, incorporated into a new model for the paranodal glial-axonal junction at the nodes of Ranvier. *J Cell Biol* 84: 261-280.
- Williamson RA, Henry MD, Daniels KJ, Hrstka RF, Lee JC, Sunada Y, Ibraghimov-Beskrovnaya O, and Campbell KP. (1997) Dystroglycan is essential for early embryonic development: disruption of Reichert's membrane in *Dag1*-null mice. *Hum Mol Genet* 6: 831-841.
- Wittmack EK, Rush AM, Craner MJ, Goldfarb M, Waxman SG, and Dib-Hajj SD. (2004) Fibroblast growth factor homologous factor 2B: association with Nav1.6 and selective co-localization at nodes of Ranvier of dorsal root axons. *J Neurosci* 24: 6765-6775.
- Xiao ZC, Ragsdale DS, Malhotra JD, Mattei LN, Braun PE, Schachner M, and Isom LL. (1999) Tenascin-R is a functional modulator of sodium channel β subunits. *J Biol Chem* 274: 26511-26517.
- Xu H, Wu XR, Wewer UM, and Engvall E (1994) Murine muscular dystrophy caused by a mutation in the laminin α2 (*Lama2*) gene. *Nat Genet* 8: 297-302.
- Yamada H, Shimizu T, Tanaka T, Campbell KP, and Matsumura K. (1994) Dystroglycan is a binding protein of laminin and merosin in peripheral nerve. *FEBS Lett* 352: 49-53.
- Yamada H, Denzer AJ, Hori H, Tanaka T, Anderson LVB, Fujita S, Fukuta-Ohi H, Shimizu T, Ruegg MA, and Matsumura K. (1996)

Dystroglycan is a dual receptor for agrin and laminin-2 in Schwann cell membrane. *J Biol Chem* 271(38): 23418-23423.

- Yamada H, Saito F, Fukuta-Ohi H, Zhong D, Hase A, Arai K, Okuyama A, Maekawa R, Shimizu T, and Matsumura K. (2001) Processing of β-dystroglycan by matrix metalloproteinase disrupts the link between the extracellular matrix and cell membrane via the dystroglycan complex. *Hum Mol Genet* 10: 1563-1569.
- Yang D, Bierman J, Tarumi YS, Zhong YP, Rangwala R, Proctor TM, Miyagoe-Suzuki Y, Takeda S, Miner JH, Sherman LS, Gold BG, and Patton BL. (2005) Coordinate control of axon defasciculation and myelination by laminin-2 and -8. *J Cell Biol* 168: 655-666.
- Yang J-F, Cao G, Koirala S, Reddy LV, and Ko C-P. (2001) Schwann cells express active agrin and enhance aggregation of acetylcholine receptors on muscle fibers. *J Neurosci* 21(24): 9572-9584.
- Yang Y, Lacas-Gervais S, Morest DK, Solimena M, and Rasband MN. (2004) βIV spectrins are essential for membrane stability and the molecular organization of nodes of Ranvier. *J Neurosci* 24: 7230-7240.
- Yoshida-Moriguchi T, Yu L, Stalnaker SH, Davis S, Kunz S, Madson M, Oldstone MBA, Schachter H, Wells L, and Campbell KP. (2010) O-mannosyl phosphorylation of α-dystroglycan is required for laminin binding. *Science* 327: 88-92.
- Yu WM, Feltri ML, Wrabetz L, Strickland S, and Chen ZL. (2005) Schwann cell-specific ablation of laminin γ1 causes apoptosis and prevents proliferation. *J Neurosci* 25: 4463-4472.
- Yurchenco PD, Quan Y, Colognato H, Mathus T, Harrison D, Yamada Y, and O'Rear JJ. (1997) The α chain of laminin 1 is independently secreted and drives secretion of its β and γ chain partners. *Proc Natl Acad Sci USA* 94: 10189-10194.
- Yurchenco PD, and Patton BL. (2009) Developmental and pathogenic

mechanisms of basement membrane assembly. *Curr Pharm Des* 15(12): 1277-1294.

- Zalc B, and Colman DR. (2000) Origin of vertebrate success. *Science* 288: 271-272.
- Zalc B, Goujet D, and Colman DR. (2008) The origin of the myelination program in vertebrates. *Curr Biol* 18(12): 511-512.
- Zhang X, Davis JQ, Carpenter S, and Bennett V. (1998) Structural requirements for association of neurofascin with ankyrin. *J Biol Chem* 273: 30785-30794.
- Zhong D, Saito F, Saito Y, Nakamura A, Shimizu T, and Matsumura K. (2006) Characterization of the protease activity that cleaves the extracellular domain of β-dystroglycan. *Biochem Biophys Res Commun* 345: 867-871.
- Zhou L, Zhang CL, Messing A, and Chiu SY. (1998) Temperature-sensitive neuromuscular transmission in Kv1.1 null mice: role of potassium channels under the myelin sheath in young nerves. *J Neurosci* 18: 7200-7215.
- Zhou W, and Goldin AL. (2004) Use-dependent potentiation of the Nav1.6 sodium channel. *J Biophys* 87: 3862-3872.
- Zhou Z, Wang J, Cao R, Morita H, Soininen R, Chan KM, Liu B, Cao Y, and Tryggvason K. (2004.) Impaired angiogenesis, delayed wound healing and retarded tumor growth in perlecan heparin sulfate-deficient mice. *Cancer Res* 64: 4699-4702.
- Zimmermann H. (1996) Accumulation of synaptic vesicle proteins and cytoskeletal specializations at the peripheral node of Ranvier. *Microsc Res Tech* 34: 462-473.

Scope of the thesis

The general aim of this thesis is to examine how the laminin receptor dystroglycan can regulate different aspects of Schwann cell architecture and peripheral nerve function. By pairing with different dystrophin-like proteins (utrophin, Dp116 and DRP2), cytoskeletal and cytoskeletal-adaptor proteins (actin) and extracellular-matrix ligands (laminins, agrin and perlecan), dystroglycan forms complexes that are differently localized throughout the nerve and that may have specific functions in radial sorting, compartmentalization of the myelinated fiber and organization of nodes of Ranvier.

In the present thesis I will focus on the role of Schwann cell dystroglycan in nodal architecture (1), and I will analyze how DG cleavage by matrix metalloproteinases 2 and 9 (MMP-2 and MMP-9) can regulate Schwann cell cytoplasm compartmentalization and internodal lenght in both physiological and pathological conditions (2).

These two sub-projects have the following specific objectives:

1. To understand if the defect in Nav clustering at nodes of Ranvier in the absence of dystroglycan is developmentally-determined or acquired with age; to unravel the mechanism/s through which Schwann cell dystroglycan aids Nav clustering (Chapter 2).
2. To understand if post-translational modification of dystroglycan by metalloproteainases 2 and 9 can alter the compartmentalization of Schwann cell cytoplasm and how this influence the Schwann cell phenotype in physiological

conditions; to evaluate if the ablation of MMP9, which is elevated in nerves of dystrophic mice (model of MDC1A), could ameliorate the peripheral neuropathy (Chapter 3).

Dystroglycan is required to build the normal architecture of peripheral nodes of Ranvier.

Cristina Colombelli,[1] Desirée Zambroni,[1] Marilena Palmisano,[1] Simona Occhi,[1] Sophie Nicole,[2] Raija Soininen,[3] Elior Peles,[4] Lawrence Wrabetz,[1] M. Laura Feltri[1]

1 Division of Genetics and Cell Biology, San Raffaele Scientific Institute, 20132 Milan, Italy.
2 Inserm, U546, Univ Paris 06, Paris, France.
3 Oulu Center for Cell-Matrix Research, Biocenter Oulu, Department of Medical Biochemistry and Molecular Biology, University of Oulu, Finland.
4 Department of Molecular Cell Biology, The Weizmann Institute of Science, Rehovot 76100, Israel.

Manuscript in preparation.

Chapter 2

Dystroglycan is required to build the normal architecture of peripheral nodes of Ranvier

2.1 Introduction

Nodes of Ranvier are periodical interruptions of the myelin sheath, where the axolemma is endowed with high densities of voltage-gated Na^+ channels (Nav) that ensure the regeneration of action potentials during fast saltatory conduction (Ranvier, 1871; Hodgkin and Huxley, 1952). How the accumulation of Nav at these focal sites is achieved has been matter of several studies, especially in the last decade. Both *in vivo* and *in vitro* studies demonstrated that in the peripheral nervous system (PNS) nodes of Ranvier assembly is the result of a finely regulated interplay between the axolemma and the overlaying Schwann cell (Vabnick et al., 1996; Ching et al., 1999; Pedraza et al., 2001; Poliak and Peles, 2003; Salzer, 2003). One peculiarity of peripheral nodes is the presence of microvilli, interdigitating cytoplasmic processes that extend from the outer collars of two neighbouring Schwann cells and closely appose the nodal axolemma (Ichimura and Ellisman, 1991). Schwann cell microvilli are embedded within a nodal gap substance that is enriched in non-sulfated mucopolysaccharides, hyaluronic acid and proteoglycans, like versican V1 (Apostolski et al., 1994; Melendez-Vasquez et al., 2005), NG2 (Martin et al., 2001) and syndecan-3 and 4 (Goutebroze et al., 2005; Melendez-Vasquez et al., 2005). In addition, Schwann cells express gliomedin, a molecule that is shed from a transmembrane

precursor in a furin-dependent manner and is incorporated into the nodal gap substance forming a molecular complex with glial NrCAM and heparan sulfates (Eshed et al., 2007; Feinberg et al., 2010). During early postnatal development, gliomedin-positive microvilli align with node intermediates, known as heminodes, (Tao-Cheng and Rosenbluth, 1983; Melendez-Vasquez et al., 2001; Gatto et al., 2003; Eshed et al., 2005) and interactions between the lateral tips of Schwann cells and the axon trigger the clustering of axonal cell adhesion molecules important for Nav clustering. According to the current model, gliomedin induces the clearance of the axonal isoform of neurofascin (Nf186) from the internodal region, allowing its accumulation at nascent nodes (Feinberg et al., 2010; Zhang et al., 2012). Subsequently, Nf186 functions as a docking protein for the recruitment of ankyrin-G and the stable accumulation of βIV-spectrin and Nav. On the axonal side, Nf186 is the pioneer molecule that triggers Nav clustering, as mice lacking Nf186, exhibit severe nodal disorganization and are not able to cluster Nav (Sherman et al., 2005; Thaxton et al., 2011). On the glial side, although gliomedin and NrCAM are required for heminodal clustering, their absence does not hamper Nav cluster formation at mature nodes. It has been proposed that, at least *in vitro*, the establishment of paranodal junctions (PNJs) can overcome the absence of heminodal molecules, facilitating the formation of nodal Nav clusters by constraining mechanisms (Feinberg et al., 2010). Another possibility is that other glial cues may also contribute to Nav clustering at nodes and function in the absence of gliomedin.

A glial molecule related to Nav clustering is dystroglycan (DG). DG comprises a α-subunit that mediates binding to laminins, agrin and perlecan in the basal lamina, and a transmembrane β-subunit linked to the cytoskeleton through different dystrophin isoforms or homologues. We previously reported that Schwann cell dystroglycan is enriched at microvilli, where its major intracellular partner is the 116 kDa dystrophin isoform, Dp116, whereas laminin 211 and laminin 511 are enriched in the basal lamina over nodes (Occhi et al., 2005). Schwann cell-specific ablation of *Dag-1* results in reduced conduction velocity, abnormal clustering of Nav and disorganization of microvilli (Saito et al., 2003). Although to a lesser extent, similar alterations were found in mice lacking laminins from Schwann cells and in a merosin deficient muscular dystrophy (MDC1A) patient (Occhi et al., 2005). However, the analysis of dystroglycan deficient mice did not reveal if DG is required for the formation of Nav clusters or if it is mainly involved in their maintenance. Furthermore, the mechanism through which this occurs is still unclear.

Here we show that dystroglycan is polarized immediately to nascent nodes and heminodes, where it is required for the formation of thight Nav clusters. In addition we observe by immunoelectron microscopy that α- and β-DG are localized at Schwann cell microvilli facing both the basal lamina and the nodal gap substance, suggesting a mechanism of action that involves interactions at both sides. Indeed, we found that dystroglycan is necessary to localize perlecan at nodes of Ranvier, which suggests a potential role for this interaction in gliomedin incorporation in the nodal gap and subsequent Nav clustering. However, the analysis of two perlecan mutant mice did not reveal any

alterations in either gliomedin accumulation or Nav clustering, possibly because of compensatory mechanisms by other heparan sulfate proteoglycans (HSPGs). Finally, we find that similarly to gliomedin, the N-terminal domain of α-DG (α-DG-N) is shed from cultured Schwann cells by a furin protesase and it can bind myelinating axons in an *in vitro* system, suggesting that it may have a role in facilitating Nav clustering.

2.2 Materials and Methods

Mice. The following mice lines were used: *dag1*$^{flox/flox}$//P0Cre (from now on referred to as dgko) (Saito et al., 2003), *caspr* null (*caspr*$^{-/-}$) (Gollan et al., 2003), *Hspg2*$^{\Delta 3/\Delta 3}$ (Rossi et al., 2003), *Hspg2* $^{KI/+}$ and *Hspg2* $^{KI/KO}$ (Stum et al., 2008). Dgko mice were produced by crossing P0Cre transgenic mice (mPoTOTCre) (Feltri et al., 1999) with dystroglycan-floxed mice (Moore et al., 2002) and were maintained by backcrosses with C57BL6/N (Charles River). *Caspr* null mice were gently provided by E. Peles (Weizmann Institute of Science, Rehovot, Israel) and were maintained by backcrosses with ICR. Double mutant dgko//*caspr*$^{-/-}$ mice were obtained by crossing heterozygous *caspr*$^{+/-}$ with *dag1*$^{flox/flox}$//P0Cre and intercrossing *dag1*$^{flox/+}$//P0Cre//*caspr*$^{+/-}$. Double knock outs were obtained with a Mendelian ratio. The analysis of dgko//*caspr*$^{-/-}$ mice was done in F1 ICR//C57Bl6/N mixed background.

In addition, Spraw-Dawley rats were used. Experiments were approved by the San Raffaele Institutional Animal Care and Use Committee and complied with NIH guidelines.

Primary/secondary antibodies and dyes. Primary antibodies included the following: rabbit anti-caspr (6061; 1:800), mouse anti-caspr (M275; 1:1), rabbit anti-olfactomedin (Ab320; 1:1000), rabbit anti-gliomedin (Ab720; 1:200) and mouse anti-gliomedin (Mab94; 1:50) (all generous gifts from E. Peles, Weizmann Institute of Science, Rehovot, Israel), mouse anti-β-dystroglycan (43DAG/8D5; Novocastra) (1:50 for IF; 1:80 for WB), mouse anti-glycosylated α-dystroglycan (IIH6) (1:100 for IF; 1:1000 for WB) (generous gift from K.P. Campbell, University of Iowa, Iowa City, IA), rabbit anti-α-DG-N (API528; 1:70 for WB) (generous gift from F. Saito, Teikyo University, Tokyo, Japan), mouse anti-Dp116 (Mandra1; Sigma) (1:100 for IF; 1:1500 for WB), rabbit anti-ezrin (1:30) (Upstate), rabbit anti-ERM and rabbit anti-ERM-P (1:50 for IF; 1:1000 for WB) (Cell Signaling), mouse anti-Nav pan (1:100) (K58/35; Sigma), rabbit anti-Nav1.6 (generous gift from J. Trimmer, University of California, Davis, CA), rabbit anti-agrin (AS204; 1:100) (generous gift from M. Ruegg, Biozentrum, University of Basel, Basel), rat anti-perlecan (1:100) (A7L6; Chemicon), rabbit anti-syndecan-3 (Abcam), rat anti-neurofilament-H (TA51, 1:20) (generous gift from V. Lee, University of Pennsylvania, PA), rabbit anti-S100 (1:200) (Dako), rabbit anti-neurofascin pan (NFC2199; 1:4000) (generous gift from P.J. Brophy, University of Edinburgh, Edinburgh, UK), mouse anti-β-tubulin (1:1000) (Sigma), rabbit anti-calnexin (1:3000 for WB) (Sigma), rabbit anti-laminin α5 (1:500 for IF; 1:1000 for WB) (generous gift from L. Sorokin, University of Muenster, Muenster, Germany). Secondary antibodies included the following: donkey anti-rabbit FITC (1:200), goat anti-rabbit DyLight™488 (1:1000), donkey anti-rat

FITC (1:200), goat anti-rat Cy5 (1:200) and goat anti-human IgGFc-specific Rhodamine (Jackson ImmunoResearch), goat anti-mouse TRITC (1:200) and goat anti-mouse IgG2a-specific FITC (1:200) (Southern Biotech), goat anti-mouse IgM TRITC (Nordic), goat anti-mouse IgGFab-specific or goat anti-mouse IgGFc-specific HRP (1:5000) (Sigma), goat anti-rabbit HRP (1:10000). Nuclei were stained with 4,6-diamidino-2-phenylindole (DAPI; Sigma).

Western blot analysis. Sciatic nerves were dissected from rats or mice, frozen and homogenized in a metal pestle and then lysed with lysis buffer containing 25 mM Tris, pH 7.4, 95 mM NaCl, 10 mM EDTA, pH 8, 2% SDS, 1 mM NaF, 1 mM Na_3VO_4, and 1% protease inhibitor cocktail (PIC; Sigma). After rocking at 4°C for 30 minutes, samples were spun at 13,200 rpm in a microcentrifuge for 10 min to eliminate insoluble material. The supernatant was recovered and stored at -80°C until use. Protein concentration was determined by BCA protein assay kit (Pierce) according to the manufacturer's instructions. Equal amounts of homogenates (containing 5-30 µg of protein) were brought up to 10 µl with lysis buffer to which was added 4.5 µl reducing sample buffer (150 mM TrisHCl, pH 6.8, 6% SDS, 0.3% bromophenol blue, 30% glycerol, 0.08 M DTT). The samples were denatured, resolved on 5-12% SDS-polyacrylamide gels and electroblotted onto a polyvinylidene fluoride microporous membrane (PVDF; PerkinElmer). To verify equal loading of proteins, membranes were stained with ponceau red. Blots were blocked with 0.1% Tween, 5% dry milk in PBS, and incubated with the appropriate antibody in 0.1% Tween, 1% dry milk in PBS. Peroxidase (HRP)-

conjugated secondary antibodies were visualized using the ECL method with autoradiography films (Amersham Biosciences). Some blots were checked directly for equal loading by amido black staining after antibody experiments were completed.

Immunofluorescence on teased nerve fibers. Sciatic nerves were dissected and immersion fixed in 4% paraformaldehyde for 30 min. For immunofluorescence on unfixed tissues, nerves were washed in PBS after dissection and teased immediately. Perineurium was removed, nerve fiber bundles were separated through stainless steel needles, and teased individually on a PBS drop in 3-aminopropyltriethoxysilane (TESPA; Sigma)-coated slides. After permeabilization in pre-chilled acetone or methanol for 5-10 min, teased fibers were blocked and permeabilized with 0.5% TritonX-100, 5% fish skin gelatine (Sigma) in PBS for 1 h at RT. Primary antibodies were applied in the same blocking solution overnight at 4°C in a humid chamber. After washes in Tris buffer saline (TBS, pH 7.4), appropriate secondary antibodies were applied for 1 h at RT, and nuclei stained with DAPI. Slides were air-dried, mounted with Vectashield (Vector Labs, Burlingame, CA), and analyzed with a Leica DM 5000B microscope or a confocal microscope. Nonspecific background staining was determined in every experiment by omitting the primary antibody and no background staining over tissue autofluorescence was detected with any of the antibodies used in this study.

Image acquisition. Immunofluorescence stainings of teased fibers

were imaged using a microscope confocal system [UltraView ERS spinning disk confocal microscope (PerkinElmer) equipped with a Plan Apochromat 63Å~/1.4 oil-immersion objective and using the UltraView ERS acquisition software]. FITC, TRITC, cy-5 fluorophores were excited with an Ar laser (488 nm), a He/Ne laser (568 nm) and a Red Diode laser (640 nm), respectively. In addition a Confocal-MRC 1024 laser-scanning confocal microscope (Bio-Rad Laboratories, Inc.), equipped with a Plan Neofluar 40Å~/1.3 oil-immersion objective and using the Laser Sharp 2000 acquisition software, was used occasionally. Figures were mounted using Photoshop software (Adobe). To quantify the frequency of abnormal Nav clusters, images were photographed using Leica TCS-SP2 confocal fluorescence microscope equipped with a Plan Apochromat 63Å~/1.4 oil-immersion objective and using the LCS confocal acquisition software (Leica). The gain of Nav fluorescence detection was maintained below the threshold of fluorochrome saturation. *z*-axis-series spanning around ~ 3.0 μm were acquired as 1024x1024 pixels images by sequentially scanning (between frames), using a step size of 0.1221 μm.

Electron microscopy. Electron microscopy was performed as described previously (Wrabetz et al., 2000).

Immunoelectron microscopy (IEM). Adult wt and DG deficient mice (used as negative controls) were anaesthetized intraperitoneally with 2,2,2-tribromoethanol (0.4 mg/g) and perfused with 4% paraformaldehyde/0.05% glutaraldehyde in 0.01M sodium periodate,

0.1M lysine, 3% sucrose in 0.1M phosphate buffer pH7.4. Sciatic nerves were dissected, fixed for 2 h, and left overnight in 3.5% sucrose in 0.1M phosphate buffer. Tissues were processed at 4°C as follows (modified from Scherer et al., 1995): they were stained with 0.25% tannic acid for 1 hour, quenched in 50mM NH_4Cl, washed in 4% sucrose in 0.1M maleate buffer (pH 6.2), followed by 1% uranyl acetate in maleate buffer for 1 h, dehydrated to 90% ethanol, then infiltrated first with 1:1 ratio of L.R.Gold (Polysciences)/ethanol, then with a 7:3 ratio of L.R.Gold/ethanol, followed by two changes of L.R.Gold for 1 h and overnight. The day after the tissues were infiltrated in L.R.Gold with 0.5% benzoin methyl ether for 1 h and then overnight, embedded in gelatin and polymerized by UV irradiation (365 nm) for 48 h at -20°C. Nerves were cut longitudinally and sections were collected on nickel formward/carbon grids, and stained according to the method of Nico et al. (Nico et al., 2010). The sections were incubated with TBS for 10 min at RT, and treated with 0.1% trypsin in TBS for 4 min. After washing in TBS and blocking with 1% BSA in TBS for 10 min at RT, sections were incubated with mouse anti-α-DG IgM antibody (IIH6; 1:100) or mouse anti-β-DG antibody (43DAG1/8D5; 1:1), rinsed with TBS, and incubated with a 10 nm gold particles-conjugated secondary antibody (British BioCell; 1:100). After staining, grids were washed on drops of TBS and dH_2O and stained with saturated uranyl acetate and lead citrate. Images were taken using a LEO 912AB Transmission Electron Microscope. This work was performed by Desirée Zambroni in the lab.

Cell culture. Schwann cells (SCs) were isolated from the sciatic nerves of 3 day old Sprague-Dawley rats stripped of perineurium using 1% collagenase and 0.25% trypsin (Brockes et al., 1979). They were expanded on poly-L-lysine-coated 100 mm^2 tissue culture plates in Dulbecco's Modified Eagle Medium (DMEM), supplemented with 10% heat-inactivated fetal calf serum (FCS), 2 μM forskolin (Fsk; Calbiochem) and 2 ng/ml of soluble NRG1-β1 (R&D Systems) (Porter et al., 1986). The cells were refed every 3-4 days and subcultured every 7 days. For pharmacological treatment, SCs were plated at $35x10^4$ on poly-L-lysine-coated 6-well plates and treated with 20 μM Furin inhibitor I (Dec-RVKR-CMK; Calbiochem) for 48 hours. Then cells were scraped and proteins extracted on ice with lysis buffer (25 mM Tris pH 7.4, 95 mM NaCl, 10 mM EDTA, 2% SDS, 1 mM NaF, 1 mM Na_3VO_4, with PIC) as described above.

Production of Fc-fusion proteins and binding experiments. 293FT cells were transfected with plasmids encoding DG-Fc2, DG-Fc5, DG-Fc6 and gliomedin Olf-Fc and ECD-Fc fusion proteins (gifts of K.P. Campbell and E. Peles; Kanagawa et al., 2004; Eshed et al., 2005) in media containing DMEM, 1% Ultra-Low IgG FBS (Invitrogen), and 2 mM L-glutamine. After 72 hours, the supernatants were collected and filtered, and Fc-proteins expression was confirmed by Western blotting. Binding experiments were performed using these Fc-fusion proteins on rat SCs, purified rat DRG neurons or rat SC-DRG neuron co-cultures. SCs were grown on poly-L-lysine-coated coverslips and incubated with conditioned media containing various Fc-fusions for 30 minutes at RT. Cells were then washed, fixed with 4%

paraformaldehyde for 5 min at RT and incubated with a Rhodamine-conjugated anti-human Fc antibody (Jackson Laboratories). Condition media containing DG-Fc2 and Olf-Fc were pre-clustered with the secondary antibody for 30 min before the binding procedure. After fixation for 15 min at RT, antibody labeling was performed: cells were washed with PBS and incubated in blocking solution [PBS, 10% normal goat serum (NGS), 0.1% Triton X-100, 1% glycine] for 30 min. Primary antibodies diluted in blocking solution were added for 1 h at RT, followed by washing with PBS and incubation with secondary antibodies diluted in blocking solution for 40 min. Coverslips were then washed, mounted in Vectashield and analyzed on a confocal microscope (UltraView ERS).

Organotypic neuron/SC co-cultures. Primary dorsal root ganglia (DRG) were dissected from embryos of 16.5 gestational days. Pregnant rats were euthanized by carbon dioxide, and the uterus removed using aseptic technique. Embryos were extracted and DRGs dissected out in L-15 (Leibovitz) medium as previously described (Einheber et al; 1997). One or two DRGs were seeded in coverslips coated with collagen in a drop of C-medium (MEM, 4g/L D-glucose, 10% FBS, 2 mM L-glutamine, 50 ng/ml NGF) plus 100 U/ml penicillin/100 µg/ml streptomycin for one night. The day after C-medium was replaced with supplemented NB medium (Neurobasal, 4g/L D-glucose, 2 mM L-glutamine, 50 ng/ml NGF, B27 supplement 1X). After one week, myelination was induced with 50 µg/ml ascorbic acid (Sigma-Aldrich). DRGs were maintained for 10-12 days with ascorbic acid before being processed for immunofluorescence and binding experiments as described above.

For the experiments in which isolated DRG neurons were used, purified DRGs were obtained cycling the cultures with NB and NBF (supplemented NB containing fluorodeoxyuridine 10 μM and uridine 10 μM) media.

2.3 Results

α- and β-dystroglycan are early markers of Schwann cell microvilli

α- and β-dystroglycan are found at nodes of Ranvier in rodent myelinated fibers. At these sites, the major intracellular partner of β-DG is dystrophin 116 kDa isoform (Dp116), whereas laminin 211 and 511 are enriched in the basal lamina over microvilli (Occhi et al., 2005). Previous studies have shown that genetic ablation of dystroglycan from Schwann cells causes a reduction in Nav clusters at peripheral nodes of Ranvier (Saito et al., 2003). In adult DG deficient mice Nav were smaller, less intense, abnormally shaped, and lacked definite corners (Occhi et al., 2005). From these studies however it was unclear if this abnormality was due to defective cluster formation during development, or to a degeneration of clusters that formed normally. Thus, we asked if dystroglycan polarization at nodes correlated with Nav cluster formation and/or to their maintenance. Double immunostaining of rat sciatic nerve teased fibers showed that both α- and β-DG co-localize with ezrin, an early marker of nodes of Ranvier, soon after birth (Fig. 1A-D, 1E-H). β-DG is polarized to nodes as early as ezrin: at postnatal day 2 (P2), 96.1% of ezrin-positive nodes are also positive for β-DG, at P5 the percentage increases to 96.9% to reach the 100% at P10 (Fig. 1I). α-DG is

polarized early to nodes as well (79.7% at P2, at 82.4% at P5 and 82.2% at P10), even if slightly later than β-DG (Fig. 1J).

Western blot analysis on sciatic nerve lysates confirmed that β-DG is present at P2, when it is already proteolitically cleaved by MMP-2 and -9, as evidenced by the presence of the cleaved 31 kDa form (β-DG_{31}) (Fig. 1J and Court et al., 2011). α-DG, recognized by a glyco-specific antibody (IIH6), increases its molecular weight from P2 to adulthood, suggesting that the extent of its glycosylation is regulated during development, as already known in nerve and other tissues (Martin, 2003; Cai et al., 2007; Court et al., 2011).

Dp116, but not laminin 511, is rapidly polarized at nodes during Nav cluster formation

We next evaluated if Dp116, the most abundant dystrophin isoform present in microvilli, and laminin 511, localized in the basal lamina over nodes and paranodes (Vagnerova et al., 2003; Occhi et al., 2005), are polarized in early node development. By Western blot analysis we confirmed previous data showing that Dp116 is expressed from P1 onwards in peripheral nerve (Fig. 2F; Cai et al., 2007). Dp116 is also polarized early at nodes, although later than the transmembrane receptor β-DG (the percentage of Dp116-positive nodes is lower than dystroglycan-positive nodes at P2, P5 and P10) (Fig. 2A-D, 2E). This may suggest that dystroglycan is first inserted in the membrane of Schwann cell microvilli and soon after Dp116 is recruited to the cytoplasm of Schwann cells at these sites. On the other hand, protein levels of laminin α5-chain are low at P5 and P10 and reach the maximum only in mature nerves, as shown by Western blot analysis

(Fig. S1D). Early in postnatal development (P2-P5) laminin α5-chain is found predominantly in perinuclear regions, and it acquires its mature localization only from P10 (Fig. S1A-C). Thus, differently from Dp116, laminin 511 is polarized at nodes of Ranvier after they are formed.

Fig. 1 (next page) **(A-D; I) β-DG is expressed and localized at nodes as early as the first nodal marker ezrin.** Images of sciatic nerve teased fibers from rats at postnatal age 2 (P2), 5 (P5), 10 (P10) and adult (Ad). **A-D**, Double immunostaining for β-DG (green; **A-D**) and the nodal marker ezrin (red; **A'-D'**). The merged confocal images are shown (**A''-D''**). Arrows indicate double positive nodes.
I, The graph summarizes data from P2 to adulthood. Data are plotted as a percentage of total sites present at each of the indicated day. Black bars, ezrin alone; gray bars, β-DG; white bars, both ezrin and β-DG. β-DG-positive nodes are 96.1% at P2, 96.9% at P5 and 100% at P10. Western blot for β-DG on rat sciatic nerve lysates at P2, P5, P10 and Ad.

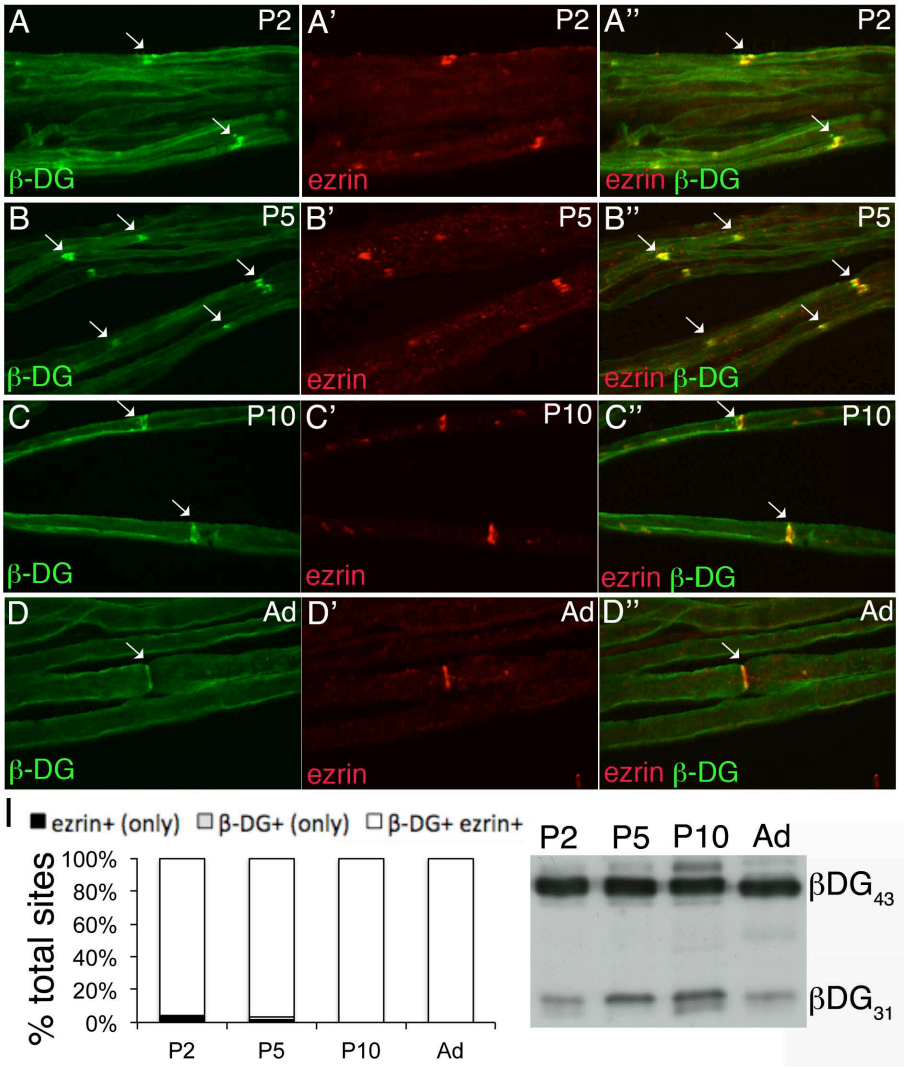
A
P2
β-DG
A'
P2
ezrin
A''
P2
ezrin β-DG
B
P5
β-DG
B'
P5
ezrin
B''
P5
ezrin β-DG
C
P10
β-DG
C'
P10
ezrin
C''
P10
ezrin β-DG
D
Ad
β-DG
D'
Ad
ezrin
D''
Ad
ezrin β-DG
I
ezrin+ (only)
β-DG+ (only)
β-DG+ ezrin+
% total sites
100%
80%
60%
40%
20%
0%
P2
P5
P10
Ad
P2
P5
P10
Ad
βDG43
βDG31

Fig. 1 (next page) **(E-H; J) α-DG is expressed and localized at nodes immediately after ezrin during postnatal development.** Images of sciatic nerve teased fibers from rats at P2, P5, P10 and adult (Ad). **E-H**, Double immunostaining for α-DG (red) and the nodal marker ezrin (green; **E'-H'**). The merged confocal images are shown (**E''-H''**). Arrows indicate double positive nodes, asterisks α-DG-negative nodes. Scale bar, 35 μm.

J, Black bars, ezrin alone; gray bars, α-DG alone; white bars, both ezrin and α-DG. α-DG-positive nodes are 79.7% at P2, 82.4% at P5 and 82.2% at P10. Western blot for α-DG on sciatic nerve lysates at P2, P5, P10 and Ad. Equal loading was verified by calnexin (clnx).

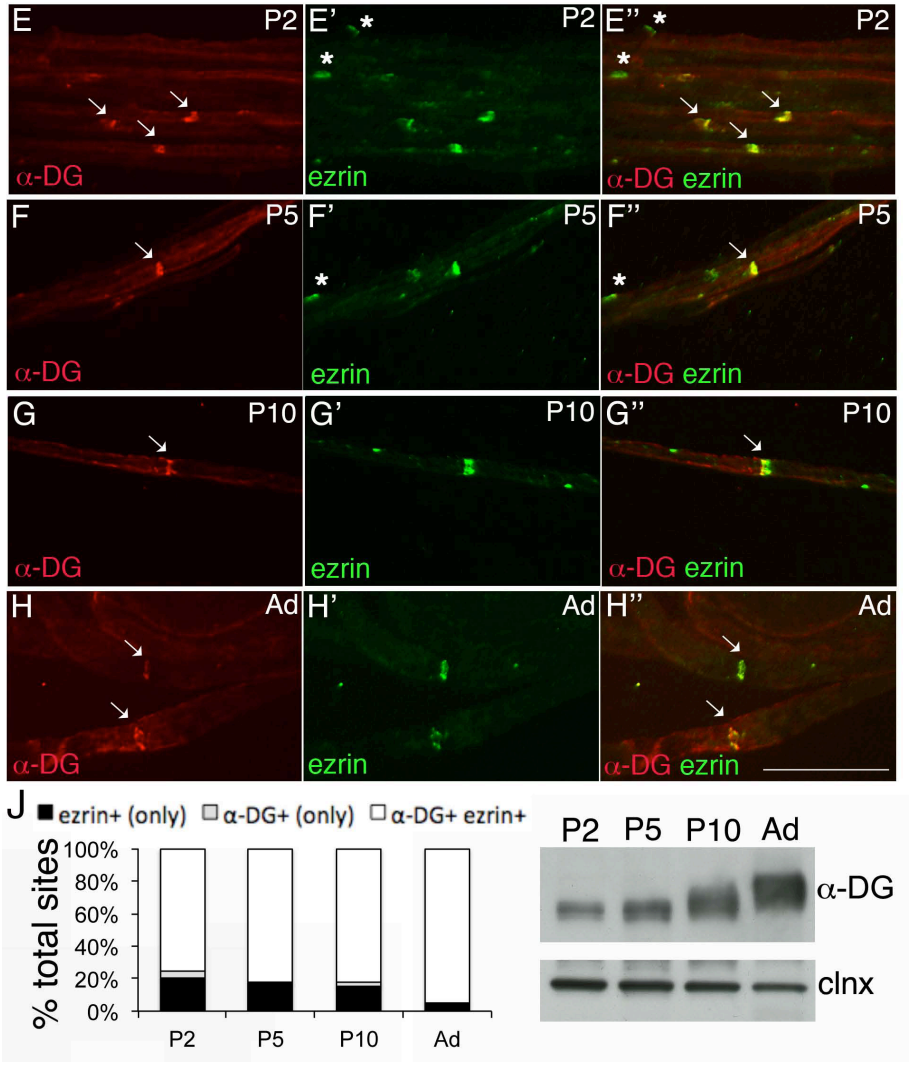
E
P2
α-DG
E'
P2
ezrin
E''
P2
α-DG ezrin
F
P5
α-DG
F'
P5
ezrin
F''
P5
α-DG ezrin
G
P10
α-DG
G'
P10
ezrin
G''
P10
α-DG ezrin
H
Ad
α-DG
H'
Ad
ezrin
H''
Ad
α-DG ezrin
J
ezrin+ (only)
α-DG+ (only)
α-DG+ ezrin+
% total sites
100%
80%
60%
40%
20%
0%
P2
P5
P10
Ad
P2 P5 P10 Ad
α-DG
clnx

Fig. 2 (next page) **Dp116 is localized at nodes early, immediately after ezrin, during node formation.** Images of sciatic nerve teased fibers from wild type rats at P2, P5, P10 and in adulthood (Ad). **A-D**, Double immunostaining for Dp116 (green; **A'-D'**) and the nodal marker ezrin (red; **A-D**). The merged confocal images are shown (**A''-D''**). Arrows indicate double positive nodes, asterisks Dp116-negative nodes. **E**, The graph summarizes data from P2 to the adult. Black bars, ezrin alone; gray bars Dp116 alone; white bars, both ezrin and Dp116. Dp116-positive nodes are 63.3% at P2, 76.8% at P5 and 97.4% at P10. **F**, Western blot on sciatic nerve lysates at P2, P5, P10 and adulthood (Ad) for Dp116 (116 kDa). Equal loading was verified by β-tubulin (β-tub).

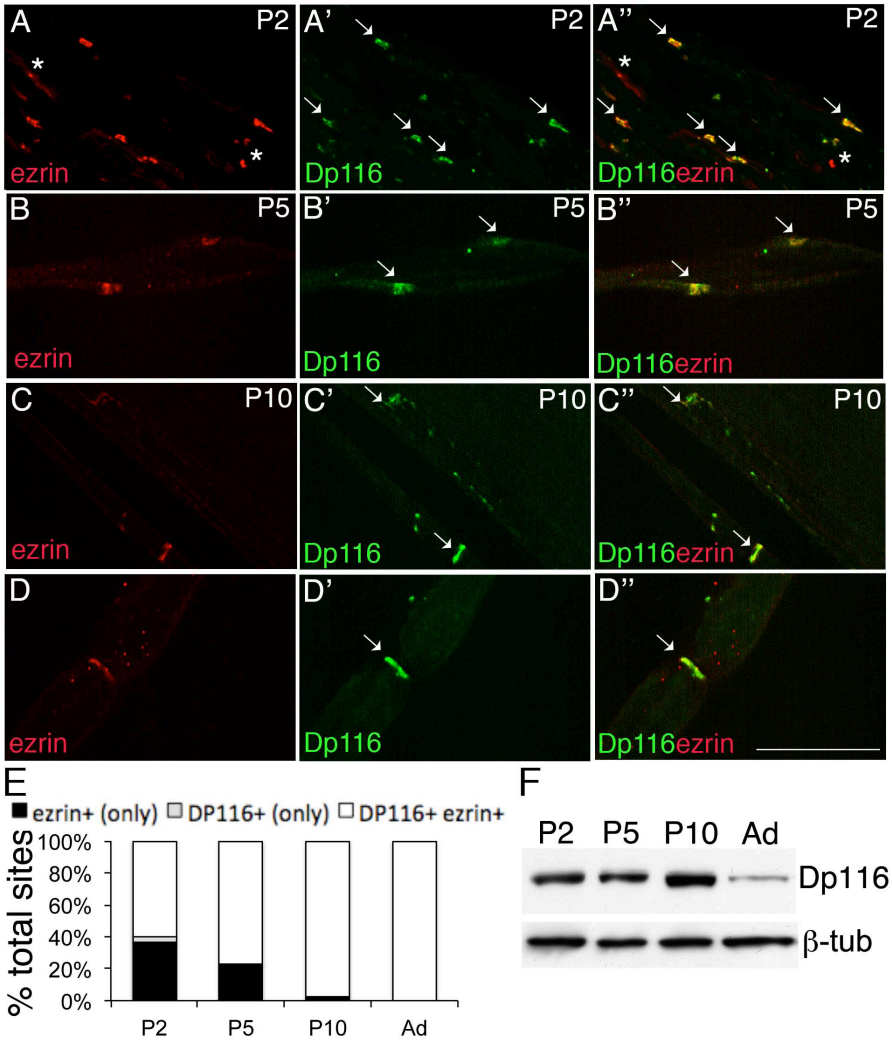
A
P2
ezrin
A'
P2
Dp116
A''
P2
Dp116ezrin
B
P5
ezrin
B'
P5
Dp116
B''
P5
Dp116ezrin
C
P10
ezrin
C'
P10
Dp116
C''
P10
Dp116ezrin
D
ezrin
D'
Dp116
D''
Dp116ezrin
E
ezrin+ (only)
DP116+ (only)
DP116+ ezrin+
% total sites
100%
80%
60%
40%
20%
0%
P2
P5
P10
Ad
F
P2
P5
P10
Ad
Dp116
β-tub

Fig. S1 (next page) **Laminin 511 polarization around nodes follows Nav and gliomedin clustering during early nerve development.** Images of sciatic nerve teased fibers from rats at P5, P10 and adult (Ad). **A-C**, Double immunostaining for laminin α5 (green; **A-C**) and the nodal marker gliomedin (red; **B'-C'**). The merged confocal images are shown at the right (**A''-C''**). Nuclei are stained with DAPI (blue). Arrows indicate double-positive nodes, asterisks perinuclear staining. Scale bar, 17.5 μm. **D**, Western blot analyis for laminin α5-chain on sciatic nerve lysates at P5, P10 and adulthood (Ad). The 450 kDa α5-chain is of the expected size. Smaller α5-immunoreactive bands (380, 320, and 210 kDa), representing post-translationally cleaved forms, were also detected. For comparison, the same blot was incubated with anti-laminin α2-chain antibody (320 kDa). Equal loading was verified by β-tubulin (β-tub).

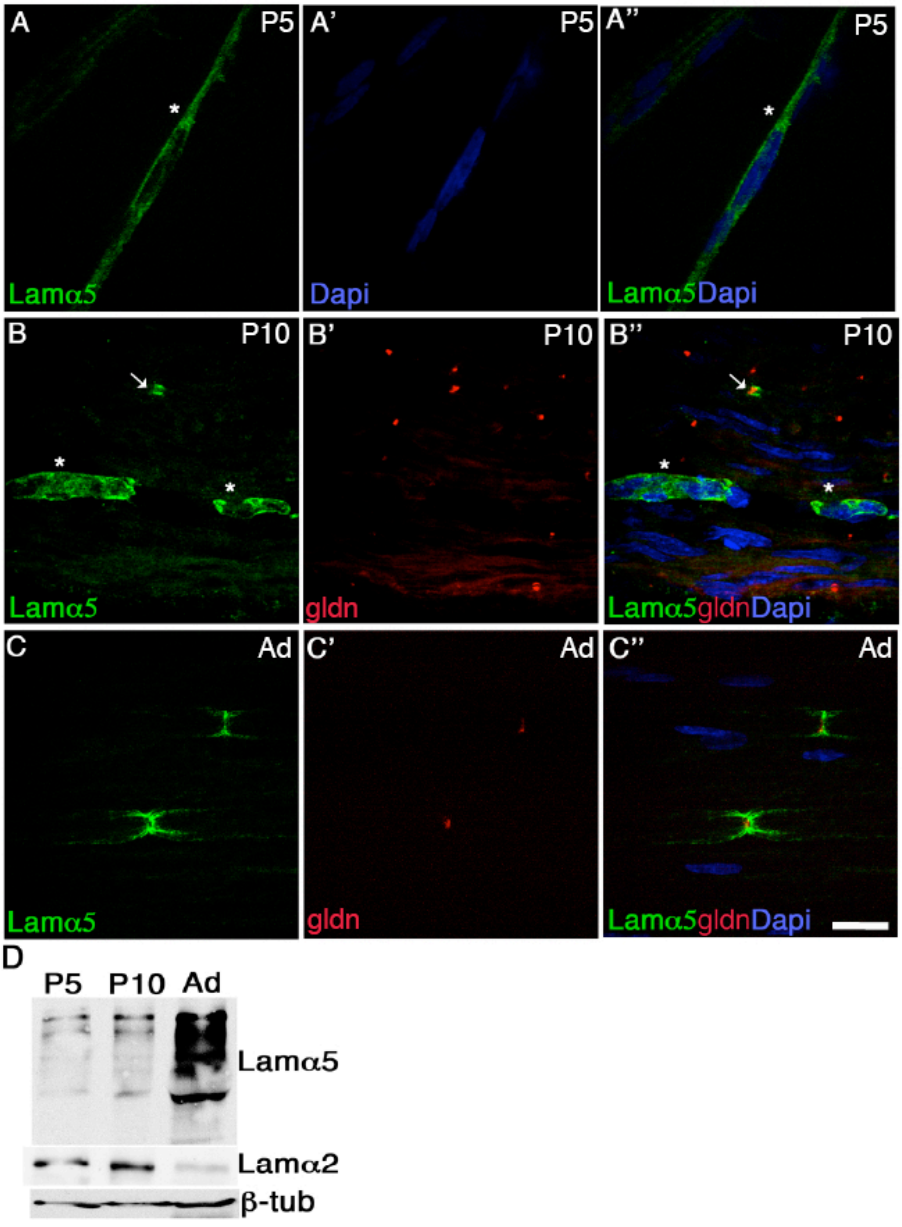
A
P5
Lamα5
A'
P5
Dapi
A''
P5
Lamα5Dapi
B
P10
Lamα5
B'
P10
gldn
B''
P10
Lamα5gldnDapi
C
Ad
Lamα5
C'
Ad
gldn
C''
Ad
Lamα5gldnDapi
D
P5
P10
Ad
Lamα5
Lamα2
β-tub

Absence of dystroglycan does not interfere with the timing of Nav cluster formation

To understand if dystroglycan is involved in Nav cluster formation, we asked if Nav clusters formed in a timely manner when DG is ablated from Schwann cells. Counting the number of clusters flanked by caspr-positive paranodes at different postnatal days (P2, P5 and P10), we found that at each time point the number of clusters per field of view was similar in DG deficient and wild type animals (Fig. 3A). Therefore, the absence of dystroglycan does not affect the timing of cluster formation, contrary to what happens in other nodal mutants such as NrCAM deficient mice, in which a slight delay of Nav clusters appearence was reported (Custer et al., 2003).

Newly formed clusters are already abnormal in the absence of dystroglycan

To understand whether dystroglycan is required for clusterization of newly formed clusters or for their maintenance in time, we evaluated the morphology of newly formed Nav clusters in early postnatal development. Sciatic nerve fibers from P4 and P7 mutant and control mice were immunostained with an antibody recognizing all the isoforms of Nav (anti-panNav). To quantify the frequency of abnormal clusters, the Nav cluster staining at the node was classified as normal (rectangular, with square corners and normal width) or abnormal (irregularly shaped and lacking square corners, diffuse and long, low intensity in every optical plane, or difficult to put into focus, see fig. 3B); the analysis was performed blindly by two independent investigators, as previously described (Occhi et al., 2005). Whereas

clusters in wt animals were rectangular and had square corners, DG deficient clusters were irregular and lacked definite corners both at P4 and P7, like in adult mice (Fig. 3B). When counted blindly, abnormal clusters were significantly more frequent in mutant than in control mice (79% of dgko nodes at P4 and 76% of dgko nodes at P7, vs 23% and 24% of wt nodes at P4 and P7 respectively; $p < 0.001$ by χ^2 test) (Fig. 3B). Thus, DG is required for proper clusterization of nascent Nav channels, not for their maintenance.

Proper heminodal clustering of Nav requires dystroglycan

During early development Nav are first clustered at heminodes located at the tips of myelinating Schwann cells, bordering each myelin segment. Longitudinal growth of the glial processes displaces these heminodal clusters, bringing them closer together until they fuse and form a single focal node (Rasband et al. 1999; Boiko et al., 2001). It has been shown that gliomedin, a component of the nodal matrix that binds neurofascin 186 and NrCAM, is required for formation of these heminodal clusters (Feinberg et al., 2010). To understand if dystroglycan is involved in the initial Nav clustering also at the level of heminodes, we examined Nav clusters in the developing sciatic nerve of wt and DG deficient mice at P6, a time when both nodes and heminodes can be detected (Schafer et al., 2006) (Fig. 3C). Two independent investigators counted Nav heminodal clusters (identified by the presence of one flanking capsr-positive paranode) and classified them as normal or abnormal/absent. Although some abnormally shaped clusters were occasionally found also in wt because of the handling of fibers during teasing, the frequency of

abnormal or absent clusters was significantly higher in mutants than controls (40% in dgko vs 14% in wt; $p < 0.001$ by χ^2 test). This result suggests that proper heminodal, not only nodal, clustering of Nav channels requires Schwann cell dystroglycan.

Fig. 3 (next page) **Dystroglycan influences the shape, not the timing, of newly formed Nav clusters, and is required for efficient heminodes formation. A**, No delay in Nav clustering at nodes of Ranvier of DG deficient mice. Number of sites were plotted versus age. Black bars, sites with both caspr-positive paranodes and Nav clustered at node; white bars, sites with caspr-positive paranodes but no detectable Nav nodal cluster. Total sites analyzed were as follows: wild type (P2, 89; P5, 362; P10, 1107); dgko (P2, 74; P5, 336; P10, 786). Results are reported as average ± SEM of three mice/genotype. **B**, Nav clusters form abnormally in the absence of dystroglycan. Sciatic nerve teased fibers from P4 and P7 wt and DG deficient mice were labeled using an antibody to panNav (red). Analysis of Nav cluster shape and morphology shows that also at P4 and P7, Nav clusters are often smaller, diffusive and irregularly shaped, in the absence of DG. On the right, quantification of frequency of normal and abnormal Nav clusters shows that both at P4 and P7 the majority of Nav clusters are abnormal in DG null (P4 n=83, 79%; P7 n=41, 69.5%) versus wild type (P4 n=27; 23%; P7 n=15, 23.8%). $p < 0.001$ by χ^2 test, N 224 (P4), N 122 (P7). **C**, Nav clusters are absent or abnormally-shaped at heminodes of dgko mice. Sciatic nerve teased fibers from P6 wt and DG deficient mice labeled using antibodies to panNav (red), caspr (green) and neurofilament (NFH; blue). For each genotype heminodes at different stages of development, and nodes, are shown. Quantification of frequency of normal and abnormal heminodal Nav clusters indicates that abnormal or absent Nav clusters are more frequent in dgko (n=186; 40%) than control (n=49; 14%). $p < 0.001$ by χ^2 test N 823. Scale bar, 17.5 μm.

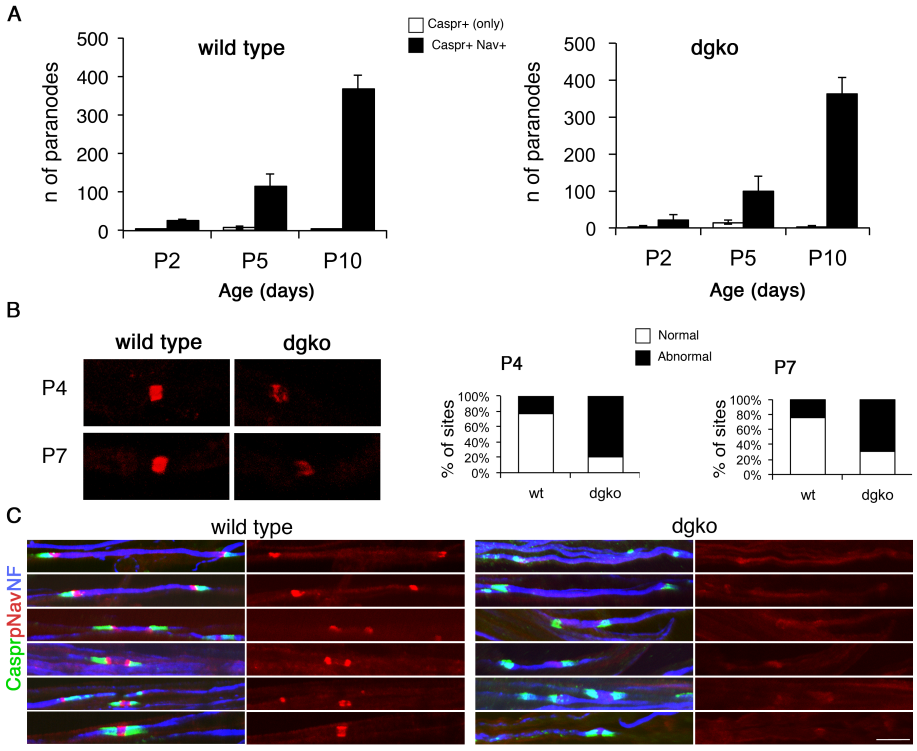
A
wild type
dgko
Caspr+ (only)
Caspr+ Nav+
n of paranodes
500
400
300
200
100
0
P2
P5
P10
Age (days)
B
wild type
dgko
P4
P7
Normal
Abnormal
% of sites
100%
80%
60%
40%
20%
0%
wt
dgko
C
wild type
dgko
CasprpNavNF

The absence of paranodal junctions only slightly worsens the Nav clustering defects of DG deficient mice

It has been proposed that two independent, yet overlapping systems (i.e.: heminodal clustering and paranodal junction-mediated restriction) cooperate to ensure high-density Nav cluster formation at peripheral nodes (Feinberg et al., 2010). To understand if the formation of defective Nav clusters in the absence of dystroglycan might be further impaired by the disrupture of the paranodal restriction mechanism, we crossed DG deficient mice (dgko) with mice lacking paranodal junctions (caspr null), thus generating dgko//caspr null (dgko//*caspr*$^{-/-}$) mutants. In agreement with previous reports (Bhat et al., 2001; Gollan et al., 2003) caspr null mice exhibit progressive neurological defects, but have a normal life span. Homozygous dgko//*caspr*$^{-/-}$ mice were macroscopically similar to *caspr*$^{-/-}$ mice without any obvious worsening of the neurological phenotype or a decrease in life span. Immunofluorescence analysis of P28 dgko//*caspr*$^{-/-}$ sciatic nerves revealed a trend towards higher percentage of abnormal clusters compared to dgko nerves (Fig. 4A, E). However, the increase in the amount of abnormal Nav clusters in double homozygous vs DG null mice is not statistically significant by Kruskal-Wallis test. Measurement of the nodal lenght does not reveal an increase in double mutants vs DG deficient mice, suggesting that the major defects pertain to the morphology of the clusters rather than to their lateral diffusion (Fig. 4F). Thus, we performed electron microscopy (EM) to analyze the nodal ultrastructure. Double homozygous showed an increased number of nodal defects when compared to single mutants. The absence of paranodal junctions

enhanced the disorganization of microvilli, which do not attach to the nodal axolemma and often penetrate the space between the paranodal loops and the axon. Moreover, elongated axonal protrusions into the nodal gap, occasionally found in DG deficient mice (Saito et al., 2003), were detected with higher frequency in double vs single homozygous mice (Fig. 4G). Abnormally large axonal protrusions contained numerous mitochondria and small vesicles, and invaded the nodal gap in place of the atrophic microvilli (Fig. 5).

Fig. 4 (next page) **Nodal abnormalities in dgko//caspr null mutants. A-D**, Sciatic nerve teased fibers from P28 wt, *caspr*$^{-/-}$, dgko and dgko//caspr$^{-/-}$ mice. Double staining for panNav (red; **A-D**) and the paranodal marker caspr (green). The merged confocal images are shown (**A'-D'**). Scale bar, 17.5 μm. **E**, Quantification of frequency of normal and abnormal Nav clusters in sciatic nerves from P28 mice of the four indicated genotypes. Abnormal clusters are more frequent in double than single mutants (n=102, 79% in dgko//*caspr*$^{-/-}$; n=72, 69% in dgko; n=49, 45% in *caspr* $^{-/-}$; n=16, 13% in wt). The difference between dgko//*caspr*$^{-/-}$and dgko is not statistically significant by Kruskal-Wallis test. **F**, Average lenght of the node of Ranvier was quantified from P28 wt, *caspr*$^{-/-}$, dgko and dgko//*caspr*$^{-/-}$ mice sciatic nerves by EM (n=61; n=60; n=72; n=79, respectively, 3 mice/genotype). No statistical significance was observed by Student's *t* test. **G**, Quantification of the number of elongated axonal 'spines' found at nodes of sciatic nerves from wt, *caspr*$^{-/-}$, dgko and dgko//*caspr*$^{-/-}$ mice at P28. The percentage of spines is reported (n=64, 9% in wt; n=70, 39% in *caspr*$^{-/-}$; n=80, 41% in dgko; n=82, 82% in dgko//*caspr*$^{-/-}$). $p < 0.001$ by χ^2 test.

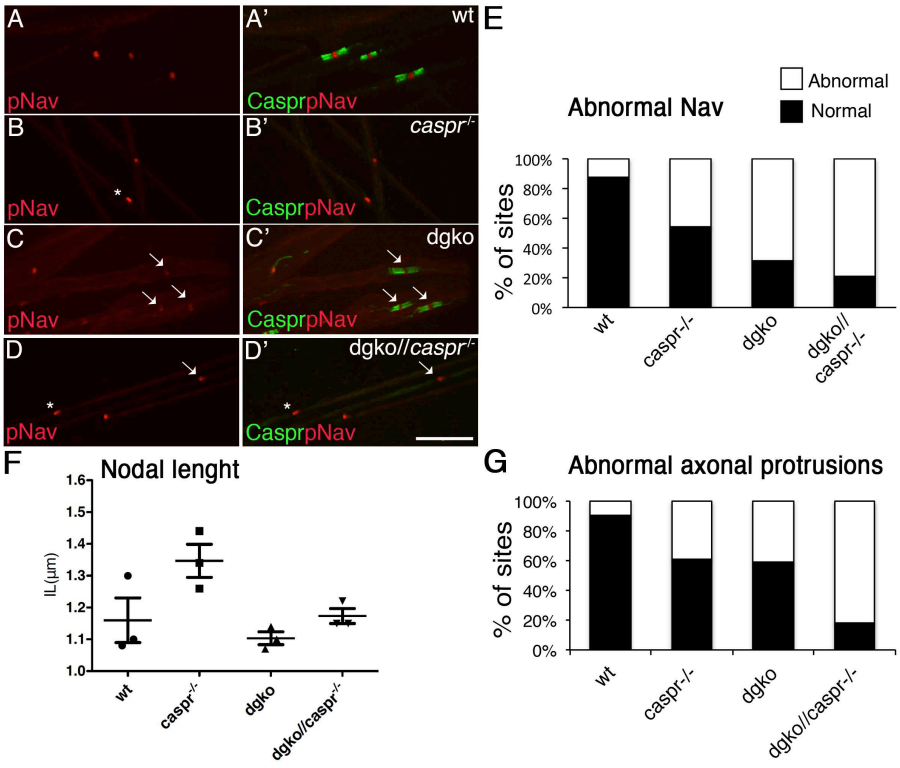
A
pNav
A'
wt
CasprpNav
B
pNav
B'
caspr-/-
CasprpNav
C
pNav
C'
dgko
CasprpNav
D
pNav
D'
dgko//caspr-/-
CasprpNav
E
Abnormal
Normal
Abnormal Nav
% of sites
100%
80%
60%
40%
20%
0%
wt
caspr-/-
dgko
dgko//caspr-/-
F
Nodal lenght
IL(µm)
1.6
1.5
1.4
1.3
1.2
1.1
1.0
wt
caspr-/-
dgko
dgko//caspr-/-
G
Abnormal axonal protrusions
% of sites
100%
80%
60%
40%
20%
0%
wt
caspr-/-
dgko
dgko//caspr-/-

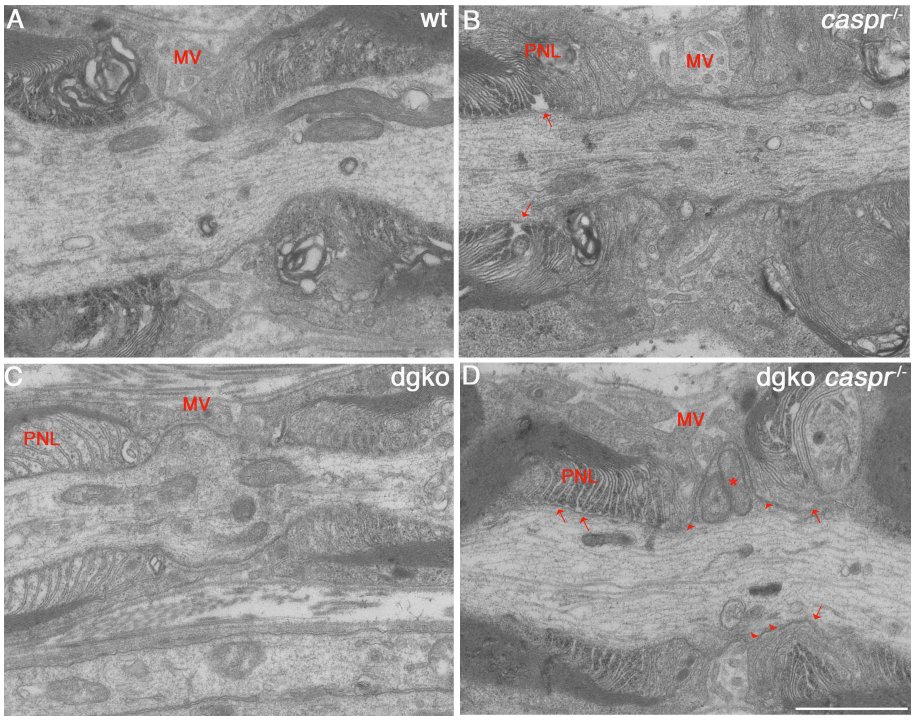

Fig. 5 Nodal ultrastructure in dgko//*caspr*$^{-/-}$ nerves. Electron microscopy images of the nodal area of sciatic nerves from P28 wt (**A**), single (**B-C**) and double mutant (**D**) animals. The location of Schwann cell microvilli (MV) and paranodal loops (PNL) are marked in red. SC microvilli of dgko//*caspr*$^{-/-}$ are disorganized and blunt, and occasionally invade beneath the paranodal loops (arrowhead), or penetrate the area between the paranodal loops and the axolemma (arrowhead). Example of an elongated axonal protrusion full of mitochondria is shown (asterisk in **D**). Note the detachment of PNL from the axolemma in *caspr*$^{-/-}$ and dgko//*caspr*$^{-/-}$ mice (arrows). Scale bar, 1 μm.

α- and β-DG are localized in the nodal gap

We previosly showed that dystroglycan colocalizes with ERM proteins at Schwann cell microvilli by confocal immunofluorescence microscopy (Occhi et al., 2005), but it is unclear whether DG is inserted solely in the Schwann cell abaxonal membrane facing the basal lamina, or if it localizes in the nodal gap and facing the axon as well. To understand the mechanism/s through which DG favours proper Nav clustering at peripheral nodes of Ranvier, we evaluated its subcellular nodal localization by performing immunogold electron microscopy (IEM) on wild type mouse sciatic nerves. Both α- and β-DG are found in Schwann cell microvilli not only adjacent to the basal lamina, but also in the nodal gap abutting onto the axon (Fig. 6A-B). No gold grains were found in DG deficient mice (not shown).

In light of this dual localization, we hypothesize two different, not mutually exclusive mechanisms through which DG aids Nav clustering. First, through its binding to the basal lamina, DG could trigger a rearrangement in the cytoskeleton of Schwann cell microvilli, thus favouring the compaction of Nav clusters at the node. This could be mediated by the cytoskeletal linker ERM proteins, in particular ezrin, which is present at Schwann cell microvilli and has been shown to interact with β-DG in other systems (Spence et al., 2004). Another possibility is that DG favours the presentation and anchoring of other cell adhesion molecules important for Nav clustering to the nodal axon.

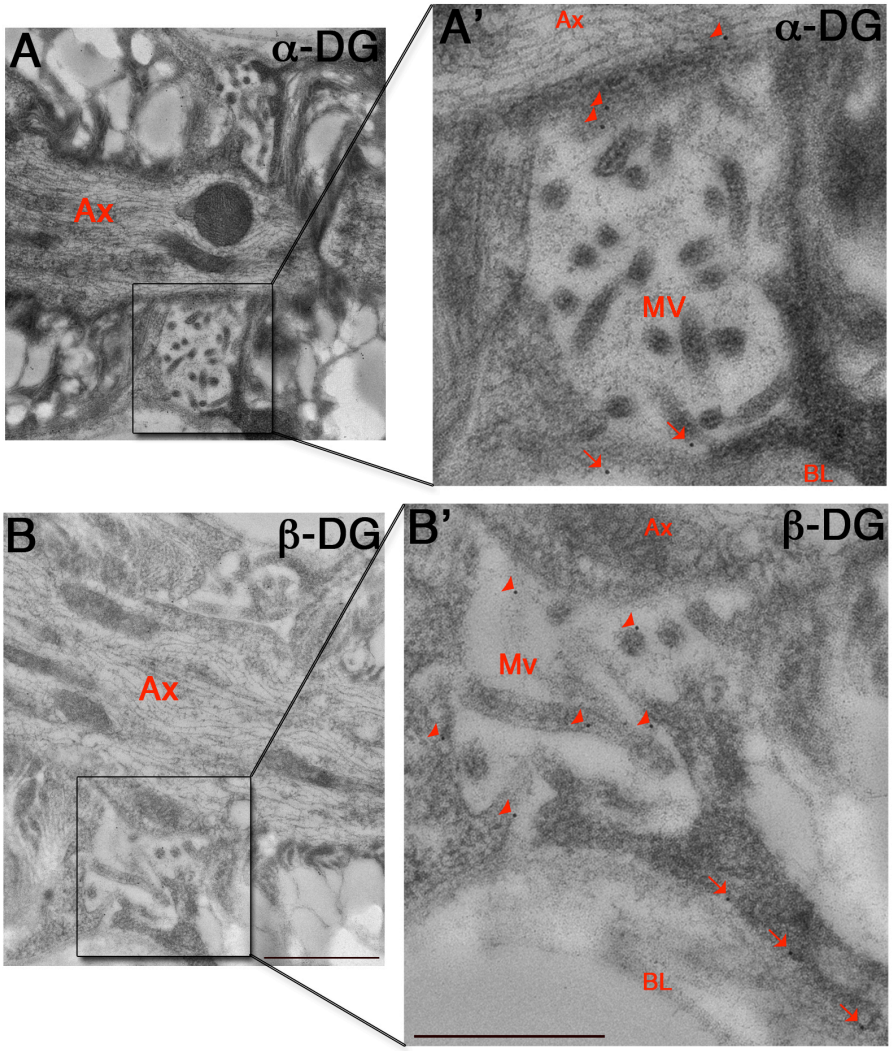

Fig. 6 α- and β-dystroglycan localization in the nodal gap. IEM on sciatic nerve of wild type adult mouse using antibodies against α-DG (**A**) and β-DG (**B**) shows gold particles decorating both the Schwann cell microvilli abaxonal surface facing the basal lamina (arrows in **A'** and **B'**, magnified at the right), and Schwann cell microvilli in the nodal gap, abutting to the axon (arrowheads in **A'** and **B'**, magnified at the right). Scale bar, 1 μm and 0.5 μm for magnifications.

Slight reduction of ERM proteins in DG deficient sciatic nerves

The first hypothesis is strengthened by the fact that even laminin mutants (*Lama2*$^{dy2J/dy2J}$ and P0Cre*Lamaγ1*null) show Nav clustering defects similar to those found in DG deficient mice (Occhi et al., 2005). Moreover, we observed that the absence of laminin 211, a known ligand of DG, alters both nodal and heminodal Nav clusters, like in DG null animals (data not shown). We then asked if ERM proteins could be involved in this mechanism as mediators of BL-driven microvillar cytoskeleton rearrengements. To this end we checked if ERMs were normally expressed and polarized at peripheral nodes in the absence of dystroglycan. Western blot analysis revealed a slight decrease in total ERMs and phosphorylated ERMs (ERM-P) when normalized to neurofascin, to account for the fact that DG deficient mice have shorter internodes and thus more nodes (Fig. 7A). Immunofluorescence of teased fibers shows that in the absence of DG ezrin is normally polarized to nodes. However, we observed a higher amount of cytoplasmic puncta all along the fiber, suggesting an impairment of ERM transport (Fig. 7C arrows). Phosphorylated ERMs are normally localized in the majority of nodes, with occasional reduction of their staininig, reflecting their decreased expression (arrows in Fig. 7E-E'). Thus, the absence of DG does not impede ERM localization at microvilli, but causes a decrease of ERM proteins possibly due to impaired trafficking.

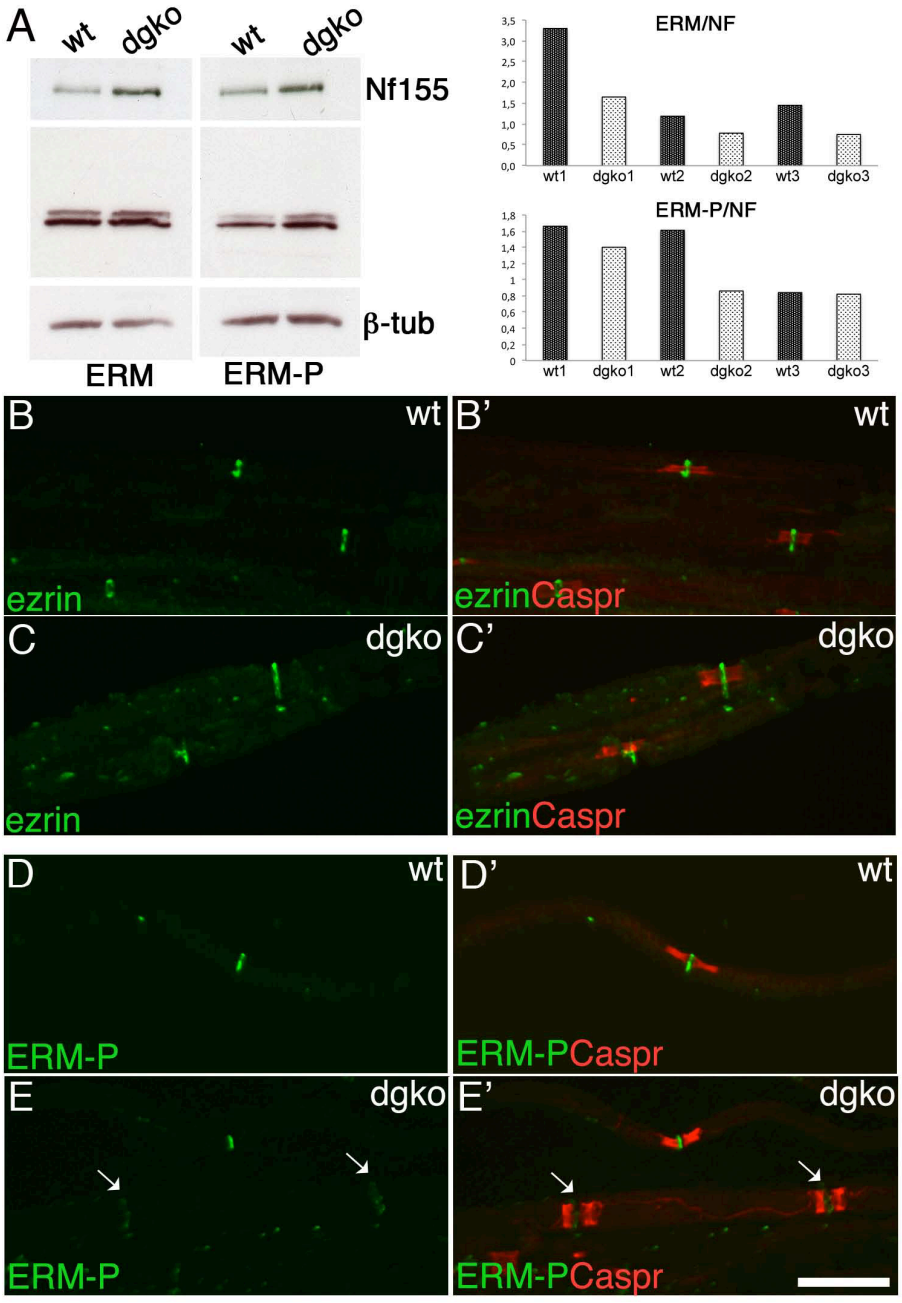
A
wt
dgko
wt
dgko
Nf155
β-tub
ERM
ERM-P
ERM/NF
3,5
3,0
2,5
2,0
1,5
1,0
0,5
0,0
wt1
dgko1
wt2
dgko2
wt3
dgko3
ERM-P/NF
1,8
1,6
1,4
1,2
1
0,8
0,6
0,4
0,2
0
wt1
dgko1
wt2
dgko2
wt3
dgko3
B
wt
ezrin
B'
wt
ezrinCaspr
C
dgko
ezrin
C'
dgko
ezrinCaspr
D
wt
ERM-P
D'
wt
ERM-PCaspr
E
dgko
ERM-P
E'
dgko
ERM-PCaspr

Fig. 7 (previous page) **ERM proteins expression is reduced in the absence of DG, but their nodal localization is not altered. A**, Western blot on sciatic nerve lysates from wt and DG deficient mice. Filters were blotted with antibodies against ezrin/radixin/moesin (ERM) and phosphorylated ERM (ERM-P). Neurofascin 155 (Nf155) was used as normalization for the higher number of nodes in dgko. Equal loading was verified by β-tubulin (β-tub). On the right, quantification of Western blot on three mice/genotype, represented as ratio of ERM/Nf155 and ERM-P/Nf155, respectively. **B-E**, Sciatic nerve teased fibers from wt and dgko adult mice were immunostained for ezrin (**B-C**; green) or ERM-P (**D-E**; green) and caspr (red). The merged confocal images are shown (**A'-E'**). Notice increased ezrin-positive puncta (**C-C'**) and lower levels of ERM-P at some dgko nodes (arrows in **E-E'**). Scale bar 17.5 μm.

Perlecan is reduced at DG deficient nodes, but two different perlecan mutants have normally clustered Nav

A second mechanism through which DG mediates Nav clustering could be by favouring the presentation or aggregation of gliomedin and/or NrCAM to the nodal axon. Similarly to DG, gliomedin and glial NrCAM are necessary for the initial clustering of Nav at peripheral heminodes (Feinberg et al., 2010). Furthermore, gliomedin is secreted by Schwann cells and deposited in the ECM of the nodal gap by binding to heparan sulfate proteoglycans (HSPGs) (Eshed et al., 2007). Given its localization in the nodal gap and its ability to bind various HSPGs, DG could properly maintain a high concentration of HSPGs which in turn favour aggregation of gliomedin and NrCAM in the nodal gap. Thus we evaluated the nodal expression of various HSPGs in wild type and DG deficient sciatic nerves. Both agrin and perlecan, two HSPGs expressed by Schwann cells, and known DG

ligands (Gesemann et al., 1998; Talts et al., 1999), are enriched at nodes of Ranvier, however in the absence of DG, only perlecan expression is decreased at these sites (Fig. 8A-F). Of note, perlecan is also polarized to nodes early in postnatal development and this polarization is absent in DG deficient nerves as early as P6 (Fig. 8G-J), further supporting a potential role in the formation of Nav clusters. To test this, we analyzed peripheral nerves isolated from two different perlecan mutant mice, one lacking the attachment sites of HS-side chains (*Hspg2*$^{\Delta 3/\Delta 3}$; Rossi et al., 2003), and the other lacking almost all the secreted protein, being a compound heterozygote of the *Hspg2* null allele and an allele carrying one missense substitution that corresponds to a human familial Schwarz-Jampel Syndrome (SJS) (*Hspg2*$^{KI/KO}$; Stum et al., 2008). In both cases nerve morphology was not altered by semithin section (not shown). *Hspg2*$^{KI/KO}$ mutants display muscle stiffness and fatigability at low frequencies of nerve stimulation. This is presumably attributable to achetilcolinesterase (AchE) deficiency at the neuromuscular junction (NMJ), but recent electrophysiological studies suggested that also peripheral nerve is involved (Echaniz-Laguna et al., 2009). The clusterization of gliomedin and Nav were not altered in *Hspg2*$^{\Delta 3/\Delta 3}$ mice, indicating that the heparan sulfate chains of perlecan are dispensable for the concentration of gliomedin at the nodal gap and for proper clustering of Nav at nodes of Ranvier (Fig. 9A). *Hspg2*$^{KI/KO}$ and *Hspg2*$^{KI/+}$ animals were immunolabeled at P6 and P60 for Nav1.6 isoform, panNav, or gliomedin, and perlecan or the paranodal marker caspr. First we confirmed that perlecan levels are markedly reduced in mutant mice and no enrichment is found at *Hspg2*$^{KI/KO}$ nodes of

Ranvier. Despite this, gliomedin normally accumulates in the nodal gap and Nav clusters are not altered either at nodes or heminodes in *Hspg2*$^{KI/KO}$ mutants (Fig. 9B). Overall, the results from the analysis of these two perlecan mutants suggest that perlecan is not involved in Nav clustering. It is probale that a significant redundancy of HSPGs exists in the nodal area, and this could overshadow the effect of absence of a single HSPG.

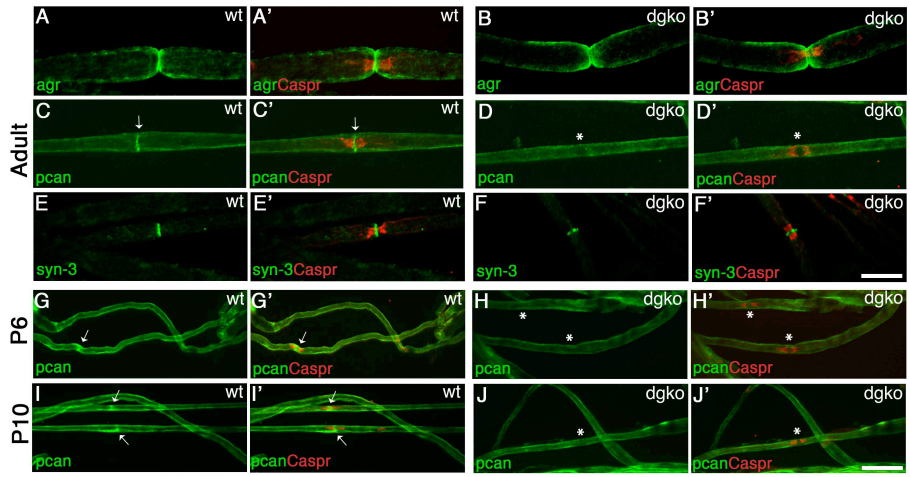

Fig. 8 Perlecan and agrin are present at nodes of Ranvier, perlecan is reduced in this location in the absence of dystroglycan. **A-F**, Images of sciatic nerve teased fibers isolated from adult wild type (wt) and DG null mice. Double staining for the HSPGs agrin (agr), perlecan (pcan) or syndecan-3 (syn-3) (green; **A-F**) and the paranodal marker caspr (red). The merged confocal images are shown (**A'-F'**). Note that perlecan is enriched at wt nodes (arrow in **C-C'**), whereas in the absence of DG it is reduced at these sites (asterik in **D-D'**). **G-J**, Perlecan is polarized early to nodes during postnatal development, and missing even at early time points in DG deficient nodes. Images of sciatic nerve teased fibers isolated from P6 and P10 wt and DG deficient mice. Double staining for perlecan (green; **G-J**), and the paranodal marker caspr (red). The merged confocal images are shown (**G'-J'**). Note that perlecan is polarized at nodes of Ranvier in wt (arrows in **G-G'** and **I-I'**), but not in dgko (asteriks in **H-H'** and **J-J'**) fibers both at P6 and P10. 68% and 87% caspr-positive paranodes are flanked by perlecan-positive nodes at P6 and P10 in wt nerves. Only 4% and 6% nodes have been quantified as perlecan-positive in dgko age-matched animals. Scale bar, 17.5 μm.

Fig. 9 (next page) **Nav clusters are not altered at nodes or heminodes of two different perlecan mutants. A-D**, Images of sciatic nerve teased fibers isolated from adult wt (**A, C**) and *Hspg2*$^{\Delta 3/\Delta 3}$ (**B, D**) mice. Double immunostaining for Nav1.6 (**A-B**; green) or gliomedin (**C-D**; green) and the paranodal marker caspr (**A'-B'**; **C'-D'**; red) does not show any obvious alterations in nodal clusters. **E-J**, Images of sciatic nerve teased fibers isolated from P6 *Hspg2*$^{KI/+}$ (**E, G, I**), used as controls, and *Hspg2*$^{KI/KO}$ (**F, H, J**). Double staining for Nav1.6 (**E-F**; red) and pcan (**E'-F'**; green). Note that whereas perlecan is enriched at nodes of controls (asterisks in **E'**), its expression is almost absent in *Hspg2*$^{KI/KO}$ nerves (asterisk in **F'**). Double immunostaining for panNav (**G-H**; red) and caspr (**G'-H'**; green), or gliomedin (**I-J**; green) and caspr (**I'-J'**; red). Fibers are counterstained with neurofilament (NF, blue). Notice that both panNav and gliomedin can form normal clusters, either heminodal (arrows) or nodal. **K-N**, Images of sciatic nerve teased fibers isolated from P60 *Hspg2*$^{KI/+}$ (**K, M**), used as controls, and *Hspg2*$^{KI/KO}$ (**L, N**). Double immunostaining for panNav (**K-L**; red) and caspr (**K'-L'**; green), or gliomedin (**M-N**; green) and caspr (**M'-N'**; red). Scale bar, 17.5 μm.

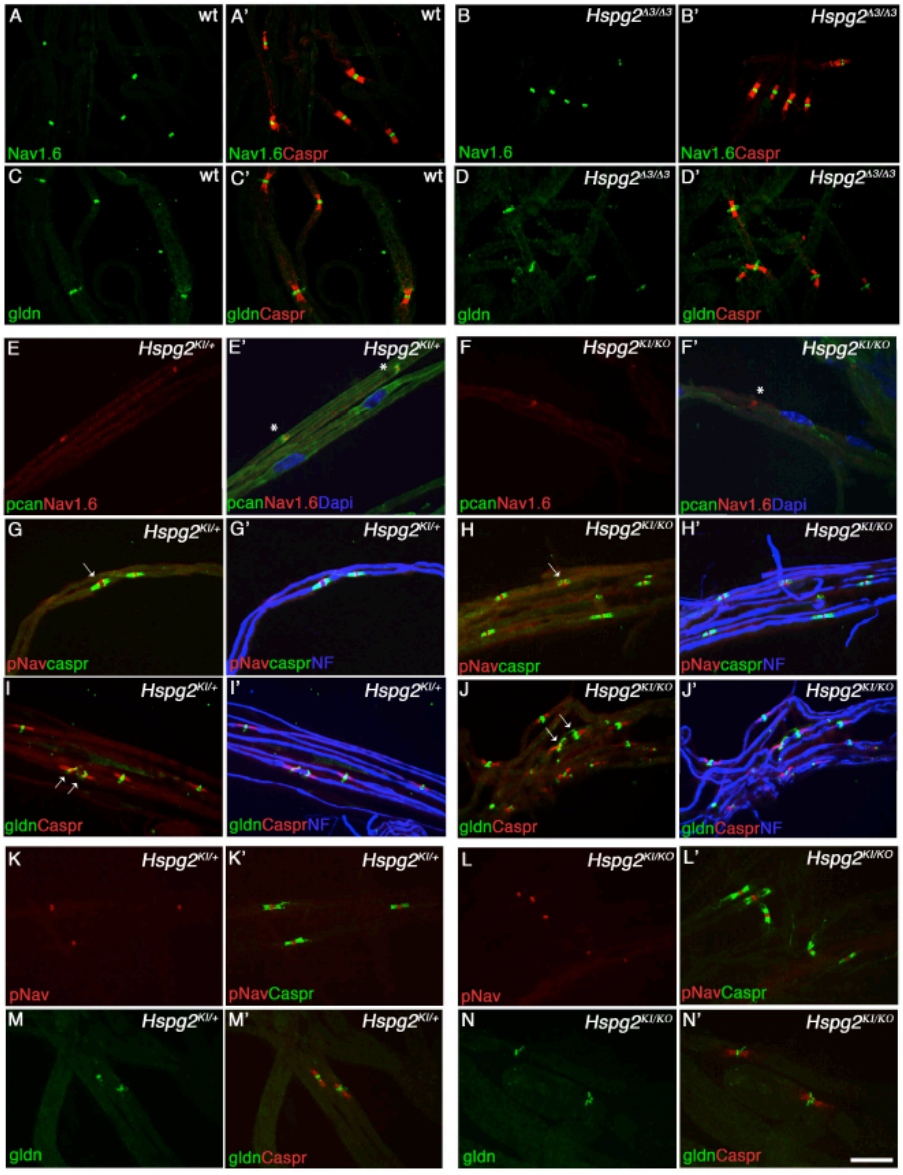
A wt
Nav1.6
A' wt
Nav1.6Caspr
B Hspg2Δ3/Δ3
Nav1.6
B' Hspg2Δ3/Δ3
Nav1.6Caspr
C wt
gldn
C' wt
gldnCaspr
D Hspg2Δ3/Δ3
gldn
D' Hspg2Δ3/Δ3
gldnCaspr
E Hspg2KI/+
pcanNav1.6
E' Hspg2KI/+
pcanNav1.6Dapi
F Hspg2KI/KO
pcanNav1.6
F' Hspg2KI/KO
pcanNav1.6Dapi
G Hspg2KI/+
pNavcaspr
G' Hspg2KI/+
pNavcasprNF
H Hspg2KI/KO
pNavcaspr
H' Hspg2KI/KO
pNavcasprNF
I Hspg2KI/+
gldnCaspr
I' Hspg2KI/+
gldnCasprNF
J Hspg2KI/KO
gldnCaspr
J' Hspg2KI/KO
gldnCasprNF
K Hspg2KI/+
pNav
K' Hspg2KI/+
pNavCaspr
L Hspg2KI/KO
pNav
L' Hspg2KI/KO
pNavCaspr
M Hspg2KI/+
gldn
M' Hspg2KI/+
gldnCaspr
N Hspg2KI/KO
gldn
N' Hspg2KI/KO
gldnCaspr

Potential role of α-DG-N at nodes of Ranvier

Gliomedin and NrCAM, two glial cell adhesion molecules that trigger Nf186 clustering by initiating heminode formation, are secreted in the nodal gap upon furin proprotein convertase cleavage (Maertens et al., 2007; Eshed et al., 2007; Feinberg et al., 2010). Then, the N-terminal fragment of gliomedin (olfactomedin) and the extracellular domain of NrCAM are incorporated in the nodal gap substance, where they form a multimeric complex whose composition is still not completely known. By analogy, the N-terminal domain of α-DG, α-DG-N (spanning from residue 30 to 316), can be cleaved by a furin protease in a wide variety of cell lines (Singh et al., 2004; Saito et al., 2008); furthermore, recent studies have shown that α-DG-N is probably secreted and can be found in human blood serum, cerebrospinal fluid and urine, but its physiological significance is unclear (Saito et al., 2008 and 2011; Hesse et al, 2011). To understand if α-DG-N could have a role in peripheral nerve, specifically at nodes of Ranvier, we first asked whether α-DG-N is cleaved and secreted by Schwann cells. To this end, rat Schwann cells were cultured in the presence of the furin inhibitor I (CMK) for 48 hours; subsequently, the cell lysate and the culture medium were analysed by Western blot. In the absence of CMK, α-DG with a molecular weight of 120 kDa was detected in cell lysates by IIH6 antibody, which recognizes the mucin-like domain of α-DG. In the same conditions, the culture medium contained a 35-40 kDa fragment that is detected by an anti-α-DG-N-specific antibody (API528) (Fig. 10A). Instead, after treatment with CMK, IIH6 antibody detected α-DG with a molecular mass of 160 kDa, whereas the 35-40 kDa band became undetectable in culture medium (Fig.

10A). These data indicate that α-DG-N is excised by a furin proprotein convertase in cultured Schwann cells and is shed in the medium immediately upon cleavage.

To unravel a possible role of α-DG-N in PNS *in vivo*, an immunofluorescence with the API528 antibody was performed on nerve teased fibers. Unfortunately, this antibody does not work in this experimental setting.

As an alternative approach, α-DGFc fusion proteins were used to perform binding assays on Schwann cells and neurons. Full-lenght and truncated α-DG molecules, fused with human IgGFc (DGFc), were generated by transfection of 293FT cells with constructs gently gifted by Kevin Campbell (Kanagawa et al., 2004). The presence of each fusion protein was confirmed in culture media by Western blot with proteinA-HRP (not shown). DGFc5 represents whole α-DG, DGFc6 has a deletion in the N-terminal domain, while DGFc2 encompasses the N-terminal domain only (Fig.7B).

Binding experiments on cultured rat Schwann cells revealed that both DGFc5 and DGFc6 bound to the Schwann cell membrane, but they were not incorporated in the associated ECM like it has been described for extracellular gliomedin (Gldn-ECDFc; Eshed et al., 2007), that was used as a positive control (Fig. 7C). We excluded that DGFc5 and DGFc6 bound to α-DG expressed on the surface of Schwann cells, as the binding did not change upon DG knock down by shRNA (not shown). In contrast, DGFc2 was not able to bind either Schwann cells or their ECM, similarly to what was previously shown for the more distal domain of gliomedin, olfactomedin (Gldn-OlfFc; Eshed et al., 2007) (Fig. 7C). Furthermore, deletion of α-DG-N

in the DGFc6 construct does not alter the ability of α-DG to bind the SC membrane, suggesting that the mucin-like and the C-terminal domains of α-DG are sufficient to mediate this interaction.

The same experiment was also performed on isolated DRG neurons. Although pre-clustered olfactomedin-Fc (Gldn-OlfFc), that was used as positive control, bound to axons, as expected (Eshed et al., 2007), none of the DGFc constructs were able to interact with DRG neurons (Fig. 7D).

However, when myelinating Schwann cell-DRG co-cultures were incubated with DGFc fusion proteins, DGFc2 bound to some Schwann cells aligned with axons, similarly to Gldn-OlfFc (Fig.7E). Instead, DGFc5 and DGFc6 robustly bound the matrix in between neurons and Schwann cells (Fig.7E). These results suggest that, similarly to the olfactomedin domain of gliomedin, α-DG-N can interact with myelinating fibers, but only after the Schwann cell-axon contact is established. This indicates that whereas gliomedin directly interacts with an axonal protein (i.e. neurofascin 186), the N-terminal fragment of DG might bind a complex of molecule that forms only when myelination is triggered. Instead, full lenght α-DG can bind components of the ECM deposited by Schwann cells either in the presence or in the absence of neurons. Most likely, full lenght α-DG interactors are represented by laminins, perlecan or agrin. Future experiments will elucidate this aspect.

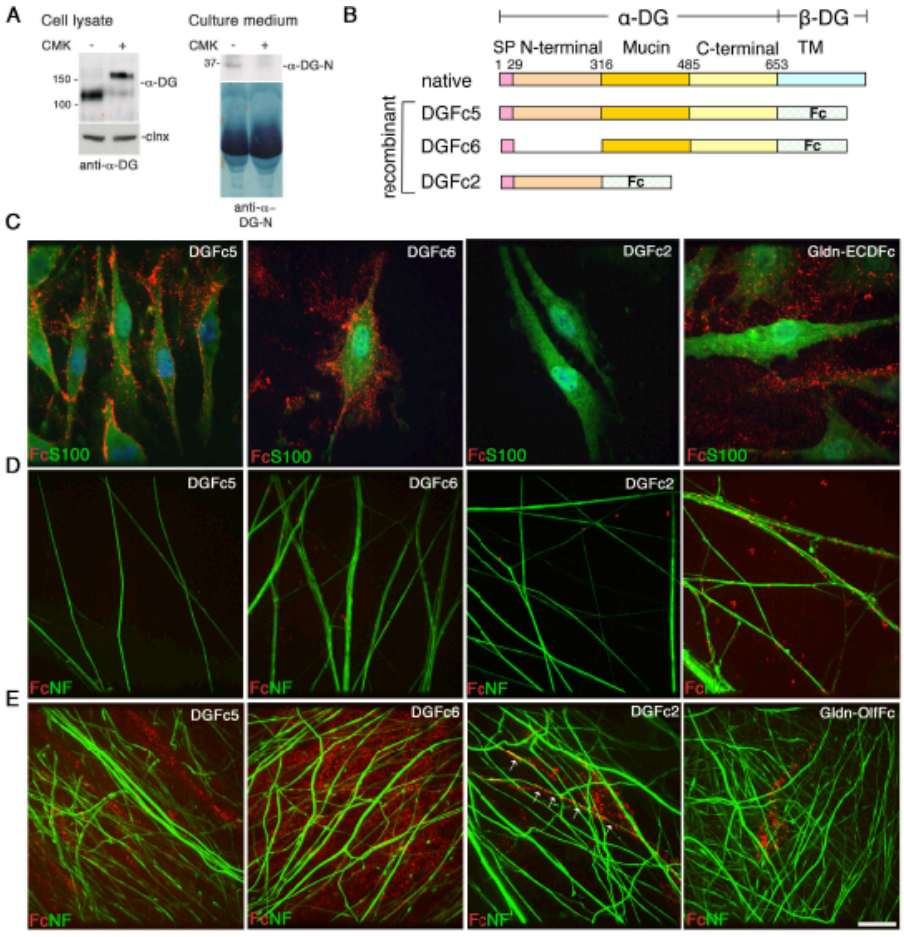
A
Cell lysate
CMK - +
150 -
100 -
-α-DG
-clnx
anti-α-DG
Culture medium
CMK - +
37-
-α-DG-N
anti-α-DG-N
B
α-DG
β-DG
SP N-terminal
Mucin
C-terminal
TM
1 29
316
485
653
native
recombinant
DGFc5
DGFc6
DGFc2
Fc
C
D
E
DGFc5
DGFc6
DGFc2
Gldn-ECDFc
Gldn-OlfFc
FcS100
FcNF

Fig. 10 (previous page) **Cultured Schwann cells secrete α-DG-N, and different portions of α-DGFc differently bind Schwann cells, DRG neurons and SC-DRG co-cultures. A,** Native α-DG-N is cleaved by a furin protease in rat Schwann cells. Rat SCs were cultured for 48 hours with (+) or without (-) furin inhibitor I (CMK). Western blot analysis on SC lysate (left) and culture medium (right) shows that in the absence of CMK a 35-40 kDa α-DG-N is secreted in cell medium and a 120 kDa α-DG is detected in cell lysate by IIH6 antibody. In the presence of CMK, α-DG is not cleaved, as shown by both the higher MW (around 160 kDa) of α-DG in SCs or the absence of α-DG-N in the cell culture medium. **B**, Schematic representation of α-DG, showing its domain composition (Signal peptide, SP, N-terminal, Mucin-like, C-terminal, and transmembrane,TM). The N-terminal domain of α-DG is cleaved by a furin proprotein convertase at residue 316. The three deletion mutants of DGFc proteins are shown: DGFc5 (whole α-DG fused with Fc), DGFc6 (deletion of α-DG-N fused with Fc) and DGFc2 (α-DG-N fused with Fc). **C**, Binding of DGFc5, DGFc6 and DGFc2 to isolated rat Schwann cells. Both DGFc5 and DGFc6, but not DGFc2, binds to the matrix associated with the SC membrane. In contrast Gldn-ECDFc, used as positive control, binds to the ECM between the SC. Fc binding is shown in red, Schwann cells were labeled with an antibody against S100 (green) and the nuclei of Schwann cells were labeled with Dapi (blue). **D**, Binding of DGFc5, DGFc6 and DGFc2 to isolated DRG neurons. Gldn-OlfFc, used as positive control, interacts with the axon, whereas none of the DGFc proteins bind isolated neurons. Fc binding is shown in red and neurons are labeled with an antibody against neurofilament (NF, green). **E**, Binding of DGFc5, DGFc6 and DGFc2 to SC-DRG co-cultures after 10 days from the induction of myelination. Fc binding is shown in red, neurons are labeled with an antibody against neurofilament (NF, green). Note the binding of DGFc2 to SCs aligned with axons (arrows). Scale bar, 17.5 μm.

2.4 Discussion

We and others previously reported that dystroglycan is enriched at Schwann cell microvilli and its absence causes abnormal clustering of Nav and variable degrees of microvilli disorganization (Saito et al., 2003; Occhi et al., 2005). Here we have demonstrated that these abnormalities depend on a defective formation of Nav clusters rather than a degeneration of normal clusters with time. We have also shown that dystroglycan is polarized immediately to Schwann cell processes at nascent nodes, and that at microvilli it faces both the basal lamina and the nodal gap substance. The analysis of the mechanism does not indicate an involvement of perlecan, we rather propose a model in which DG stabilizes newly formed Nav clusters by interactions with laminin 211 in the basal lamina, and yet unknown molecules in the nodal gap, possibly through its shed N-terminal domain.

Our findings support the notion that Schwann cell microvilli contribute to the proper formation of Nav clusters at nodes of Ranvier. Several observations go in the same direction. First, in the peripheral nervous system, a direct contact between Schwann cells and the axon is necessary for Nav to cluster (Ching et al., 1999; Vabnick et al., 1996). Second, in early postnatal development, Nav clusters appear in close association with ERM-positive Schwann cell processes, early precursors of Schwann cell microvilli (Melendez-Vasquez et al., 2001; Gatto et al., 2003). Third, gliomedin and NrCAM, glial cues that promote the initial clustering of axonal CAMs, are polarized early to microvilli (Eshed et al., 2005; Feinberg et al., 2010), and their absence leads to microvillar disorganization, absence of heminodal

clusters (Feinberg et al., 2010) and delay in Nav appearence (Custer et al., 2003).

Early polarization of DG at nascent nodes of Ranvier is consistent with a role in Nav cluster formation

We have confirmed the observation that in rodent peripheral nerves dystroglycan is expressed during early postnatal development, and we have extended this notion to its nodal polarization. Previous works have shown that expression of β-DG is low and not confined to the Schwann cell outer membrane from embryonic day 18, when only β-DG mRNA was found in spinal nerves (Previtali et al., 2003), to birth (Masaki et al., 2002). Just prior the onset of myelination DG is detected at the protein level and soon after its expression increases, as confirmed by Western blot analysis for both α- and β-DG at P2, and in accordance with other reports (Cai et al., 2007). In the present work we found that in rat sciatic nerves, the majority of ezrin-positive Schwann cell processes were also positive for α- and β-DG as soon as P2. We also noticed that for each one of the analyzed time points the percentage of α-DG-positive nodes was always lower than β-DG. The extent of α-DG glycosylation increases during development, thus it is possible that a glyco-specific antibody as the one used in this analysis exhibits a lower affinity for a not completely glycosylated target. Alternatively, it might be that a minority of the nodal dystroglycan complex lacks α-DG as a consequence of β-DG cleavage by MMP-2 and -9, that are active during early postnatal development (Court et al., 2011). The same immunofluorescence analysis performed with

antibodies recognizing either α-DG core protein or the cleaved β-DG_{31} fragment could clarify this aspect.

Dystroglycan is required for proper Nav clustering at nodes and heminodes

Data from the developmental analyses are consistent with the idea that dystroglycan in Schwann cell processes have a role in mediating the formation of Nav clusters because newly formed Nav clusters have the same abnormalities found in adult mice, indicating that DG mediates Nav clustering rather than their maintenance. In addition, even heminodal clusters were defective in DG deficient mice, strongly suggesting that, in virtue of its temporal and spatial localization, DG contributes with gliomedin and glial NrCAM to promote the first steps of Nav accumulation. However, an important difference between mice lacking gliomedin or NrCAM and DG deficient mice is that the former completely lack Nav clusters at heminodes, whereas in the absence of DG clusters can generally be detected, albeit with the same morpholgical defects of nodal clusters. This indicates that DG is required for the stabilization of both nodal and heminodal clusters as they form, but it is not necessary to induce clusterization per se. This finding is supported by the fact that gliomedin and Nf186 are still found at DG deficient nodes (not shown and Saito et al., 2003), where they can trigger Nav clustering, although in a defective way due to the lack of DG stabilization.

Removal of paranodal junctions worsens the nodal defects of DG deficient mice

It has been proposed that, when nodal axo-glial contact is impaired, like in the absence of gliomedin and NrCAM, a paranodal junction-dependent mechanism allows Nav to accumulate at mature nodes by restricting their distribution between two growing myelin internodes (Feinberg et al., 2010). Indeed, removal of paranodal junctions in gliomedin and NrCAM deficient mice resulted in a remarkable decrease of the total amount of Nav clusters (Feinberg et al., 2010). However, the idea that PNJs can substitute heminodal interactions is controversial, as *Nfasc*^{NF186} null mice are not able to cluster Nav, despite the presence of intact paranodes (Sherman et al., 2005; Thaxton et al., 2011).

Here we asked whether ablation of the paranodal junction mechanism would worsen cluster abnormalities in DG deficient nerves. Dgko//caspr-null mice exhibit a higher number of abnormal Nav clusters and an overall worsening of the nodal architecture. Ultrastructurally, concomitant elimination of caspr and a microvillar protein (gliomedin, NrCAM or dystroglycan) causes microvilli to invade the space between the axolemma and the detached paranodal loops. Moreover, in dgko//caspr null mice we observed a significant increment of the number and the dimensions of bulging axonal protrusions into the nodal gap. These structures, full of vesicles and mitochondria, could be either an adaptive mechanism of the axon to overcome the higher energetic load, or the tendency of the neurite to form sprouts in the absence of a stable glial covering.

Overall, these data suggest that properly formed microvilli and

intact paranodal axo-glial junctions, if not equally required for the clustering, do cooperate in stabilizing Nav clusters at nodes of Ranvier.

Dp116 and perlecan, but not laminin 511, are polarized early to nascent nodes.

Specific laminins and specific dystrophin-glycoprotein complexes are expressed at mature nodes of Ranvier (Occhi et al., 2005). This regional polarization might have a functional significance for the nodal architecture, and the analysis of the temporal expression of DG intracellular and extracellular partners could suggest which complex might regulate Nav clustering. Here we have shown that Dp116, the major dystrophin isoform found at nodes of Ranvier, accumulates at sites of Schwann cell-axon contact as early as P2. We also noticed that Dp116 nodal localization is slightly delayed compared to that of dystroglycan, suggesting a progression of events in which DG is first inserted in the membrane of Schwann cell microvilli, followed by the recruitment of Dp116 to the cytoplasm of these structures. Thus, in the first days of postnatal development, the nodal DG complex could function independently of Dp116. To elucidate this eventuality it could be interesting to analyze Nav clustering in mice deficient in all dystrophin isoforms, including Dp116 (*mdx*$^{3cv/3cv}$), or *mdx*$^{3cv/3cv}$//utr$^{-/-}$ mice that also lack utrophin, to avoid compensation issues. Previous analysis of these mutants did not show evident signs of peripheral nerve disease (Rafael et al., 1998 and 1999), however a more careful investigation might be required.

In the basal lamina over nodes, potential DG ligands are laminin 211 and 511, and the heparan sulfate proteoglycans agrin and perlecan (Gesemann et al., 1998; Talts et al., 1999; Ido et al., 2004), which are enriched in the nodal region. Immunofluorescence analysis revealed that laminin α5-chain acquires its mature polarization around nodes and paranodes only after P10, a period when nodes have already formed. Thus, it is more likely that laminin 511 has a role unrelated to the maintenance of the nodal architecture; the generation of Schwann cell specific *Lama5* null mice would be the best way to gain insight into its function.

On the contrary, laminin 211 and perlecan become polarized to nodes earlier, indicating that their interaction with DG might be involved in the first steps of Nav clustering. For laminin 211, this is confirmed by the observation of abnormal Nav clusters in mice and humans with defective laminin α2-chain (Occhi et al., 2005). Furthermore, in the murine model of MDC1A we also found abnormalities in heminodal clusters (Colombelli and Feltri, unpublished observation), suggesting that together with dystroglycan, laminin 211 is involved in node formation. Specifically, we propose that interactions between α-DG and laminin 211 can trigger rearrangements in the cytoskeleton of microvilli that in turn favour the compaction of Nav clusters in the nodal axolemma. This mechanism is supported by three experimental observations. First, laminin mutants phenocopy the clustering defects of DG deficient mice, even if with lower severity. Second, β-dystroglycan can directly interact with actin and ezrin, which are enriched at Schwann cell microvilli (Chen et al., 2003; Spence et al., 2004). Third, Schwann cell microvilli are disorganized in the absence

of dystroglycan (Saito et al., 2003). Ezrin is part of the ERM family proteins that, when activated by phosphorylation at a conserved threonine residue, function as linkers between transmembrane receptors and the cytoskeleton (Bretscher et al., 2002; McClatchey and Fehon, 2009). In epithelial cells the interaction between β-DG and phospho-ezrin induces actin-rich surface protrusions (Spence et al., 2004), hinting at a potential involvement of this alternative dystroglycan complex in the formation of peripheral filopodia and microvilli. Indeed, in the absence of DG, we found a slight reduction in ERM protein levels. How dystroglycan can modulate ERM expression in nerves is not known, but it is possible that the Cajal band/apposition disorganization in DG deficient mice (Court et al., 2009) slows ERM transport to microvilli, thus reducing their localization to the microvilli. In support, we found higher amounts of ERM-positive puncta along the nerve fibers of DG deficient mice. However, ERM nodal localization is generally preserved; probably, in the absence of DG, the interaction between cytoskeletal F-actin and the microvillar membrane is maintained, at least in part, by syndecan-3 that, akin to syndecan-2, might bind ezrin (Granes et al., 2000 and 2003). An analysis of β-DG/ezrin or β-DG/F-actin interactions during node formation may clarify this aspect.

Perlecan is dispensable for Nav clustering

In the last few years growing evidence pointed to the nodal gap substance as a region where communication between the Schwann cell and the axolemma, critical for Nav clustering, takes place. Specifically, gliomedin is able to bind Nf186 only when shed in the

nodal gap and incorporated in a multimolecular complex in a heparan sulfate-dependent manner (Eshed et al., 2007). The composition of the nodal gap substance, earlier termed 'cementing disc of Ranvier' (Landon and Langley, 1971), is still poorly defined, but many proteoglycans and non-sulfated mucopolysaccharides have been identified (Hess and Young, 1952; Quick and Waxman, 1977). Through their HS-chains, heparan sulfate proteoglycans (HSPGs) can sequester and trap growth factors as a form of protection against proteolytic degradation, or to present them for high-affinity receptor binding. For instance, perlecan presents FGF-2 to its receptor and lack of perlecan HS-chains causes delayed wound healing and retarded tumor growth due to reduced FGF-2 signalling (Zhou et al., 2004). Similarly, in the perinodal matrix the HS-chains of a still undetermined HSPG bind gliomedin, creating high local concentrations that may favour its interaction with Nf186 and subsequent Nav clustering. We hypothesized that DG may serve to immobilize such a HSPG in this specific location. One open question is whether perlecan and agrin, two HSPGs expressed by Schwann cells and able to bind DG, are present solely in the basal lamina or are also secreted in the nodal gap substance. We found that both agrin and perlecan are localized at nodes of Ranvier in wild type nerves, and in the absence of DG perlecan nodal enrichment is lost, indicating that dystroglycan is necessary for the positioning of this HSPG in this specialized area. Nonetheless, the absence of perlecan HS-chains does not affect gliomedin accumulation or Nav clustering at peripheral nodes. To avoid the possibility that the C-terminal HS chain that is still present in *Hspg2*$^{\Delta 3/\Delta 3}$ mice compensated for the absence of the

other 3 N-terminal HS-chains, we also analyzed mice lacking almost all secreted perlecan. However, even these mutants did not present abnormalities in gliomedin and Nav clusters. We conclude that perlecan is dispensable for Nav clustering, even if it is likely that other HSPGs present at nodes of Ranvier, like syndecan-3 and -4, NG2 proteoglycan, versican V1 and agrin, are redundant with perlecan in this function (Martin et al., 2001; Goutebroze et al., 2003; Melendez-Vasquez et al., 2005). Of note, syndecan-3 and NG2 deficient mice exhibit normal nodal organization and unaltered clustering of Nav (Melendez-Vasquez et al., 2005; Colombelli and Feltri, unpublished observation), making it necessary the generation of multiple HSPG knock outs to unveil heparan sulfate function in the nodal region. Similarly, CNS nodes present a specialized extracellular matrix that contains the chondroitin-sulfate proteoglycans (CSPGs) brevican, versican V2 and phosphacan, the glycoprotein tenascin-R and brain-specific hyaluronan-binding link protein Bral1 (Rasband, 2010). It has been proposed that these ECM proteins may have a role in active clustering of channels at CNS nodes, but genetic loss of any single one of them does not affect the clustering of Nav (Weber et al., 1999; Brakebusch et al., 2002; Dours-Zimmerman et al., 2009; Bekku et al., 2010). As in PNS, redundancy could play a role, but alternative functions, including buffering of ions and stabilization of clusters, have been advocated (Hedstrom et al., 2007; Bekku et al., 2010).

Potential role of α-DG-N at nodes

The hypothesis that, with or without a HSPG, dystroglycan might have a role in coordinating the NrCAM-gliomedin multimolecolar

complex is supported by the finding that at microvilli DG not only faces the basal lamina, but also the nodal gap substance. Moreover, like glial NrCAM and gliomedin, α-DG contains a consensus sequence for furin-mediated cleavage. It has been shown that the N-terminal domain of α-DG (α-DG-N) is released in culture media of several cell types (Singh et al., 2004; Saito et al., 2008), and can also be found in different body fluids, like plasma, urine and cerebrospinal fluid (Saito et al., 2008 and 2011; Hesse et al., 2011). Some reports, but not others, suggested that α-DG-N can bind laminins and other ECM ligands, and promote neurite extension *in vitro* (Hall et al., 2003; Kangawa et al., 2004). Nonetheless, its biological function is still elusive. By analogy with gliomedin and NrCAM, we hypothesized that α-DG-N is shed in the nodal gap substance where it can exert a stabilizing effect on the NrCAM-gliomedin/Nf186 complex. Indeed, we demonstrated that in the absence of furin inhibitor Schwann cells released α-DG-N in the culture medium. Although direct detection of native α-DG-N *in vivo* was hampered by the absence of a suitable antibody, dystroglycan-Fc binding assays revealed that the N-terminal fragment of DG is able to bind myelinating fibers in an *in vitro* system. Complete α-DG, comprising the mucin-like domain deposited onto the surface of cultured Schwann cells, probably binding laminins, perlecan and/or agrin. Instead, α-DG-N was not able to interact with either Schwann cells or isolated neurons, but interaction could be detected upon ascorbic acid addition, in SC-DRG co-cultures. From preliminary experiments, similarly to the olfactomedin domain of gliomedin, α-DG-N decorates the surface of Schwann cells aligned with axons and progressively accumulates at

nodes of Ranvier as myelination proceeds (not shown). This suggests that α-DG-N binds one or more molecules that are expressed by or complexed onto the axonal surface only when myelination is triggered. Future experiments are aimed at confirming the exact localization of α-DG-N in myelinating fibers in respect to nodal and paranodal markers, and at different stages of myelination. Potential α-DG-N binding partners in the nodal gap are not known, but α-DG-N is an autonomous folding unit, with an Ig-like domain, a module that is commonly implicated in cell-cell interactions and adhesion (Barclay, 1999). A recent study describes the extracellular protein DIG-1, a new potential interactor of the N-terminal domain of the DG ortholog in *C. elegans* (DGN1) (Johnson and Kramer, 2012). DIG-1 has been first described as a giant secreted protein containing many protein interaction domains, with high similarity to mammalian hyalectans, like aggrecan and versican. Its function is to mantain axons and cell bodies in place whithin axonal fascicles and ganglia (Bénard et al., 2006; Burket et al., 2006). It has been shown that a direct or an indirect interaction between DIG-1 and the N-terminal domain of DGN-1 is required for the maintenance of lumbar neuron position (Johnson et al., 2012). As cell-matrix interactions are important in nematode embryonic positional maintenance, in a similar way vertebrate α-DG-N could favour the positioning of microvilli by mediating the binding between a nodal gap proteoglycan and the NrCAM-gliomedin/Nf186 multimeric complex. This proteoglycan could be perlecan, that is in fact reduced in the absence of DG, or alternatively versican V1.

Dystroglycan mediates Nav clustering through two distinct mechanisms

In conclusion, our study demonstrated that dystroglycan is required for the formation of properly shaped Nav clusters at peripheral nodes and heminodes. We propose a model implying two cooperating mechanisms. On the basal lamina side DG-laminin 211 interaction induces the reorganization of the cytoskeleton of Schwann cell tips, during the formation of microvilli, thus stabilizing Nav clusters in the nodal axolemma. On the axonal side, the N-terminal domain of α-DG might be shed in the nodal gap where it stabilizes the glial complex that induces axonal neurofascin and Nav accumulation (Fig. 12).

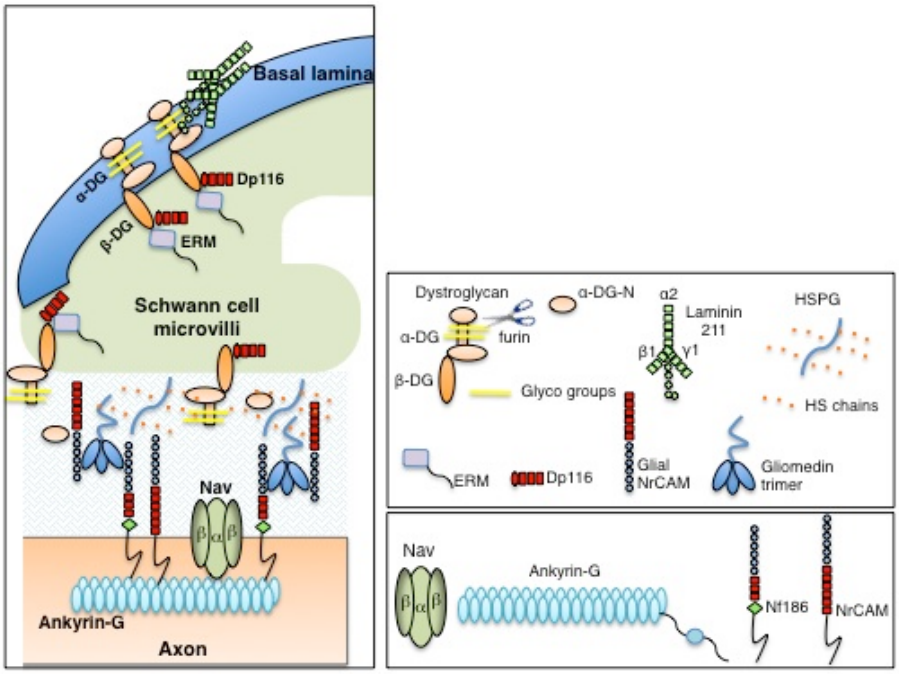

Fig. 12 Schematic representation of the potential mechanisms through which DG mediates proper Nav clustering at nodes of Ranvier. We propose that dystroglycan aids axonal Nav clustering via two different, not mutually exclusive, mechanisms. At the side of basal lamina (in blue), DG interaction with laminin 211 can trigger a remodeling of the cytoskeleton of microvilli through ERM proteins. The interactions of β-DG with ERMs and Dp116 can occur simultaneously (Spence et al., 2004). We also hypothesize that α-DG-N is cleaved and released in the nodal gap substance (in light blue) where it can stabilize gliomedin/NrCAM-complex through interactions with a still undefined molecule. This could be an HSPG, like perlecan, agrin or versican V1. It is not known if furin cleavage occurs intracellularly or at the membrane and whether β-DG is also cleaved by MMP-2 and -9 at nodes of Ranvier. It is possible that two sequential cleavages, by MMPs and furin, can release two forms of α-DG, with distinctive functions in Nav clustering.

2.5 References

- Apostolski S, Sadiq SA, Hays A, Corbo M, Suturkova-Milosevic L, Chaliff P, Stefansson K, LeBaron RG, Ruoslahti E, Hays AP, and Latov N. (1994) Identification of Gal(β1-3)GalNAc bearing glycoproteins at the nodes of Ranvier in peripheral nerve. *J Neurosci Res* 38(2): 134-41.
- Barclay AN. (1999) Ig-like domains: evolution from simple interaction molecules to sophisticated antigen recognition. *Proc Natl Acad Sci USA* 96(26): 14672-14674.
- Bekku Y, Vargova L, Goto Y, Vorisek I, Dmytrenko L, Narasaki M, Ohtsuka A, Fässler R, Ninomiya Y, Syková E, and Oohashi T. (2010) Bral1: its role in diffusion barrier formation and conduction velocity in the CNS. *J Neurosci* 30(8): 3113-23.
- Bénard CY, Boyanov A, Hall DH, and Hobert O. (2006) DIG-1, a novel giant protein, non-autonomously mediates maintenance of nervous system architecture. *Dev* 133: 3329-40.
- Bhat MA, Rios JC, Lu Y, Garcia-Fresco GP, Ching W, St Martin M, Li J, Einheber S, Chesler M, Rosenbluth J, Salzer JL, and Bellen HJ. (2001) Axon-glia interactions and the domain organization of myelinated axons requires neurexin IV/Caspr/Paranodin. *Neuron* 30: 369-383.
- Boiko T, Rasband M, Levinson S, Caldwell J, Mandel G, Trimmer J, and Mathews G. (2001) Compact myelin dictates the differential targeting of two sodium channel isoforms in the same axon. *Neuron* 30: 91-104.
- Bozic D, Sciandra F, Lamba D, and Brancaccio A. (2004) The structure of the N-terminal region of murine skeletal muscle α-dystroglycan discloses a modular architecture. *J Biol Chem* 279: 44812-44816.
- Brakebusch C, Seidenbecher CI, Asztely F, Rauch U, Matthies H, Meyer H, Krug M, Bockers TM, Zhou X, Kreutz MR, Montag D, Gundelfinger

ED, and Fässler R. (2002) Brevican-deficient mice display impaired hippocampal CA1 long-term potentiation but show no obvious deficits in learning and memory. *Mol Cell Biol* 22: 7417-7427.

- Bretscher A, Edwards K, and Fehon RG. (2002) ERM proteins and merlin: integrators at the cell cortex. *Nat Rev Mol Cell Biol* 3: 586-599.
- Brockes JP, Fields P, and Raff MC. (1979) Studies on cultured rat Schwann cells. I. Establishment of purified populations from cultures of peripheral nerve. *Brain Res* 165: 105-118.
- Burket CT, Higgins CE, Hull LC, Berninsone PM, and Ryder EF. (2006) The *C. elegans* gene *dig-1* encodes a giant member of the immunoglobulin superfamily that promotes fasciculation of neuronal processes. *Dev Biol* 299: 193-205.
- Cai H, Erdman RA, Zweier L, Chen J, Shaw IV JH, Baylor KA, Stecker MM, Carey DJ, and Chan Y-MM. (2007) The sarcoglycan complex in Schwann cells and its role in myelin stability. *Exp Neurol* 205(1): 257-269.
- Chen YJ, Spence HJ, Cameron JM, Jess T, Ilsley JL, and Winder SJ. (2003) Direct interaction of β-dystroglycan with F-actin. *Biochem* 375(2): 329-337.
- Ching W, Zanazzi G, SR Levinson, and Salzer JL. (1999) Clustering of neuronal sodium channels requires contact with myelinating Schwann cells. *J Neurocytol* 28: 295-301.
- Court FA, Zambroni D, Pavoni E, Colombelli C, Baragli C, Figlia G, Sorokin L, Ching W, Salzer JL, Wrabetz L, and Feltri ML. (2011) MMP2-9 cleavage of dystroglycan alters the size and molecular composition of Schwann cell domains. *J Neurosci* 31(34): 12208-17.
- Custer AW, Kazarinova-Noyes K, Sakurai T, Xu X, Simon W, Grumet M, and Shrager P. (2003) The role of the ankyrin-binding protein NrCAM in node of Ranvier formation. *J Neurosci* 23(31): 10032-10039.

- Dours-Zimmerman MT, Maurer K, Rauch U, Stoffel W, Fässler R, and Zimmermann DR. (2009) Versican V2 assembles the extracellular matrix surrounding the nodes of Ranvier in the central nervous system. *J Neurosci* 29: 7731-42.
- Echaniz-Laguna A, Rene F, Marcel C, Bangratz M, Fontaine B, Loeffler J-P, and Nicole S. (2009) Electrophysiological studies in a mouse model of Schwartz-Jampel syndrome demonstrate muscle fiber hyperactivity of peripheral nerve origin. *Muscle Nerve* 40(1): 55-61.
- Einheber S, Zanazzi G, Ching W, Scherer S, Milner TA, Peles E, and Salzer JL. (1997) The axonal membrane protein Caspr/neurexin IV is a component of the septate-like paranodal junctions that assemble during myelination. *J Cell Biol* 139: 1495-1506.
- Eshed Y, Feinberg K, Poliak S, Sabanay H, Sarig-Nadir O, Spiegel I, Bermingham JR Jr, and Peles E. (2005) Gliomedin mediates Schwann cell-axon interaction and the molecular assembly of nodes of Ranvier. *Neuron* 47(2): 215-29.
- Eshed Y, Feinberg K, Carey DJ, and Peles E. (2007) Secreted gliomedin is a perinodal matrix component of peripheral nerves. *J Cell Biol* 177: 551-562.
- Feinberg K, Eshed-Eisenbach Y, Frechter S, Amor V, Salomon D, Sabanay H, Dupree JL, Grumet M, Brophy PJ, Shrager P, and Peles E. (2010) A glial signal consisting of gliomedin and NrCAM clusters axonal Na^+ channels during the formation of nodes of Ranvier. *Neuron* 65: 490-502.
- Feltri ML, D'Antonio M, Previtali S, Fasolini M, Messing A, and Wrabetz L (1999) P0-Cre transgenic mice for inactivation of adhesion molecules in Schwann cells. *Ann NY Acad Sci* 883: 116-123.

- Gatto CL, Walker BJ, and Lambert S. (2003) Local ERM activation and dynamic growth cones at Schwann cell tips implicated in efficient formation of nodes of Ranvier. *J Cell Biol* 162: 489-498.
- Gesemann M, Brancaccio A, Schumacher B, and Ruegg MA. (1998) Agrin is a high-affinity binding protein of dystroglycan in non-muscle tissue. *J Biol Chem* 273: 600-605.
- Gollan L, Salomon D, Salzer JL, and Peles E. (2003) Caspr regulates the processing of contactin and inhibits its binding to neurofascin. *J Cell Biol* 163: 1213-1218.
- Goutebroze L, Carnaud M, Denisenko N, Boutterin MC, and Girault JA. (2003) Syndecan-3 and syndecan-4 are enriched in Schwann cell perinodal processes. *BMC Neurosci* 4: 29-37.
- Granes F, Urena JM, Rocamora N, and Vilaro S. (2000) Ezrin links syndecan-2 to the cytoskeleton. *J Cell Sci* 113(7): 1267-1276.
- Granes F, Berndt C, Roy C, Mangeat P, Reina M, and Vilaro S. (2003) Identification of a novel ezrin-binding site in syndecan-2 cytoplasmic domain. *FEBS Lett* 547: 212-216.
- Hall H, Bozic D, Michel K, and Hubbell JA. (2003) N-terminal α-dystroglycan binds to different extracellular matrix molecules expressed in regenerating peripheral nerves in a protein mediated manner and promotes neurite extension of PC12 cells. *Mol Cell Neurosci* 24: 1062-1073.
- Hedstrom KL, Xu X, Ogawa Y, Frischknecht R, Seidenbecher CI, Shrager P, and Rasband MN. (2007) Neurofascin assembles a specialized extracellular matrix at the axon initial segment. *J Cell Biol* 178(5): 875-86.
- Hess A, and Young JZ. (1952) The Nodes of Ranvier. *Proc R Soc Lond B* 140: 301-320.
- Hesse C, Johansson I, Mattsson N, Bremell D, Andreasson U, Halim A,

Anckarsäter R, Blennow K, Anckarsäter H, Zetterberg H, Larson G, Hagberg L, and Grahn A. (2011) The N-terminal domain of α-dystroglycan is released as a 38 kDa protein and is increased in cerebrospinal fluid in patients with Lyme neuroborreliosis. *Biochem Biophys Res Comm* 412(3): 494-9.

- Hodgkin AL, and Huxley AF. (1952) A quantitative description of membrane current and its application to conduction and excitation in nerve. *J Physiol* 117: 500-544.
- Ichimura T, and Ellisman MH. (1991) Three-dimensional fine structure of cytoskeletal-membrane interactions at nodes of Ranvier. *J Neurocytol 20*: 667-681.
- Ido H, Harada K, Futaki S, Hayashi Y, Nishiuchi R, NatsukaY, Li S, Wada Y, Combs AC, Ervasti JM, and Sekiguchi K. (2004) Molecular dissection of the α-dystroglycan- and integrin-binding sites within the globular domain of human laminin-10. *J Biol Chem* 279(12): 10946-10954.
- Johnson RP, and Kramer JM. (2012) Neural maintenance roles for the matrix receptor dystroglycan and the nuclear anchorage complex in *C. elegans*. *Genetics* [Epub ahead of print].
- Kanagawa M, Saito F, Kunz S, Yoshida-Moriguchi T, Barresi R, Kobayashi YM, Muschler J, Dumanski JP, Michele DE, Oldstone BA, and Campbell KP. (2004) Molecular recognition by LARGE is essential for expression of functional dystroglycan. *Cell* 117: 953-964.
- Landon DN, and Langley OK. (1971) The local chemical environment of nodes of Ranvier: a study of cation binding. *J Anat* 108: 419-432.
- Maertens B, Hopkins D, Franzke CW, Keene DR, Bruckner-Tuderman L, Greenspan DS, and Koch M. (2007) Cleavage and oligomerization of gliomedin, a transmembrane collagen required for node of Ranvier formation. *J Biol Chem* 282(14): 10647-59.

- Martin PT. (2003) Dystroglycan glycosylation and its role in matrix binding in skeletal muscle. *Glycobiol* 13(8): 55R-66R.
- Martin S, Levine AK, Chen ZJ, Ughrin Y, and Levine JM. (2001) Deposition of the NG2 proteoglycan at nodes of Ranvier in the peripheral nervous system. *J. Neurosci.* 21: 8119-8128.
- Masaki T, Matsumura K, Hirata A, Yamada H, Hase A, Arai K, Shimizu T, Yorifuji H, Motoyoshi K, and Kamakura K. (2002) Expression of dystroglycan and the laminin-α2 chain in the rat peripheral nerve during development. *Exp Neurol* 174, 109-117.
- McClatchey AI, and Fehon RG. (2009) Merlin and the ERM proteins-regulators of receptor distribution and signaling at the cell cortex. *Trends Cell Biol* 19: 198-206.
- Melendez-Vasquez CV, Rios JC, Zanazzi G, Lambert S, Bretscher A, and Salzer JL. (2001) Nodes of Ranvier form in association with ezrin-radixin-moesin (ERM)-positive Schwann cell processes. *Proc Natl Acad Sci USA* 98: 1235-1240.
- Melendez-Vasquez C, Carey DJ, Zanazzi G, Reizes O, Maurel P, and Salzer JL. (2005) Differential expression of proteoglycans at central and peripheral nodes of Ranvier. *Glia* 52: 301-308.
- Moore SA, Saito F, Chen J, Michele DE, Henry MD, Messing A, Cohn RD, Ross-Barta SE, Westra S, Williamson RA, Hoshi T, Campbell KP (2002) Deletion of brain dystroglycan recapitulates aspects of congenital muscular dystrophy. *Nature* 418: 422-425.
- Nico B, Tamma R, Annese T, Mangieri D, De Luca A, Corsi A, Benagiano V, Longo V, Crivellato E, Salmaggi A and Ribatti D. (2010) Glial dystrophin-associated proteins, laminin and agrin, are downregulated in the brain of mdx mouse. *Lab Invest* 90: 1645-1660.
- Occhi S, Zambroni D, Del Carro U, Amadio S, Sirkowski EE, Scherer SS, Campbell KP, Moore SA, Chen ZL, Strickland S, Di Muzio A,

Uncini A, Wrabetz L, and Feltri ML. (2005) Both laminin and Schwann cell dystroglycan are necessary for proper clustering of sodium channels at nodes of Ranvier. *J Neurosci* 25(41): 9418-9427.

- Pedraza L, Huang JK, and Colman DR. (2001) Organizing principles of the axoglial apparatus. *Neuron* 30: 335-344.
- Poliak S, and Peles E. (2003) The local differentiation of myelinated axons at nodes of Ranvier. *Nat Rev Neurosci* 4: 968-980.
- Previtali SC, Nodari A, Taveggia C, Pardini C, Dina G, Villa A, Wrabetz L, Quattrini A, and Feltri ML. (2003) Expression of laminin receptors in Schwann cell differentiation: evidence for distinct roles. *J Neurosci* 23: 5520-5530.
- Quick DC, and Waxman SG. (1977) Ferric ion, ferrocyanide, and inorganic phosphate as cytochemical reactants at peripheral nodes of Ranvier. *J Neurocytol* 6(5): 555-70.
- Rafael JA, Tinsley JM, Potter AC, Deconinck AE, and Davies KE. (1998) Skeletal muscle-specific expression of a utrophin transgene rescues utrophin-dystrophin deficient mice. *Nat Genet* 19: 79-82.
- Rafael JA, Trickett JI, Potter AC, and Davies KE. (1999) Dystrophin and utrophin do not play crucial roles in nonmuscle tissues in mice. *Muscle Nerve* 22: 517-519.
- Ranvier L. (1871) Sur les éléments conjonctifs de la moelle épinière. *Compt Rend* 73: 1168-1171.
- Rasband MN, Peles E, Trimmer JS, Levinson SR, Lux SE, and Shrager P. (1999) Dependence of nodal sodium channel clustering on paranodal axoglial contact in the developing CNS. *J Neurosci* 19: 7516-7528.
- Rasband MN. (2010) Composition, assembly, and maintenance of excitable membrane domains in myelinated axons. *Semin Cell Dev Biol* 22(2):178-84.
- Rossi M, Morita H, Sormunen R, Airenne S, Kreivi M, Wang L, Fukai

N, Olsen BR, Tryggvason K, and Soininen R. (2003) Heparan sulfate chains of perlecan are indispensable in the lens capsule but not in the kidney. *EMBO J* 22(2): 236-245.

- Saito F, Moore SA, Barresi R, Henry MD, Messing A, Ross-Barta SE, Cohn RD, Williamson RA, Sluka KA, Sherman DL, Brophy PJ, Schmelzer JD, Low PA, Wrabetz L, Feltri ML, and Campbell KP. (2003) Unique role of dystroglycan in peripheral nerve myelination, nodal structure, and sodium channel stabilization. *Neuron* 38: 747-758.
- Saito F, Saito-Arai Y, Nakamura A, Shimizu T, and Matsumura K. (2008) Processing and secretion of the N-terminal domain of a-dystroglycan in cell culture media. *FEBS Lett* 582(3): 439-44.
- Saito F, Saito-Arai Y, Nakamura-Okuma A, Ikeda M, Hagiwara H, Masaki T, Shimizu T, and Matsumura K. (2011) Secretion of N-terminal domain of α-dystroglycan in cerebrospinal fluid. *Biochem Biophys Res Commun* 411(2): 365-9.
- Salzer JL. (2003) Polarized domains of myelinated axons. *Neuron* 40: 297-318.
- Schafer DP, Custer AW, Shrager P, and Rasband MN. (2006) Early events in node of Ranvier formation during myelination and remyelination in the PNS. *Neuron Glia Biol* 2(2): 69-79.
- Scherer SS, Xu Y, Bannerman PGC, Sherman DL, and Brophy PJ. (1995) Periaxin expression in myelinating Schwann cells: modulation by axon-glial interactions and polarized localization during development. *Dev* 121: 4265-4273.
- Sherman DL, Tait S, Melrose S, Johnson R, Zonta B, Court FA, Macklin WB, Meek S, Smith AJ, Cottrell DF, and Brophy PJ. (2005) Neurofascins are required to establish axonal domains for salutatory conduction. *Neuron* 48: 737-742.
- Singh J, Itahana Y, Knight-Krajewski S, Kanagawa M, Campbell KP,

Bissell MJ, and Muschler J. (2004) Proteolytic enzymes and altered glycosylation modulate dystroglycan function in carcinoma cells. *Canc Res* 64: 6152-6159.

- Spence HJ, Chen YJ, Batchelor CL, Higginson JR, Suila H, Carpen O, and Winder SJ. (2004) Ezrin-dependent regulation of the actin cytoskeleton by b-dystroglycan. *Hum Mol Gen* 13(15): 1657-1668.
- Stum M, Girard E, Bangratz M, Bernard V, Herbin M, Vignaud A, Ferry A, Davoine CS, Echaniz-Laguna A, René F, Marcel C, Molgó J, Fontaine B, Krejci E, and Nicole S. (2008) Evidence of a dosage effect and a physiological endplate acetylcholinesterase deficiency in the first mouse models mimicking Schwartz-Jampel syndrome neuromyotonia. *Hum Mol Genet* 17(20): 3166-79.
- Talts JF, Andac Z, Gohring W, Brancaccio A, and Timpl R. (1999) Binding of G domains of laminin α1 and α2 chains and perlecan to heparin, sulfatides, α-dystroglycan and several extracellular matrix proteins. *EMBO J* 18: 863-870.
- Tao-Cheng JH, and Rosenbluth J. (1983) Axolemmal differentiation in myelinated fibers of rat peripheral nerves. *Brain Res* 285: 251-263.
- Thaxton C, Pillai AM, Pribisko AL, Dupree JL, and Bhat MA. (2011) Nodes of Ranvier act as barriers to restrict invasion of flanking paranodal domains in myelinated axons. *Neuron* 69: 244-257.
- Vabnick I, Novakovic SD, Levinson SR, Schachner M, and Shrager P. (1996) The clustering of axonal sodium channels during development of the peripheral nervous system. *J Neurosci* 16: 4914-4922.
- Vagnerova KT, Tarumi YS, Proctor TM, and Patton BL. (2003) A specialized basal lamina at the node of Ranvier. Abstract 29:351.18 at *Soc for Neurosci Meeting*.
- Weber P, Bartsch U, Rasband MN, Czaniera R, Lang Y, Bluethmann H, Margolis RU, Levinson SR, Shrager P, Montag D, and Schachner M.

(1999) Mice deficient for tenascin-R display alterations of the extracellular matrix and decreased axonal conduction velocities in the CNS. *J Neurosci* 19(11): 4245-62.

- Wrabetz L, Feltri ML, Quattrini A, Imperiale D, Previtali S, D'Antonio M, Martini R, Yin X, Trapp BD, Zhou L, Chiu SY, and Messing A. (2000) P(0) glycoprotein overexpression causes congenital hypomyelination of peripheral nerves. *J Cell Biol* 148: 1021-1034.
- Zhang Y, Bekku Y, Dzhashiashvili Y, Armenti S, Meng X, Sasaki Y, Milbrandt J, and Salzer JL. (2012) Assembly and maintenance of nodes of Ranvier rely on distinct sources of proteins and targeting mechanisms. *Neuron* 73: 92-107.
- Zhou Z, Wang J, Cao R, Morita H, Soininen R, Chan KM, Liu B, Cao Y, and Tryggvason K. (2004) Impaired angiogenesis, delayed wound healing and retarded tumor growth in perlecan heparan sulfate-deficient mice. *Canc Res* 64: 4699-4702.

MMP2-9 cleavage of dystroglycan alters the size and molecular composition of Schwann cell domains.

Felipe A. Court,[1] Desirée Zambroni,[1] Ernesto Pavoni,[1] Cristina Colombelli,[1] Chiara Baragli,[1] Gianluca Figlia,[1] Lydia Sorokin,[2] William Ching,[3] James L. Salzer,[3] Lawrence Wrabetz,[1] and M. Laura Feltri[1]

1 Division of Genetics and Cell Biology, San Raffaele Scientific Institute, 20132 Milan, Italy.
2 Institute of Physiological Chemistry and Pathobiochemistry, University of Muenster, 48149 Muenster, Germany.
3 Department of Cell Biology and Neurology, and the Smilow Neuroscience Program, New York University School of Medicine, New York, New York 10016.

Published in:
Journal of Neuroscience, 31(34): 12208-12217 (2011).

Chapter 3

Dystroglycan regulation of Schwann cell cytoplasm compartmentalization and internodes

3.1 Introduction

Function of many cell types depends on polarization, the formation of different anatomical, and molecular domains. Myelinating Schwann cells are highly polarized both radially and longitudinally, a configuration required for action potential propagation (Salzer, 2003). In addition, the cytoplasm outside myelin is organized into regions in which the outer cell membrane and myelin are apposed or cytoplasmic channels extending from perinuclear to nodal regions (Cajal bands and *trabeculae*) (Ramón y Cajal, 1933). These structures probably fulfill the metabolic and transport requirement of Schwann cells (Kidd et al., 1994; Court et al., 2004), which must extend up to 1 mm in length and produce 50-100 wraps of spiraling membrane during myelination. It has been proposed that this pattern is also required to achieve the correct length of a myelin segment (internodal length), which in turn regulates nerve conduction velocity (Court et al., 2004). We recently demonstrated that the dystrophin-glycoprotein complex (dystroglycan complex), containing utrophin and laminin 211, plays a role in this process (Court et al., 2009). This may explain the internodal abnormalities seen in mice and patients lacking laminin 211 in congenital muscular dystrophy 1A (MDC1A) (Bradley and Jenkison, 1973; Di Muzio et al., 2003). The dystroglycan complex connects the

cytoskeleton to extracellular matrix, and, in Schwann cells, it consists of α- and β-dystroglycan (DG), sarcoglycans, dystrobrevins, synthrophins, and the dystrophin family members utrophin, Dp116, and DRP2. The dystroglycan complex provides a scaffold for specific proteins required for myelin stability (Sherman et al., 2001; Cai et al., 2007; Albrecht et al., 2008), and its composition varies in different Schwann cell compartments: utrophin, Dp116, α-dystrobrevin1, and syntrophins are in Cajal bands (Albrecht et al., 2008; Court et al., 2009), DRP2 and periaxin are in appositions (Sherman et al., 2001), and Dp116 is enriched in microvilli (Occhi et al., 2005). How the differential distribution of dystroglycan complex components is achieved is unknown. Here we provide evidence that selective proteolytic processing is a mechanism contributing to this cell polarization.

DG is processed after synthesis into transmembrane β-dystroglycan (β-DG) and extracellular α-dystroglycan (α-DG), which binds laminins and proteoglycans (Ibraghimov-Beskrovnaya et al., 1992; Holt et al., 2000). β-DG can be further cleaved extracellularly by matrix metalloproteinase 2 and 9 (MMP-2 and -9), yielding a transmembrane protein unable to bind α-DG, therefore disrupting the linkage between the basement membrane and the cytoskeleton (Yamada et al., 2001; Zhong et al., 2006). With few exceptions, this processing has been associated with pathological conditions, including cancer invasion, autoimmune encephalomyelitis, and muscular dystrophies (Matsumura et al., 2003; Jing et al., 2004; Agrawal et al., 2006; Shang et al., 2008).

Here we show that the composition and localization of components of the dystroglycan complex change depending on cleavage of β-dystroglycan by MMP-2 and MMP-9 and that this is a physiological process that Schwann cells may use to remodel subcellular compartments. In contrast, excessive dystroglycan cleavage results in abnormal compartments in nerves from *Lama2*$^{dy2J/dy2J}$ mice, an animal model of MDC1A (Bradley and Jenkison, 1973; Di Muzio et al., 2003). Inhibition of DG proteolysis restores normal compartments and partially rescues internodal lenght in myelinating *Lama2*$^{dy2J/dy2J}$ cultures. However, the genetic ablation of MMP-9 from two murine models of MDC1A (*Lama2*$^{dy2J/dy2J}$ and *Lama2*$^{dy3k/dy3k}$) is not sufficient to rescue these parameters *in vivo*.

3.2 Materials and Methods

Mice. P0CreDGko (dgko), *Lama2*$^{dy2J/dy2J}$ (*Dy2j/2j*), and *Lama2*$^{3k/3k}$ (Dy3k/3k) (from S. Takeda) mice were reported previously (Meier and Southard, 1970; Miyagoe et al., 1997; Feltri et al., 1999; Saito et al., 2003) and were on a C57BL/6 background. MMP-2 knock out (KO) mice (C57BL/6) were from S. Itohara (Riken Institute, Tokyo, Japan) (Itoh et al., 1997), MMP-9KO mice were from G. Odenakker (University of Leuven, Leuven, Belgium) (Dubois et al., 1999) (C57BL/6) and The Jackson Laboratory (Vu et al., 1998) (FVB). Experiments were approved by the San Raffaele Institutional Animal Care and Use Committee and complied with NIH guidelines.

Primary/secondary antibodies and dyes. Primary antibodies included the following: rabbit anti-DRP2 (1:400 for IF; 1:2000 for WB) and rabbit anti-periaxin (1:30000 for WB) (both generous gifts from P.J. Brophy and D. Sherman, University of Edinburgh, Edinburgh, UK), mouse anti-β-tubulin (Sigma) (1:1000), FITC- and TRITC-conjugated phalloidin (Sigma), mouse anti-β-dystroglycan (43DAG/8D5; Novocastra) (1:50 for IF; 1:80 for WB), mouse anti-Dp116 (Mandra1; Sigma) (1:100 for IF; 1:1500 for WB), mouse anti-glycosylated α-dystroglycan (IIH6) (1:100 for IF; 1:1000 for WB) and goat anti-core α-dystroglycan G20 (1:20 for IF) (both generous gifts from K.P. Campbell, University of Iowa, Iowa City, IA), rat anti-myelin basic protein (MBP; 1:10 for IF) (generous gift from V. Lee, University of Pennsylvania, Philadelphia, PA), mouse anti-utrophin (1:1000 for WB) (NovoCastra Laboratories), mouse anti-utrophin (1:10 for IF) (generous gift from G.E. Morris), rat anti-β1-integrin (1:20 for IF) (R&DSystems), mouse anti-β1-integrin (BD Trans Lab) (1:1000 for WB), goat anti-MMP-9 (1:1000 for WB) (R&DSystems), rabbit anti-neurofilament (1:3000 for WB) (Chemicon), and rabbit anti-calnexin (1:3000 for WB) (Sigma). Secondary antibodies included the following: goat anti-rabbit FITC or TRITC and goat anti-mouse Cy5 (1:200) (Jackson ImmunoResearch), goat anti-mouse (Fab-specific) or goat anti-mouse (Fc-specific) HRP (1:5000) (Sigma), donkey anti-goat HRP (1:5000) (Tebu-Bio), goat anti-rabbit HRP (1:10000), and DAPI (Sigma). The goat anti-mouse secondary antibodies were used to reveal the mouse anti-β-dystroglycan 43DAG/8D5 antibody (see Fig. 2-9). When using the Fab-specific or

Fc-specific goat anti-mouse antibody, a non specific band of 25 or 55 kDa, respectively, appeared, which was present even when the primary antibody was omitted (marked with * in the figures) and represented Ig in the nerves recognized by the secondary antibody.

Western blot analysis. Sciatic nerves and dorsal root ganglia or coverslips with explants were frozen and homogenized in a metal pestle and then lysed with buffer PN1 containing 25 mM Tris, pH 7.4, 95 mM NaCl, 10 mM EDTA, 2% SDS, 1 mM NaF, 1 mM Na_3VO_4, and 1% protease inhibitor cocktail (PIC) (Sigma-Aldrich). Western blot was performed using standard techniques.

Gelatin zymography. Sciatic nerves were dissected and perineurium removed. Nerves were homogenized in 100 mM Tris, pH 7.4, 200 mM NaCl, 1% Triton X-100, 1 mM 4-(2-aminoethyl)benzenesulfonyl fluoride (AEBSF), and 1% PIC and centrifuged for 15 min at 4°C. Supernatants were recovered, and proteins were quantified (BCA kit; Invitrogen). Proteins, 60 μg, were mixed with 3X sample buffer and loaded in an SDS gel containing 1 mg/ml pig skin gelatin (Fluka) in the running part of the gel. Samples were not boiled or treated with DTT to avoid loss of enzymatic activity. After running, the gel was washed in distilled water (dH_2O) twice, incubated in a solution containing 2.5% Triton X-100 in dH_2O, washed, and incubated in 50 mM Tris, pH 7.6, 5 mM $CaCl_2$, and 0.02% NaN_3 at 37°C. After two washes in dH_20, gels were stained with Coomassie Brilliant Blue and destained until degradative, negative bands appear.

Wheat germ agglutinin pull-down. Sciatic nerves were frozen and grinded in a metal pestle. From this step, all procedures were performed at 4°C. Nerve powders were incubated with lysis buffer B (50 mM Tris-HCl, pH 7.5, 120mM NaCl, 1% digitonin, 0.25mM AEBSF, and 1% PIC) for 2 hs in a rotating apparatus, lysates were centrifuged at 13,200 rpm for 30 min, and the supernatant (input) was mixed with wheat germ agglutinin agglutinin (WGA)-Sepharose (washed in buffer B overnight). After centrifugation, the supernatant was stored (void), and WGA-bound proteins were washed in buffer B and eluted using 0.6 M *N*-acetyl-D-glucosamine for 5 min at room temperature (WGA). After spinning, eluted proteins were loaded in an SDS gel for Western blot. Although β-DG is also glycosylated, our protocol allows us to obtain a fraction rich in α-DG.

Electron microscopy. Electron microscopy was performed as described previously (Wrabetz et al., 2000).

Immunofluorescence. For immunofluorescence, sciatic nerve fibers were teased and immediately stained with mild permeabilization to preserve the abaxonal subcortical Schwann cell structure as described (Court et al., 2009), with the following modification for dystroglycan complex proteins: nerves permeabilized for 5 min in methanol at room temperature and blocked with 1% fish skin gelatin. Dorsal root ganglia were fixed for 10 min in 4% paraformaldehyde and blocked/permeabilized with 5% fish skin gelatin and 0.5% Triton X-100.

Drug injection. Intraperineurial drug injection (IL-1β, 20 μg/ml; GM6001 (Sigma-Aldrich) (*N*-[(2*R*)-2(hydroxamidocarbonylmethyl)-4 methylpantanoyl]-L-tryptophan methylamide), 1mM) was performed as described (Court and Alvarez, 2000).

Rat dorsal root ganglia-Schwann cell co-cultures. Primary rat dorsal root ganglia and Schwann cell cultures were prepared from embryos of 15-17 gestational days following the method described (Einheber et al., 1997).

Mouse dorsal root ganglia explants. Dorsal root ganglia were dissected from embryos of 14.5 gestational days as described previously (Nodari et al., 2007). After 3 days, ascorbic acid (50 μg/ml) was added to the medium to induce myelination for 2-3 weeks, in the presence or absence of GM6001 (4-20 μM) or vehicle.

Teasing of osmicated fibers and internodal lenght measurement. Sciatic nerves from adult mice were dissected and fixed 1 hour at 4°C in 2% glutaraldehyde in 0.12 M phosphate buffer. Nerves were then washed in 0.12 M phosphate buffer and osmicated in 1% OsO_4 for 2 hours at room temperature. After 3 washes in 0.12 M phosphate buffer, osmicated nerves were left in 66% glycerol overnight at RT. The day after they were transferred to 100% glycerol and stored at 4°C until teasing. With pointed forceps and using a dissecting microscope, epineurium and perineurium were stripped away from endoneurium on lightly glycerinated glass slides. Next, small strands

of nerve fibers were torn from the endoneurium and a single fiber or a small bundle of fibers was pulled away from the main strand. The proximal end of each separated fiber strand was grasped with forceps and slid onto a clean slide through a minute drop of glycerine. Coverslips were applied and sealed with nail polish. Images of single fibers were taken in bright field using a Leica DM 5000B microscope. This procedure permits evaluation of consecutive internodes of the same myelinated nerve fiber and is used to establish the frequency of certain neuropathologic abnormalities, such as tomacula, segmental demyelination, presence of myelin ovoids (Griffin et al., 1993; Krinke et al., 2000). For internodal length analysis, the length between two nodes of Ranvier was measured using *ImageJ* software. Around 100 internodes were measured for each animals, and 3 animals/genotypes were analyzed.

Morphological analysis, *f*-ratio, and imaging. All images were acquired with either a spinning Nipkow disk confocal microscope (UltraVIEW; PerkinElmer Life and Analytical Sciences) using a 63X objective or with a TCS SP2 Laser Scanning Confocal microscope using a 63X objective. Images were composed using Photoshop software (Adobe Systems). Any image manipulation was equally applied to all the panels in a figure. *f*-ratio analysis at the light (LM) and electron (EM) microscopic level was performed as described previously (Court et al., 2009). Semiquantitative estimate of dystroglycan complex proteins was performed using a mask corresponding to either DRP2 staining or actin staining using TRITC-

conjugated phalloidin. The signal intensity was measured in each domain and normalized to the total intensity of the complete optic slice.

3.3 Results

β-DG is present without α-DG in Cajal bands

We first assessed the localization of dystroglycan complex components by staining freshly isolated nerve fibers. Interestingly, we observed that α-DG is detectable only in appositions, where it forms a complex with DRP2 and periaxin (Sherman et al., 2001), whereas β-DG is also present in Cajal bands where it colocalizes with utrophin and Dp116 (Fig. 1). Staining with antibodies recognizing either the core α-DG protein or its glycosylated epitope colocalized in patches/appositions, excluding the possibility that α-DG was not detectable in Cajal bands because of potential differences in glycosylation that affect antibody binding (Fig. 1B). Therefore, utrophin, Dp116, and DRP2 are not only segregated in different subcellular domains but are found with two different DGs: complete DG (α and β) in appositions or β-DG alone in Cajal bands. Absence of α-DG in Cajal bands does not preclude linkage to the basal lamina in these regions, because other laminin receptors such as α6β1 or α6β4 integrins are localized in Cajal bands (Fig. 1F) (Nodari et al., 2008).

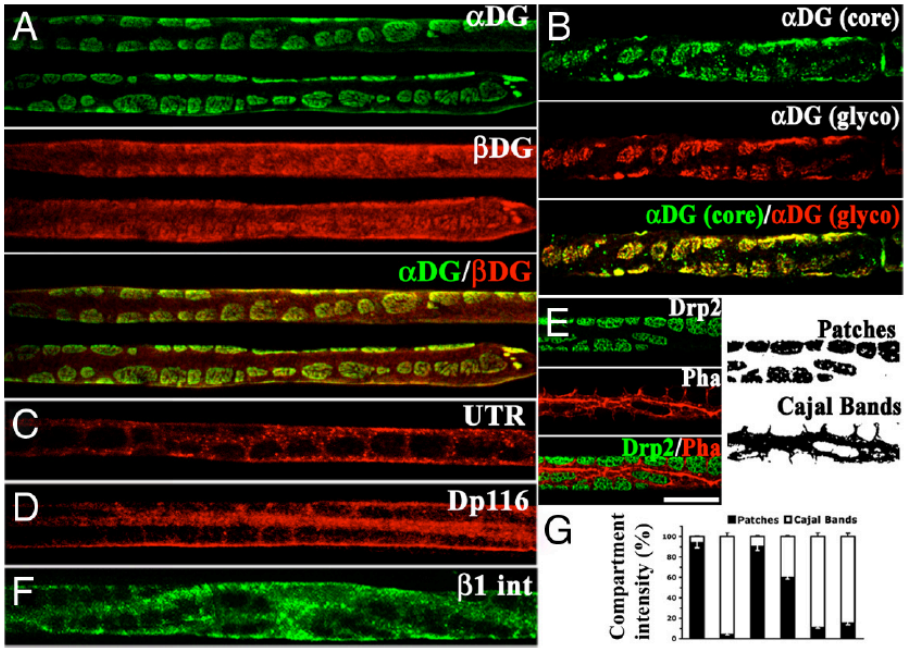

Fig. 1 β-DG, not α-DG, is localized in Cajal bands. Teased fibers from adult sciatic nerves stained with anti-DG complex antibodies. **A,** α-DG (green) is restricted to patches corresponding to appositions, in which DRP2 is also localized (**E**). In contrast β-DG (red) is also present in Cajal bands. **B**, Antibodies against glycosylated α-DG (red) or the α-DG core protein (green) colocalize and are both restricted to patches. Utrophin (UTR) (**C**), Dp116 (**D**), and β1integrin (**F**) are in Cajal bands. The fluorescence intensity of each protein in patches (black) or Cajal bands (white) is represented in **G**. Error bars corresponds to SEM. Scale bar, 10 μm.

Metalloproteinase-cleaved β-DG copurifies with different dystrophin-like proteins

The presence of β-DG without α-DG in Cajal bands suggested cleavage of the extracellular domain of β-DG. In several tissues the gelatinases MMP-2 and -9 cleave β-DG in its N-terminal extracellular portion, releasing α-DG (Yamada et al., 2001). We confirmed that also in peripheral nerves the proteolysis of full length β-DG ($\beta\text{-DG}_{43}$) occurs, and gives rise to a 31 kDa fragment ($\beta\text{-DG}_{31}$) (Fig. 2A, input lane; Yamada et al., 2001).

To support that the cleavage of N-terminal β-DG explains the absence of α-DG in Cajal bands, we asked whether only $\beta\text{-DG}_{43}$ copurified with glycosylated α-DG after pull down of nerve lysates using wheat germ agglutinin (WGA). As expected, WGA pulled down α-DG from nerves (Fig. 2A). $\beta\text{-DG}_{43}$, but not $\beta\text{-DG}_{31}$, was associated with the WGA fraction, whereas the void fraction contained $\beta\text{-DG}_{31}$, but little $\beta\text{-DG}_{43}$, strongly suggesting that β-DG in Cajal bands is mainly cleaved (Fig. 2). Furthermore, from the immunolocalization data, we expected that components of the dystroglycan complex in appositions (α-DG , $\beta\text{-DG}_{43}$ and DRP2) would copurify in the WGA fraction, while components of the dystroglycan complex in Cajal bands ($\beta\text{-DG}_{31}$, Dp116, utrophin) would be absent. Indeed, only DRP2 was in the WGA fraction, whereas utrophin and Dp116 were almost completely found in the void fraction with $\beta\text{-DG}_{31}$ (Fig. 2). DRP2 was also detected in the void, probably representing DRP2 protein not efficiently pulled-down. These results indicate that when not cleaved,

β-DG interacts with α-DG and forms a complex preferentially with DRP2, which is localized in appositions; vice versa β-DG cleavage favours the dystroglycan-utrophin/Dp116 complex in Cajal bands that corresponds to the void fraction. This model is represented in Fig. 2B.

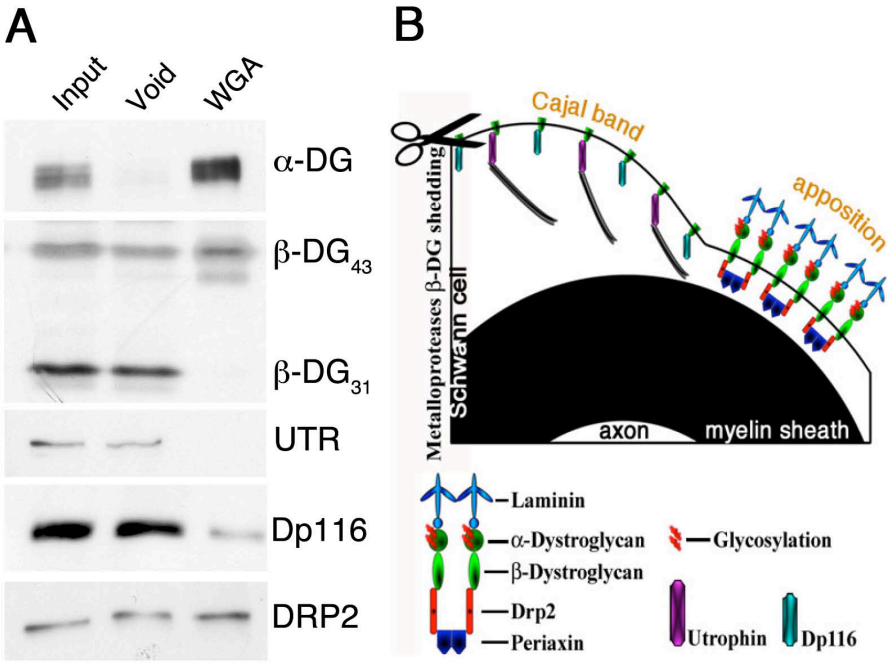

Fig. 2 β-DG$_{43}$ and β-DG$_{31}$ copurify with different intracellular partners. A, WGA pull-down from adult mouse sciatic nerves. Notice that the WGA fraction, enriched in α-DG, contains β-DG$_{43}$, whereas β-DG$_{31}$ is present only in the void fraction. The only dystrophin in the WGA fraction is DRP2, while utrophin and Dp116 are found preferentially in the void fraction. Both β-DG$_{43}$ and β-DG$_{31}$ are detected by an antibody recognizing β-DG C-terminus. **B,** Proposed model of the localization of different dystroglycan complexes in Schwann cells. β-DG$_{31}$ is cleaved by MMP-2/9 (scissor) and

associates with utrophin or Dp116 in Cajal bands. Uncleaved β-DG_{43} associates with α-DG extracellularly, DRP2 and periaxin intracellularly, and localizes at appositions.

β-DG cleavage by MMP-2 and -9 is developmentally regulated and correlates with the expression of the corresponding dystrophin family member

We wondered whether gelatinase activity and cleavage of β-DG were regulated during development. We showed previously that compartmentalization of Schwann cell cytoplasm *in vivo* starts at approximately P10, with formation of an actin scaffold around nascent appositions (Court et al., 2009). We found that MMP-9 is expressed at low levels throughout development and up-regulated after nerve injury, as previously reported (La Fleur et al., 1996) (Fig. 3A). In contrast, active MMP-2 is detected at P10 and 4 weeks, but not early in development or in mature nerves (Fig. 3A). This temporal expression/activation of MMPs correlates with the timing of Cajal band/apposition formation, and supports the idea that the modulation of β-DG cleavage could regulate the establishment of these specific compartments in Schwann cells. Furthermore, during the first postnatal days (P2-P10), a period in which appositions have not formed yet, β-DG is highly cleaved (Fig. 1I in Chapt. 2 and Fig. 3B) and Dp116 and utrophin are expressed at high levels (Fig. 2F in Chapt.2 and Fig. 3B); conversely, as appositions first appear (P10) and progressively grow (4 weeks), β-DG_{43} with its partner DRP2 increase, while β-DG_{31}, utrophin and Dp116 show a decrease,

suggesting a redistribution of these components to Cajal bands (Fig. 3B). α-DG expression does not change during development but its glycosylation does, a modification that might modulate the susceptibility of β-DG to MMP cleavage (Fig. 1J in Chapt. 2 and Fig. 3B).

These data suggest that MMP cleavage of β-DG may be directly involved in cytoplasmic compartmentalization by regulating the amount and composition of dystroglycan complex required for the formation of each cytoplasmic domain.

Modulation of MMP acitvity in nerves leads to modification of Schwann cell compartments

Selective α-DG shedding in Cajal bands may regulate formation and maintenance of compartments in Schwann cells, because this requires linkage between the cortical cytoskeleton and the basement membrane (Court et al., 2009).

To ask whether manipulation of MMP activity *in vivo* leads to changes in compartments, we injected the MMP-activating recombinant protein IL-1β (Wu et al., 2009) or the general MMP inhibitor GM6001 into the endoneurium of adult mice. Injection of IL-1β quickly increased β-DG_{31}/β-DG_{43} ratio, resulting in a reduction of the definition and intensity of DRP2 staining in patches (Fig. 4A and D). Conversely, acute treatment with GM6001 lead to depletion of β-DG_{31} and resulted in increased patch size with fusion in the longitudinal orientation (Fig. 4A and D). Furthermore, Western blot analysis confirmed that inhibition of DG cleavage lead to an increase

in DRP2 protein levels and decreased utrophin content (Fig. 4B), as expected from the existence of different dystroglycan complexes independently regulated by cleavage of β-DG. Thus, acute modulation of MMP activity by a single *in vivo* injection in nerves dynamically regulates β-DG cleavage, the amount of different dystroglycan complexes, and the size of subcortical cytoplasmic compartments in Schwann cells.

One surprising aspect of this experiment was its short time frame. Cleaved β-DG_{31} disappeared within two hours, and this translated into a rapid increase in steady-state levels of DRP2 and to an increase in patches/apposition size. The rapid disappearance of β-DG_{31} suggested degradation. When GM6001 was injected with the general proteasomal inhibitor MG132 (carbobenzoxy-L-leucyl-L-leucyl-L-leucinal), β-DG_{31} was still detectable 1 hour after injection (Fig. 4C). MG132 also increased the amount of β-DG_{31} normally present in sciatic nerve, suggesting that the proteasome constitutively degrades the β-DG_{31} that is produced in physiological conditions.

These results indicate that the ratio between the transmembrane dystroglycan forms β-DG_{31}/β-DG_{43}, which is regulated by endogenous gelatinase activity, dynamically regulate compartments in the Schwann cell cytoplasm.

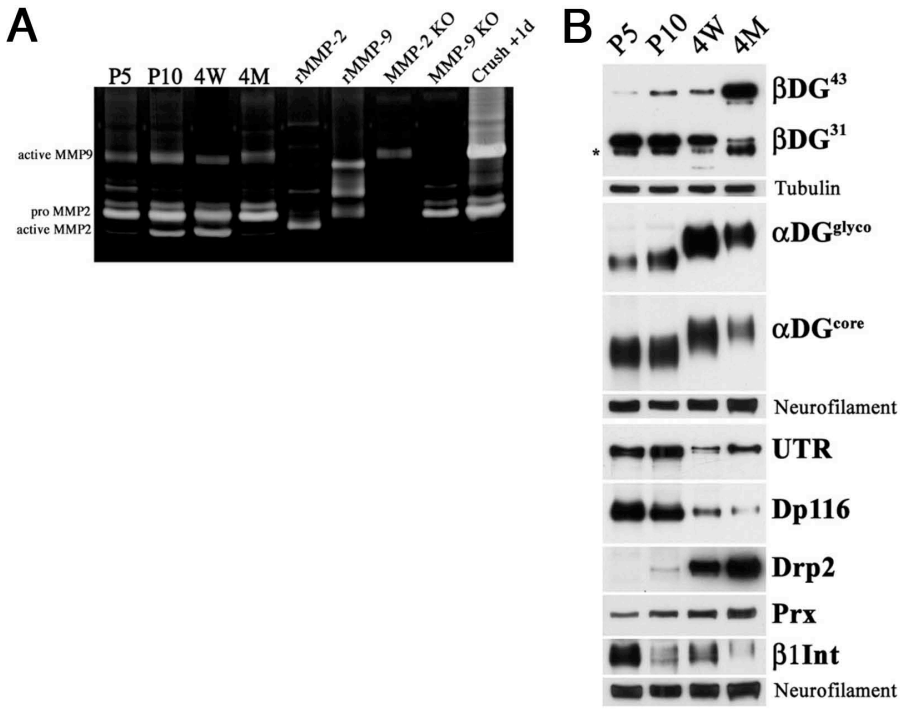

Fig. 3 Expression of DG complex proteins during development correlates with β-DG processing. A, Gelatin zymography of sciatic nerves shows active MMP-2 and -9 during development. Recombinant MMP-2 and MMP-9 (rMMP-2/9), nerves from MMP-2- and MMP-9-deficient mice or 1 day after crush injury were used as controls. **B**, Western blot of sciatic nerves. Before compartments form in Schwann cells (P5), β-DG is mostly cleaved (β-DG_{31}). When appositions appear (P10) and progressively grow [4 weeks (4W) to 4 months (4M)], the uncleaved β-DG_{43} form increases and β-DG_{31} decreases. The abundance of the proposed partners (utrophin and Dp116 for β-DG_{31}; DRP2, periaxin, and α-DG for β-DG_{43}) changes accordingly. α-DG also shows a developmental increase from 90-100 to 120-130 kDa as a result of glycosylation. β-tubulin and neurofilament were used as loading controls. (* marks an Ig non-specific band recognized by the secondary antibody).

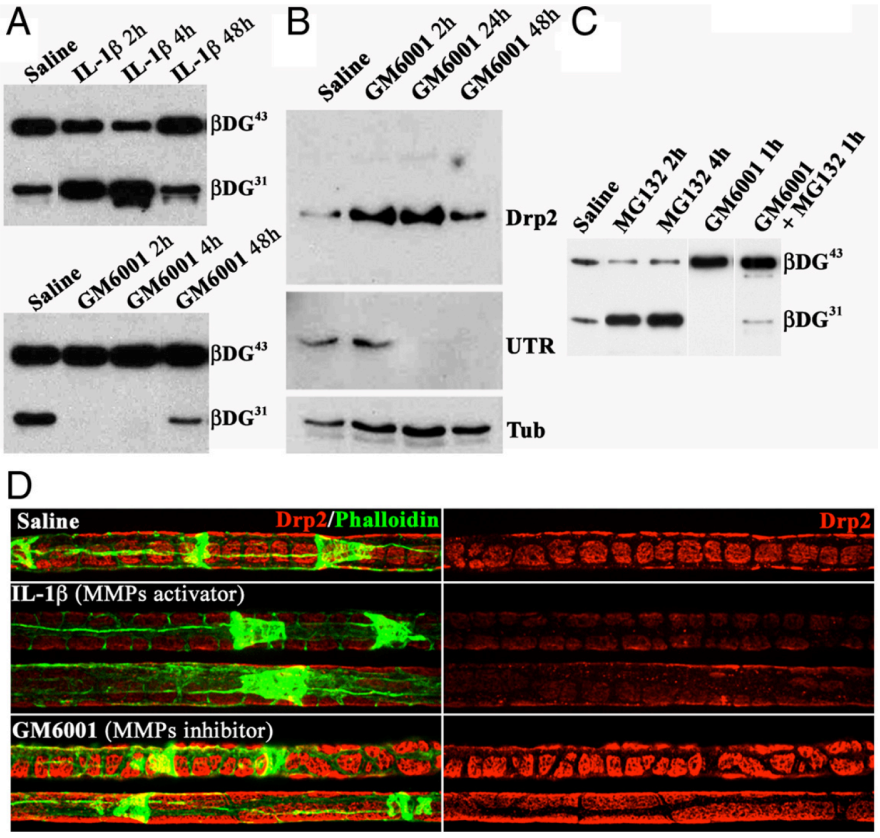

Fig. 4 MMPs cleave β-DG in Schwann cells and modifies compartments. A, Western blot of β-DG in adult sciatic nerves injected with saline, the MMP activator IL-1β (20 μg/ml), or the MMP inhibitor GM6001 (1 mM). MMP activation increases, whereas MMP inhibition decreases, β-DG_{31} in nerves. **B**, GM6001 increases DRP2 expression, whereas utrophin (UTR) disappears. **C**, The proteasome inhibitor MG132 increases β-DG_{31}. **D**, Immunofluorescence on teased fibers from nerves 24 hs after injection stained for DRP2 and FITC-phalloidin. Activation of MMPs with IL-1β (middle) decreases the intensity and definition of DRP2-positive patches. In contrast, MMPs inhibition using GM6001 increases DRP2 patches size, with longitudinal fusion of patches (bottom fiber).

Absence of MMP-2 and MMP-9 *in vivo* alters Schwann cell compartmentalization

β-DG cleavage appears to play a role in the dynamic regulation of cytoplasmic compartments. To investigate whether this regulation also has long term effects, we analyzed mice lacking MMP-2, MMP-9, or both (Itoh et al., 1999; Vu et al., 1998; Dubois et al., 1999). In adult mutant nerves, cleavage of β-DG was inhibited in double null nerves, decreased in MMP-2 null nerves, and variable in MMP-9 null nerves (Fig. 5B and data not shown). Compartmentalization of the Schwann cell cytoplasm was quantified as the previously described ratio between the Schwann cell membrane found above Cajal bands and above appositions on electron-microscopy samples (f-ratio^{EM}) or above Cajal bands and DRP2-positive patches on immunostained fibers (f-ratio^{LM}) (Court et al., 2009). The f-ratio is a constant of 1-1.5 in mature myelinated fibers of any caliber, and it is high when appositions are too small as a result of laminin 211 or dystroglycan deficiency (Court et al., 2009). In one (Dubois et al., 1999) of two independently generated strains of MMP-9 null mice, appositions were larger and the f-ratio decreased (Fig. 5A), whereas in a second strain (Vu et al., 1998), f-ratio was not decreased (data not shown). In mice lacking MMP-2 and both MMP-2 and MMP-9, f-ratio was also decreased (Fig. 5A). Thus, the absence of MMP-2 and MMP-9 causes a long term reduction in the size of Cajal bands.

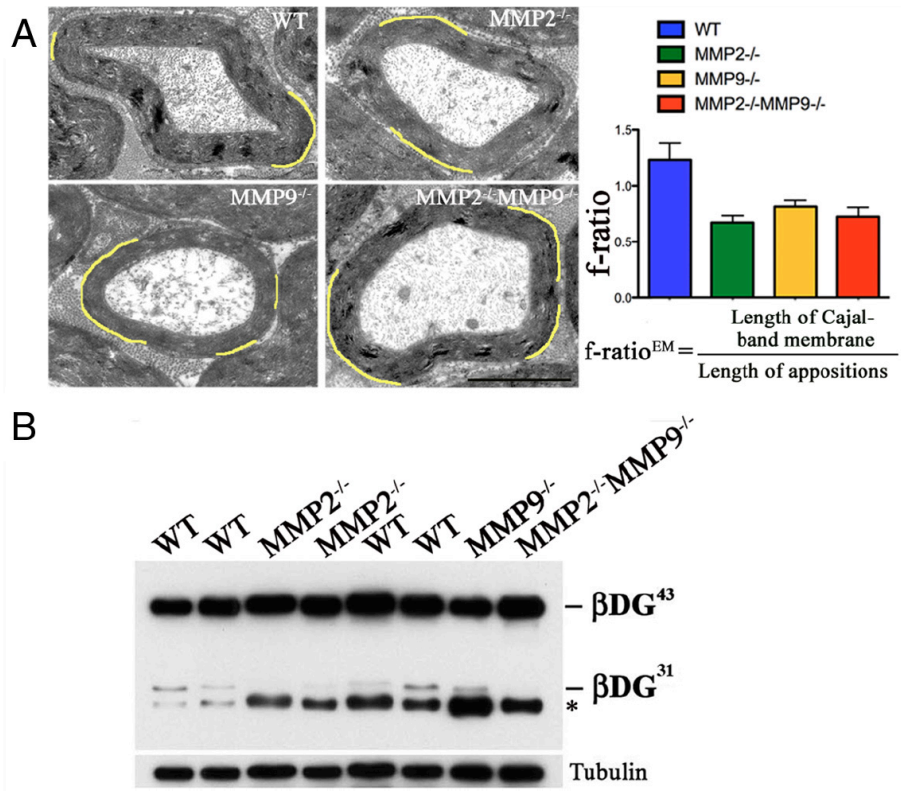

Fig. 5 Deletion of MMP-2 and MMP-9 in mice results in smaller Cajal bands. MMP-2 and MMP-9 deficient mice sciatic nerves were analyzed by EM (**A**) and Western blot (**B**) at 8 months. **A**, EM showed larger appositions (pseudocolored in yellow) in MMP-2 and MMP-9 null mice; consequently, the *f*-ratio^{EM} is decreased (wt vs MMP-9 or MMP-2 null, $p < 0.0001$; wt vs double null, $p < 0.01$; n=25 fibers for wt, 18 for MMP-9 null, 25 for MMP-2 null, and 28 for double null, by Student's *t* test; error bars indicate SEM). Scale bar, 2 μm. **B**, Western blot shows absence of β-DG$_{31}$ when both gelatinases are deleted. Equal loading was verified by β-tubulin (* marks an Ig non-specific band recognized by the secondary antibody; see Methods).

Increase in β-DG cleavage underlies the defect in dystrophic nerves

Unregulated and prolonged activation of MMP-2 and -9 has been observed in many peripheral neuropathies (Hartung and Kieseier, 2000; Shubayev and Myers, 2000). It would be interesting to know if the resulting excessive β-DG proteolysis would negatively affect Schwann cell compartments and internodal lenghts in these pathological conditions.

Different mouse models of MDC1A, known as dystrophic mice, exhibit reduced internodal lenghts (Jaros and Jenkison, 1983) and the *Lama2*$^{dy2J/dy2J}$ mouse show an altered Schwann cell cytoplasm compartmentalization into Cajal bands and appositions (Court et al., 2009). We wondered if such a phenotype might be correlated to a dysregulation of metalloproteinase activity and β-DG cleavage. To test this, we analyzed the expression levels of MMP-9 in sciatic nerves from two different dystrophic mouse models, *Lama2*$^{dy2J/dy2J}$ and *Lama2*$^{dy3k/dy3k}$. As shown by Western blot analysis, MMP-9 was increased in both mutants (Fig. 6A). To determine whether MMP-9 protein present in sciatic nerves of dystrophic mice was enzymatically active, we performed gelatin zymography. A remarkable increase in the gelatinolytic activity of MMP-9 was observed in both *Lama2*$^{dy2J/dy2J}$ and *Lama2*$^{dy3k/dy3k}$ mice (Fig. 6B and not shown); in addition, the activity of MMP-2 was slightly increased (Fig. 6B). Next we evaluated β-DG cleavage and found an increase in β-DG_{31} in nerve lysates from dystrophic mice (Fig. 6C). To ask whether this was responsible for the disruption of appositions, we inhibited MMPs

during myelination *in vitro* and asked if we could rescue the phenotype of *Lama2*$^{dy2J/dy2J}$ Schwann cells. We used dorsal root ganglia (DRG) explants from *Lama2*$^{dy2J/dy2J}$ and *Lama2*$^{dy2J/+}$ mice embryos and induced myelination in the presence of the MMP inhibitor GM6001. Cleavage of β-DG was inhibited in explants of both genotypes treated with GM6001 (Fig. 7C). Myelin segments formed *in vitro* and were visualized with anti-MBP antibody and co-stained with DRP2. As *in vivo* (Court et al., 2009), *Lama2*$^{dy2J/dy2J}$ Schwann cells have smaller DRP2 patches, larger Cajal bands, and higher *f*-ratio than heterozygous Schwann cells (Fig. 7A, B). Of note, inhibition of MMP activity increased patches size and reduced Cajal bands and *f*-ratio in both *Lama2*$^{dy2J/dy2J}$ and *Lama2*$^{dy2J/+}$ Schwann cells (Fig. 7A, B). Thus, after MMP inhibition and reduced β-DG cleavage, the increased *f*-ratio in *Lama2*$^{dy2J/dy2J}$ Schwann cells was normalized.

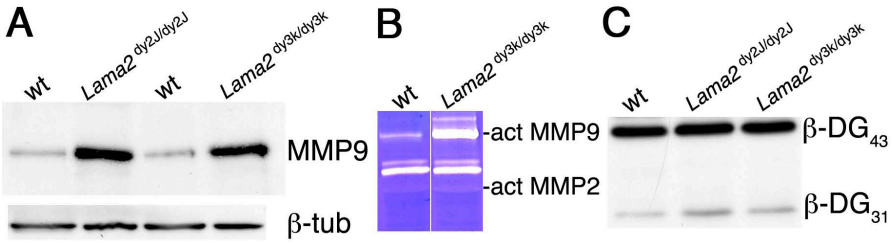

Fig. 6 MMP-9 is increased in dystrophic nerves. A, Western blot analysis of MMP-9 on sciatic nerves from P28 *Lama2*$^{dy2J/dy2J}$ and *Lama2*$^{dy3k/dy3k}$ animals and age-matched littermate controls (wt). Equal loading was verified by β-tubulin. **B**, Gelatin zymography on sciatic nerves from P28 *Lama2*$^{dy3k/dy3k}$ and wt. MMP-9 is hyperactive in *Lama2*$^{dy3k/dy3k}$ nerves. **C**, Western blot analysis of β-DG on sciatic nerves of P28 *Lama2*$^{dy2J/dy2J}$, *Lama2*$^{dy3k/dy3k}$ and control shows that β-DG_{31} is higher in dystrophic mutants vs control.

Fig. 7 (next page) **Inhibition of excessive DG proteolysis restores compartmentalization defects in *Lama2*$^{dy2J/dy2J}$ Schwann cells. A**, DRG explants from *Lama2*$^{dy2J/+}$ and *Lama2*$^{dy2J/dy2J}$ embryos myelinating in the presence or absence of the MMP inhibitor GM6001. *Lama2*$^{dy2J/+}$ and *Lama2*$^{dy2J/dy2J}$ explants stained with antibodies against DRP2 (red) and MBP (green). Bottom panels show the DRP2 signal above an arbitrary threshold in black and white (for details, see Court et al., 2009). *Lama2*$^{dy2J/dy2J}$ Schwann cells form smaller DRP2-positive patches, and this is prevented by GM6001. Scale bar, 10 μm. **B**, β-DG31 is decreased after GM6001 treatment. Asterisk marks a non-specific band. **C**, Quantitative analysis of DRG compartments (mean *f*-ratio, calculated as cytoplasmic area/DRP2 patches area, as described by Court et al., 2009) (n=4 explants for each genotype and treatment; *$p < 0.0001$ by Student's t test; error bars indicate SEM). Dy/+, *Lama2*$^{dy2J/+}$; Dy/Dy, *Lama2*$^{dy2J/dy2J}$.

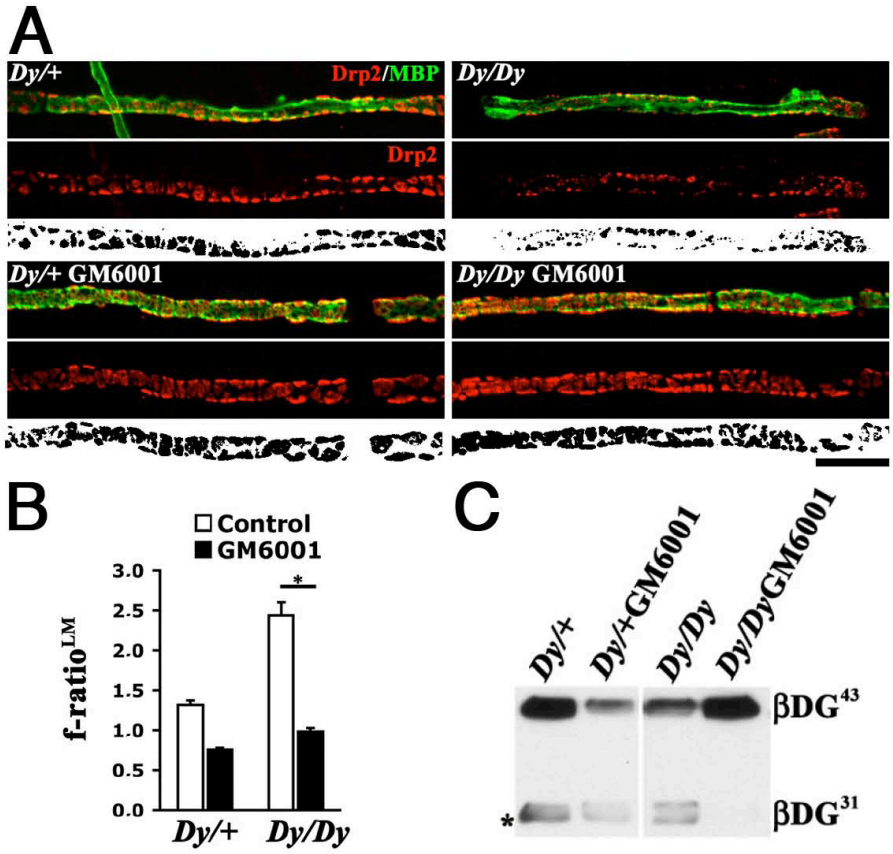
A
Dy/+
Drp2/MBP
Drp2
Dy/Dy
Dy/+ GM6001
Dy/Dy GM6001
B
Control
GM6001
f-ratio^LM
3.0
2.5
2.0
1.5
1.0
0.5
0.0
*
Dy/+
Dy/Dy
C
Dy/+
Dy/+GM6001
Dy/Dy
Dy/DyGM6001
βDG43
βDG31
*

Elongation defects in *Lama2*$^{dy2J/dy2J}$ Schwann cells are partially rescued by MMP inhibition

Internodal lengths are reduced in *Lama2*$^{dy2J/dy2J}$ animals and MDC1A patients (Jaros and Jenkison, 1983; Di Muzio et al., 2003; Court et al., 2009). In several, but not all, instances (Court et al., 2004 and 2009; Triolo et al., 2009), defective cytoplasmic compartmentalization (smaller appositions/larger Cajal bands) was associated with reduced internodal length. We thus asked whether inhibition of DG cleavage and normalization of compartments in *Lama2*$^{dy2J/dy2J}$ Schwann cells also restores internodal lengths. We first confirmed that, even in myelinating explants, *Lama2*$^{dy2J/dy2J}$ internodes were shorter than those in *Lama2*$^{dy2J/+}$ Schwann cells (Fig. 8). When MMP activation was inhibited, *Lama2*$^{dy2J/dy2J}$ myelin segments increased in length by 23%, even if they did not reach the length of wild type internodes (Fig. 8), indicating that reducing MMP activation in this pathological context improves Schwann cell elongation.

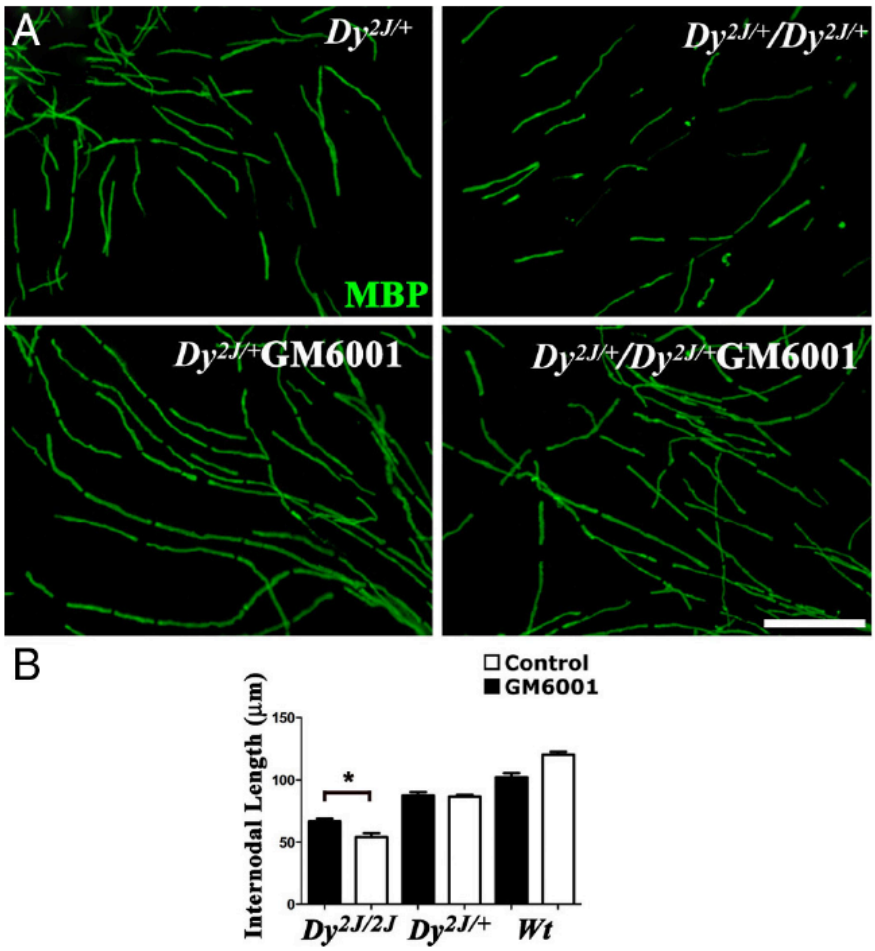

Fig. 8 Shorter internodes of *Lama2*$^{dy2J/dy2J}$ SCs are partially rescued by MMP inhibition. DRG explants from wt, *Lama2*$^{dy2J/+}$, and *Lama2*$^{dy2J/dy2J}$ embryos were treated during myelination with the MMP inhibitor GM6001 and stained with an antibody against MBP (green). **A**, *In vitro*, internodal lengths of *Lama2*$^{dy2J/dy2J}$ SCs are smaller than wt and *Lama2*$^{dy2J/+}$, but continuous MMP inhibition increases length of internodes in *Lama2*$^{dy2J/dy2J}$. Scale bar, 100 μm. In **B**, the mean internodal length for each genotype and treatment are plotted, respectively (at least 10 explants/genotype and treatment were used; *$p < 0.0001$, by Student's *t* test; error bars indicate SEM).

Genetic ablation of MMP9 is not sufficient to rescue either compartmentalization defect or internodal lenght in dystrophic mice

To confirm these results *in vivo*, and taken into account the prominent increase of MMP-9 activity in dystrophic nerves (Fig. 6A, B), we crossed *Lama2*$^{dy2J/dy2J}$ and *Lama2*$^{dy3k/dy3k}$ mice with MMP-9 null mice (*Mmp9*$^{-/-}$; Vu et al., 1998), thus generating *Mmp9*$^{-/-}$//*Lama2*$^{dy2J/dy2J}$ and *Mmp9*$^{-/-}$//*Lama2*$^{dy3k/dy3k}$ double mutants.

Both double homozygous were born in expected Mendelian ratios and were macroscopically similar to dystrophic littermates. Like homozygous *Lama2*$^{dy2J/dy2J}$ mice, *Mmp9*$^{-/-}$//*Lama2*$^{dy2J/dy2J}$ animals have a normal life span and suffer from a congenital muscular dystrophy and a peripheral neuropathy. Similarly, *Mmp9*$^{-/-}$//*Lama2*$^{dy3k/dy3k}$ animals do not survive longer than the 3-5 weeks already observed for *Lama2*$^{dy3k/dy3k}$ mutants (Miyagoe et al., 1997), primarly due to the severity of the muscular dystrophy. Hence, we analyzed peripheral nerves of *Mmp9*$^{-/-}$//*Lama2*$^{dy3k/dy3k}$ at P28, and *Mmp9*$^{-/-}$//*Lama2*$^{dy2J/dy2J}$ at 4 months of age.

First we confirmed that the deletion of a single allele of the *Mmp9* gene reduced the protein levels of MMP-9 in sciatic nerves of dystrophic mice and there was no detectable MMP-9 protein in double homozygous mice (Fig. 9A and not shown). Gelatin zymography also showed reduced or absent MMP-9 acitvity in dystrophic mice heterozygous and homozygous for *Mmp9* respectively (Fig. 9B). Then, we asked whether β-DG cleavage was reduced in nerves of dystrophic mice lacking MMP-9. Indeed, β-DG$_{31}$/β-DG$_{43}$ ratio

decreased when MMP-9 was absent or partially deleted, indicating that a reduced MMP-9 activity results in higher amounts of uncleaved β-DG_{43} (Fig. 9C). Nonetheless residual levels of β-DG_{31} were still detectable, likely due to the presence of MMP-2 (Fig. 9B). Reduction of β-DG cleavage was expected to translate into an increase in α-DG that could favour attachment to the basal lamina. However, albeit partial decrease of β-DG_{31}, α-DG was actually reduced (Fig. 9D).

Since pharmacological inhibition of MMPs lead to an amelioration of dystrophic Schwann cell compartment organization and elongation *in vitro*, we asked whether the removal of MMP-9 had a similar effect *in vivo*. As a measure of compartmentalization of the Schwann cell cytoplasm, *f*-ratio was quantified at the EM level. The mean *f*-ratio of *Lama2*$^{dy3k/dy3k}$ nerves was increased than expected for a wild type nerve, as previously shown (Court et al., 2009); however, in *Mmp9*$^{-/-}$ //*Lama2*$^{dy3k/dy3k}$, this parameter was not decreased (Fig. 10C).

Our second endpoint was internodal lenght. As anticipated by *f*-ratio measurements, also internodal lenghts, measured on osmicated teased fibers (Fig. 10A), were similar between *Lama2*$^{dy/dy}$ and *Mmp9*$^{-/-}$ //*Lama2*$^{dy/dy}$ mice (Fig. 10B). In line with these findings, we were also unable to detect any significative increase in nerve conduction velocity in dystrophic mice with MMP-9 deficiency (Fig. 10D).

Overall, both morphometric and electrophysiological data suggest that *in vivo*, genetic ablation of MMP-9 is not sufficient to rescue either the compartmentalization defect or the shorter internodal lenghts of dystrophic mice. This is might be due to redundancy of MMP-2, which is slightly increased in dystrophic nerves lacking MMP-9.

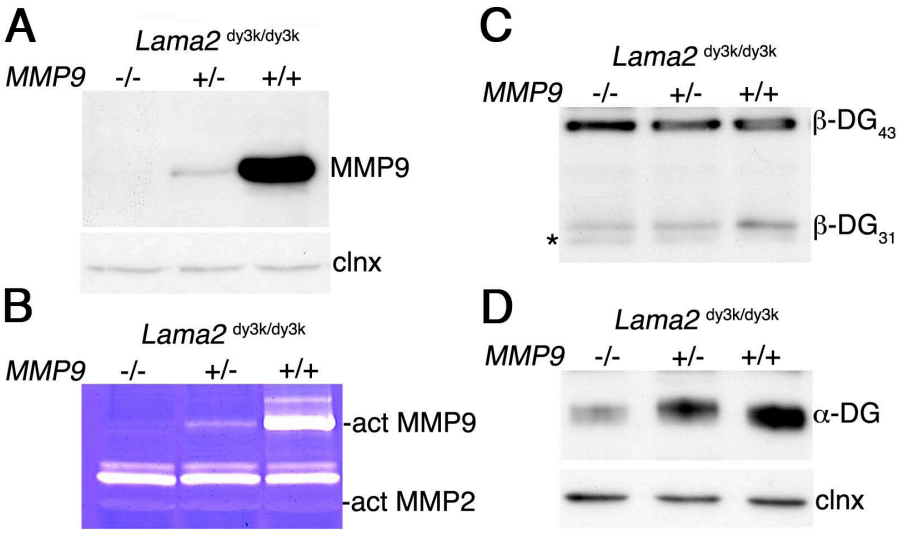

Fig. 9 β-DG cleavage is reduced in dystrophic mice lacking MMP-9. A and **C-D**, Western blot analysis of MMP-9 (**A**), β-DG (**C**), and α-DG (**D**) on sciatic nerve lysates from P28 *Mmp9*$^{-/-}$//*Lama2*$^{dy3k/dy3k}$, *Mmp9*$^{+/-}$//*Lama2*$^{dy3k/dy3k}$ and *Mmp9*$^{+/+}$//*Lama2*$^{dy3k/dy3k}$. Equal loading was verified with calnexin (clnx). **B**, Gelatin zymography on the same nerve lysates. MMP-9 activity is absent or reduced in *Mmp9*$^{-/-}$ //*Lama2*$^{dy3k/dy3k}$ and *Mmp9*$^{+/-}$//*Lama2*$^{dy3k/dy3k}$ mice respectively.

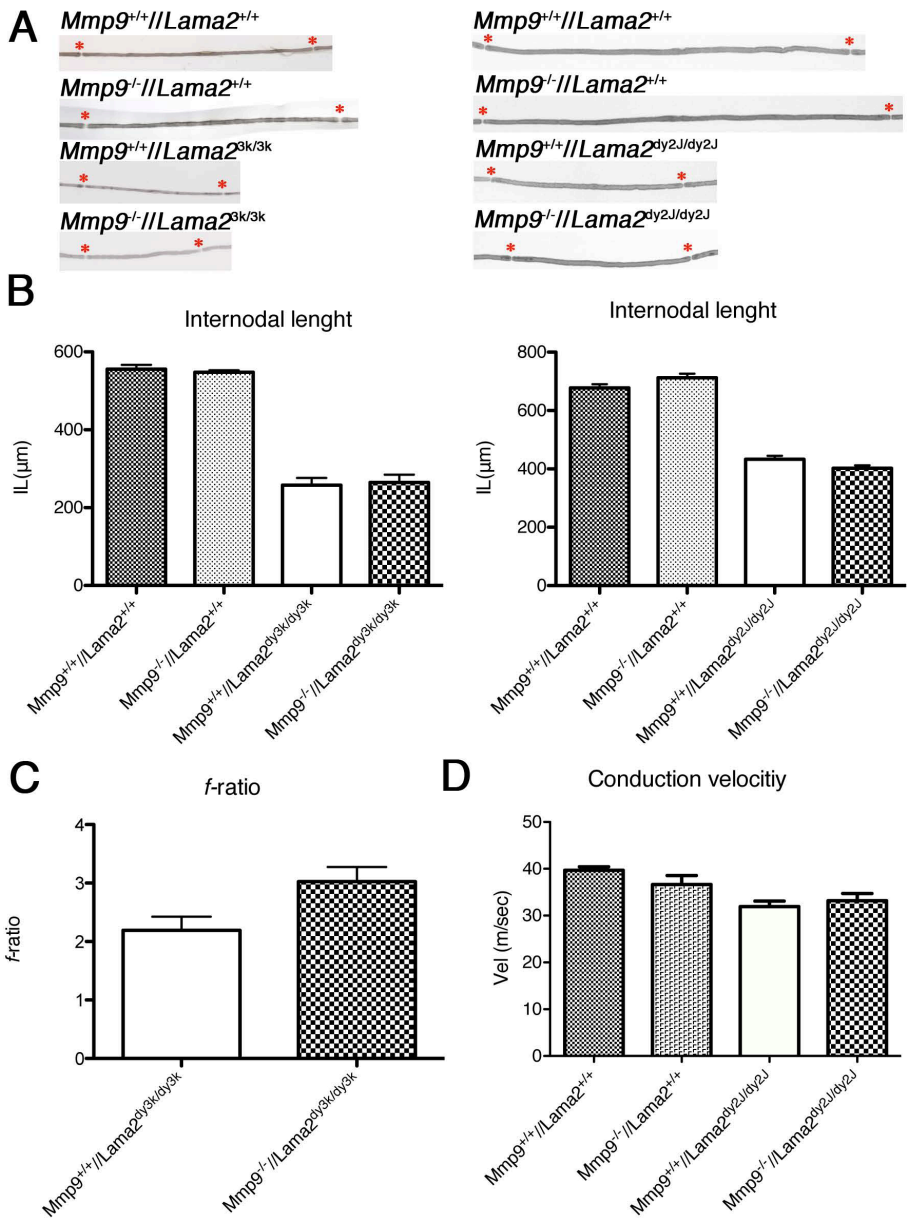
A
Mmp9+/+//Lama2+/+
Mmp9-/-//Lama2+/+
Mmp9+/+//Lama23k/3k
Mmp9-/-//Lama23k/3k
Mmp9+/+//Lama2dy2J/dy2J
Mmp9-/-//Lama2dy2J/dy2J
B
Internodal lenght
IL(µm)
600
400
200
0
Mmp9+/+/Lama2+/+
Mmp9-/-/Lama2+/+
Mmp9+/+/Lama2dy3k/dy3k
Mmp9-/-/Lama2dy3k/dy3k
Internodal lenght
IL(µm)
800
600
400
200
0
Mmp9+/+/Lama2+/+
Mmp9-/-/Lama2+/+
Mmp9+/+/Lama2dy2J/dy2J
Mmp9-/-/Lama2dy2J/dy2J
C
f-ratio
f-ratio
4
3
2
1
0
Mmp9+/+/Lama2dy3k/dy3k
Mmp9-/-/Lama2dy3k/dy3k
D
Conduction velocitiy
Vel (m/sec)
50
40
30
20
10
0
Mmp9+/+/Lama2+/+
Mmp9-/-/Lama2+/+
Mmp9+/+/Lama2dy2J/dy2J
Mmp9-/-/Lama2dy2J/dy2J

Fig. 10 (previous page) **Neither *f*-ratio nor internodal lenght and conduction velocity are ameliorated in dystrophic mice upon MMP-9 ablation. A**, Examples of osmicated teased fibers from sciatic nerves of *Mmp9*//*Lama2*^{dy3k} and *Mmp9*//*Lama2*^{dy2J} mice (nodes of Ranvier are marked by red asterisks). **B**, Mean internodal lenghts were calculated for P28 *Mmp9*//*Lama2*^{dy3k} mice and 4 month old *Mmp9*//*Lama2*^{dy2J} mice (Error bars indicate SEM). 3 animals/genotype were analyzed: *Mmp9*$^{+/+}$//*Lama2*$^{+/+}$, 553 µm (n=281); *Mmp9*$^{-/-}$//*Lama2*$^{+/+}$, 547 µm (n=268); *Mmp9*$^{+/+}$//*Lama2*$^{dy3k/dy3k}$, 255 µm (n=344); *Mmp9*$^{-/-}$//*Lama2*$^{dy3k/dy3k}$, 260 µm (n=460). *Mmp9*$^{+/+}$//*Lama2*$^{+/+}$, 678 µm (n=123); *Mmp9*$^{-/-}$//*Lama2*$^{+/+}$, 695 µm (n=134); *Mmp9*$^{+/+}$//*Lama2*$^{dy2J/dy2J}$, 433 µm (n=152); *Mmp9*$^{-/-}$//*Lama2*$^{dy2J/dy2J}$, 402 µm (n=198). **C**, Quantitative analysis of compartments in *Mmp9*$^{+/+}$//*Lama2*$^{dy3k/dy3k}$ and *Mmp9*$^{-/-}$//*Lama2*$^{dy3k/dy3k}$ mice. Mean *f*-ratios^{EM} were calculated as cytoplasmic area/apposition area in EM sections of sciatic nerves (5 animals/genotype were analyzed. Error bars indicate SEM). **D**, Conduction velocities were measured in 4 month old MMP9dy2J and littermate controls. Mean conduction velocities (m/sec) are plotted (Error bars indicate SEM): *Mmp9*$^{+/+}$//*Lama2*$^{+/+}$, 39.7±0.73 (n=8); *Mmp9*$^{-/-}$//*Lama2*$^{+/+}$, 36.7±1.91 (n=4); *Mmp9*$^{+/+}$//*Lama2*$^{dy2J/dy2J}$, 31.9±1.18 (n=17); *Mmp9*$^{-/-}$//*Lama2*$^{dy2J/dy2J}$, 33.2±1.51. *Mmp9*$^{+/+}$//*Lama2*$^{dy2J/dy2J}$ vs *Mmp9*$^{-/-}$//*Lama2*$^{dy2J/dy2J}$ not significative by Student's *t* test (p=0.5083).

3.4 Discussion

Protein polarization in specific cell domains is crucial for cell function. In myelinated nerve fibers, several specialized domains are required for fast propagation of action potentials. The cytoplasm and membrane outside myelin in the peripheral nervous system are compartmentalized into two domains characterized by the expression of different dystroglycan complexes. Here we show that this differential distribution and the size of these domains depend on β-DG cleavage by MMP-2 and MMP-9 (Fig. 11). Modulation of MMP activity quickly remodels subcellular domains in physiological situations. In contrast, during a peripheral neuropathy, excessive and unregulated β-DG cleavage causes disruption of cytoplasmic domains. Importantly, inhibition of β-DG cleavage is able to restore the normal domain organization of Schwann cells *in vitro*. However, genetic ablation of MMP-9 from two murine models of MDC1A is not sufficient to rescue defective compartments *in vivo*. Our results present a novel mechanism regulating both normal and abnormal subcellular polarization, dependent on physiological cleavage of β-DG by MMP-2 and MMP-9.

MMP-mediated β-DG cleavage leads to spatially distinct dystroglycan complexes in Schwann cells

Dystroglycan is best known for its function in muscle, but it also occurs in non-muscle tissues within diverse supramolecular complexes, each with a precise subcellular distribution (Haenggi and Fritschy, 2006). These complexes act as a scaffold for segregating

functional proteins into specific cellular subdomains. Examples are aquaporin 4 at the astrocytic endfeet (Neely et al., 2001), Kir4.1 channels in retinal Müller glia (Noël et al., 2005), aquaporin 4 and neuronal nitric oxide synthase in sarcolemma (Adams et al., 2008), acetylcholine receptors at neuromuscular junctions (Grady et al., 2000), and laminins and polarity proteins in mammary epithelia (Weir et al., 2006). Similarly, in Schwann cells, dystroglycan complex with DRP2 localizes periaxin in appositions possibly to bind the outer myelin wrap, whereas the dystroglycan complex with utrophin, Dp116, dystrobrevin, and syntrophins in Cajal bands localizes the ABCA1 cholesterol transporter (Albrecht et al., 2008). We show that β-DG cleavage changes the relative amount of these spatially distinct complexes and the size of the domain in which they reside.

In physiological conditions, we detected high levels of cleaved β-DG, Dp116 and utrophin, during early postnatal development, a period in which appositions have not formed yet. When DRP2 starts to be polarized to appositions, β-DG cleavage is reduced, and Dp116 and utrophin levels decrease, indicating that these complexes are gradually confined to cytoplasmic bands. Treatment of nerves with either inhibitors or activators of MMPs results in higher DRP2 expression and larger appositions or higher β-DG cleavage and decreased size of appositions respectively. This indicates that β-DG cleavage is responsible for the distribution of the different dystroglycan complexes not only during the formation of Cajal bands and appositions, but also in adult nerve, where a fine modulation of MMP activity is required to maintain the correct proportion between these

domains.

How β-DG cleavage can regulate the sorting of different complexes to different domains remains obscure. It is possible that interaction with both intracellular or extracellular ligands might favour the localization in a specific domain. For instance, α-DG in apposition can bind laminin 211, agrin, or perlecan in the basal lamina, and DRP2 intracellularly. This interactions can be protective, reducing β-DG accessibility to MMPs. The rapid increase in DRP2 protein seen by Western blot after inhibition of β-DG cleavage likely reflects an increase in protein stabilization after linkage within a stable complex. The concomitant decrease in utrophin and β-DG_{31}, the latter delayed by proteasome inhibition, suggests that active and regulated degradation of the whole dystroglycan complex located in Cajal bands is taking place constituvely. Indeed dystroglycan complex components are degraded by the proteasome (Bonnuccelli et al., 2003; Gazzerro et al., 2010). β-DG shedding could also favour lateral movement of β-DG_{31} and association with Dp116/utrophin in Cajal bands, similar to the way cleavage of α/β-DG precursor changes its affinity for laminin binding (Akhavan et al., 2008). Finally, the rate of β-DG cleavage may vary depending on the association with other protein(s) (Singh et al., 2004) that also direct targeting to either appositions or Cajal bands. DRP2 is a good candidate because it appears in development after utrophin and Dp116, and is targeted to future appositions (regions free of actin) (Court et al, 2009). It is salso known that DRP2 in parallel binds a basic domain of periaxin that contains a nuclear localization signal in embryonic Schwann cells

(Sherman and Brophy, 2000). When DRP2 is expressed, it may trigger formation of appositions by sequestering periaxin from its nuclear localization and by linking it to the abaxonal membrane through the DG complex (Wrabetz and Feltri, 2001). Here, interactions with basal lamina guarantee the stability of the complex by preventing β-DG cleavage. This is supported by the finding that shedding of β-DG is increased in perlecan-deficient fibroblasts (Herzog et al., 2004). Independently of the mechanism, because altering β-DG cleavage rapidly changes the amount of dystroglycan complex proteins and the size of cellular domains, we propose that this mechanism represents a dynamic way to regulate the sorting of functional proteins depending on the mechanic or metabolic requirement of myelinating cells.

Physiological function of β-DG cleavage and α-DG shedding

Contrary to other tissues, like skeletal muscle, where β-DG cleavage is detected only in pathological conditions (Yamada et al., 2001; Matsumura et al., 2003), we demonstrated that in peripheral nerve dystroglycan cleavage by MMP-2 and -9 occurs constitutively, both during early postnatal development and in mature nerves. The idea that MMPs can regulate DG function in a physiological context is not completely new. A previous report showed that β-DG is digested by MMP-9 at some CNS synapses in response to neuronal activity (Michaluk et al., 2007). In addition, β-DG is proteolytically released from the surface of normal cutaneous cells, although the functional role of the cleavage is unknown (Herzog et al., 2004). We show that in peripheral nerve β-DG is present in two forms, full-length (β-DG_{43})

and cleaved (β-DG_{31}), and that their preferential aggregation with specific DGC components influences their spatial segregation, affecting the formation of cytoplasmic bands and appositions. For long time dystroglycan has been described as a merely structural protein with the main function to link extracellular matrix to cytoplasmic cytoskeleton. Upon MMP cleavage the non-covalent α-DG/β-DG binding is lost and α-DG is shed in the ECM. Two questions arise. One is whether β-DG_{31}, which is not able to bind basal lamina, could have any unconventional role in Schwann cells; the second is if shed α-DG could have an active function as well. It is known that through its C-terminal domain β-DG can bind a host of proteins, ranging from actin, cytoskeletal adaptors, such as ERMs, plectins, ankyrin-G and vinculin, to signaling molecules, as Grb2 (Moore and Winder, 2010); thus, it is plausible that β-DG_{31} in Cajal bands might act independently of basal lamina binding. Moreover, it is worth noting that in the absence of dystroglycan, utrophin remains in Schwann cells, although not bound to the membrane, and small DRP2-positive patches can still form (Saito et al., 2003; Court et al., 2009). This suggests that members of the dystroglycan complex, such as utrophin, can function independently of α-DG.

Another intriguing idea is that shed α-DG or the cleaved N-terminal β-DG may have some active roles after cleavage. This is supported by the fact that shed α-DG is released in cell culture media (Herzog et al., 2004) and it would parallel a myriade of ECM molecules that become bioactive only upon cleavage, such as collagen XVIII/endostatin (O'Reilly et al., 1997), perlecan/endorepellin, collagenIV/tumstatin

(Bix and Iozzo, 2005), or gliomedin/olfactomedin (Eshed et al., 2007).

Timescale of DG cleavage and the remodeling of Schwann cell compartments

The rapid changes in protein level and in the size of cytoplasmic compartments after acute manipulation of β-DG cleavage were surprising. DRP2 and utrophin protein levels changed rapidly after pharmacological inhibition of gelatinases. The increase of β-DG_{31} after proteasome inhibition suggests that β-DG cleavage occurs constitutively and that β-DG_{31} is rapidly degraded. Finally, mice lacking MMP-2 and MMP-9 had increased size of appositions. These data suggest that abaxonal cytoplasmic compartments in Schwann cells are quickly remodeled by metalloproteinases, possibly in response to mechanic or metabolic requirements. Additional experiments will be required to explore this intriguing possibility.

Increased β-DG cleavage in pathological conditions results in Schwann cell compartmentalization defect

MMP-2 and MMP-9 have been shown to be up-regulated in several pathological conditions, such as muscular dystrophies (Kherif et al., 1999; Matsumura et al., 2003), tumor progression and metastasis, multiple sclerosis (Agrawal et al., 2006), brain injury and vascular cognitive impairment (Rosenberg, 2009). As a consequence, abnormal β-DG cleavage has been demonstrated in many of these diseases. In peripheral nerves, MMP-2 and -9 initiate early degenerative events of Schwann cell activation, macrophage recruitment and demyelination,

as demonstrated in experimentally induced nerve injuries (Shubayev and Myers, 2000 and 2002; Siebert et al., 2001; Shubayev et al., 2006; Chattopadhyay et al., 2007; Kherif et al., 1998), inflammatory neuropathies (Zhao et al., 2010), pure neuritic leprosy (Teles et al., 2007) and other clinical neuritic processes (Mawrin et al., 2003; Gurer et al., 2004). Furthermore, it has been long established that myelin segments formed after remyelination are shorter than normal (Hiscoe, 1947). We provide evidence that this could potentially be caused by excessive cleavage of β-DG and formation of defective compartments, which has been linked to internodal lenght.

We have analyzed peripheral nerves of two different murine models of MDC1A, a congenital muscular dystrophy with a peripheral neuropathy characterized by reduced internodal lengths and defective Schwann cell compartments (Jaros and Jenkison, 1983; Court et al., 2009). Surprisingly, we found increased levels and enzymatic activity of MMP-9 in sciatic nerves of mutant mice, even if MDC1A has not previously described to have an inflammatory component. Indeed, the analysis of nerves from these animals did not show the presence of infiltrating macrophages. Moreover, the SC-DRG co-culture system, that lacks macrophages, is characterized by the same increase in gelatinolytic activity (not shown), suggesting that Schwann cells release MMP-2 and MMP-9 as part of a cell-autonomous mechanism regulating cytoplasmic compartmentalization. It is likely that absence of laminin 211, or its inability to polymerize, which results in a defective basal lamina, induces Schwann cells to increase MMP expression in the attempt to remodel the extracellular matrix. In

addition, the dystroglycan complex might be destabilized by the absence of its major extracellular ligand, becoming exposed to MMP-dependent proteolytic processing. Similarly, perlecan (Herzog et al., 2004) and sarcoglycans might mask the MMP cleavage site on β-DG (Roberds et al., 1993; Straub et al., 1998; Yamada et al., 2001). Inhibition of MMP-2/9 in all these situations may help to reserve the integrity of the dystroglycan complex and may explain in part the beneficial effect recently demonstrated in mdx mice (Li et al., 2009).

Genetic ablation of MMP-9 does not ameliorate the peripheral neuropathy in mouse models of MDC1A

We showed that pharmacological inhibition of MMPs rescues the compartmentalization and elongation defects of dystrophic Schwann cells *in vitro*. Importantly, shorter internodal lenghts in DG deficient Schwann cells are not rescued by MMP inhibition (not shown), which demonstrates that DG is a substrate of MMPs required for the observed effects. However, when we crossed dystrophic mice with MMP-9 deficient mice, although a reduction of β-DG_{31} was observed, *f*-ratios were not reduced. This could depend on the presence of active MMP-2 that in this pathological condition might be sufficient to cleave β-DG. Although less cleavage was detected, in the absence of laminin 211, MMP-2 might cleave β-DG indiscriminately, leading to disruption of compartments. This is supported by the fact that less β-DG cleavage is not paralleled by higher levels of α-DG, on the contrary α-DG shedding is actually increased .

Thus, ablation of the sole MMP-9 is not sufficient to restore normal

compartments, proper internodal lenght and conduction velocity in dystrophic mice. Future experiments involving MMP-2//MMP-9 double null mice would be necessary to address this issue.

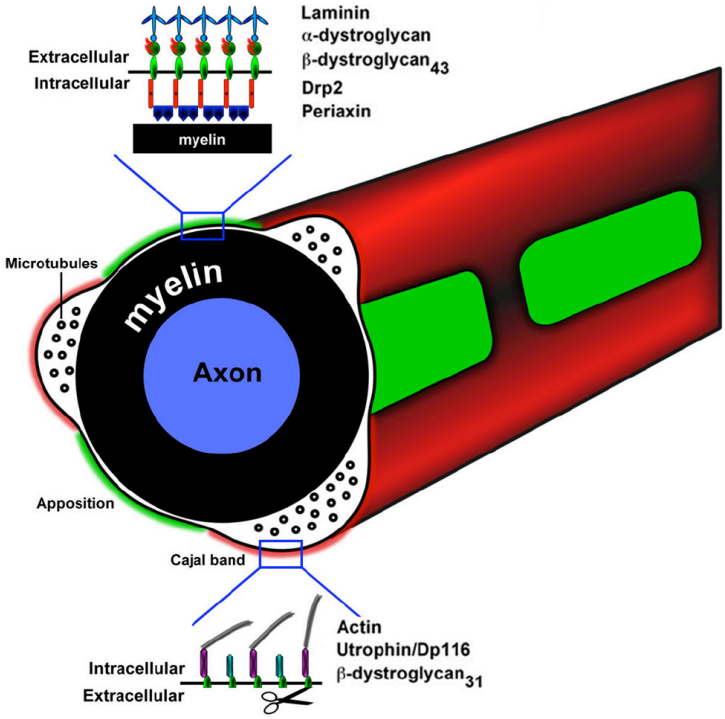

Fig. 11 Schematic representation of Schwann cell abaxonal domains and their molecular composition. Appositions are formed by a complex consisting of β-DG, full-length β-DG_{43}, DRP2, and periaxin. In contrast, in Cajal bands, β-DG is cleaved by MMP-2 and MMP-9, α-DG is shed, and the resulting β-DG_{31} is found with utrophin and Dp116 and in part degraded by the proteasome. Utrophin can bind actin and possibly organizes the Cajal bands cytoskeleton. Linkage to the basal lamina in Cajal bands is ensured by other laminin receptors found in this location, such as α6β4 and α6β1 integrins.

3.5 References

- Adams ME, Tesch Y, Percival JM, Albrecht DE, Conhaim JI, Anderson K, and Froehner SC. (2008) Differential targeting of nNOS and AQP4 to dystrophin deficient sarcolemma by membrane-directed α-dystrobrevin. *J Cell Sci* 121: 48-54.
- Agrawal S, Anderson P, Durbeej M, van Rooijen N, Ivars F, Opdenakker G, and Sorokin LM. (2006) Dystroglycan is selectively cleaved at the parenchymal basement membrane at sites of leukocyte extravasation in experimental autoimmune encephalomyelitis. *J Exp Med* 203: 1007-1019.
- Akhavan A, Crivelli SN, Singh M, Lingappa VR, and Muschler JL. (2008) SEA domain proteolysis determines the functional composition of dystroglycan. *FASEB J* 22: 612-621.
- Albrecht DE, Sherman DL, Brophy PJ, and Froehner SC. (2008) The ABCA1 cholesterol transporter associates with one of two distinct dystrophin-based scaffolds in Schwann cells. *Glia* 56(6): 611-618.
- Bix G, and Iozzo RV. (2005). Matrix revolutions: 'tails' of basement membrane components with angiostatic functions. *Trends Cell Biol* 15: 52-60.
- Bonuccelli G, Sotgia F, Schubert W, Park DS, Frank PG, Woodman SE, Insabato L, Cammer M, Minetti C, and Lisanti MP. (2003) Proteasome inhibitor (MG-132) treatment of mdx mice rescues the expression and membrane localization of dystrophin and dystrophin-associated proteins. *Am J Pathol* 163: 1663-1675.
- Bradley WG, and Jenkison M. (1973) Abnormalities of peripheral nerves in murine muscular dystrophy. *J Neurol Sci* 18: 227-247.
- Cai H, Erdman RA, Zweier L, Chen J, Shaw IV JH, Baylor KA, Stecker MM, Carey DJ, and Chan Y-MM. (2007) The sarcoglycan complex in

Schwann cells and its role in myelin stability. *Exp Neurol* 205(1): 257-269.

- Chattopadhyay S, Myers RR, Janes J, and Shubayev V. (2007) Cytokine regulation of MMP-9 in peripheral glia: implications for pathological processes and pain in injured nerve. *Brain Behav Immun* 21: 561-568.
- Court F, and Alvarez J. (2000) Nerve regeneration in Wld(s) mice is normalized by actinomycin D. *Brain Res* 867: 1-8.
- Court FA, Sherman DL, Pratt T, Garry EM, Ribchester RR, Cottrell DF, Fleetwood-Walker SM, and Brophy PJ. (2004) Restricted growth of Schwann cells lacking Cajal bands slows conduction in myelinated nerves. *Nature* 431: 191-195.
- Court FA, Hewitt JE, Davies K, Patton BL, Uncini A, Wrabetz L, and Feltri ML. (2009) A laminin-2, dystroglycan, utrophin axis is required for compartmentalization and elongation of myelin segments. *J Neurosci* 29(12): 3908-19.
- Di Muzio A, De Angelis MV, Di Fulvio P, Ratti A, Pizzuti A, Stuppia L, Gambi D, and Uncini A. (2003) Dysmyelinating sensory-motor neuropathy in merosin-deficient congenital muscular dystrophy. *Muscle Nerve* 27: 500-506.
- Dubois B, Masure S, Hurtenbach U, Paemen L, Heremans H, van den Oord J, Sciot R, Meinhardt T, Hammerling G, Opdenakker G, and Arnold B. (1999) Resistance of young gelatinase B-deficient mice to experimental autoimmune encephalomyelitis and necrotizing tail lesions. *J Clin Invest* 104: 1507-1515.
- Einheber S, Zanazzi G, Ching W, Scherer S, Milner TA, Peles E, and Salzer JL. (1997) The axonal membrane protein Caspr/neurexin IV is a component of the septate-like paranodal junctions that assemble during myelination. *J Cell Biol* 139: 1495-1506.

- Eshed Y, Feinberg K, Carey DJ, and Peles E. (2007) Secreted gliomedin is a perinodal matrix component of peripheral nerves. *J Cell Biol* 177: 551-562.
- Feltri ML, D'Antonio M, Previtali S, Fasolini M, Messing A, and Wrabetz L. (1999) P0-Cre transgenic mice for inactivation of adhesion molecules in Schwann cells. *Ann NY Acad Sci* 883: 116-123.
- Gazzerro E, Assereto S, Bonetto A, Sotgia F, Scarfi S, Pistorio A, Bonuccelli G, Cilli M, Bruno C, Zara F, Lisanti MP, and Minetti C. (2010) Therapeutic potential of proteasome inhibition in Duchenne and Becker muscular dystrophies. *Am J Pathol* 176: 1863-1877.
- Grady RM, Zhou H, Cunningham JM, Henry MD, Campbell KP, and Sanes JR. (2000) Maturation and maintenance of the neuromuscular synapse: genetic evidence for roles of the dystrophin-glycoprotein complex. *Neuron* 25: 279-293.
- Griffin JW, Low PA, and Podsulo JF. (1993) Peripheral Neuropathy. Dyck PJ and Thomas PK. Third Edition. Vol (1): 528-547.
- Gurer G, Erdem S, Kocaefe C, Ozguc M, and Tan E. (2004) Expression of matrix metalloproteinases in vasculitic neuropathy. *Rheumatol Int* 24: 255-259.
- Haenggi T, and Fritschy JM. (2006) Role of dystrophin and utrophin for assembly and function of the dystrophin glycoprotein complex in non-muscle tissue. *Cell Mol Life Sci* 63: 1614-1631.
- Hartung HP, and Kieseier BC. (2000) The role of matrix metalloproteinases in autoimmune damage to the central and peripheral nervous system. *J Neuroimmunol* 107: 140-147.
- Herzog C, Has C, Franzke CW, Echtermeyer FG, Schlötzer-Schrehardt U, Kröger S, Gustafsson E, Fässler R, and Bruckner-Tuderman L. (2004) Dystroglycan in skin and cutaneous cells: β-subunit is shed from

the cell surface. *J Invest Dermatol* 122: 1372-1380.

- Hiscoe HB. (1947) Distribution of nodes and incisures in normal and regenerated nerve fibers. *Anat Rec* 99: 447-475.
- Holt K H, Crosbie RH, Venzke DP, and Campbell KP. (2000) Biosynthesis of dystroglycan: processing of a precursor propeptide. *FEBS Lett* 468: 79-83.
- Ibraghimov-Beskrovnaya O, Ervasti JM, Leveille CJ, Slaughter CA, Sernett SW, and Campbell KP. (1992) Primary structure of dystrophin-associated glycoproteins linking dystrophin to the extracellular matrix. *Nature* 355: 696-702.
- Itoh T, Ikeda T, Gomi H, Nakao S, Suzuki T, and Itohara S. (1997) Unaltered secretion of β-amyloid precursor protein in gelatinase A (matrix metalloproteinase 2)-deficient mice. *J Biol Chem* 272: 22389 - 22392.
- Jaros E, and Jenkison M. (1983) Quantitative studies of the abnormal axon-Schwann cell relationship in the peripheral motor and sensory nerves of the dystrophic mouse. *Brain Res* 258: 181-196.
- Jing J, Lien CF, Sharma S, Rice J, Brennan PA, and Gorecki DC. (2004) Aberrant expression, processing and degradation of dystroglycan in squamous cell carcinomas. *Eur J Cancer* 40: 2143-2151.
- Kherif S, Dehaupas M, Lafuma C, Fardeau M, Alameddine HS. (1998) Matrix metalloproteinases MMP-2 and MMP-9 in denervated muscle and injured nerve. *Neuropathol Appl Neurobiol* 24: 309-319.
- Kherif S, Lafuma C, Dehaupas M, Lachkar S, Fournier JG, Verdiere-Sahuque M, Fardeau M, and Alameddine HS. (1999) Expression of matrix metalloproteinases 2 and 9 in regenerating skeletal muscle: a study in experimentally injured and mdx muscles. *Dev Biol* 205: 158-170.

- Kidd GJ, Andrews SB, and Trapp BD. (1994) Organization of microtubules in myelinating Schwann cells. *J Neurocytol* 23: 801-810.
- Krinke GJ, Vidotto N, and Weber E. (2000) Teased-fiber technique for peripheral myelinated nerves: methodology and interpretation. *Toxicol Pathol* 28: 113-122.
- La Fleur M, Underwood JL, Rappolee DA, and Werb Z. (1996) Basement membrane and repair of injury to peripheral nerve: defining a potential role for macrophages, matrix metalloproteinases, and tissue inhibitor of metalloproteinases-1. *J Exp Med* 184: 2311-2326.
- Li H, Mittal A, Makonchuk DY, Bhatnagar S, and Kumar A. (2009) Matrix metalloproteinase-9 inhibition ameliorates pathogenesis and improves skeletal muscle regeneration in muscular dystrophy. *Hum Mol Genet* 18: 2584 -2598.
- Matsumura K, Arai K, Zhong D, Saito F, Fukuta-Ohi H, Maekawa R, Yamada H, and Shimizu T. (2003) Disruption of dystroglycan axis by β-dystroglycan processing in cardiomyopathic hamster muscle. *Neuromuscul Disord* 13: 796-803.
- Mawrin C, Brunn A, Rocken C, Schroder JM. (2003) Peripheral neuropathy in systemic lupus erythematosus: pathomorphological features and distribution pattern of matrix metalloproteinases. *Acta Neuropathol (Berl)* 105: 365-372.
- Meier H, and Southard JL. (1970) Muscular dystrophy in the mouse caused by an allele at the dy-locus. *Life Sci* 9: 137-144.
- Michaluk P, Kolodziej L, Mioduszewska B, Wilczynski GM, Dzwonek J, Jaworski J, Gorecki DC, Ottersen OP, and Kaczmarek L. (2007) β-dystroglycan as a target for MMP-9, in response to enhanced neuronal activity. *J Biol Chem* 282: 16036 -16041.
- Miyagoe Y, Hanaoka K, Nonaka I, Hayasaka M, Nabeshima Y, Arahata

K, and Takeda S. (1997) Laminin α2 chain null mutant mice by targeted disruption of the Lama2 gene: a new model of merosin (laminin 2)-deficient congenital muscular dystrophy. *FEBS Lett.* 415: 33-39.

- Moore CJ, and Winder SJ. (2010) Dystroglycan versatility in cell adhesion: a tale of multiple motifs. *Cell Commun Signal* 8: 3.
- Neely JD, Amiry-Moghaddam M, Ottersen OP, Froehner SC, Agre P, and Adams ME. (2001) Syntrophin-dependent expression and localization of Aquaporin-4 water channel protein. *Proc Natl Acad Sci USA* 98: 14108-14113.
- Nodari A, Zambroni D, Quattrini A, Court FA, D'Urso A, Recchia A, Tybulewicz VL, Wrabetz L, and Feltri ML. (2007) β1 integrin activates Rac1 in Schwann cells to generate radial lamellae during axonal sorting and myelination. *J Cell Biol* 177: 1063-1075.
- Nodari A, Previtali SC, Dati G, Occhi S, Court FA, Colombelli C, Zambroni D, Dina G, Del Carro U, Campbell KP, Quattrini A, Wrabetz L, and Feltri ML. (2008) α6β4 integrin and dystroglycan cooperate to stabilize the myelin sheath. *J Neurosci* 28: 6714-6719.
- Noël G, Belda M, Guadagno E, Micoud J, Klöcker N, and Moukhles H. (2005) Dystroglycan and Kir4.1 coclustering in retinal Müller glia is regulated by laminin-1 and requires the PDZ-ligand domain of Kir4.1. *J Neurochem* 94: 691-702.
- Occhi S, Zambroni D, Del Carro U, Amadio S, Sirkowski EE, Scherer SS, Campbell KP, Moore SA, Chen ZL, Strickland S, Di Muzio A, Uncini A, Wrabetz L, and Feltri ML. (2005) Both laminin and Schwann cell dystroglycan are necessary for proper clustering of sodium channels at nodes of Ranvier. *J Neurosci* 25(41): 9418-9427.
- O'Reilly MS, Boehm T, Shing Y, Fukai N, Vasios G, Lane WS, Flynn E, Birkhead JR, Olsen BR, Folkman J. (1997) Endostatin: an

endogenous inhibitor of angiogenesis and tumor growth. *Cell* 88: 277-285.

- Ramón y Cajal. (1933) *S. Histology* (Bailliere, Tindall & Cox, London).
- Roberds SL, Ervasti JM, Anderson RD, Ohlendieck K, Kahl SD, Zoloto D, and Campbell KP. (1993) Disruption of the dystrophin-glycoprotein complex in the cardiomyopathic hamster. *J Biol Chem* 268: 11496 - 11499.
- Rosenberg GA. (2009) Matrix metalloproteinases and their multiple roles in neurodegenerative diseases. *Lancet* 8: 205-216.
- Saito F, Moore SA, Barresi R, Henry MD, Messing A, Ross-Barta SE, Cohn RD, Williamson RA, Sluka KA, Sherman DL, Brophy PJ, Schmelzer JD, Low PA, Wrabetz L, Feltri ML, and Campbell KP (2003) Unique role of dystroglycan in peripheral nerve myelination, nodal structure, and sodium channel stabilization. *Neuron* 38: 747-758.
- Salzer JL. (2003) Polarized domains of myelinated axons. *Neuron* 40: 297-318.
- Shang ZJ, Ethunandan M, Gorecki DC, and Brennan PA. (2008) Aberrant expression of β-dystroglycan may be due to processing by matrix metalloproteinases-2 and -9 in oral squamous cell carcinoma. *Oral Oncol* 44: 1139-1146.
- Sherman DL, and Brophy PJ. (2000) A tripartite nuclear localization signal in the PDZ-domain protein L-periaxin. *J Biol Chem* 275: 4537-4540.
- Sherman DL, Fabrizi C, Gillespie CS, and Brophy PJ. (2001) Specific disruption of a Schwann cell dystrophin-related protein complex in a demyelinating neuropathy. *Neuron* 30: 677-687.
- Shubayev VI, and Myers RR. (2000) Upregulation and interaction of TNFα and gelatinases A and B in painful peripheral nerve injury. *Brain*

Res 855: 83-89.

- Shubayev VI, and Myers RR. (2002) Endoneurial remodeling by TNFα and TNFα-releasing proteases. A spatial and temporal co-localization study in painful neuropathy. *J Peripher Nerv Syst* 7: 28-36.
- Shubayev VI, Angert M, Dolkas J, Campana WM, Palenscar K, Myers RR. (2006) TNFα-induced MMP-9 promotes macrophage recruitment into injured peripheral nerve. *Mol Cell Neurosci* 31: 407-415.
- Siebert H, Dippel N, Mäder M, Weber F, Brück W. (2001) Matrix metalloproteinase expression and inhibition after sciatic nerve axotomy. *J Neuropathol Exp Neurol* 60: 85-93.
- Singh J, Itahana Y, Knight-Krajewski S, Kanagawa M, Campbell KP, Bissell MJ, and Muschler J. (2004) Proteolytic enzymes and altered glycosylation modulate dystroglycan function in carcinoma cells. *Canc Res* 64: 6152-6159.
- Straub V, Duclos F, Venzke DP, Lee JC, Cutshall S, Leveille CJ, and Campbell KP. (1998) Molecular pathogenesis of muscle degeneration in the δ-sarcoglycan-deficient hamster. *Am J Pathol* 153: 1623-1630.
- Teles RMB, Antunes SLG, Jardim MR, Oliveira AL, Nery JAC, Sales AM, Sampaio EP, Shubayev V, and Sarno EN. (2007) Expression of metalloproteinases (MMP-2, MMP-9, and TACE) and TNF-α in the nerves of leprosy patients. *J Peripher Nerv Syst* 12: 195-204.
- Triolo D, Cerri F, Taveggia C, Porrello E, Bolino A, Colombelli C, Feltri ML, Dina G, D'Adamo P, Del Carro U, Morana P, Sherman DL, Babinet C, Quattrini A, Previtali SC. (2009) Abnormal Schwann cell-axon units and myelination in vimentin-deficient mice. Abstract at *Periph Nerve Soc Meeting. J Periph Nerv Syst* 1163.
- Vu TH, Shipley JM, Bergers JE, Helms JA, Hanahan D, Shapiro SD, Senior RM, and Werb Z. (1998) MMP-9/Gelatinase B is a key regulator

of growth plate angiogenesis and apoptosis of hypertrophic chondrocytes. *Cell* 93: 411-422.

- Weir ML, Oppizzi ML, Henry MD, Onishi A, Campbell KP, Bissell MJ, and Muschler JL. (2006) Dystroglycan loss disrupts polarity and β-casein induction in mammary epithelial cells by perturbing laminin anchoring. *J Cell Sci* 119: 4047- 4058.
- Wrabetz L, Feltri ML, Quattrini A, Imperiale D, Previtali S, D'Antonio M, Martini R, Yin X, Trapp BD, Zhou L, Chiu SY, and Messing A. (2000) P(0) glycoprotein overexpression causes congenital hypomyelination of peripheral nerves. *J Cell Biol* 148: 1021-1034.
- Wrabetz L, and Feltri ML. (2001) Do Schwann cells stop, DR(o)P2, and roll? *Neuron* 30: 642-644.
- Wu CY, Hsieh HL, Sun CC, and Yang CM. (2009) IL-1β induces MMP-9 expression via a Ca2+-dependent CaMKII/JNK/c-JUN cascade in rat brain astrocytes. *Glia* 57: 1775-1789.
- Yamada H, Saito F, Fukuta-Ohi H, Zhong D, Hase A, Arai K, Okuyama A, Maekawa R, Shimizu T, and Matsumura K. (2001) Processing of β-dystroglycan by matrix metalloproteinase disrupts the link between the extracellular matrix and cell membrane via the dystroglycan complex. *Hum Mol Genet* 10: 1563-1569.
- Zhao XL, Li GZ, Sun B, Zhang ZL, Yin YH, Tian YS, Li H, Li HL, Wang de S, Zhong D. (2010) MMP-mediated cleavage of β-dystroglycan in myelin sheath is involved in autoimmune neuritis. *Biochem Biophys Res Commun* 392: 551-556.
- Zhong D, Saito F, Saito Y, Nakamura A, Shimizu T, and Matsumura K. (2006) Characterization of the protease activity that cleaves the extracellular domain of β-dystroglycan. *Biochem Biophys Res Commun* 345: 867-871.

Chapter 4

Conclusions and future perspectives

Dystroglycan is an intriguing molecule with a fascinatingly complex biogenesis, a large number of interacting partners, and a wide-reaching biological involvement in a broad range of processes. It has been extensively studied as part of the dystrophin-glycoprotein complex (DGC) in skeletal muscle, where it serves as a physical link between extracellular matrix and subsarcolemmal cytoskeleton, providing the sarcolemma with the structural stability necessary during contraction and extension. Dystroglycan is also expressed in many other cell types and growing evidence shows that it plays different functional roles beyond muscle tissue (Cohn, 2005). For instance, it has been implicated in epithelial development (Durbeej et al., 1995), somitegenesis (Hidalgo et al., 2009), synaptogenesis (Jacobson et al., 1998; Montanaro et al., 1998), cell polarization (Deng et al., 2003; Li et al., 2003; Weir et al., 2006; Masuda-Hirata et al., 2009), immunological synapse formation (Gong et al., 2008), carcinogenesis (Henry et al., 2001; Jing et al., 2004; Sgambato and Brancaccio, 2005), infective pathogen targeting (Cao et al., 1998; Rambukkana et a., 1998 and 2003), visual function (Satz et al., 2008 and 2009), and development of the central nervous system (Moore et al., 2002; Schröder et al., 2007; Satz et al., 2010).

In the peripheral nervous system, dystroglycan has been shown to regulate several processes, like infection of *Mycobacterium leprae* (Rambukkana et al., 1998), radial sorting of axons (Berti et al., 2011), stabilization of the myelin sheath (Saito et al., 2003; Nodari et al.,

2008), establishment of proper Schwann cell cytoplasmic compartments and correct internodal lenghts (Court et al., 2009), and stabilization of the nodal architecture (Saito et al., 2003; Occhi et al., 2005). The mechanisms through which DG mediates each one of these processes are currently under study, and the comprehension of the molecular bases underlying DG function might be useful to understand the pathogenesis of a series of diseases involving not only the peripheral nervous system, but also other tissues. Due to its nearly ubiquitous distribution and multiple functions also in embryonic development, only one mutation in the *DAG1* gene has been described so far (Hara et al., 2011). The affected patient suffered from a limb-girdle muscular dystrophy with mental retardation; unfortunately, the peripheral nervous system was not analyzed in this patient. However, many forms of human congenital muscular dystrophies with peripheral nervous system (PNS) involvement have been described. In particular, loss of function mutations in the gene encoding laminin α2-chain causes MDC1A, a congenital muscular dystrophy characterized by a dysmyelinating and mild demyelinating peripheral neuropathy (Shorer et al., 1995; Di Muzio et al., 2003). In addition, α-DG hypoglycosylation, due to deficiency of at least six glycosyltransferases, causes secondary α-dystroglycanopathies with major involvement of muscle, eye and brain, but also PNS abnormalities have been described in some patients (Kimura et al., 1992; Jang et al., 2012). Many pathological features observed in these conditions resemble peripheral nerve defects found experimentally in the Schwann cell-specific conditional DG null mouse. This has suggested that dystroglycan interaction with laminin 211, which

largely depends on α-DG glycosylation, is functionally important for certain processes occurring in the peripheral nerve.

In the present work, we have analyzed the differential roles of Schwann cell dystroglycan in two specialized domains of the peripheral myelinated fiber, the node of Ranvier and the internode. Proper clustering of Nav at nodes of Ranvier and a correct length of internodes, together with an intact myelin sheath, are prerequisites for a fast and efficient electrical conduction in myelinated fibers. Reduced conduction contributes to disability in patients affected with peripheral neuropathies. Hence, understanding the underlying molecular mechanisms would be important to determine the targets of potential therapeutic treatments.

4.1 Dystroglycan at nodes of Ranvier

In the first part of this thesis we demonstrated that dystroglycan stabilizes the formation of Nav clusters during early postnatal development in mice. Absence of DG causes clusters to form abnormally and this has been correlated to slowed nerve conductions. Previously in our lab, the analysis of a sural nerve biopsy from a MDC1A patient revealed Nav cluster abnormalities similar to those found in mice lacking DG or laminins (Occhi et al., 2005). This suggests that the interaction of DG with laminin 211 is important for Nav clustering in both humans and mice. However, one report did not detect Nav clustering defects in a murine model of a glycosyltransferase deficiency (Levedakou et al., 2005). The analysis of other mutants and, possibly, nerve biopsies from α-

dystroglyconopathy patients would clarify this point.

The idea that Nav clustering could be regulated by other DG ligands in addition to laminins is supported by our finding of a potential role for the N-terminal domain of α-DG (α-DG-N) in the nodal gap substance. Further investigations are aimed at assessing the presence of α-DG-N at peripheral nodes *in vivo*, and at determining its interacting partners in this specific context. In the last few years α-DG-N has been detected not only in several types of cultured cells, but also in body fluids, like blood serum and cerebrospinal fluid (CSF) (Saito et al., 2008 and 2011). Although its biological function is still unclear, it has been suggested that α-DG-N could be used as a biomarker for some neuromuscular or neurological diseases (Bozzi et al., 2009); for instance, increased levels of α-DG-N were recently found in the CSF of patients with Lyme neuroborreliosis (Hesse et al., 2011). Nonetheless, an urgent issue is to determine whether the N-terminal cleavage of α-DG takes place in all DG-expressing tissues, or only in specific districts, and if it is regulated during development and/or under pathologic conditions. This may shed light on a molecule that, similarly to other furin substrates, including growth factors, hormones and receptors, might be synthetized as an inactive proprotein (complete DG) and then processed to become a biologically active protein by proteolytic cleavage (Nakayama, 1997; Thomas, 2002). Another intriguing possibility is that at nodes of Ranvier, also laminin 211 is cleaved by furin protease. It is known that laminin α2 chain can be cleaved by furin in its LG3 domain (Talts et al., 1998), and the released processed form, lacking LG4-LG5 domains, is able to induce agrin-independent AchR clustering in

myotubes (Smirnov et al., 2002). The function of both α-DG and laminin 211 could be regulated at nodes by the same protease that activates them for their 'Nav clustering activity'. Future experiments will assess laminin 211 cleavage in peripheral nerves and furin activity at nodes of Ranvier.

From a more general point of view, the study of the mechanisms of Nav clustering and nodal domain assembly is useful because different pathological conditions, either inherited or acquired, causing demyelination, dysmyelination and altered neuron-glia interaction, lead to loss or misexpression of nodal ion channel clusters and altered nerve conduction. For instance, in the *Trembler-J* mouse, an authentic model of a dominantly inherited demyelinating neuropathy in humans (CMT1A), segmental demyelination and remyelination have been associated with unusual expression of Nav1.8 and Kv3.1b isoforms at nodes and heminodes (Devaux and Scherer, 2005). A similar ectopic expression of Nav1.8 was also reported in the *Mpz*-null mouse that develops a severe and early onset dysmyelinating neuropathy (Ulzheimer et al., 2004).

Nodes of Ranvier have also been proposed to be the direct targets of autoantibodies in some forms of PNS autoimmune diseases (Pollard and Armati, 2011). In acute motor axonal neuropathy, a form of Guillain-Barré syndrome (GBS), autoantibodies against the gangliosides GM1 and GD1a bind preferentially to the nodal region, with subsequent dismantling of nodes of Ranvier due to the activation of the complement cascade (Susuki et al., 2007). More interestingly, autoantibodies against two nodal components involved in Nav clustering, gliomedin and neurofascin 186, were also found in a form

of experimental allergic neuritis (EAN), another model of GBS. In this situation, the nodal axo-glial unit is selectively affected before the onset of the disease, suggesting that disruption of nodes themselves maybe a major contributor to the pathophysiology of the disease (Lonigro and Devaux, 2009). It would be interesting to know if also dystroglycan might be the target of an immune response in this pathology.

In conclusion, these studies suggest that disruption or alteration of ion channel clusters may be a common early consequence or a common cause of many types of peripheral nervous system diseases. Given the central role played by clustered ion channels in nervous system function, it will be important to understand the developmental mechanisms that lead to channel clustering when considering therapeutic strategies aimed at nervous system repair.

4.2 Dystroglycan at internodes

In the second part of this thesis we have shown that the post-translational cleavage of β-dystroglycan by MMP-2 and -9 regulates the size and the molecular composition of Schwann cell domains and this has been related to changes in internodal length (Court et al., 2009 and 2011).

Internodal length influences nerve conduction velocity because the presence of more nodes in a given segment (decreased internodal length) increases the action potential regeneration events, thus increasing the time for the action potential to travel along the nerve fiber. This has been predicted theoretically by mathematical models (Brill et al., 1977; Moore et al., 1978) and proved experimentally

(Court et al., 2004).

Moreover, the proper distribution of Cajal bands and appositions in the outer Schwann cell cytoplasm has been associated with the establishment of a correct internodal length (Court et al., 2004 and 2009). Although this correlation is not absolute (Triolo et al., 2009; Brophy P.J., personal communication), loss or mutation of some components of the dystroglycan complex, like DG, utrophin and periaxin, or one of its ligand, laminin 211, result in defective Schwann cell compartmentalization and reduced internodal lengths (Court et al., 2004 and 2009). Future studies are aimed at understanding if other parameters regulate the ability of Schwann cells to form normal cytoplasmic channels, allowing them to properly elongate. Microtubule (MT) organization and connection with the actin-based cytoskeleton have been advocated as potential regulators of internodal length. In this regard, it is worth noting that both Dp116 and utrophin contain a microtubule-binding domain (Prins et al., 2009), making them potential cytolinker between DG, the actin- and the MT-cytoskeleton.

Metalloproteinases have been implicated in the regulation of a plethora of physiological and pathological processes, such as embryo implantation, bone remodelling and organogenesis, or inflammation, wound healing and tumor invasion (Page-McCaw et al., 2007). Here we have shown that in peripheral nerve MMP-2 and -9 are important regulators of Schwann cell compartmentalization in physiological conditions. However, their dysregulated expression might be detrimental in certain pathological circumstances. This holds true in a series of neurodegenerative and neurovascular diseases, and also in

PNS disorders, like experimental allergic neuritis in rats (Rosenberg, 2009). We have shown that also in the mouse model of MDC1A, metalloproteinases are abnormally upregulated and we associated the unregulated cleavage of β-DG to the reduced internodes and conduction, that have been reported also in MDC1A patients (Di Muzio et al., 2003; Court et al., 2009). As a proof of principle, the inhibition of β-DG cleavage by a MMP inhibitor rescued defective SC compartmentalization and, at least in part, internodal length of dystrophic mice *in vitro*. However, the genetic ablation of MMP-9 in dystrophic mice did not show the same ameliorations, probably due to redundancy mechanisms by MMP-2, or to the fact that MMP-9 ablation would have been modulated in time. To address this point, the analysis of MMP-2 MMP-9 double knockouts and the generation of an inducible knockout mouse in the dystrophic background might be useful. In addition, a pre-clinical study with a MMP inhibitor in dystrophic mice should be designed. Defining the temporal expression of active gelatinases during the development of the peripheral neuropathy would be important to determine the timing of the treatment. A second crucial issue is the choice of the inhibitor: specificity, high selectivity and ability to cross the blood-nerve barrier are three prerequisites to avoid the onset of dramatic side effects and to guarantee the correct bioavailability (Hu et al., 2007). A group of completely novel and promising type of MMP inhibitors are the mechanism-based inhibitors developed by the group of Mobashery (Brown et al., 2000). The first prototype was named SB-3CT and is highly selective for gelatinases. Specifically, this compound contains a thiirane group that coordinates with the active-site zinc. In turn, this

leads to a conformational change and a covalent attachment to the active-site Glu. This is the reason why this class of inhibitors is also called suicide inhibitors. New variants were recently designed, synthetized and proved to be active *in vivo*.

Last, but not least, a treatment with such an inhibitor should take into account the dystrophic pathology affecting the skeletal muscle. Recently, the removal of MMP-9, but not MMP-2, proved to be beneficial in *mdx* mice, a model of Duchenne muscular dystrophy (Li et al., 2009; Miyazaki et al., 2011). Thus, the analysis of gelatinases and their role in the pathogenesis of muscular dystrophy in MDC1A should be performed.

In principle, our finding that the regulation of β-DG cleavage by MMPs can be modulated to ameliorate peripheral nerve pathology could be useful in other PNS pathological conditions, especially inflammatory demyelinating diseases, in which excessive gelatinase activation was detected. In this direction, the use of captopril, a broad-spectrum MMP inhibitor, improved the clinical signs of EAN in rats and this was associated with a reduced cleavage of β-DG (Zhao et al., 2010).

In addition, MMP-2 and -9 generally increase after nerve injury, promoting the breakdown of blood-nerve barrier, macrophage recruitment into injured nerve, MBP degradation, and causing neuropathic pain. It would be interesting to determine if also in these situations higher gelatinase activity results in abnormal β-DG cleavage and SC compartmentalization, possibly determining the reduced internodal lengths observed in remyelinated fibers.

It has been shown that MMP-9 removal protects nerve fibers from

demyelination and axonal degeneration, and reduces neuropathic pain after injury (Shubayev et al., 2006; Chattopadhyay et al., 2007). However, MMPs also exert beneficial effects during regeneration of the damaged nervous system. Hence, the necessity to use MMP inhibitors only in finely regulated temporal windows.

4.3 References

- Berti C, Bartesaghi L, Ghidinelli M, Zambroni D, Figlia G, Chen Z-L, Quattrini A, Wrabetz L, and Feltri ML. (2011) Non-redundant function of dystroglycan and β1 integrins in radial sorting of axons. *Dev* 138: 4025-4037.
- Bozzi M, Morlacchi S, Bigotti MG, Sciandra F, and Brancaccio A. (2009) Functional diversity of dystroglycan. *Matr Biol* 28: 179-187.
- Brill MH, Waxman SG, Moore JW, and Joyner RW. (1977) Conduction velocity and spike configuration in myelinated fibres: computed dependence on internode distance. *J Neurol Neurosurg Psych* 40: 769-774.
- Brown S, Bernardo MM, Li ZH, Kotra LP, Tanaka Y, Fridman R, and Mobashery S. (2000) Potent and selective mechanism-based inhibition of gelatinases. *J Am Chem Soc* 122: 6799-6800.
- Cao W, Henry MD, Borrow P, Yamada H, Elder JH, Ravkov EV, Nichol ST, Compans RW, Campbell KP, and Oldstone MBA. (1998) Identification of α-dystroglycan as a receptor for lymphocytic choriomeningitis virus and Lassa fever virus. *Science* 282(5396): 2079-2081.
- Chattopadhyay S, Myers RR, Janes J, and Shubayev V. (2007) Cytokine regulation of MMP-9 in peripheral glia: implications for pathological processes and pain in injured nerve. *Brain Behav Immun* 21: 561-568.

- Cohn RD. (2005) Dystroglycan: important player in skeletal muscle and beyond. *Neuromusc Dis* 15: 207-217.
- Court FA, Sherman DL, Pratt T, Garry EM, Ribchester RR, Cottrell DF, Fleetwood-Walker SM, and Brophy PJ. (2004) Restricted growth of Schwann cells lacking Cajal bands slows conduction in myelinated nerves. *Nature* 431: 191-195.
- Court FA, Hewitt JE, Davies K, Patton BL, Uncini A, Wrabetz L, and Feltri ML. (2009) A laminin-2, dystroglycan, utrophin axis is required for compartmentalization and elongation of myelin segments. *J Neurosci* 29(12): 3908-19.
- Court FA, Zambroni D, Pavoni E, Colombelli C, Baragli C, Figlia G, Sorokin L, Ching W, Salzer JL, Wrabetz L, and Feltri ML. (2011) MMP2-9 cleavage of dystroglycan alters the size and molecular composition of Schwann cell domains. *J Neurosci* 31(34): 12208-17.
- Deng W-M, Schneider M, Frock R, Castillejo-Lopez C, Gaman EA, Baumgartner S, and Ruohola-Baker H. (2003) Dystroglycan is required for polarizing the epithelial cells and the oocyte in Drosophila. *Dev* 130(1): 173-184.
- Devaux JJ, and Scherer SS. (2005) Altered ion channels in an animal model of Charcot-Marie-Tooth disease type IA. *J Neurosci* 25(6): 1470-80.
- Di Muzio A, De Angelis MV, Di Fulvio P, Ratti A, Pizzuti A, Stuppia L, Gambi D, and Uncini A. (2003) Dysmyelinating sensory-motor neuropathy in merosin-deficient congenital muscular dystrophy. *Muscle Nerve* 27: 500-506.
- Durbeej M, Larsson E, Ibraghimov-Beskrovnaya O, Roberds SL, Campbell KP, and Ekblom P. (1995) Non-muscle α-dystroglycan is involved in epithelial development. *J Cell Biol* 130(1): 79-91.

- Gong Y, Zhang R, Zhang J, Xu L, Zhang F, Xu W, Wang Y, Chu Y, and Xiong S. (2008) α-dystroglycan is involved in positive selection of thymocytes by participating in immunological synapse formation. *FASEB J* 22(5): 1426-39.
- Hara Y, Balci-Hayta B, Yoshida-Moriguchi T, Kanagawa M, Beltran-Valero de Bernabé D, Gündeşli H, Willer T, Satz JS, Crawford RW, Burden SJ, Kunz S, Oldstone MBA, Accardi A, Talim B, Muntoni F, Topaloğlu H, Dincer P, and Campbell KP. (2011) A dystroglycan mutation associated with Limb-Girdle Muscular Dystrophy. *N Engl J Med* 364(10): 939-946.
- Henry MD, Cohen MB, and Campbell KP. (2001) Reduced expression of dystroglycan in breast and prostate cancer. *Hum Pathol* 32: 791-795.
- Hesse C, Johansson I, Mattsson N, Bremell D, Andreasson U, Halim A, Anckarsäter R, Blennow K, Anckarsäter H, Zetterberg H, Larson G, Hagberg L, and Grahn A. (2011) The N-terminal domain of α-dystroglycan is released as a 38 kDa protein and is increased in cerebrospinal fluid in patients with Lyme neuroborreliosis. *Biochem Biophys Res Comm* 412(3): 494-499.
- Hidalgo M, Sirour C, Bello V, Moreau N, Beaudry M, and Darribère T. (2009) In vivo analyzes of dystroglycan function during somitogenesis in *Xenopus laevis*. *Dev Dyn* 238(6): 1332-1345.
- Hu J, Van den Steen PE, Sang Q-XA, and Opdenakker G. (2007) Matrix metalloproteinase inhibitors as therapy for inflammatory and vascular diseases. *Nature* 6: 480-498.
- Jacobson C, Montanaro F, Lindenbaum M, Carbonetto S, and Ferns M. (1998) α-dystroglycan functions in acetylcholine receptor aggregation but is not a coreceptor for agrin-MuSK signaling. *J Neurosci* 18: 6340-6348.

- Jang DH, Sung IY, and Ko TS. (2012). Peripheral nerve involvement in Fukuyama Congenital Muscular Dystrophy: a case report. *J Child Neurol*, Epub ahead of print.
- Jing J, Lien CF, Sharma S, Rice J, Brennan PA, and Górecki DC. (2004) Aberrant expression, processing and degradation of dystroglycan in squamous cell carcinomas. *Eur J Cancer* 40: 2143-2151.
- Kimura S, Kobayashi T, Sasaki Y, Hara M, Nishino T, Miyake S, Iwamoto H, Misugi N. (1992) Congenital polyneuropathy in Walker-Warburg syndrome. *Neuroped* 23(1): 14-17.
- Levedakou EN, Chen XJ, Soliven B, and Popko B. (2005) Disruption of the mouse *Large* gene in the enr and myd mutants results in nerve, muscle, and neuromuscular junction defects. *Mol Cell Neurosci* 28: 757-769.
- Li H, Mittal A, Makonchuk DY, Bhatnagar S, Kumar A. (2009) Matrix metalloproteinase-9 inhibition ameliorates pathogenesis and improves skeletal muscle regeneration in muscular dystrophy. *Hum Mol Genet* 18: 2584 -2598.
- Li S, Edgar D, Fässler R, Wadsworth W, and Yurchenco PD. (2003) The role of laminin in embryonic cell polarization and tissue organization. *Dev Cell* 4(5): 613-624.
- Lonigro A, and Devaux JJ. (2009) Disruption of neurofascin and gliomedin at nodes of Ranvier precedes demyelination in experimental allergic neuritis. *Brain* 132(1): 260-73.
- Masuda-Hirata M, Suzuki A, Amano Y, Yamashita K, Ide M, Yamanaka T, Sakai , Imamura M, and Ohno S. (2009) Intracellular polarity protein PAR-1 regulates extracellular laminin assembly by regulating the dystroglycan complex. *Gen Cell* 14(7): 835-850.
- Miyazaki D, Nakamura A, Fukushima K, Yoshida K, Takeda S, and Ikeda S. (2011) Matrix metalloproteinase-2 ablation in dystrophin-

deficient mdx muscles reduces angiogenesis resulting in impaired growth of regenerated muscle fibers. *Hum Mol Genet* 20: 1787-1799.

- Montanaro F, Gee SH, Jacobson C, Lindenbaum MH, Froehner SC and Carbonetto S. (1998) Laminin and α-dystroglycan mediate acetylcholine receptor aggregation via a MuSK-independent pathway. *J Neurosci* 18: 1250-1260.
- Moore JW, Joyner RW, Brill MH, Waxman SD, and Najar-Joa M. (1978) Simulations of conduction in uniform myelinated fibers. Relative sensitivity to changes in nodal and internodal parameters. *Biophys J* 21: 147-160.
- Moore SA, Saito F, Chen J, Michele DE, Henry MD, Messing A, Cohn RD, Ross-Barta SE, Westra S, Williamson RA, Hoshi T, and Campbell KP. (2002) Deletion of brain dystroglycan recapitulates aspects of congenital muscular dystrophy. *Nature* 418: 422-425.
- Nakayama K. (1997) Furin: a mammalian subtilisin/Kex2p-like endoprotease involved in processing of a wide variety of precursor proteins. *Biochem J* 327: 625-635.
- Nodari A, Previtali SC, Dati G, Occhi S, Court FA, Colombelli C, Zambroni D, Dina G, Del Carro U, Campbell KP, Quattrini A, Wrabetz L, and Feltri ML. (2008) α6β4 integrin and dystroglycan cooperate to stabilize the myelin sheath. *J Neurosci* 28(26): 6714-6719.
- Occhi S, Zambroni D, Del Carro U, Amadio S, Sirkowski EE, Scherer SS, Campbell KP, Moore SA, Chen ZL, Strickland S, Di Muzio A, Uncini A, Wrabetz L, and Feltri ML. (2005) Both laminin and Schwann cell dystroglycan are necessary for proper clustering of sodium channels at nodes of Ranvier. *J Neurosci* 25(41): 9418-9427.
- Page-McCaw A, Ewald AJ, and Werb Z. (2007) Matrix metalloproteinases and the regulation of tissue remodelling. *Nat Rev Mol Cell Biol* 8: 221-233.

- Pollard JD, and Armati PJ. (2011) CIDP - the relevance of recent advances in Schwann cell/axonal neurobiology. *J Periph Nerv Syst* 16: 15-23.
- Prins KW, Humston JL, Mehta A, Tate V, Ralston E, and Ervasti JM. (2009) Dystrophin is a microtubule-associated protein. *J Cell Biol* 186(3): 363-9.
- Rambukkana A, Yamada H, Zanazzi G, Mathus T, Salzer JL, Yurchenco PD, Campbell KP, and Fischetti VA. (1998) Role of α-dystroglycan as a Schwann cell receptor for *Mycobacterium leprae*. *Science* 282(5396): 2076-2079.
- Rambukkana A, Kunz S, Min J, Campbell KP, and Oldstone MBA. (2003) Targeting Schwann cells by nonlytic arenaviral infection selectively inhibits myelination. *Proc Natl Acad Sci USA* 100(26): 16071-16076.
- Rosenberg GA. (2009) Matrix metalloproteinases and their multiple roles in neurodegenerative diseases. *Lancet* 8: 205-216.
- Saito F, Moore SA, Barresi R, Henry MD, Messing A, Ross-Barta SE, Cohn RD, Williamson RA, Sluka KA, Sherman DL, Brophy PJ, Schmelzer JD, Low PA, Wrabetz L, Feltri ML, and Campbell KP. (2003) Unique role of dystroglycan in peripheral nerve myelination, nodal structure, and sodium channel stabilization. *Neuron* 38: 747-758.
- Saito F, Saito-Arai Y, Nakamura A, Shimizu T, and Matsumura K. (2008) Processing and secretion of the N-terminal domain of α-dystroglycan in cell culture media. *FEBS Lett* 582(3): 439-44.
- Saito F, Saito-Arai Y, Nakamura-Okuma A, Ikeda M, Hagiwara H, Masaki T, Shimizu T, and Matsumura K. (2011) Secretion of N-terminal domain of α-dystroglycan in cerebrospinal fluid. *Biochem Biophys Res Commun* 411(2): 365-9.

- Satz JS, Barresi R, Durbeej M, Willer T, Turner A, Moore SA, and Campbell KP. (2008) Brain and eye malformations resembling Walker-Warburg syndrome are recapitulated in mice by dystroglycan deletion in the epiblast. *J Neurosci* 28: 10567-10575.
- Satz JS, Philp AR, Nguyen H, Kusano H, Lee J, Turk R, Riker MJ, Hernández J, Weiss RM, Anderson MG, Mullins RF, Moore SA, Stone EM, and Campbell KP. (2009) Visual impairment in the absence of dystroglycan. *J Neurosci* 29: 13136 -13146.
- Satz JS, Ostendorf AP, Hou S, Turner A, Kusano H, Lee JC, Turk R, Nguyen H, Ross-Barta SE, Westra S, Hoshi T, Moore SA, and Campbell KP. (2010) Distinct functions of glial and neuronal dystroglycan in the developing and adult mouse brain. *J Neurosci* 30(43): 14560-14572.
- Schröder JE, Tegeler MR, Grosshans U, Porten E, Blank M, Lee J, Esapa C, Blake DJ, and Kröger S. (2007) Dystroglycan regulates structure, proliferation and differentiation of neuroepithelial cells in the developing vertebrate CNS. *Dev Biol* 307: 62-78.
- Sgambato A, and Brancaccio A. (2005) The dystroglycan complex: from biology to cancer. *J Cell Phys* 205(2): 163-169.
- Shorer Z, Philpot J, Muntoni F, Sewry C, and Dubowitz V. (1995) Demyelinating peripheral neuropathy in merosin-deficient congenital muscular dystrophy. *J Child Neurol* 10: 472-475.
- Shubayev VI, Angert M, Dolkas J, Campana WM, Palenscar K, and Myers RR. (2006) TNFα-induced MMP-9 promotes macrophage recruitment into injured peripheral nerve. *Mol Cell Neurosci* 31: 407-415.
- Smirnov SP, McDearmon EL, Li S, Ervasti JM, Tryggvason K, and Yurchenco PD. (2002) Contributions of the LG modules and furin processing to laminin-2 functions. *J Biol Chem* 277(21): 18928-18937.

- Susuki K, Rasband MN, Tohyama K, Koibuchi K, Okamoto S, Funakoshi K, Hirata K, Baba H, and Yuki N. (2007) Anti-GM1 antibodies cause complement-mediated disruption of sodium channel clusters in peripheral motor nerve fibers. *J Neurosci* 27(15): 3956-67.
- Talts JF, Mann K, Yamada Y, and Timpl R. (1998) Structural analysis and proteolytic processing of recombinant G domain of mouse laminin α2 chain. *FEBS Lett* 426: 71-76.
- Thomas G. (2002) Furin at the cutting edge: from protein traffic to embryogenesis and disease. *Nat Rev Mol Cell Biol* 3: 753-766.
- Triolo D, Cerri F, Taveggia C, Porrello E, Bolino A, Colombelli C, Feltri ML, Dina G, D'Adamo P, Del Carro U, Morana P, Sherman DL, Babinet C, Quattrini A, Previtali SC. (2009) Abnormal Schwann cell-axon units and myelination in vimentin-deficient mice. Abstract at *Periph Nerve Soc Meeting. J Periph Nerv Syst* 1163.
- Ulzheimer JC, Peles E, Levinson SR, and Martini R. (2004) Altered expression of ion channel isoforms at the node of Ranvier in P0-deficient myelin mutants. *Mol Cell Neurosci* 25: 83-94.
- Weir ML, Oppizzi ML, Henry MD, Onishi A, Campbell KP, Bissell MJ, and Muschler JL. (2006) Dystroglycan loss disrupts polarity and β-casein induction in mammary epithelial cells by perturbing laminin anchoring. *J Cell Sci* 119: 4047-4058.
- Zhao XL, Li GZ, Sun B, Zhang ZL, Yin YH, Tian YS, Li H, Li HL, Wang de S, and Zhong D. (2010) MMP-mediated cleavage of β-dystroglycan in myelin sheath is involved in autoimmune neuritis. *Biochem Biophys Res Commun* 392: 551-556.

Publications

- Court FA, Zambroni D, Pavoni E, Colombelli C, Baragli C, Figlia G, Sorokin L, Ching W, Salzer J, Wrabetz L and Feltri ML. (2011) MMP2-9 cleavage of dystroglycan alters the size and molecular composition of Schwann cell domains. *J Neurosci* 31(34): 12208-12217.

- Nodari A, Previtali SC, Dati G, Occhi S, Court FA, Colombelli C, Zambroni D, Dina G, Del Carro U, Campbell KP, Quattrini A, Wrabetz L, and Feltri ML. (2008) α6β4 integrin and dystroglycan cooperate to stabilize the myelin sheath. *J Neurosci* 28(26): 6714-6719.

- Pellegatta S, Tunici P, Poliani PL, Dolcetta D, Cajola L, Colombelli C, Ciusani E, Di Donato S, and Finocchiaro G. (2006) The therapeutic potential of neural stem/progenitor cells in murine globoid cell leukodystrophy is conditioned by macrophage/ microglia activation. *Neurobiol Dis* 21: 314-323.

Acknowledgements

In the end, I just want to thank all the people who sincerely helped me the last 6 years in the lab. They all well know who they are, without the need to be mentioned one by one. What really matters is what they have done for me.

So thanks for having shared reagents, space, time and ideas, thanks for all the scientific, technical and more human advice, for the infinite comprehension and sincere friendship, even at distance. Thanks for having shared tremendous meeting trips (!), for the mid-morning breaks - they were absolutely necessary - and for having inspired me with your passion for science. Thanks for the jokes and music, for making me laugh even when I was not willing to, you rendered life in the lab enjoyable.

Thank you for having spent hours and hours at Leo, your (I)EM were simply great, thanks for valuable suggestions and help with dissections, for artwork tips, and for having the suitable statistical test whenever it was needed! Thank you for having this thesis timely revised and for all the scientific and even more personal discussions. Thanks for mentoring me, and for both pre- and post-LWLF lab meetings, I've learned a lot from them. Thanks for having introduced me to the magic world of Schwann cells, I have to admit that it is really exciting!

I'm thankful for the infinite and continuos support during these years at university, for the love and care, for having stimulated me to go on, despite several difficulties. Thanks for the life outside the lab, simple things can be so precious and regenerating when a friend is there.

Thanks for having always encouraged me to explore several fields, I've learned that knowledge is a unique continuum, and science is just a little part of it.